# Contributions of Biogenic and Anthropogenic Hydrocarbons to Photochemical Smog Formation

Thesis by

Suzanne Elizabeth Paulson

In Partial Fulfillment of the Requirements

for the Degree of

Doctor of Philosophy

Environmental Engineering Science

California Institute of Technology

Pasadena, California

1991

(Submitted May 28, 1991)

# Acknowledgments

Many people have helped in the many varied steps leading to the developments which comprise this thesis. First comes my advisor, John Seinfeld, who provided guidance, much perspective, and, in addition to financial support, the freedom to pursue my own ideas, beginning with my desire to study gas phase chemistry. Rick Flagan also provided help and encouragement at some important times, including at the critical push to add GCMS to this work.

I owe special thanks to many folks, including Spyros Pandis for many lively and illuminating discussions on the "Roof" and at "the Office", as well as occasional reprieves from computational quagmires, Bruce Daube for assistance with instrumentation and a determination for doing things right, Yuk Yung for his enthusiasm and global (sometimes other-worldly) perspectives on science, Dr. Norman Brooks for reading this 'out of field' thesis and being a first-class executive officer, Roger Atkinson at the University of California at Riverside for very relevant discussions, Mike Hoffmann for discussions on a surprising range of topics, as well as many of the air pollution people at Caltech; Evelina Cui, Glen Cass, Jennifer Stern, Brian Wong, Sue Larson, Shih-Chen Wang, Martha Shaw, Fang-dong Yin, and Daniel Grosjean.

I very much appreciate the scholarships and fellowships I have received while at Caltech from the Switzer Foundation, The American Association of University Women, the Earl C. Anthony Endowment and the Hewlett Foundation.

Among the most valuable lessons I have learned at Caltech is the navigation of iniquitous waters. For all the things that just cannot be found elsewhere, my friends Catherine

Brinson and Andrea Ghez couldn't have done better. I also much appreciate M. Kennedy, J. Blank, K. Penix, J. Lazar, and many other friends, for all they do.

My parents, of course deserve very special thanks. They've provided support in so many ways, and excellent, if sometimes reluctant, advice on many issues. Thanks to Mom for not asking when I'm going to graduate and Dad for trying hard not to embarrass me. In all seriousness, thanks for everything.

And to my great friend Neil, who has been amazingly supportive of both science and athletics, I must express my appreciation. He has been my faithful and encouraging climbing partner, who gave me a key to the vertical world (Jane's addiction; suspended animation), didn't flinch much when I ran off with it, and without whom I should never have touched 5.12, and reached beyond. Thanks, babe.

# Abstract

Photochemical oxidation of biogenic (Isoprene) and anthropogenic (1-octene) hydrocarbons are examined. Experiments studied the individual daylight reactions of both isoprene and 1-octene, including those of OH, $O_3$, and $O(^3P)$. Results from both the smog chamber experiments and computer kinetic modeling were then used to develop photochemical oxidation mechanisms for each hydrocarbon. Aerosols formed by isoprene and another biogenic, ß-pinene, are characterized.

The OH reaction with isoprene is studied. Methyl nitrite photolysis experiments were carried out in an outdoor smog chamber in an attempt to identify as completely as possible OH-isoprene product spectrum. Emphasis was placed on identification and quantification of oxygenated products. The design of a Tenax-based cryo-trap thermal desorber used to trap, concentrate, and dry chamber samples for identification on a GC/MS is described. Analysis of the products revealed that $O(^3P)$ can form in reaction systems designed to study OH reactions that include high concentrations of NO, and consequently $NO_2$, hence this reaction is also examined. The yields of methacrolein and methyl vinyl ketone are determined as 25±3 and 35.5±4%, respectively, with an additional 5.1±3% as 3-methyl furan, totaling 66±3%. These results, combined with those of previous studies allow 80% of isoprene's products to be explicitly identified, and the general structure of the remaining products to be ascertained. The $O(^3P)$ reaction produces 84±8% epoxides, and 8.±3% species which result in production of $HO_2$, and subsequently OH. A heretofore unidentified product of the $O(^3P)$ reaction, 2,2 methyl butenal, is identified. The rate constant of the $NO_2$ -isoprene reaction is measured.

A series of experiments have been carried out to study the ozone-isoprene reaction in a smog chamber using externally produced $O_3$, added to the hydrocarbon in the dark. A

chemical tracer, methyl cyclohexane, was added to probe the OH formation in the system. $O(^3P)$ formation was also examined using the known distribution of products that are unique to the $O(^3P)$-isoprene reaction (part 1). The results provide clear evidence that both OH and $O(^3P)$ are produced from the $O_3$ -isoprene reaction directly in large quantities; about 0.68±0.15 and 0.45±0.15 per $O_3$ -isoprene reaction, respectively. These additional radicals severely complicate the analysis of the $O_3$ reaction, hence computer kinetic modeling was necessary to ascertain the products of the $O_3$ reaction itself. The product spectrum, which differs dramatically from that published previously, is: 67±9% methacrolein, 26±6% methyl vinyl ketone, and 7±3% propene, accounting for 100±10% of the reacted isoprene. Applicability of these results to the gas-phase $O_3$ reaction with other unsaturated hydrocarbons is briefly discussed.

The photooxidation chemistry of 1-octene is examined in detail. Formation of OH from the $O_3$ reaction was examined with the use of a tracer/absorber, methyl cyclohexane. The $O_3$ - 1-octene reaction is found to produce, apparently directly, significant quantities of OH, 0.55±0.2 on a per molecule reacted 1-octene basis. Almost 100% of the reacted 1-octene could be accounted for as 80±10% heptanal, 11±6% thermally stabilized Criegee biradical, and about 1% hexane. The OH - 1-octene reaction was found to produce only 15±5% heptanal. The remainder is assumed to result in the formation of alkyl nitrates (32%), and isomerization and eventual formation of multisubstituted products (52%). A separate experiment examining the $O(^3P)$-1-octene reaction, showed that 1-octyl oxide accounted for about 80% of the reacted 1-octene. A photochemical model was developed for 1-octene oxidation, and is compared with smog chamber results from $NO/NO_2$/1-octene experiments. The most crucial factor in the performance of the model is the quantity of assumed alkyl nitrate formation.

A mechanism for the oxidation of isoprene is developed and includes the recent developments on each of isoprene's atmospherically important reactions: $O_3$, OH, $O(^3P)$, and $NO_3$. The mechanism is tested against chamber data that includes a range of mixtures of these reactions. While it performs reasonably well under conditions where the OH and $O(^3P)$ reactions dominate, it tends to over predict $O_3$ formation, as well as the speed of development of $O_3$ under conditions where the $O_3$ and $NO_3$ reactions are important. The $NO_3$ reaction is the most uncertain aspect of the isoprene mechanism, and may be responsible for a large part of this discrepancy. The discrepancy may also arise from the difficulty in extrapolating the results of $O_3$ experimental results, necessarily carried out in the absence of $NO_x$, to conditions that include significant concentrations of $NO_x$.

An extensive set of outdoor smog chamber experiments was carried out to study aerosol formation by two representative biogenic hydrocarbons: isoprene and ß-pinene. The hydrocarbons, at concentrations ranging from a few ppb to a few ppm, were photooxidized in the presence of $NO_x$. Isoprene was found to produce negligible aerosol at ambient conditions, whereas ß-pinene aerosol carbon yields were as high as 8%, depending strongly on the hydrocarbon to $NO_x$ ratio. Aerosol samples subjected to infrared absorption spectroscopy revealed that the dominant aerosol products for both isoprene and ß-pinene are organic nitrates, organic acids, as well as other carbonyls and hydroxy compounds. GCMS of the neutral fraction of the ß-pinene aerosol revealed nopinone and several other compounds with molecular weights ranging from 138-200 amu, indicating mainly mono- and dioxygenated products. The average vapor pressure of the ß-pinene aerosol was estimated to be $37 \pm 24$ ppt at 31 C. Scanning electron micrographs showed that the particles consist of both liquid droplets and agglomerates of small (40-60 nm) solid particles.

# Table of Contents

# List of Tables

# List of Figures

CHAPTER 3



CHAPTER 4

CHAPTER 5

# CHAPTER 1

# Introduction

*The average adult female goes through about 11 kg of air in a day, compared to about 1.0 kg of food, and 1.6 kg of water. (adapted from Wayne, 1985).*

Photochemical smog requires three ingredients: hydrocarbons, $NO_x$, and sunlight. The nature and severity of the smog that forms of course depend on many other factors; including meteorology which controls the dilution of pollutants, insolation, ambient temperature and relative humidity, the nature of the hydrocarbons involved, the hydrocarbon/$NO_x$ ratio, and other inorganic pollutants like $SO_2$ and $NH_3$. The effort to understand the chemistry of photochemical smog formation began in Los Angeles in at least the early 1950's. The initial target hydrocarbons in these studies were small alkenes (e.g. propene), cousins of the hydrocarbons which are the subject of this thesis (Haagen-Smit et al. 1953).

The chemistry of individual hydrocarbons controls the "how fast" and "how much" of photochemical smog, hence essential to any accurate model of smog formation is an accurate understanding of the chemistry of individual hydrocarbons, or at the very least, groups of hydrocarbons. Recent moves toward regulating hydrocarbons on the basis of some formulation of their reactivity makes the chemical oxidation mechanisms even more critical. That these studies also address some fundamental aspects of organic chemistry in the gas phase should not be overlooked. Hydrocarbons, as they are oxidized, form compounds that have reduced vapor pressures, in some cases low enough to condense

and form aerosols. These processes are critical to understanding particle pollution formation.

When this thesis was commenced, it appeared that there were four types of atmospherically important hydrocarbons for which there were large gaps in the understanding of their chemistry. They were: the biogenics, long-chain alkanes and alkenes, and the aromatics. This thesis examines two of these areas in detail; the biogenics, in the form of isoprene (2-methyl butadiene), and the long-chain alkenes, in the form of 1-octene. The biogenics may be broken down into two groups: isoprene and the terpenes. Several other hydrocarbons are emitted by plants but at much lower rates than isoprene and the terpenes. Isoprene is emitted primarily by deciduous trees (Isidorov et al. 1985, Lamb et al. 1985), but is the dominant hydrocarbon emitted by at least one conifer as well (red spruce, Ennis et al. 1990). The terpenes with a few minor exceptions, are a series of isomeric dimers of isoprene, and are usually the dominant hydrocarbon emission from coniferous trees. Isoprene and the terpenes are also released from a variety of other shrubs and plants. Many vascular plants release about 1% of the carbon they fix as isoprene or terpenes, hence the natural hydrocarbon source is very large, and has been estimated at 30-60 Mt/Yr for the continental United States, of which isoprene is responsible for about 4.4 Mt/Yr, compared to an estimated anthropogenic hydrocarbon source of 27 Mt/Yr (Lamb et al. 1987).

The long-chain hydrocarbons (5 carbons or more), anthropologically derived, still suffer from significant gaps in the understanding of their chemistry. The atmospheric chemistry community, for lack of data, have assumed that the chemistry of these compounds parallels that of their smaller cousins; e.g. butene, butane, propene. Whether or not they do has only been minimally investigated. Indeed, few studies have indicated that their chemistry may in fact be dramatically different than their smaller cousins. The situation for alkanes is slightly better than for alkenes; the formation of organonitrates

during the photochemical oxidation of these compounds in the presence of $NO_x$ has been investigated (Atkinson et al. 1983). This process is very important, but provides for at most about 33% of the reactions of the long chain hydrocarbons.

Four oxidants each play a role in the breakdown of hydrocarbons in the troposphere under certain conditions; $O_3$, OH, $NO_3$, and $O(^3P)$. $O_3$ and OH are the main oxidants during daylight, when $O(^3P)$ can sometimes play a minor role. $NO_3$, and to some degree $O_3$ are the major oxidants after the sun sets. A fifth oxidant, $NO_2$, plays a role under some experimental conditions, particularly with conjugated dialkenes. The work in this thesis focuses on daylight reactions, and hence on $O_3$ and OH. In an effort to understand the potential for interference from other species, I have also examined the $O(^3P)$ and $NO_2$ reactions. In general, experiments on both isoprene and 1-octene have each been designed to examine an individual oxidant; $O_3$ , OH, $NO_2$ , or $O(^3P)$. A series of experiments to aid in the development of overall oxidation mechanisms for these hydrocarbons were also carried out, where an oxidant mixture (OH, $O_3$, and $O(^3P)$), roughly representative of urban smog, was used.

The OH reaction with hydrocarbons has long been recognized as a major oxidation pathway in the atmosphere. The OH initiated reactions of small molecules are relatively straightforward; e.g. in the case of alkenes, OH adds to the double bond:

(1) 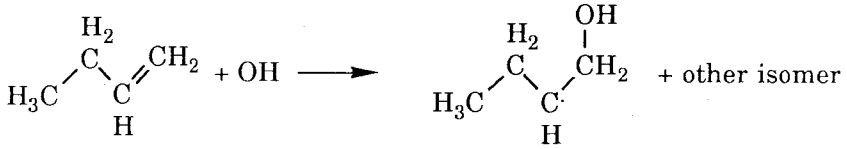


In the Earth's atmosphere, this (hydroxy) alkyl radical adds $O_2$, to produce an alkyl peroxy radical:

(2) 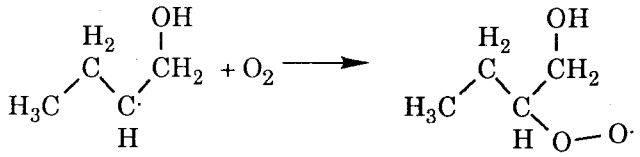

In polluted atmospheres, reaction with NO is the dominant reaction pathway for the alkyl peroxy radicals:

(3) 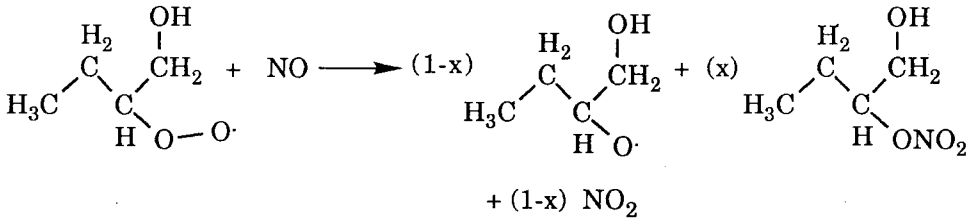

producing an alkoxy radical, some organonitrate, and partially oxidizing NO to $NO_2$ (Atkinson 1990). The amount of organonitrate formed depends on the nature of the parent hydrocarbon. The amount of organonitrate formation is very important in the atmosphere as it controls the amount of chain propagation (NO to $NO_2$ conversions) vs. the degree to which a hydrocarbon is a chain terminator and $NO_x$ sink. The organonitrate formation has been explicitly examined for only a few alkenes; hence it is unclear what effect the ß-OH group has on the formation of organonitrates. This issue is examined in chapters 4 (isoprene) and 5 (1-octene). The b-hydroxy alkoxy radical decomposes:

(4) 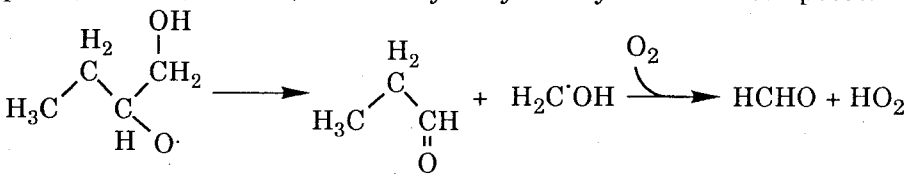

Larger hydrocarbons can undergo various internal isomerizations at the alkoxy radical stage, sometimes resulting in dramatically different amounts of $HO_2$ produced and NO to $NO_2$ conversions (Carter et al. 1976, Baldwin et al. 1977, Dobe et al. 1986). The extent to which they do this is investigated in chapters 2 (isoprene), and 5 (1-octene).

The $O_3$ reaction is a major atmospheric loss process for many alkenes, and consequently has been a subject of interest and study for decades. Most studies of $O_3$ -alkene reaction have entailed, in a broad sense, mixing $O_3$ with the alkene and measuring the carbonyl products (for example Kamens et al. 1982, Niki et al. 1983). A few studies have reported indirect evidence of OH formation in this type of experiment (Japar et al. 1976, Herron and

Huie 1978, Niki et al. 1987, Atkinson et al. 1990); for example excess reaction of hydrocarbon beyond the stoichiometric quantity of reacted $O_3$. These reports of OH formation, while in some cases as large as 70% of the reacted alkene (Niki et al. 1987), have generally been overlooked by the atmospheric chemistry community and have not been included in photooxidation mechanisms. I have devised a more direct measurement method for OH which involves adding alkane (alkanes do not react with $O_3$) to scavenge and trace OH formation, and can provide the first direct assessment of OH formation in this system. Epoxides have been observed in several studies of the $O_3$ reaction with alkenes. Herron et al. (1982) proposed a pathway for direct formation from the $O_3$-alkene reaction of $O(^3P)$ which then reacts with the parent alkene to produce epoxides. Other pathways for epoxide formation have been proposed for the alkene-$O_3$ reaction in the liquid phase (Criegee 1977). The source of epoxides is made clear in chapter 3, where it becomes clear that while this has previously been thought to be a minor pathway, it is in fact a dominant pathway. The results and analyses of the reaction with $O_3$ with isoprene and 1-octene, which include many other surprising results, are described in chapters 3 and 5 respectively.

The $O(^3P)$ reactions with alkenes have been recognized since the 1950's (this work has been reviewed by Cvetanovic 1963) when many studies of addition of atoms to alkenes were carried out. This reaction was found to form a suite of products which included epoxides from direct addition of $O(^3P)$ to the double bond, and ketones and/or aldehydes resulting from 1,2 hydrogen shifts. A portion of the $O(^3P)$-alkene adduct has been thought to decompose, producing alkyl and alkoxy radicals. These species can lead to $O_3$ production in the atmosphere, and can lead to additional reactions of the parent hydrocarbon in experimental systems that include NO. As the usual source for $O(^3P)$ is $NO_2$ photolysis, NO is present in most experimental systems. The decomposition pathway has been shown to be pressure dependant; e.g. it is an inverse function of the lifetime of the $O(^3P)$-alkene

adduct. Indeed, Cvetanovic and co-workers showed that hydrocarbon size was positively correlated with yields of the non-radical products, epoxides, aldehydes and ketones. The lifetime of the $O(^3P)$-alkene adduct presumably scales with the available vibrational modes in the molecule. Cvetanovic and Doyle (1960), however, found that butadiene did not fit well into this pattern; it had an apparent lifetime that was less than propene. These observations made difficult to predict the behavior of isoprene (2-methyl butadiene). As Cvetanovic and other workers did not carry their studies to species as large as 1-octene, the degree of stabilization for 1-octene was also unclear, as was the extent of 1,2 hydrogen transfer. These issues are examined in chapters 3 and 5 respectively.

$NO_2$ has been found to react very slowly with most alkenes, however the reaction with conjugated dialkenes, including isoprene, is much faster (Ohta 1986, Tuazon and Atkinson 1990, Glasson and Tuesday 1970). We have measured the rate constant for the $NO_2$ reaction with both isoprene and 1-octene; these results are included in chapters 3 and 5, respectively.

Chapter 5 delineates efforts to develop an overall mechanism for isoprene oxidation for use in smog formation models and other studies. This requires the development of theories and results for the unknown reactions of products, as well as the still-missing (albeit relatively small as a result of this work) aspects of the isoprene chemistry and the chemistry of its products. This method allows the overall mechanism to be refined, and illuminates remaining questions. The results are particularly useful for urban situations. This mechanism is checked against experimental data where $O_3$, OH and $O(^3P)$ reactions all take place in the same reactor.

The link between gas-phase chemistry and aerosol formation is critical to understanding and predicting the formation of organic aerosols over the range of conditions that occur in

the atmosphere. This link is also one of the least understood aspects of aerosol formation. Chapter 6 presents an effort to close this gap and applies a suite of techniques to the problem of characterizing the chemical composition of aerosol samples collected in isoprene and β-pinene photooxidation experiments reported elsewhere (Pandis et al. 1991).

# *References*


Atkinson, R. (1990) Gas Phase Tropospheric Chemistry of Organic Compounds: A Review. *Atmospheric Environment* **24A**, 1-41.

Atkinson, R., S.M. Aschmann, W.P.L. Carter, A. M. Winer and J.N. Pitts (1983) Alkyl Nitrate Formation from the $NO_x$ - air photooxidations of $C_2$ - $C_8$ n-alkanes. *J. Phys. Chem.* **86**, 4563-4569.

Atkinson, R., D. Hasegawa, and S.M Aschmann (1990) Rate constants for the gas-phase reactions of $O_3$ with a series of monoterpenes and related compounds. *Int'l J. Chemical Kinetics* **22**, 871-887.

Atkinson R. and A.C. Lloyd (1984) Evaluation of Kinetic and Mechanistic Data for Modeling of Photochemical Smog. *J. Phys. Chem. Ref. Data* **13**, 315-444.

Baldwin, A.C., J.R. Barker, D.M. Golden, and D.G. Hendry (1977) Photochemical smog. Rate parameter estimates and computer simulations. *J. Phys. Chem.* **81**, 2483-2492.

Carter, W.P.L., K.R. Darnall, A.C. Lloyd, A.M. Winer, and J.N. Pitts (1976) Evidence for alkoxy radical isomerization in photooxidations of $C_4$-$C_6$ alkanes under simulated atmospheric conditions. *Chem. Phys. Lett.* **42**, 22-27.

Cvetanovic, R.J., and L.C. Doyle (1960) Reaction of oxygen atoms with butadiene. *Can. J. Chemistry*, **36**, 2187-2198.

Cvetanovic, R.J. (1963) Addition of atoms to olefins in the gas phase. *Adv. in Photochem*, **1**, 115-182.

Dobe, S., T. Berces, and F. Marta (1986) Gas phase decomposition and isomerization reactions of 2-pentoxy radicals. *Int'l J. Chemical Kinetics* **18**, 329-344.

Ennis, C.A., A.L. Lazarus, P.R. Zimmerman and R.K. Monson (1990) Flux determinations and physiological response in the exposure of red spruce to gaseous hydrogen peroxide, ozone, and sulfur dioxide. *Tellus* **42B**, 183-199.

Glasson, W.A. and C.S. Tuesday (1970) The reaction of nitrogen dioxide with olefins. *Environ. Sci. Technol.* 4, 752-761.

Haagen-Smit, A.J., C.E. Bradley, and M.M. Fox (1953) Ozone formation photochemical oxidation of organic substances, *Indust. Eng. Chem.* **45**, 2086-2098.

Herron, J. T., R.I. Martinez, and R.E. Huie (1982) Kinetics and energetics of the Criegee intermediate in the gas phase. I. The Criegee intermediate in ozone-alkene reactions. *Int'l J. Chemical Kinetics* **14**, 201-224 .

Herron, J.T., and R.E. Huie (1978) Stopped flow studies of the mechanisms of ozone-alkene reactions in the gas phase: propene and isobutene. *Int'l J. Chemical Kinetics* **10**, 1019-1041.

Isidorov V.A., I.G. Zenkevich, B.V. Ioffe (1985) Volatile Organic Compounds in the Atmosphere of Forests. *Atmospheric Environment* **19**, 1-8.

Japar, S.M., C.H. Wu, and H.Niki (1976) Effect of molecular oxygen on the gas phase kinetics of the ozonolysis of olefins *J. Phys. Chem.* **80**, 2057-2062.

Kamens, R. M., M. W. Gery, H. E Jeffries, M. Jackson, and E. I. Cole (1982) Ozone-Isoprene Reactions: Product Formations and Aerosol Potential, *Int'l J. Chemical Kinetics* **14**, 955-975.

Lamb, B., H. Westburg, G. Allwine and T. Quarles (1985) Biogenic Hydrocarbon Emissions from Deciduous and Coniferous Trees in the Uniter States. *J. Geophys. Res.* **90**, 2380-2390.

Lamb, B., A. Guenter, D. Gay, H. Westburg (1987) A National Inventory of Biogenic Hydrocarbon Emissions, *Atmospheric Environment* **21:** 1695-1705.

Niki, H., P.D. Maker, C.M. Savage, and L.P. Breitenbach (1983) The reaction of ozone with alkenes. *Environ. Sci. Technol.* **17**, 312a-322a.

Ohta, T., H. Nakagura, and S. Suzuki (1986) Rate constants for the reactions of conjugated olefins with $NO_2$ in the gas phase. *Int'l J. Chemical Kinetics* **18**, 1-11 .

Pandis, S.N., S.E. Paulson, R.C. Flagan, and J.H. Seinfeld (1991) Aerosol Formation in the Photooxidation of Isoprene and Beta-Pinene. *Atmospheric Environ.* **25a**, 997-1008.

Tuazon, E.C., and R. Atkinson (1990) A product study of the gas-phase reaction of methacrolein with the OH radical in the presence of $NO_x$. *Int'l J. Chemical Kinetics* **22**, 591-602.

Tuazon, E.C., and R. Atkinson (1989) A product study of the gas-phase reaction of methyl vinyl ketone with the OH radical in the presence of $NO_x$. *Int'l J. Chemical Kinetics* **22**, 1141-1152 (1989).

Wayne, R.P. (1985) Chemistry of Atmospheres. Oxford University Press (Oxford).

# CHAPTER 2

# Atmospheric Photooxidation of Isoprene

# Part 1: The Hydroxyl Radical and Ground State Atomic Oxygen Reactions

Suzanne E. Paulson[a], Richard C. Flagan[b] and John H. Seinfeld[b]

[a]Environmental Engineering Science

[b]Chemical Engineering

California Institute of Technology

Pasadena, CA 91125

*International Journal of Chemical Kinetics*

In Press

*Nature....is being more and more rapidly transformed into the "environment."*

(V.A. Isidorov, 1990)

# *Abstract*

The OH reaction with isoprene is studied. Methyl nitrite photolysis experiments were carried out in an outdoor smog chamber in an attempt to identify as completely as possible OH-isoprene product distribution. Emphasis was placed on identification and quantification of oxygenated products. A Tenax-based cryo-trap thermal desorber used to trap, concentrate, and dry chamber samples for identification on a GC/MS is described. Analysis of the products revealed that $O(^3P)$ can form in reaction systems designed to study OH reactions that include high concentrations of NO, and consequently $NO_2$, hence this reaction is also examined. The yields of methacrolein and methyl vinyl ketone are determined as 25±3 and 35.5±4%, respectively, with an additional 4±2% as 3-methyl furan, totaling 65±4%. These results, combined with those of previous studies allow 80% of isoprene's products to be explicitly identified, and the general structure of the remaining products to be ascertained. The $O(^3P)$ reaction produces 84±8% epoxides, and 8.±3% species which result in production of $HO_2$, and subsequently OH. A heretofore unidentified product of the $O(^3P)$ reaction, 2-methyl 2-butenal, is identified. The rate constant of the $NO_2$ -isoprene reaction is measured.

# *Introduction*

Isoprene (2-methyl 1,3 butadiene) is the most abundant natural hydrocarbon emitted by deciduous trees, as well as a component of coniferous trees and other plant emissions (1,2,3). Isoprene emissions, estimated at 4.4 Mt/year in the Continental United States, are significant when compared to anthropogenic hydrocarbon emissions, estimated at 27 Mt/year (4). Because Isoprene is exceptionally reactive, it is expected to be important in the photochemistry of both rural and many urban areas (4,5).

Isoprene, a conjugated dialkene, can react in the troposphere with hydroxyl radical (OH), ozone ($O_3$), ground state atomic oxygen ($O(^3P)$), $NO_3$, and $NO_2$. Of these, $NO_3$ is the most important during nighttime, and $NO_2$ is insignificant. Most isoprene is emitted during daylight hours, when OH, and to a lesser degree, $O_3$ and $O(^3P)$ contribute to its loss, where the individual contribution of each species is dependent on the concentrations of $O_3$ and $NO_x$. Several studies have been carried out to determine the products of OH reaction with isoprene. Approximately, 2/3 of the products on a per molecule reacted basis have been explicitly identified (6,7,8). The ground state oxygen atom reaction with isoprene has not been studied previously.

We have carried out an extensive set of outdoor smog chamber experiments, coupled with GCMS product studies to examine isoprene's daylight oxidation pathways. Each experimental design attempted to isolate one oxidant. The necessity of adding NO to simulate reactions that occur in the atmosphere, combined with the closely interwoven chemistry of OH, and $O(^3P)$, and to a lesser degree $NO_2$, often make unambiguous identification of individual reaction pathways difficult. We have characterized these interfering species when they occur using tracers and simulations with reaction mechanisms. Certain of the interfering reactions examined in these studies have not been included in prior analysis of these and similar reactions carried out in both smog chambers and flow reactors.

# *Experimental System*

The experiments were performed in a flexible outdoor smog chamber constructed by heat sealing together 4 panels of 51 μm thick Teflon, each measuring 1.38 m by 5 m. The seams

were reinforced with Mylar type. The fully inflated chamber volume was approximately 7 $m^3$. The smog chamber facility and much of the instrumentation have been described previously (9), hence we have included descriptions only of the instrumentation and procedures unique to this study.

The gas-phase species measured on-line include NO, $NO_x$, $HNO_3$, $O_3$, isoprene and its major products. Chamber temperature, UV radiation, and total solar radiation were measured on-line as well. Hydrocarbons were monitored using a Hewlett Packard 5890 gas chromatograph/flame ionization detector, with 30mx0.32 mm DB-1 (thick film) or 30mx0.25mm DB-5 (standard film) columns (J&W Scientific). Temperature programs were typically 1 min. at 40°C, 35 °C/min. ramp, and 1 min. at 32 °C, 55°C/min. ramp, for the DB-1 and DB-5 columns, respectively. Injections were made using a 6-port gas valve (Valco), integrated with the gas chromatograph (GC) to sample automatically at identical intervals (7 to 12 minutes) throughout the experiment. The GC was calibrated for each experiment using certified cylinders containing mixtures of ultra pure air and isoprene (20 ppm) and methyl cyclohexane (31.3 ppm). Certified cylinders containing methyl vinyl ketone (21 ppm) and 2-methyl furan (18 ppm) (assumed to have the same FID response as 3-methyl furan) were initially used for these compounds, however for later experiments, responses relative to isoprene were used to calculate their concentrations. GC response factors for the product species methacrolein and 2-ethenyl 2-methyl oxirane relative to isoprene were carried out by injecting a gas-phase calibration mixture created by injecting known volumes of the liquids into an 8 liter Teflon bag and allowing them to completely evaporate, with isoprene as an internal standard. This procedure was carried out with several different volumes of the liquid hydrocarbons to verify that the liquid had completely evaporated. Final concentrations ranged from 2-30 ppm. Methacrolein, methyl vinyl ketone, 2-ethenyl 2-methyl oxirane, biacetyl, and 2-methyl 2-butenal, as well as isoprene (99%) and methyl cyclohexane (99+%) used for injection into the smog chamber

were all obtained from Aldrich. The value assumed for the unknown products of the $O(^3P)$/isoprene reaction, which elute between 2-ethenyl 2-methyl oxirane and 2-(1-methylethenyl) oxirane from both the DB-1 and DB-5 columns was the 2-ethenyl 2-methyl oxirane response factor. For 2-methyl 2-butenal, the response factor of isomeric 2-ethenyl 2-methyl oxirane was used. Calibration gas cylinders, obtained from Scott-Marrin, were certified to within ± 2%. Calibration gas cylinders containing isoprene and methyl cyclohexane were also checked periodically by calculating the response of, for example, isoprene compared to 1-octene and methyl cyclohexane vapor from liquid volumes of those compounds injected into the 8 liter Teflon bag, and the calibration cylinders appeared to be within 0.5% of their reported concentration, and did not appear to shift over a period of several months. The stability of methyl vinyl ketone or 2-methyl furan in cylinders was not verified; later calculations were carried out based the relative response factor for this compound relative to isoprene.

Samples for GCMS (Hewlett Packard model 5890 with mass selective detector) analyses were collected on Tenax (GC), and thermally-desorbed and cryo-focussed on an instrument built in this laboratory. Positive GCMS identifications of most of the compounds were made by comparisons to authentic standards (obtained from Aldrich), injected into the Tenax, and desorbed in the same manner as a smog chamber sample. 3-Methyl furan and methyl glyoxal were identified by comparison with the NIST mass spectral library (10). The 2-ethenyl 2-methyl oxirane obtained from Aldrich was reported to contain a 5% impurity. The mass spectrum of the impurity showed a molecular weight of 84 amu, and a fragmentation pattern consistent with 2-(1-Methylethenyl) oxirane. This structure was further confirmed by comparison of the 400 MHz NMR spectrum of the impurity to a reference spectrum of ethenyl oxirane (11). Biacetyl co-eluted with methyl vinyl ketone on both DB-5 and DB-1 columns regardless of conditions, however it was possible to separate the two compounds using a DB-wax column and cumbersome liquid

nitrogen pre-focusing. One experiment was carried out with the OH system using the DB-wax column technique. In this analysis the biacetyl formed was negligible (less than 1%, data not shown), hence we believe that it does not interfere significantly with the methyl vinyl ketone analysis.

# *Experimental Designs*

A summary of the experiments performed appears in Table 1. The basic experimental design involved introduction of the desired reactants into the smog chamber, and allowing the reactants to mix until their concentrations have stabilized while the chamber is covered to eliminate light. Once the reactant concentrations have stabilized, the reaction is initiated by removing the cover and exposing the reactants to sunlight. In the experiments with $NO_2$, which reacts directly with isoprene, isoprene was injected first and allowed to stabilize. Specific descriptions and considerations for the more complicated systems are presented below.

## *Hydroxyl Radical*

Methyl nitrite, which produces OH radicals when photolyzed in air in the presence of NO, was synthesized using the method described by Taylor et al. (12) by dropwise addition of 50% $H_2SO_4$ to a saturated solution of $NaNO_2$ in methanol. The methyl nitrite, which bubbles out of the $NaNO_2$ solution, was carried in a stream of ultra high purity $N_2$ through a saturated NaOH solution and then over anhydrous $CaCl_2$, trapped in a dry-ice acetone slush bath and stored in liquid $N_2$. Small quantities were transferred under vacuum into a 500 $cm^3$ glass bulb which was then flushed into the smog chamber. Methyl nitrite photolysis was initiated after the reactants were well mixed, by removing the dark tarpaulin. As this system is very reactive, care was taken to eliminate light leaks before the inception of the experiment.

### *Ground State Atomic Oxygen*

To create a system where $O(^3P)$ is produced in large quantities with only minimal $O_3$ formation, we filled and emptied the smog chamber twice with 3 $m^3$ of ultra pure $N_2$, and finally filled the chamber with 6 $m^3$ of ultra high purity $N_2$ . Isoprene and $NO_2$ were then added and allowed to mix. The reactions were initiated with removal of the dark tarpaulin, allowing $NO_2$ to photolyze. Molecular oxygen was measured with a mass spectrometer by withdrawing matrix air samples from the chamber one hour after the end of one of the $O(^3P)$ experiments, and was found to be about 1%.

## *Hydroxyl Radical-Isoprene Reaction*

The hydroxyl radical reaction is the most important daylight reaction for isoprene. The initial OH attack produces a suite of alkyl peroxy radicals, that are presumed to react with NO. Methyl nitrite photolysis offers a way to produce high concentrations of OH in situ (12), with little interference from $O_3$. Methyl nitrite photolyzes and leads to OH formation as follows:

(1) $CH_3ONO + h\upsilon \rightarrow CH_3O\cdot + NO$

(2) $CH_3O\cdot + O_2 \rightarrow HCHO + HO_2\cdot$

(3) $HO_2\cdot + NO \rightarrow OH\cdot + NO_2$

We conducted five methyl nitrite experiments, varying the initial concentrations of isoprene, $CH_3ONO$ and NO, and consequently $NO_2$ (Table 1). Experiments IOH4 and IOH5 nearly duplicate one another, as do IOH6 and IOH7, hence we show the product yield curves for IOH4, IOH6, and IOH8 (Figs. 1, 2, and 3). The same line/symbol combinations are used for each compound throughout these figures. Additionally, methacrolein, methyl vinyl ketone, 2-ethenyl 2-methyl oxirane and 2-ethenyl 2-methyl oxirane data from all

five experiments are shown in Figs. 4, 5, and 6. The products include the established species methacrolein, methyl vinyl ketone and 3-methyl furan, but also include up to 30% 2-ethenyl 2-methyl oxirane and 10% 2-(1-methylethenyl) oxirane. The total yield of observed products, on a per-molecule reacted isoprene basis, varies dramatically from about 50% (IOH6&7) to 80% (IOH4&5), increasing in the order IOH7, IOH6, IOH8, IOH4, IOH5. When plotted as a function of isoprene reacted, the product data give downward-convex curves, indicating reaction of the products themselves with the oxidants in the system. However, the amounts of the products relative to one another vary widely between the experiments, e.g. the dominant product is methyl vinyl ketone in IOH6, but 2-ethenyl 2-methyl oxirane in IOH4, and in between for IOH8, indicating that some parameter must have varied significantly among the experiments. Methacrolein and methyl vinyl ketone display similar behavior; the apparent yield for these runs decreases in the order: IOH6 > IOH7 ~ IOH8 > IOH4 > IOH5. On the other hand the 2-ethenyl 2-methyl oxirane and 2-(1-methylethenyl) oxirane yields, decrease in the opposite order: IOH5 > IOH4 > IOH8 > IOH7 > IOH6; mirroring the pattern observed in the total yield. This ordering of experiments (IOH5 > IOH4 > IOH8 > IOH7 > IOH6) also correlates with the initial concentrations of $NO_2$, indicating that the source of the variation in the experiments is either $NO_2$ or $O(^3P)$, which results from the photolysis of $NO_2$.

Yield data for the minor products are missing for several experiments where the concentrations of these products remained too low to provide reliably integratable GC peaks. However, the partial data for unknown 1 mirrors the oxide data, with decreasing yields in the same experimental order, while 3-methyl furan appears to mirror the methacrolein and methyl vinyl ketone data. Data on the concentration of 2-methyl 2-butenal was collected during IOH6 and 8 follow the epoxide pattern. The 2-methyl 2-butenal yield increases further in IO3P2 (discussed in detail below), where a greater portion still of the isoprene reacts with $O(^3P)$, hence we believe the source of 2-methyl 2-

butenal is the $O(^3P)$ reaction. Methyl glyoxal was also observed in Tenax-concentrated samples, but was not quantified. This product is the main product of the OH-methacrolein and methyl vinyl ketone reactions (13,14).

### *Formation of $O(^3P)$ in the methyl nitrite-high NO system*

Insight may be gained from plotting yield curves for the products against one another. As shown in Fig. 4, the yields of methacrolein and methyl vinyl ketone are directly correlated, as are 2-ethenyl 2-methyl oxirane vs 2-(1-methylethenyl) oxirane (Fig. 5); both data sets fall on straight lines. The slight positive deviation from a straight line in Fig. 4 results from the difference in the OH reaction rates for methacrolein and methyl vinyl ketone (these and other relevant rate constants are listed in Table 2). unknown 1 also correlates directly with 2-ethenyl 2-methyl oxirane (not shown). In Fig. 6, the concentration of methacrolein is plotted vs 2-ethenyl 2-methyl oxirane and shows an inverse relationship; the higher the 2-ethenyl 2-methyl oxirane yield from a given experiment, the lower the methacrolein yield. A plot of methyl vinyl ketone vs. 2-ethenyl 2-methyl oxirane is nearly identical (not shown). The data clearly indicate that isoprene is reacting with two or more radical species, at least two of which have dramatically different product spectra. As the $NO_2$ -isoprene reaction is very slow (below), the most likely source for the epoxide formation is the reaction of $O(^3P)$ with isoprene.

The inclusion of high concentrations of NO in the methyl nitrite reaction system introduces pathways for the formation of potentially interfering species, including $NO_2$ and $O(^3P)$. While the simple scheme (reactions 1-3) predicts the formation of only one $NO_2$ per OH molecule, several other processes lead to unavoidable high concentrations of $NO_2$ in the methyl nitrite system. Each OH reaction with isoprene converts roughly two molecules of NO to $NO_2$ via the $RO_2$ and $HO_2$ reactions with NO. Further, the dark reaction:

(4) $NO + NO + O_2 \rightarrow 2\ NO_2$

is significant at the high concentrations of NO necessary to suppress $O_3$ formation in the methyl nitrite reaction system (e.g. this reaction converts about 1 ppm NO to $NO_2$ per hour at 10 ppm NO). The $NO_2$ both reacts with isoprene itself and photolyzes, giving $O(^3P)$. While high concentrations of NO suppress $O_3$ production ($O_3$ did not exceed 50 ppb in any of our experiments), the $O(^3P)$ reacts quickly with isoprene; we have estimated $k=5.8\pm1.5\times10^{-11}$ $cm^3$ $molec^{-1}$ $s^{-1}$, based on the OH/$O(^3P)$ rate constant correlations derived by Atkinson (15). Atkinson's work (15) indicates that OH reaction rate constants correlate very well with $O(^3P)$ rate constants for a wide range of compounds, hence the uncertainty in this and other estimated $O(^3P)$ rate constants is relatively small. While OH and $NO_2$ may lead to roughly the same products, the product distribution from the $O(^3P)$ - isoprene reaction (discussed below) is dramatically different from that which has been previously observed from the OH - isoprene reaction (6,7).

To attempt to understand the $O(^3P)$ reaction and its contribution to the observed products of the OH reaction, we carried out several experiments to specifically examine that chemistry. These are discussed in detail below. We also measured the $NO_2$ -isoprene rate constant to determine its importance on the OH chemistry (also discussed below).

## *Calculations of Carbonyl and Furan Yields*

Simulations of the methyl nitrite experiments using the mechanism listed in Table 2 indicate that interference in the methyl nitrite system from $O(^3P)$ can be significant, while interference from $NO_2$ is small. The mechanism includes the methyl nitrite photolysis rate measured by Taylor et al. (13), as well as preliminary reactions of methyl vinyl ketone and methacrolein (14, 15, 17), and reactions of 2-ethenyl 2-methyl oxirane and 2-(1-methylethenyl) oxirane, which were assumed to have the same reaction rates as methyl vinyl ketone and methacrolein, respectively. The simulations were carried out

using the computational chemical kinetics scheme and inorganic mechanism (not shown) of Carter and Atkinson (18). The inorganic portion of the mechanism includes the updates of Atkinson et al. (19). The products of the reactions of methacrolein, methyl vinyl ketone, 3-methyl furan, and the two epoxides, with $O(^3P)$, and 3-methyl furan and the epoxides with OH, are not included specifically in Table 2. These second generation products are unknown, hence we assumed that they were analogous to the products of isoprene, and assumed the same radical yields and the appropriate hydrocarbon products. These reactions generally have small effects on the outcomes of the simulations, as the first generation products do not accumulate to significant concentrations before the termination of the experiments, and the rate constants for their reactions with $O(^3P)$ and OH are smaller than those for isoprene. In our experiments, the percent of reacted isoprene consumed by $O(^3P)$ ranged from 11% (IOH6 and 7) to 55% (IOH5). The amount of isoprene reacting with $NO_2$ did not exceed 2% for any of the experiments. The mechanism that we initially constructed, using the following yields: from the OH reaction, methacrolein, 21%, methyl vinyl ketone, 29%, (7), 3-methyl furan, 4.4%, (8), and from the $O(^3P)$ reaction, 2-ethenyl 2-methyl oxirane, 63%, 2-(1-methylethenyl) oxirane, 23%, and unknown 1, 9.1%, (this work, below), performed well in predicting the concentrations of the epoxides (2-ethenyl 2-methyl oxirane and 2-(1-methylethenyl) oxirane), 3-methyl furan and unknown 1, but consistently underpredicted methacrolein and methyl vinyl ketone concentrations. Simulations revealed that the methacrolein, methyl vinyl ketone, and 3-methyl furan concentrations necessary to account for the data were 35.5%, 25%, and 4%, respectively. Simulations carried out with the mechanism in Table 2 are shown with the data for each of the methyl nitrite experiments in Figs. 1-3. As the simulated curves generally coincide with the data they are not labeled individually for clarity. The overall agreement with the experiments is excellent. The yield values for both epoxides from the $O(^3P)$ reaction and carbonyls and 3-methyl furan from the OH reaction are subjected to further scrutiny in the $O(^3P)$ experiments below, where the ratio of OH to $O(^3P)$ reactions with isoprene is further

varied. The $O(^3P)$ reaction leads to some alkyl radical formation, which allows OH to form in those experiments, hence the combination of the methyl nitrite experiments and the $O(^3P)$ experiments provides a full range of OH / $O(^3P)$ mixtures, from IOH6&7 at 89% OH to MIO3P1 at about 13% OH. The yield values listed in Table 3 represent the optimized fit of the data from the full range of conditions.

Reexamination of the Tuazon and Atkinson data (7) shows that the reported yields were low by 12-15% because of the contribution of $O(^3P)$ atom reactions in the system used (R. Atkinson, personal communication). They used an indoor chamber with low light intensity, which reduces the $O(^3P)$ formation relative to our experiments. Recalculation of Tuazon and Atkinsons' yields (7) gives 0.33, 0.24 and 0.051 for methacrolein, methyl vinyl ketone, and 3-methyl furan, respectively compared to our values of 0.355, 0.25, and 0.04. The results of our two laboratories are therefore in excellent agreement as to the yields of methacrolein and methyl vinyl ketone, and 3-methyl furan. The methacrolein, methyl vinyl ketone and 3-methyl furan yields of Gu et al. (6) at about 0.23, 0.17, and 0.032, respectively, show the same proportions as those from this work and Tuazon and Atkinson (7), but are lower, probably due to $O(^3P)$ or possibly other artifacts in the Gu et al. experiments. The results of our study and that of Tuazon and Atkinson (7) show that the methyl vinyl ketone, methacrolein, and 3-methyl furan account for about 65% of the isoprene reacting with OH. When these results are combined with the additional FTIR measurements for multisubstituted compounds of Tuazon and Atkinson (7), we can account for 100% of the reacted isoprene. Tuazon and Atkinson (7) estimated that the FTIR signal for carbonyl and hydroxy carbonyl compounds other than those that could be specifically identified accounted for 19-25% of the reacted isoprene, and that the composite alkyl nitrate (arising from reactions 15 & 16, below) signal accounted for 12%. This value, when corrected for $O(^3P)$ interference, may be as high as 14%. Tuazon and Atkinson (7) also measured a 59% formaldehyde yield, consistent with the sum of

methacrolein and methyl vinyl ketone. It is unclear whether this yield requires correction for $O(^3P)$ interference, as some formaldehyde may be a product of the $O(^3P)$ reaction.

Combining results from the present study with those of the other studies cited, the product yield from the isoprene-OH reaction is: 25 ± 3% methacrolein, 35.5 ± 4% methyl vinyl ketone, 5.1 ± 1% 3-methyl furan, 12 ± 5% alkyl nitrates, and 23 ± 5% unidentified carbonyls. It is likely that 0.4-0.8% of the reacted isoprene in these experiments does not remain in the gas phase, but instead becomes sufficiently substituted (2-3 functional groups, mainly carbonyls with some hydroxyl groups) that it condenses into the aerosol phase (19). In a series of experiments designed to study aerosol formation, we observed that the aerosol yield from isoprene rose from about 0.4 to 0.8% over the initial isoprene concentration range 1 - 6 ppm (10). The yields from the OH and $O(^3P)$ reactions are summarized in Table 3. The reported uncertainties reflect a combination of experimental uncertainties of about 5% with an estimated calculation error of 10-20%, which accounts for the uncertainties in the rate constants for each compound, combined with the small uncertainties in the chamber temperature and those inherent in the numerical analysis. The final product yields are particularly sensitive to the rate constants for their reactions with OH and $O(^3P)$.

Isoprene reacts with OH, forming the following set of hydroxy alkyl radicals, probably favoring addition to the terminal carbon forming the more stable secondary and tertiary alkyl radicals:

(5) 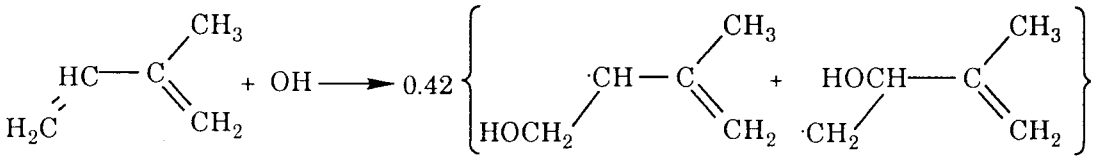

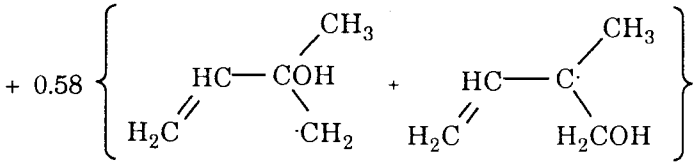

These radicals then add $O_2$ and react with NO; e.g.,

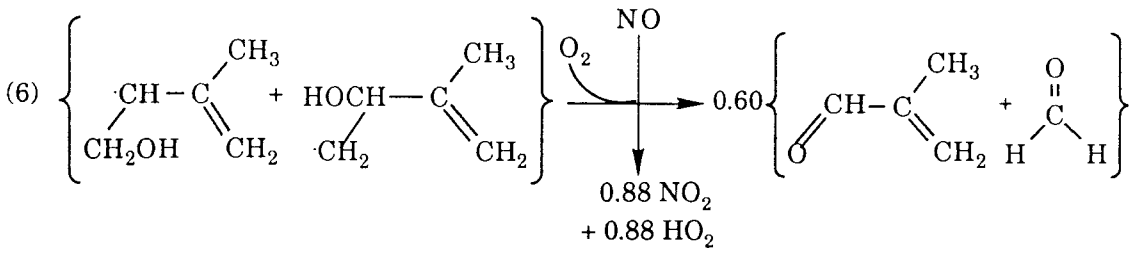

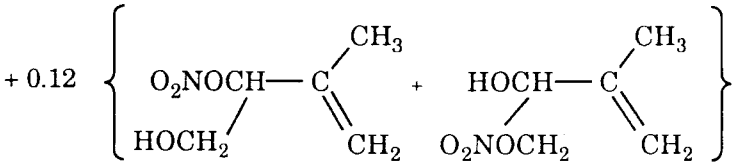

The reactions of the remaining portion of the alkyl radicals in reaction (6) are shown in reaction (7), below. The alkyl nitrate yield observed by Tuazon and Atkinson (7) (corrected for $O(^3P)$ reaction) was 0.14±0.05. Since some of the alkyl peroxy radicals which do not result in methacrolein and methyl vinyl ketone reaction probably react with more than one molecule of NO each, we use a yield of 0.12 in this mechanism, but assumed that the overall yield was 0.14 in the simulations.

The remaining alkyl radicals undergo various isomerizations to form 3-methyl furan, the multisubstituted compounds found in the aerosol phase, and in all likelihood several other minor products. It is unlikely that the studies of the OH-isoprene reaction carried out as part of this work, Tuazon and Atkinson (7), and Gu et al. (6), which have collectively included GC/MS, GC/FID and FTIR analyses, have failed to identify other major reaction products (e.g., more than 5-10% each). One possible reaction pathway for the remaining carbon is via the same allyl radical intermediate that leads to the formation of 2-methyl 2-butenal from the $O(^3P)$-isoprene reaction, discussed below, and has been proposed as one of

the pathways to explain the formation of 3-methyl furan (6). This allyl radical may undergo several other isomerizations.

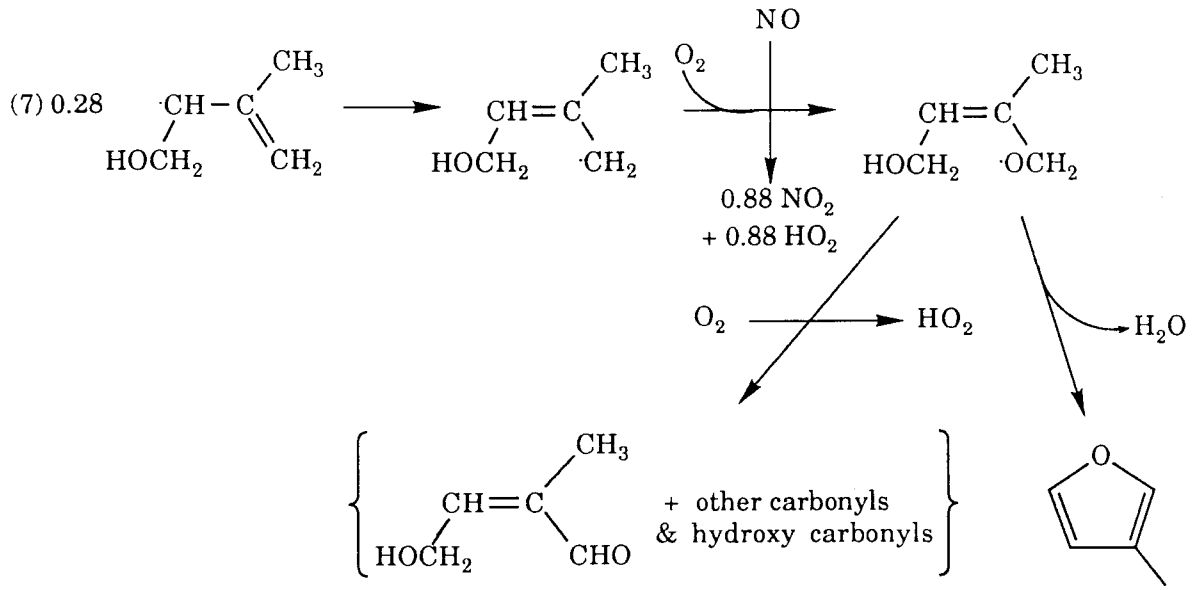


The other set of isoprene-OH adducts reacts to give the analogous set of products:

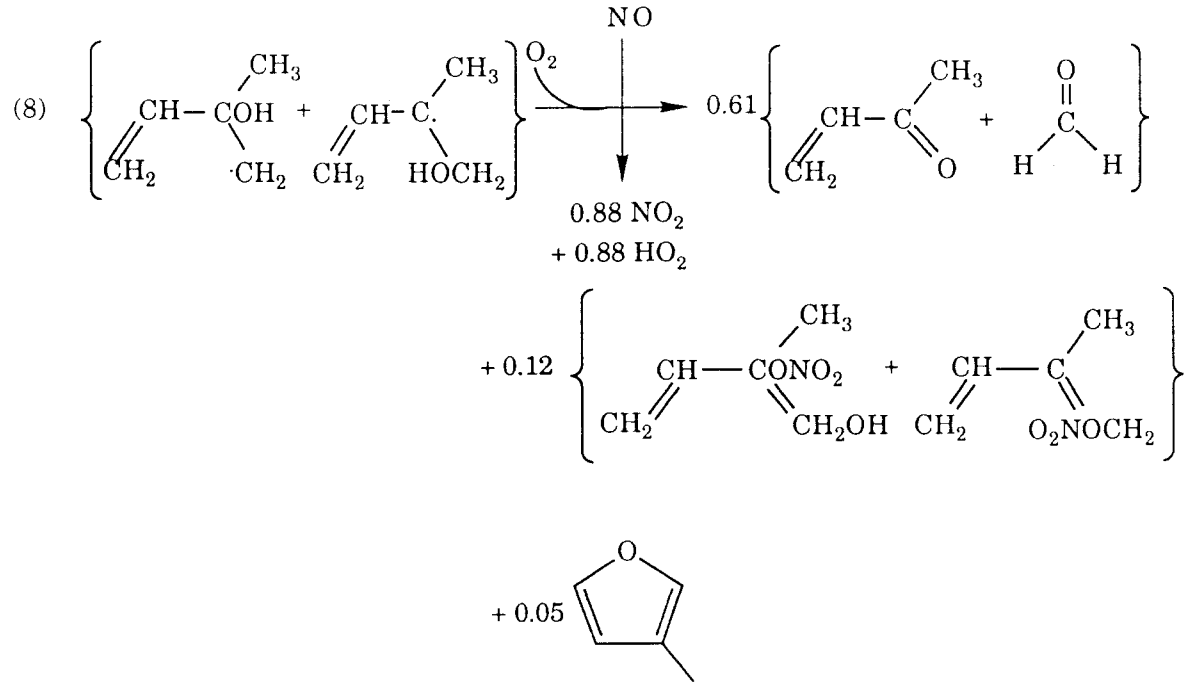

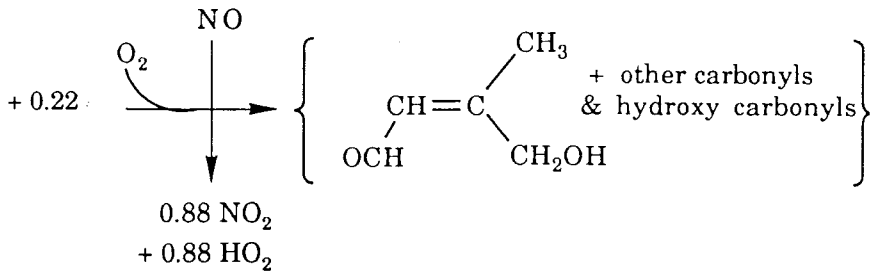


Hence with the combination of our work and that of Tuazon and Atkinson (7), we have accounted for essentially all of the reaction pathways. The portion that has not been specifically identified is probably a collection of $C_4$ - $C_5$ carbonyls and hydroxy carbonyls many of whose formation pathways produce two molecules of $HO_2$ per reaction. The measurement of the nitrate yield (7), however, is a good tracer of the overall yield of $HO_2$ from the isoprene-OH reaction; every NO to $NO_2$ conversion is followed by production of one molecule of $HO_2$ hence the total $HO_2$ yield can be expected to be 0.86±0.05. These unidentified compounds probably react with similar rate constants and chemistry as methacrolein and methyl vinyl ketone, and may reasonably be treated as such in models.

## *Ground State Atomic Oxygen-Isoprene Reaction*

While of minor importance in the atmosphere, the $O(^3P)$-isoprene reaction is important in experimental systems where the isoprene concentration is in the ppm range and significant amounts of $O(^3P)$ form. We have conducted three experiments to examine isoprene oxidation by ground state atomic oxygen. In these experiments, mixtures of $NO_2$ and isoprene in $N_2$ with about 1% oxygen were exposed to sunlight (see experimental section). Two experiments were performed in the absence of methyl cyclohexane (IO3P1 and 2), and the third (MIO3P1) included a large concentration of methyl cyclohexane to consume as much OH as possible, as well as to trace OH in the system. The product yield curves (product concentration vs. isoprene reacted) from IO3P2 and MIO3P1 for each of seven of the product species are shown in Fig. 7 (2-ethenyl 2-methyl oxirane, 2-(1-

methylethenyl) oxirane, and the major unidentified peak that is unique to the $O(^3P)$-isoprene reaction labeled unknown 1) and Fig. 8 (methacrolein, methyl vinyl ketone, 3-methyl furan, 2-methyl 2-butenal, and unknown 2), and the loss of methyl cyclohexane is shown in Fig. 9. Only one or two data points were obtained from experiment IO3P1, as essentially all of the isoprene was consumed within 10 minutes of initiation of the reactions, which is about the recycle time for the GC/FID. Yields, for 2-ethenyl 2-methyl oxirane, 2-(1-methylethenyl) oxirane, unknown 1, methacrolein and methyl vinyl ketone from experiment IO3P1 agree within experimental error with those observed in IO3P2 (data not shown). The total yield of the observed products, on a per molecule reacted basis, was about 92% in experiment IO3P2 and 96% for MIO3P1. The results of simulations, discussed in detail below, are also included in Figs. 7-9. The simulated results are shown as lines with the same identification as that used for the corresponding product.

The addition of methyl cyclohexane (MIO3P1) has a dramatic effect on the product yield curves. The products divide themselves into two categories in response. The oxide and unknown yields either greatly increase or remain about the same (Fig. 7), while methacrolein, methyl vinyl ketone, and 3-methyl furan (Fig. 9) all drop dramatically upon addition of methyl cyclohexane (Fig. 9). The methyl cyclohexane data clearly show OH formation in the reaction system, hence the results may be understood as follows. With some OH forming in the system (e.g. IO3P2), some of the isoprene that disappears reacts with OH rather than $O(^3P)$, lowering the apparent yield of the oxides and unknown 1, and leading to the production of methacrolein, methyl vinyl ketone, and 3-methyl furan. When methyl cyclohexane is added, scavenging OH radicals, more isoprene reacts with $O(^3P)$ rather than OH, and the yields of 2-ethenyl 2-methyl oxirane and 2-(1-methylethenyl) oxirane approach their correct yields and the methacrolein, methyl vinyl ketone, and 3-methyl furan yields dramatically decrease. The inverse behavior of the carbonyls (methacrolein, methyl vinyl ketone) plus 3-methyl furan vs. the epoxides (2-

ethenyl 2-methyl oxirane and 2-(1-methylethenyl) oxirane) indicates that they originate from different reactions; most of the former from OH and the latter from $O(^3P)$. A small amount of organic radical production by the $O(^3P)$ - isoprene reaction can lead to OH formation in this high $NO_x$ system via the pathway:

(9) $R^{\cdot} \xrightarrow{O_2 \quad NO} RO^{\cdot} + NO_2$

(10) $RO^{\cdot} \rightarrow HO_2 + R{=}O$ , via decomposition or reaction with $O_2$ ,

(11) $HO_2 + NO \rightarrow OH + NO_2$ .

It is also possible that the $NO_2$ reaction with isoprene leads to OH production by forming alkyl or alkoxy radicals that then form OH through reactions (9)-(11). We have assumed the hydrocarbon products from the $NO_2$ reaction are the same as those from the OH reaction.

To deduce the correct product distribution from the $O(^3P)$ - isoprene reaction, we carried out simulations of the experiments using the mechanism in Table 2. Rate constants for isoprene, methacrolein, and methyl vinyl ketone with $O(^3P)$ were estimated based on their OH rate constants using the empirical correlation between OH and $O(^3P)$ rate constants developed by Atkinson (16). 2-ethenyl 2-methyl oxirane and 2-(1-methylethenyl) oxirane were assumed to have the same rate constants as methyl vinyl ketone and methacrolein, respectively. Simulations are shown in Figs. 7, 8, and 9. An excellent fit of the methyl cyclohexane data was attained by adjusting the organic radical yield from the $O(^3P)$ + isoprene reaction to 8%. Using this radical source, the simulations and the methacrolein and methyl vinyl ketone data are close to agreement with the data from both experiment IO3P2 and MIO3P1, although in both cases the simulation results are somewhat low (Fig. 9). That the agreement is not exact is not surprising; these results are significantly affected by the unknown $NO_2$ - isoprene reaction product distribution; the $NO_2$ reaction is responsible for about 9% of the reacted isoprene, compared to 27% due to OH reaction for

IO3P2; for MIO3P1 the values are: 3% ($NO_2$), compared to 15% (OH). The $O_3$ and $NO_3$ reactions are responsible for about 1% of the reacted isoprene each (IO3P2) and <0.5% for MIO3P1. We assumed that the $NO_2$ product distribution was the same as the OH distribution, which assumes only a 60.5% carbonyl yield. This may indicate that the methacrolein, methyl vinyl ketone, and possibly the 3-methyl furan yields are higher for the $NO_2$ reaction than for the OH reaction. After calculation of the organic radical yields of the $O(^3P)$ reaction, the 2-ethenyl 2-methyl oxirane and 2-(1-methylethenyl) oxirane yields could be calculated, and were found to be about 63 and 22%, respectively. These results may be understood qualitatively by considering that the initial ratio of methyl cyclohexane to isoprene for this experiment is 9.31, hence initially the methyl cyclohexane consumes only about 50% of the OH that forms (the methyl cyclohexane-OH rate constant is about a factor of 10 slower than the isoprene-OH rate constant (17)). The apparent yield of the 2-ethenyl 2-methyl oxirane goes from 39 to 52% upon addition of this quantity of methyl cyclohexane, but since the methyl cyclohexane is insufficient to consume all of the OH, the correct yield should be still higher, around the 62% predicted by the mechanism.

Interference in the $O(^3P)$ experiments from other reactive species was minimal. As $O_2$ was maintained at about 1% in the reaction mixture, $O_3$ formation was minimal, measured at 55 ppb for IO3P1 and less than 2 ppb for IO3P2 and MIO3P1. Less than 0.1% of the isoprene is predicted to have reacted with ozone.

The following mechanism for the reaction of $O(^3P)$ with isoprene is proposed based on our experimental results:

(13) 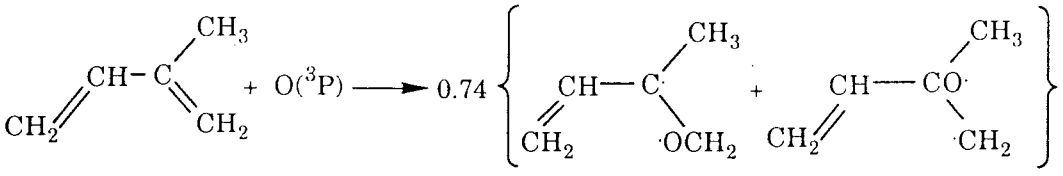

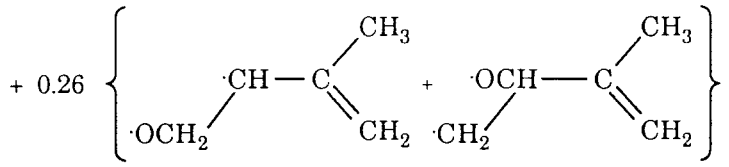

The $O(^3P)$ attack takes place preferentially on the thermodynamically favored methyl substituted double bond, presumably favoring addition to the terminal carbons of each double bond. The initial adducts are mainly stabilized to form 2-ethenyl 2-methyl oxirane and 2-(1-methylethenyl) oxirane, e.g.:

(14) 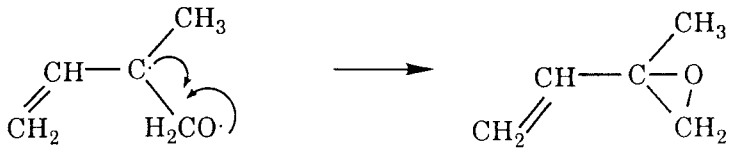

The adducts may also decompose or rearrange; e.g.:

(15) 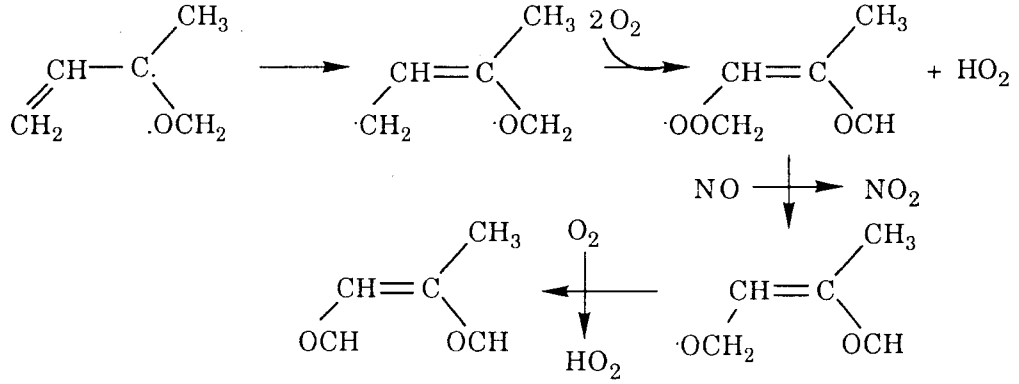

and:

(16) 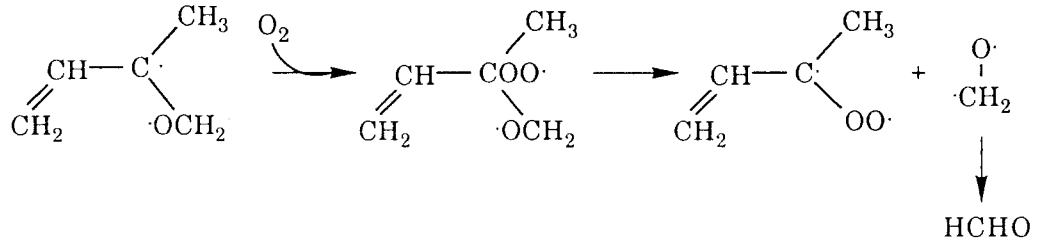

Both of these pathways produce some $HO_2$ which is efficiently converted to OH by NO. The formation of 2-methyl 2-butenal may result from a 5-membered ring transition state from the allylic radical resulting in hydrogen transfer between the two ends of the molecule's butyl backbone:

(17) 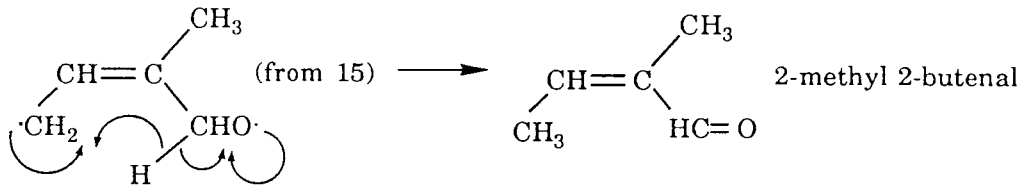 (from 15) 2-methyl 2-butenal

The unidentified peaks may also result from similar rearrangements, or they may be the products of the same reactions that result in the formation of OH.

The mechanism for this reaction differs significantly from the results for the butene isomers, butadiene, and those that have been proposed for isoprene by Killus and Whitten (21). Trans-2-butene and 1-butene produce roughly 40% epoxides, 30-40% aldehydes or ketones (resulting from 1,2 hydrogen transfer), and 20% partially decomposed products that lead to further radical formation (e.g. OH and $HO_2$) (22). For isoprene, Killus and Whitten (21) hypothesized 40% epoxides, and 30% aldehydes and 30% decomposition products with concomitant free radical production. Cvetanovik and Doyle (23) studied the $O(^3P)$ reaction with butadiene and found about 30% butene oxide and 22% 3-butenal (which results from 1,2 hydrogen transfer), uncorrected for any reactions with other radicals that may have formed in their system. In sharp contrast, we find about 84% epoxides, 3-12% decomposition products, and 9-19% terminal aldehydes and rearranged products, of which 0-9% result from 1,2 hydrogen transfer. The uncertainty in these yield numbers results from the fact that we did not identify the peaks labeled unknown 1 and 2. The $O(^3P)$ - isoprene adduct strongly favors the stabilization pathway over decomposition and rearrangement. 1,2 Hydrogen transfer is much less facile than for 1-butene or butadiene, although it may be partially supplanted by a rearrangement involving a 5-membered ring, leading to the formation of 2-methyl 2-butenal. The preference toward stabilization means that the free radical production is much lower than expected; at about 8% instead of 30-40% as previously believed. Cvetanovic and co-workers (24) carried out extensive studies on the reactions of $O(^3P)$ with alkenes. They observed that the larger the parent alkene, the longer the lifetime of the $O(^3P)$-alkene adduct and the less likely that adduct

would decompose; they also showed that the fragmentation pathway decreased with increasing pressure for all alkenes. However, Cvetanovic and co-workers found that the butadiene-O($^3$P) adduct decomposition appeared favorable relative to the propene adduct; hence from their data we might expect that the importance of isoprene's fragmentation pathway might be more similar than it is to 1-butene. Clearly the isoprene results further the notion that decomposition is diminished for larger hydrocarbons due to increased stability of the larger O($^3$P)-alkene adducts.

# *Nitrogen Dioxide-Isoprene Reaction*

To determine if the isoprene reaction with $NO_2$ was important in either the $O(^3P)$ or OH experiments, we carried out one experiment with $NO_2$ and isoprene in the dark, INO21. The isoprene and $NO_2$ disappear at about the same rate (not shown). A rate constant for the reaction may be obtained in the following way:

$$3)\ -d[Iso]/dt = k[Iso][NO_2] = -d[NO_2]/dt$$

where [Iso] and $[NO_2]$ are the time variant concentrations of isoprene and $NO_2$, respectively, t is time, and k is the isoprene/$NO_2$ rate constant. For this system, when $NO_2$ reacts only with isoprene and *vice versa*, we can express the concentrations of isoprene and $NO_2$ as follows:

$$4)\ [NO_2] = [Iso] + C$$

where C is the difference between [Iso] and $[NO_2]$, and should remain constant throughout the experiment. For this experiment, C is nearly constant, and C = 3.0 ± 0.1 ppm. Substitution of equation 4) into equation 3) allows integration of 3) to give:

$$5)\ k(t-t_0) = (1/C)\{\ln|([Iso]+ C)/[Iso]| - \ln|(([Iso]_0+ C)/[Iso]_0)|,$$

and likewise:

$$6)\ k(t-t_0) = -(1/C)\{\ln|[NO_2]- C)/[NO_2]| - \ln([NO_2]_0- C)/[NO_2]_0\}.$$

Plots of $(1/C)\{\ln|([Iso]+ C)/[Iso]| - \ln|(([Iso]_0+ C)/[Iso]_0)\}$ and $-(1/C)\{\ln|[NO_2]- C)/[NO_2]| - \ln([NO_2]_0- C)/[NO_2]_0\}$ vs. t are shown in Fig. 9. Using the slopes of these plots, we obtain $k=2.02 \times 10^{-19}$ and $1.59 \times 10^{-19}$ $cm^3$ $molec^{-1}$ $s^{-1}$ from the isoprene and $NO_2$ data respectively, yielding an average value of $1.8 \times 10^{-19}$ $cm^3$ $molec^{-1}$ $s^{-1}$. This result is in good agreement with the results of previous studies, which range from $k=1.0 \times 10^{-19}$ to $k=1.8 \times 10^{-19}$ $cm^3$ $molec^{-1}$ $s^{-1}$ (6, 25, 26, 27). The reaction is quite slow, and hence may suffer some contamination from other radicals that form in small quantities; for example $HO_2$ and subsequently OH, explaining the somewhat higher rate constant derived from the isoprene data relative to that derived from the $NO_2$ data. The products were not quantified, but

included essentially the same suite of products found from other reactions: methacrolein, methyl vinyl ketone, 3-methyl furan, 2-(1-methylethenyl) oxirane, and 2-ethenyl 2-methyl oxirane.

# *Conclusions*

Our results, when combined with those of Tuazon and Atkinson (7) allow us to account for virtually 100% of the OH-isoprene products. The hydroxyl radical reaction yields (on a per molecule isoprene reacted basis) 60.5% carbonyls, 4% 3-methyl furan, and 14% organonitrates, leaving 21% of the product not individually identified. These are a collection of multisubstituted carbonyl products, 2-4% of which condense to the aerosol phase. The OH reaction is difficult to study because of the necessity of including NO, which provides a formation pathway for $O(^3P)$, complicating the analysis of any OH-alkene reaction. This problem is likely to have interfered with previous studies of OH-alkene reaction systems to some degree, independent of the source used for OH, resulting in carbonyl product yields that are low.

While we were not able to determine the products of the $NO_2$ -isoprene reaction, we measured its rate constant and found 1.8 $x10^{-19}$ $cm^3$ $molec^{-1}$ $s^{-1}$.

We have found that the $O(^3P)$ -isoprene reaction results in smaller quantities of free radicals than previously believed; only about 8% produces species that result in $HO_2$ formation. Most of the remainder forms epoxides; the epoxide yield, at 84% is about double that expected based on results for 1-butene (20,21). The 1,2 hydrogen shifts that appear to be prevalent for 1-butene are minimal if they occur at all; however, the reaction forms 2-methyl 2-butenal via an isomerization involving a 5-membered ring.

# *Acknowledgements*

This work was supported by National Science Foundation Grant ATM-9003186. One of the authors (S.E.P.) gratefully acknowledges the support of a Dissertation Fellowship from the American Association of University Women. The authors also appreciate helpful discussions with W.P.L. Carter and R. Atkinson of the University of California at Riverside.

# *References*

(1) Isidorov V.A., I.G. Zenkevich, and B.V. Ioffe *Atmospheric Environment* **19,** 1 (1985).

(2) Lamb, B., H. Westburg, G. Allwine and T. Quarles *J. Geophys. Res.* **90**, 2380(1985).

(3) Ennis, C.A., A.L. Lazarus, P.R. Zimmerman and R.K. Monson *Tellus* **42B**, 183 (1990).

(4) Lamb, B., A. Guenter, D. Gay, H. Westburg *Atmospheric Environment* **21**, 1695 (1987).

(5) Trainer, M., E.Y. Hsie, S.A. McKeen, R. Tallamraju, D.D. Parrish, F.C. Fehsenfeld, and S.C. Liu *Nature* **329**, 705 (1987).

(6) Gu, C.L., C.M. Rynard, D. G. Hendry, T. Mill *Envir. Sci. Technol.* **19,** 151 (1985).

(7) Tuazon, E.C., and R. Atkinson *Int'l J. Chemical Kinetics* **22**, 1221 (1990).

(8) Atkinson R., S. M. Aschmann, E. C. Tuazon, J. Arey and B. Zelinska *Int'l J. Chemical Kinetics* **21,** 593 (1989).

(9) Pandis, S.N., S.E. Paulson, R.C. Flagan, and J.H. Seinfeld *Atmospheric Environ.* **25a**, 997 (1991).

(10) National Institute of Standards and Technology Mass Spectral Library (1990).

(11) Aldrich Nuclear Magnetic Resonance Library of Reference Spectra, Aldrich Chemical Company, Milwaukee, WI (1983).

(12) Pitts, J.N. Jr., A.M. Winer, S.M. Aschmann, W.P.L. Carter and R. Atkinson Experimental Protocol for Determining Hydroxyl Radical Reaction Rate Constants for Organic Compounds. Final Report, EPA Cooperative Agreement CR-810214 (1985).

(13) Taylor, W.D., T.D. Allston, M.J. Moscato, G.B. Fazekas, R. Kozlowski, G.A. Takas *Int'l J. Chemical Kinetics* **12**, 231 (1980).

(14) Tuazon, E.C., and R. Atkinson *Int'l J. Chemical Kinetics* **22**, 591 (1990).

(15) Tuazon, E.C., and R. Atkinson *Int'l J. Chemical Kinetics* **22**, 1141 (1989).

(16) Atkinson R., *Chemical Rev.* **19**, 799 (1985).

(17) Atkinson R. *Atmospheric Environment* **24A**, 1 (1990).

(18) Carter, W., and R. Atkinson, Development and implementation of an up-to-date photochemical mechanism for use in airshed modeling, Summary final report, Calif. Air Resources Board (1988).

(19) Atkinson, R., D.L. Baulch, R.A. Cox, R.F. Hampson Jr., J.A. Kerr, and J. Troe *J. Phys. Chem. Ref. Data* **18**, 881 (1989).

(20) Paulson, S.E., S.N. Pandis, U. Baltensburger, J.H. Seinfeld, R.C. Flagan, E.J. Palen, D.T. Allen, C. Schaffner, W. Giger, A. Portmann. *J. Aerosol Sci.* **21**, S245 (1991).

(21) Killus, P. and G. Z. Whitten, Isoprene: a Photochemical Kinetic Mechanism, *Environ. Sci. Technol.* **18**, 142-148 (1984).

(22)Atkinson R. and A. C. Lloyd *J. Phys. Chem. Ref. Data* **13**, 315 (1984).

(23) Cvetanovic, R.J., and L.C. Doyle *Can. J. Chemistry* **36**, 2187 (1960).

(24) Cvetanovic, R.J., *Adv. in Photochem* **1**, 115 (1963).

(25) Ohta, T., H. Nakagura, and S. Suzuki *Int'l J. Chemical Kinetics* **18**, 1 (1986).

(26) Glasson, W.A., and C.S. Tuesday *Environ. Sci. Technol.* **4**, 752 (1970).

(27) Atkinson, R., S.M. Aschmann, A.M. Winer, and J.N.Pitts, Jr. *Int'l J. Chemical Kinetics* **16**, 697 (1984).

(28) Dlugokencky, E.J., and C.J. Howard *J. Phys. Chem.* **93**, 1091 (1989).

(29) Atkinson, R. *Int'l J. Chemical Kinetics* **19**, 799 (1987).

*Table 1.*

*Summary of Initial Conditions*

| Expt.* | Primary Reaction | Initial Concentration (ppm) HC | NO | $NO_2$ | $CH_3ONO$ | $O_3$ max. |
|---|---|---|---|---|---|---|
| IOH4 | Isoprene + OH | 2.87 | 9.5 | 3.9** | 0.5 | 0.058 |
| IOH5 | Isoprene + OH | 3.45 | 8.3 | 3.9** | 0.6** | 0.06 |
| IOH6 | Isoprene + OH | 1.69 | 5.5 | 0.45 | 0.86 | 0.036 |
| IOH7 | Isoprene + OH | 1.65 | 5.5 | 0.5 | 0.9 | 0.033 |
| IOH8 | Isoprene + OH | 4.71 | 6.8 | 1.3** | 0.75** | 0.059 |
| IO3P1 | Isoprene + $O(^3P)$ | 3.20 | 0.067 | 4.7 | -- | 0.055 |
| IO3P2 | Isoprene + $O(^3P)$ | 45.1 | 0.065 | 8.8 | -- | 0.00 |
| MIO3P3 | Isoprene + $O(^3P)$ | 24.2 | 0.064 | 10.0 | -- | 0.00 |
| + Methyl cyclohexane | | 225. | | | | |
| INO21 | Isoprene + $NO_2$ | 5.66 | 0.00 | 8.35 | -- | -- |

*Experiments are numbered as follows: hydrocarbon(s) (1 letter each), primary oxidant (up to 3 letters) and a number differentiating experiments of a given type.

** indicates a value that was estimated from the input volumes rather than measured.

# *Table 2.*

## *OH/O($^3$P) Oxidation Mechanism for Isoprene*

| Rate constant at 298 K | Activation Energy ($E_a$/RT) (K) | Reactants | Products | Reference for Rate Constant | Reference for Product Spectrum |
|---|---|---|---|---|---|
| 1) 1.01E-10, | -410 | isoprene + OH | → 0.42 ISOH1 + 0.58 ISOH2 | | 17,a&7 |
| 2) 7.6E-12, | 180 | ISOH1 + NO | → 0.1 ISNI1 + 0.60 methacrolein + 0.59 HCHO + 0.24 IALD1 + 0.9 $HO_2$ + 0.9 $NO_2$ + 0.04 3-methyl furan | | 19,a |
| 3) 7.6E-12, | 180 | ISOH2 + NO | → 0.1 ISNI2 + 0.61 methyl vinyl ketone + 0.61 HCHO + 0.04 3-methyl furan + 0.23 IALD1 + 0.9 $HO_2$ + 0.9 $NO_2$ | | 19,a |
| 4) 7.6E-12, | 180 | IALD1 +NO | → 0.1 ISNI1 + 0.9 IALD2 + 0.9 $HO_2$ + 0.9 $NO_2$ | | 17,a |
| 5) 5.8E-11 | | isoprene + O | → 0.63 2-ethenyl 2-methyl oxirane + 0.22 2-(1-methylethenyl) oxirane + 0.085 I3PR | | b,a |
| 6) 7.6E-12, | 180 | I3PR + NO | → 0.88 $NO_2$ + 0.88 IALD1 + 0.12 ISNI1 + 0.88 $HO_2$ | | 17,c |
| 7) 1.7E-19 | | isoprene + $NO_2$ | → 0.42 ISOH1 + 0.58 ISOH2 + NO | | a&7,d |
| 8) 6.69E-13, | 450 | isoprene + $NO_3$ | → 0.73 ISOH1 + 0.27 ISOH2 + $NO_2$ + HCHO | | 28,e |
| 9) 3.1E-12 | | 2-ethenyl 2-methyl oxirane + O | → | | f,g |
| 10) 7.9E-12 | | 2-(1-methylethenyl) oxirane + O | → | | f,g |
| 11) 1.88E-11 | | 2-ethenyl 2-methyl oxirane + OH | → VOH1 | | f,h |
| 12) 3.35E-11 | | 2-(1-methylethenyl) oxirane + OH | → AOH1 | | f,h |
| 13) 1.88E-11 | | methyl vinyl ketone + OH | → 0.72 VOH1 + 0.28 VOH2 | | 17,1 |
| 14) 7.6E-12, | 180 | VOH1 + NO | → 0.92 hydroxy acetaldehyde + | | 17,15 |

| | | |
|---|---|---|
| | 0.92 $CH_3C(O)OO\cdot$ + 0.08 MVNI + 0.92 $NO_2$ | |
| 15) 7.6E-12, 180 | VOH2 + NO → 0.92 methyl glyoxal + 0.92 HCHO + 0.08 MVNI + 0.92 $NO_2$ + 0.92 $HO_2$ | 17,15 |
| 16) 3.1E-12 | methyl vinyl ketone + O → | 16,g |
| 17) NO2 photolysis x2.7E-6 | methyl vinyl ketone + HV → | h,g |
| 18) 3.35E-11 | methacrolein + OH → 0.42 AOH1 + 0.08 AOH2 + 0.5 $CH_2=C(CH_3)CC(O)OO\cdot$ | 17,14 |
| 19) 7.6E-12, 180 | AOH1 + NO → 0.92 $HO_2$ + 0.92 CO + 0.92 OHAC + 0.08 MANI + 0.92 $NO_2$ | 19,14 |
| 20) 7.6E-12, 180 | AOH2 + NO → 0.92 methyl glyoxal + 0.92 $HO_2$ + 0.92 HCHO + 0.08 MANI + 0.92 $NO_2$ | 19,14 |
| 21) 8.4E-12 | $CH_2=C(CH_3)CC(O)OO\cdot$ + $NO_2$ → $CH_2=C(CH_3)CC(O)OONO_2$ | i,i |
| 22) 5.8E-4, -13435 | $CH_2=C(CH_3)CC(O)OONO_2$ → $CH_2=C(CH_3)CC(O)OO\cdot$ + $NO_2$ | i,i |
| 23) 7.6E-12, 180 | $CH_2=C(CH_3)CC(O)OO\cdot$ + NO → PO2 + $NO_2$ + $CO_2$ | 17,14 |
| 24) 7.9E-12 | methacrolein + O → | b,g |
| 25) NO2 photolysis x 2.7E-6 | methacrolein + HV + PK3 → | h,g |
| 26) 2.E-11 | IALD2 + OH → IALD3 | j |
| 27) 7.6E-12, 180 | IALD3 + NO → 0.9 IALD2 + 0.9 $NO_2$ + 0.9 ISNI1 + 0.9 $HO_2$ | 17,j |
| 28) 5.E-13 | IALD2 + O → | b,g |
| 29) 9.35E-11 | 3-methyl furan + OH → IALD2 | 8 |
| 30) 1.04e-11 | methyl cyclohexane + OH → MCHR | 17,17 |
| 31) 7.6E-12, 180 | MCHR + NO → 0.84 IALD2 + 0.16 ISNI1 + 0.78 $HO_2$ + 0.84 $NO_2$ | 17,k |

---

a) This work.

b) Estimated from correlations between the rate constants of OH and $O(^3P)$ developed by Atkinson (16).
c) Assumed to produce the same fraction of nitrate as isoprene as this species should have five carbons.
d) Products unknown/assumed to be the same as the OH-isoprene reaction.
e) These rate constants were assumed to equal the values for methyl vinyl ketone (2-ethenyl 2-methyl oxirane) and methacrolein (2-(1-methylethenyl) oxirane. Products were also assumed to react in the fashion of the appropriate methacrolein and methyl vinyl ketone derived radicals.
f) $NO_3$ was assumed to have the same product branching as $O_3$ because of steric hindrance.
g) Products unknown/assumed to be exactly analogous to the products of isoprene; same radical yields and the appropriate hydrocarbon products. The hydrocarbon products of these reactions are expected to have a negligible effect on any simulation carried out with the mechanism (see text).
h) Assumed to equal the values for acetone (19).
i) Assumed to react like acetaldehyde, as reported by Atkinson et.al. (19)
j) Most of IALD2 is expected to be a suite of 5-carbon mono-unsaturated compounds with two carbonyls/hydroxy groups, although it is also used as a surrogate for other minor products. OH rate constant and product estimates were made on this assumption.
k) Based on extensive estimates of the branching ratios, products and rate constants from structure-activity relationships developed by Atkinson (29).

| | |
|---|---|
| ISOH1 | isoprene-adduct; addition to the 3,4 double bond. |
| ISOH2 | isoprene-adduct; addition to the 1,2 double bond. |
| ISNI1 | generalized organic nitrate, with hydroxyl group. |
| IALD1 | surrogate for unidentified products of isoprene reaction. |
| IALD2 | Most of IALD2 is expected to be a suite of 5-carbon mono-unsaturated compounds with two carbonyls/hydroxy groups, although it is also used as a surrogate for other minor products. |
| IALD3 | reaction intermediate for IALD2 |
| O | $O(^3P)$ |
| I3PR | $CH_2$=C-CO·($CH_3$)-$CH_2$O-O· + 3 other isomers |
| OXA | generalized epoxide from reaction of $O(^3P)$ with 2-methyl 3-butene oxide, 2-(1-methylethenyl) oxirane, methacrolein, or methyl vinyl ketone. |
| VOH1 | $CH_2$=C-COH($CH_3$)$CH_2$O-O· + $CH_2$=C-COO·($CH_3$)$CH_2$OH |
| AOH1 | ·O-O-CH($CH_2$OH)-C($CH_3$)=$CH_2$ + $CH_2$=CH(OO·)-C($CH_3$)=$CH_2$ |
| MCHR | generalized methyl cyclohexane-OH adduct |
| MVNI | generalized methyl vinyl ketone-derived organo-nitrate |
| MANI | generalized methacrolein-derived organo-nitrate |
| PAN | Peroxy acetyl nitrate |

*Table 3. Summary of Product Yields*

| Reaction | Product | Yield (% of Isoprene reacted leading to product) |
|---|---|---|
| OH + Isoprene | Methyl vinyl ketone | 35.5 ±3 |
| | Methacrolein | 25. ±3 |
| | 3-Methyl furan | 4. ± 2 |
| | Other carbonyls, | 21 ± 5* |
| | hydroxy carbonyls, | 0.4-0.8 |
| | including condensible products | |
| | Formaldehyde | 67 ± 7** |
| | Alkyl nitrates | 14 ± 5** |
| Total | | 100 |

*Consistent with the observations of Tuazon and Atkinson (7).
**These are values derived from the work of Tuazon and Atkinson (7).

| | | |
|---|---|---|
| $O(^3P)$ + Isoprene | 2-ethenyl 2-methyl oxirane | 63.± 8 |
| | 2-(1-Methylethenyl) oxirane | 22.± 3 |
| | unknown 1 | 11.± 4° |
| | unknown 2 | 1.0± .5° |
| | 2,2 methylbutenal | 1.7± .8 |
| | Organic Radicals | 8.± 3°° |
| Total | | 96.8-105.3 |

°These species are unidentified peaks that elute from the GC between 2-ethenyl 2-methyl oxirane and 2-(1-methylethenyl) oxirane.
°°These radical species, derived from model calculations 1) may have a stoichiometry of between 1 and 2, and 2) may result in formation of the unknowns, and hence should not necessarily be included in the total.

Figure 1. Methacrolein, methyl vinyl ketone, unknown 1, 2-ethenyl 2-methyl oxirane, and 2-(1-methylethenyl) oxirane yields vs. isoprene reacted for experiment IOH4. The symbols show data; the lines show the simulation results. Note that 2-(1-methylethenyl) oxirane is plotted with respect to the right-hand axis.

Figure 2. Methacrolein, methyl vinyl ketone, 2-ethenyl 2-methyl oxirane, and 2-(1-methylethenyl) oxirane yields vs. isoprene reacted for experiment IOH6. The symbols show data; the lines with matching identification show the simulation results. Note that both epoxides (2-ethenyl 2-methyl oxirane and 2-(1-methylethenyl) oxirane) are plotted with respect to the right-hand axis.

Figure 3. Methacrolein, methyl vinyl ketone, 2-ethenyl 2-methyl oxirane, and 2-(1-methylethenyl) oxirane yields vs. isoprene reacted for experiment IOH8. The symbols show data; the lines show simulation results. Simulations for unknown 2 and 2-methyl 2-butenal are not shown. Note that 2-ethenyl 2-methyl oxirane and unknown 1 are plotted with respect to the right-hand axis.

Figure 4. Methacrolein concentration vs. methyl vinyl ketone concentration for experiments IOH4-IOH8.

Figure 5. 2-(1-methylethenyl) oxirane vs. 2-ethenyl 2-methyl oxirane concentration for experiments IOH4-IOH8.

Figure 6. Methacrolein concentrations vs. 2-ethenyl 2-methyl oxirane concentration for experiments IOH4-IOH8. The experiments with higher initial $NO_2$ concentrations show higher epoxide yields and lower methacrolein yields (IOH4 and 5), for those with lower initial $NO_2$ concentrations, the reverse is observed (IOH6 and 7); IOH8 is intermediate (see Table 1 for a summary of the initial conditions).

Figure 7. 2-ethenyl 2-methyl oxirane, 2-(1-methylethenyl) oxirane, and unknown 1 vs. isoprene reacted for $O(^3P)$-isoprene experiments IO3P2 and MIO3P1. Data are indicated with symbols; lines are simulation results. MIO3P1 contains added methyl cyclohexane.

Figure 8. Methacrolein, methyl vinyl ketone, 3-methyl furan, 2-methyl 2-butenal and unknown 2 vs. isoprene reacted for experiments IO3P2 and MIO3P1. 3-Methyl furan is plotted with respect to the right-hand axis. Data are indicated with symbols; lines are simulation results.

Figure 9. Methyl cyclohexane reacted vs. isoprene reacted for experiment MIO3P1. Data are indicated with filled diamonds; dotted line shows the simulation results.

Figure 10. Plots of $(1/C)\{\ln|([Iso]+C)/[Iso]| - \ln|(([Iso]_0+C)/[Iso]_0)|\}$ and $-(1/C)\{\ln|[NO_2]-C)/[NO_2]| - \ln([NO_2]_0-C)/[NO_2]_0\}(ppm^{-1})$ vs. time. The slopes of the lines give estimates of the $NO_2$-isoprene rate constant.

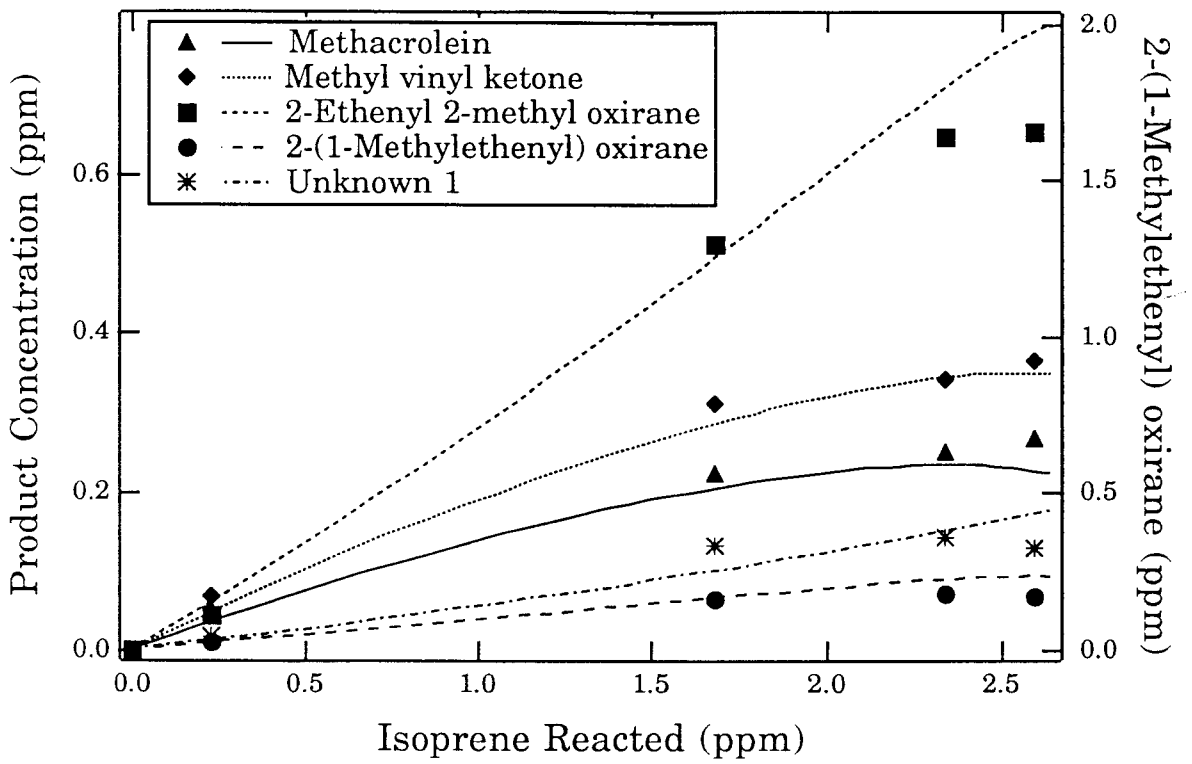
Methacrolein
Methyl vinyl ketone
2-Ethenyl 2-methyl oxirane
2-(1-Methylethenyl) oxirane
Unknown 1
Product Concentration (ppm)
2-(1-Methylethenyl) oxirane (ppm)
Isoprene Reacted (ppm)
0.0
0.2
0.4
0.6
0.5
1.0
1.5
2.0
2.5

Figure 1.

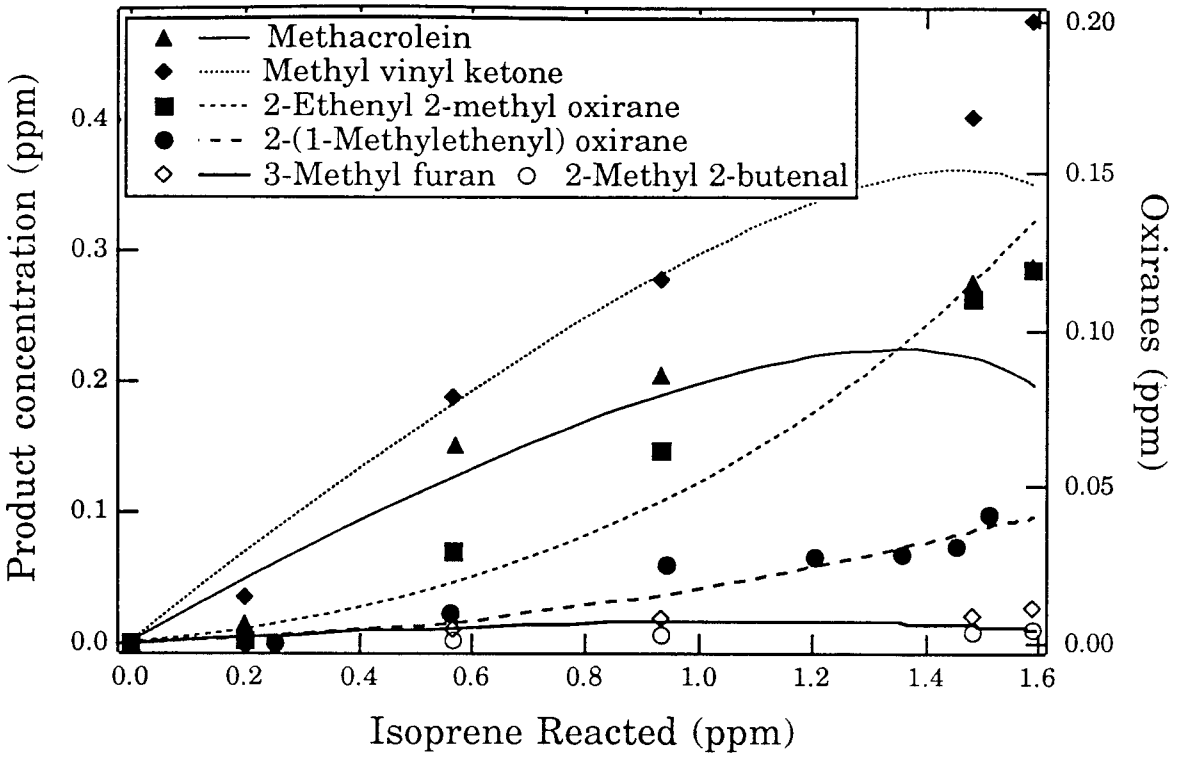
Methacrolein
Methyl vinyl ketone
2-Ethenyl 2-methyl oxirane
2-(1-Methylethenyl) oxirane
3-Methyl furan
2-Methyl 2-butenal
Product concentration (ppm)
Oxiranes (ppm)
Isoprene Reacted (ppm)
0.0
0.1
0.2
0.3
0.4
0.00
0.05
0.10
0.15
0.20
0.0
0.2
0.4
0.6
0.8
1.0
1.2
1.4
1.6

Figure 2.

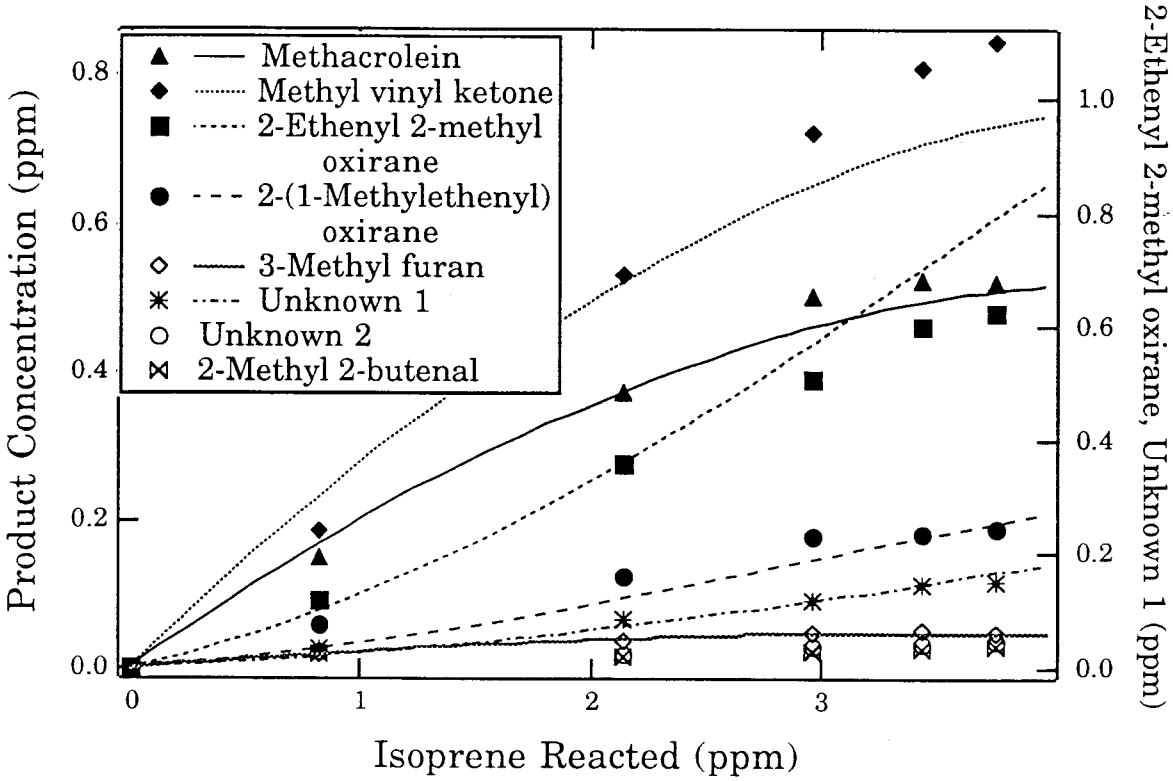
Methacrolein
Methyl vinyl ketone
2-Ethenyl 2-methyl oxirane
2-(1-Methylethenyl) oxirane
3-Methyl furan
Unknown 1
Unknown 2
2-Methyl 2-butenal
Product Concentration (ppm)
2-Ethenyl 2-methyl oxirane, Unknown 1 (ppm)
Isoprene Reacted (ppm)
0.0
0.2
0.4
0.6
0.8
1.0
0
1
2
3

Figure 3.

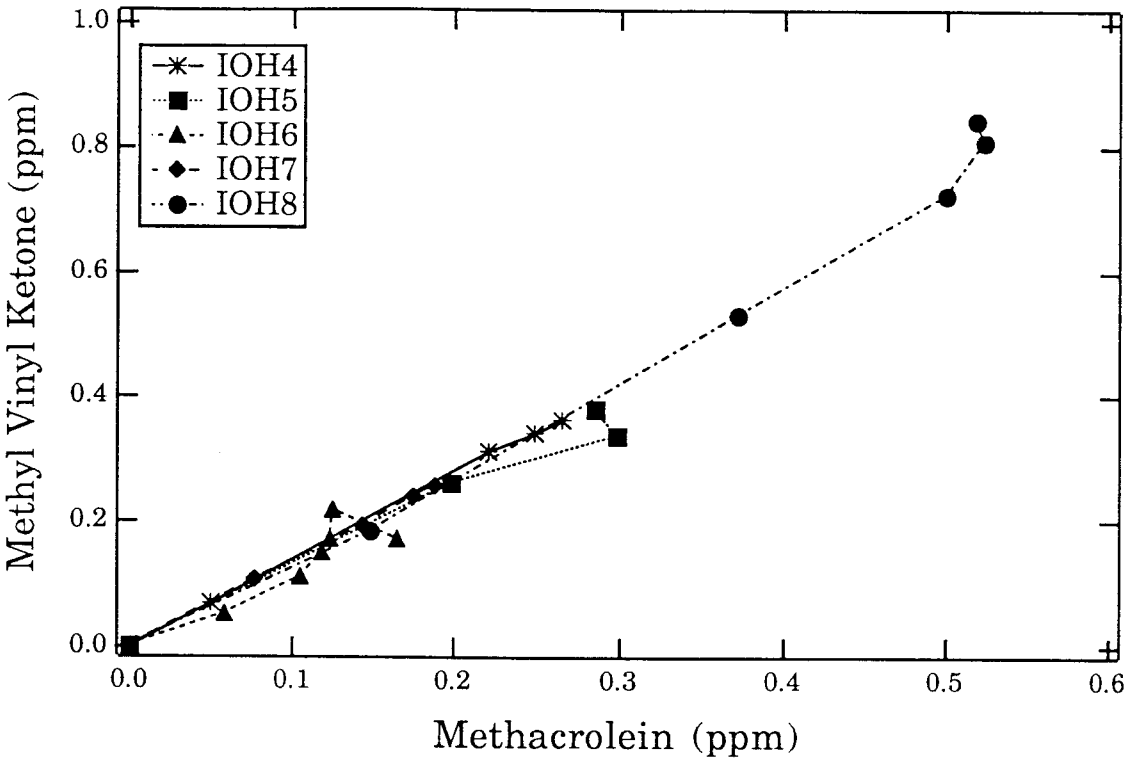
IOH4
IOH5
IOH6
IOH7
IOH8
Methyl Vinyl Ketone (ppm)
Methacrolein (ppm)
0.0
0.2
0.4
0.6
0.8
1.0
0.0
0.1
0.2
0.3
0.4
0.5
0.6

Figure 4.

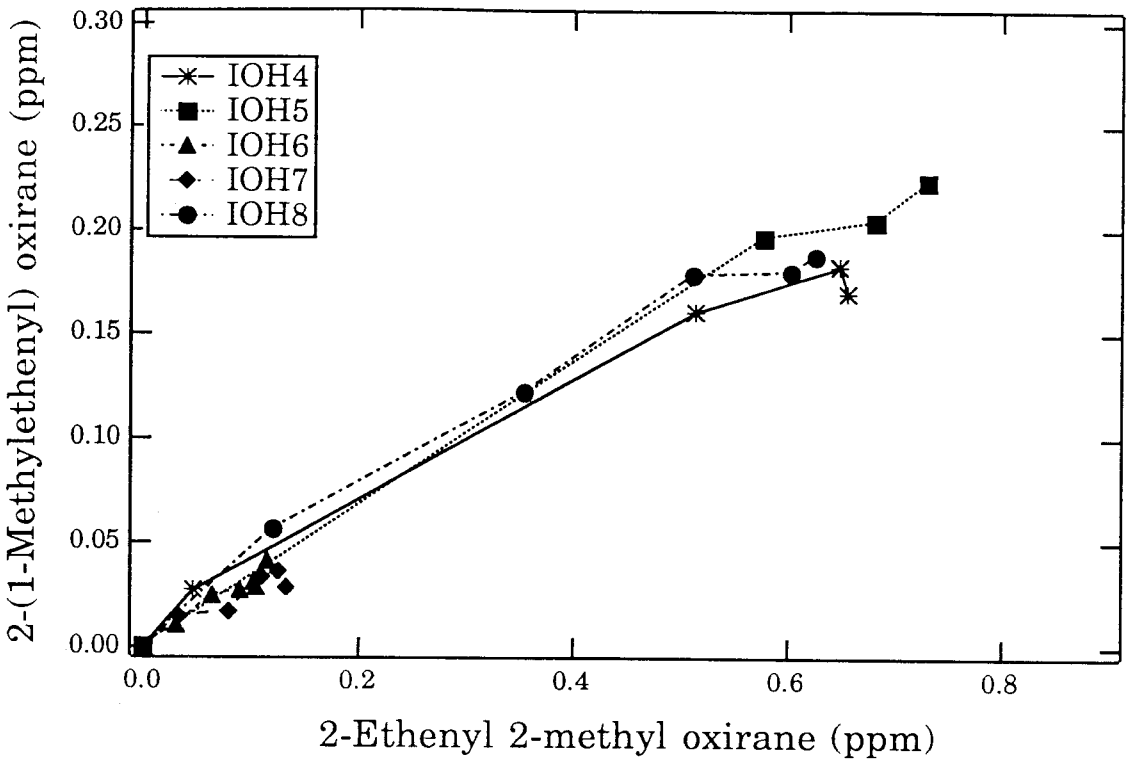
IOH4
IOH5
IOH6
IOH7
IOH8
0.30
0.25
0.20
0.15
0.10
0.05
0.00
0.0
0.2
0.4
0.6
0.8
2-(1-Methylethenyl) oxirane (ppm)
2-Ethenyl 2-methyl oxirane (ppm)

Figure 5.

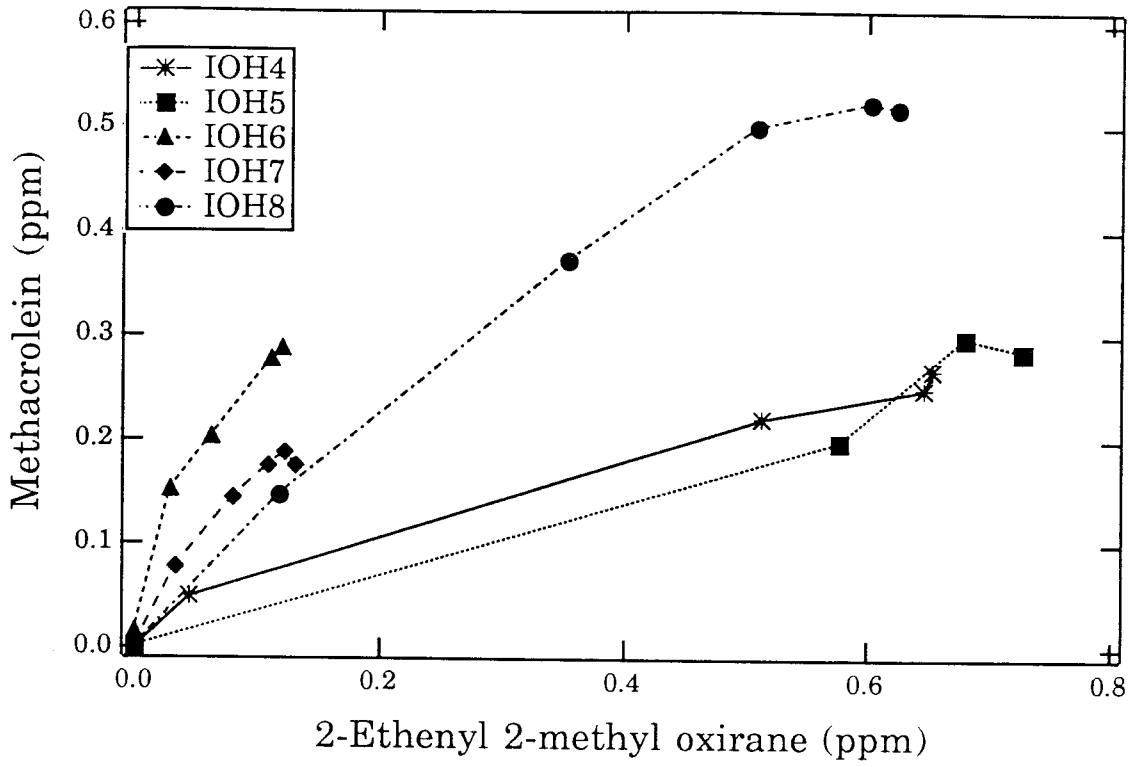
IOH4
IOH5
IOH6
IOH7
IOH8
Methacrolein (ppm)
2-Ethenyl 2-methyl oxirane (ppm)
0.0
0.1
0.2
0.3
0.4
0.5
0.6
0.0
0.2
0.4
0.6
0.8

Figure 6.

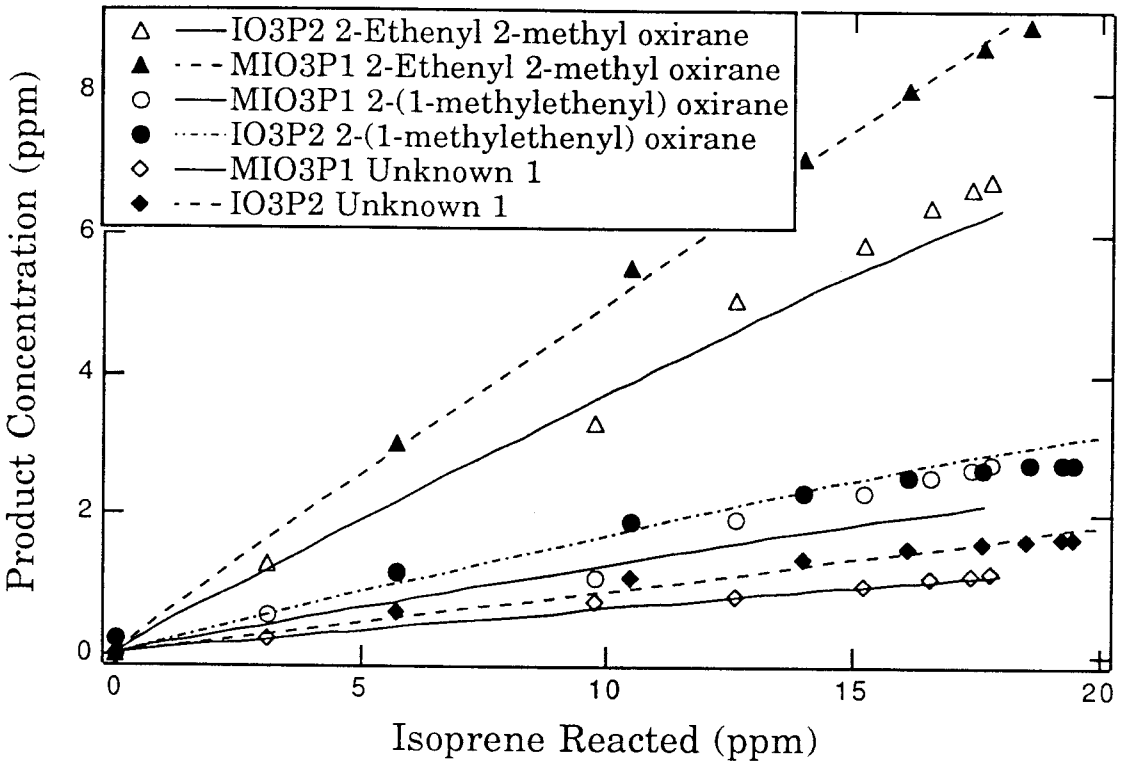
IO3P2 2-Ethenyl 2-methyl oxirane
MIO3P1 2-Ethenyl 2-methyl oxirane
MIO3P1 2-(1-methylethenyl) oxirane
IO3P2 2-(1-methylethenyl) oxirane
MIO3P1 Unknown 1
IO3P2 Unknown 1
Product Concentration (ppm)
Isoprene Reacted (ppm)
0
2
4
6
8
0
5
10
15
20

Figure 7.

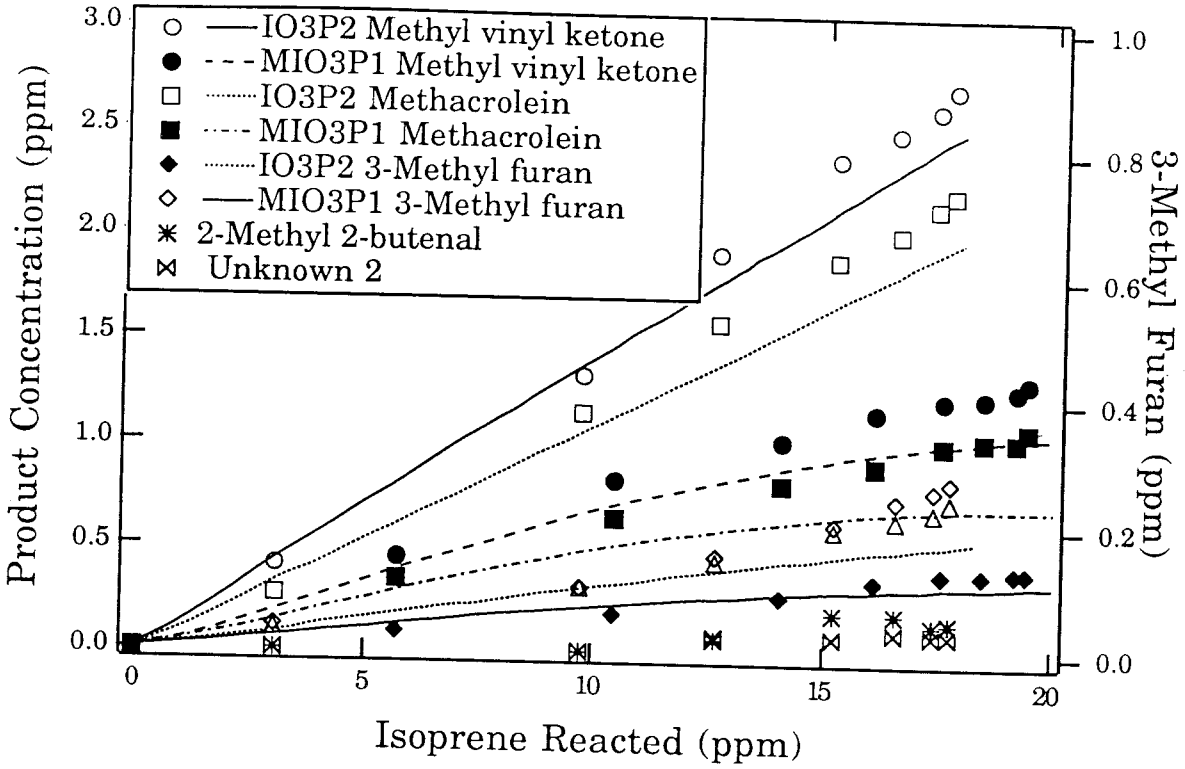
IO3P2 Methyl vinyl ketone
MIO3P1 Methyl vinyl ketone
IO3P2 Methacrolein
MIO3P1 Methacrolein
IO3P2 3-Methyl furan
MIO3P1 3-Methyl furan
2-Methyl 2-butenal
Unknown 2
Product Concentration (ppm)
3-Methyl Furan (ppm)
Isoprene Reacted (ppm)
0.0
0.5
1.0
1.5
2.0
2.5
3.0
0.2
0.4
0.6
0.8
1.0
0
5
10
15
20

Figure 8.

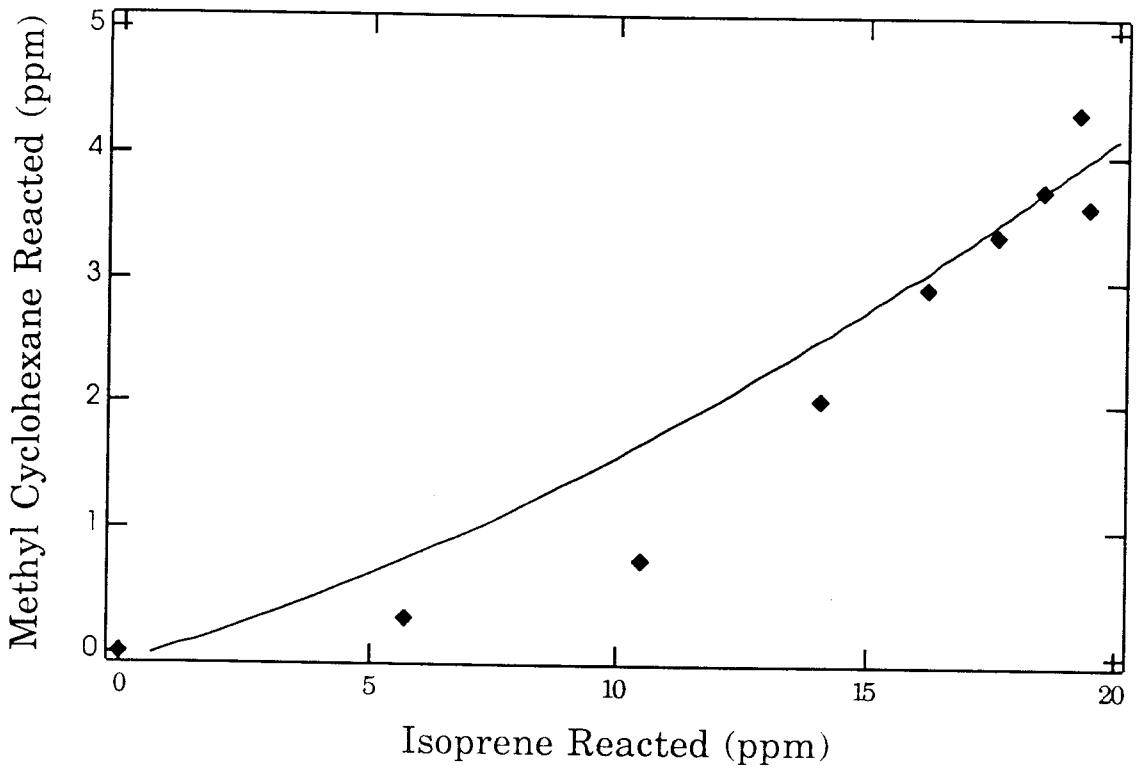
Methyl Cyclohexane Reacted (ppm)
5
4
3
2
1
0
0
5
10
15
20
Isoprene Reacted (ppm)

Figure 9.

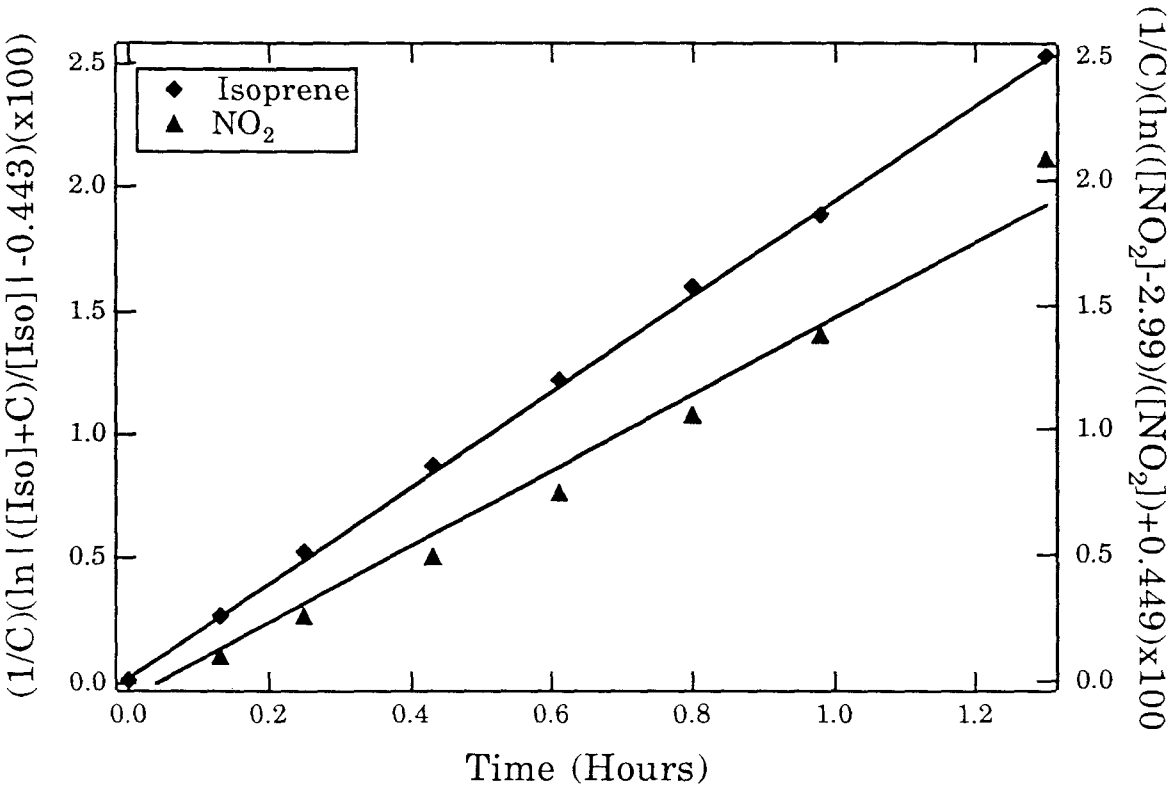
Isoprene
$NO_2$
(1/C)(ln|([Iso]+C)/[Iso]|-0.443)(x100)
(1/C)(ln(([$NO_2$]-2.99)/([$NO_2$])+0.449)x100
Time (Hours)
0.0
0.2
0.4
0.6
0.8
1.0
1.2
0.5
1.5
2.0
2.5

Figure 10.

# CHAPTER 3

# Atmospheric Photooxidation of Isoprene

# Part 2: The Ozone - Isoprene Reaction

Suzanne E. Paulson[a], Richard C. Flagan[b] and John H. Seinfeld[b]

[a]Environmental Engineering Science

[b]Chemical Engineering

California Institute of Technology

Pasadena, CA 91125

*International Journal of Chemical Kinetics*

In Press

*I don't exist when you don't see me*

*I want more*

(The Sisters of Mercy, 1990)

# *Abstract*

A series of experiments have been performed to study the ozone-isoprene reaction in a smog chamber by adding externally produced $O_3$ to the hydrocarbon in the dark. A chemical tracer, methyl cyclohexane, was added to probe the OH formation in the system. $O(^3P)$ formation was also examined using the known distribution of products that are unique to the $O(^3P)$-isoprene reaction (part 1). The results provide clear evidence that both OH and $O(^3P)$ are produced by the $O_3$-isoprene reaction directly in large quantities; about 0.68±0.15 and 0.45±0.20 per $O_3$-isoprene reaction, respectively. These additional radicals severely complicate the analysis of the $O_3$ reaction, hence computer kinetic modeling was necessary to ascertain the products of the $O_3$ reaction itself, corrected for OH and $O(^3P)$ reactions. The product distribution, which differs dramatically from that published previously, is: 67±9% methacrolein, 26±6% methyl vinyl ketone, and 7±3% propene, accounting for 100±10% of the reacted isoprene. Applicability of these results to the gas-phase $O_3$ reaction with other unsaturated hydrocarbons is briefly discussed.

# *Introduction*

A substantial portion of the atmospheric oxidation of all alkenes is due to reaction with ozone, hence an accurate description of both urban and rural ozone formation requires an understanding of the ozone-alkene reactions. Although ozone-alkene reactions have been studied for decades, many questions remain, particularly as to the fate of the Criegee biradicals in the gas phase (1, and references therein). A few of these studies have found evidence for substantial quantities of OH formation from the $O_3$ reaction with alkenes, including tetramethylethylene (2), propene (3,4), isobutene (3), and a series of terpenes (5). The studies of tetramethylethylene (2) and propene (4) provide the only quantification of this OH source, at 0.7 and roughly 0.3 per molecule of alkene reacted. Quantification and analysis of the effect of the OH source on other measured quantities remain very scarce, as does an explanation of the pathway to the formation of OH. Further, despite its importance, the formation of OH in the $O_3$-alkene reactions has not been included in models used to understand chemical processes in the atmosphere. If the isoprene-$O_3$ reaction results in a

significant source of free radicals, its impact on atmospheric chemistry may be greater than generally believed.

We have undertaken to examine the free radical as well as carbonyl production from the $O_3$-isoprene reaction in an effort to delineate the mechanism for this reaction. We have carried out a series of batch-reactor experiments, some with the addition of an alkane (methyl cyclohexane) to trace OH formation. We have focused on identifying and quantifying even relatively minor products to understand the reaction pathways of the Criegee biradicals. Two studies of the products of the reaction of isoprene with ozone have been carried out to date (6,7); these were successful in identifying about 50% of the reacted isoprene as two products, methacrolein and methyl vinyl ketone. These studies also quantified formaldehyde formation. In addition to quantifying the methacrolein and methyl vinyl ketone yields, we have measured yields of two epoxides, 2-ethenyl 2-methyl oxirane and 2-(1-methylethenyl) oxirane, and propene, as well as OH radical. We have further derived the yield and probable formation pathway of $O(^3P)$ in the $O_3$ reaction with isoprene.

## *Experimental System*

The smog chamber facility, instrumentation, and description of materials and methods used have been described previously (8) and in part 1, hence we have included descriptions only of the instrumentation and procedures unique to this study. Table 1 contains a summary of the initial conditions for the experiments.

Ozone experiments were carried out in the dark, and lasted from 1.5 to 3 hours. Isoprene was added to the smog chamber, and allowed to mix until a stable concentration was obtained. The temperature of the chamber was 298 ± 8° C. Ozone was generated with a

corona-less discharge device, supplied with a stream of pure molecular oxygen. The effluent of the discharge flowed through a 3.6 m x 0.635 cm O.D. Teflon tube, and into the chamber. It is important to consider whether such discharges result in the introduction of any species other than $O_3$ and $O_2$ to the smog chamber. In a pure molecular oxygen stream, the only species that may result from the discharge are the neutral and ionized dissociation products of $O_2$ itself; mainly $O(^3P)$, $O(^1D)$, $O^-$, $O^+$, and $O_2^-$. The dominant reactions for the radical species are:

(a) $O(^3P) + O_2 \xrightarrow{O_2} O_3 + O_2$;

(b) $O(^1D) + O_2 \rightarrow O(^3P) + O_2$;

The ionic species may react rapidly with neutrals, but the important reactions to consider are the recombination reactions, which remove the ions from system. Ion-ion recombination reactions tend to have similar rates (9); a typical recombination reaction in this system is:

(c) $O^+ + O^- + M \rightarrow O_2 + M$;

where $k_{(a)}=6.02\times10^{-34}$ $cm^6$ $molec^{-2}$ $s^{-1}$ (10), $k_{(b)}=4.0\times10^{-11}$ $cm^3$ $molec^{-1}$ $s^{-1}$ (10), $k_{(c)}=3\times10^{-8}$ $cm^3$ $molec^{-1}$ $s^{-1}$ (9). The residence time in the tube between the ozone generator and the smog chamber is approximately 30 ms, and the effluent of the tube is approximately 240 ppm ozone, indicating that the $O_2$ concentration at the discharge is at least 99%. It follows that atomic oxygen concentrations of both the ground and excited states, as well as the ionic species, at the exit of the tube are totally negligible (the maximum concentration we calculated for the ions were $10^4$ $cm^{-1}$, and the radical concentrations were much lower, at less than 1 $cm^{-1}$).

Propene was identified by comparison of its retention time with the calibration cylinder on two different columns (DB-1 and DB-5 columns, J&W Scientific). A relative GC/FID response factor was calculated for propene by comparing sequential runs from certified

cylinders of propene and isoprene. Identification and quantification procedures for all other product species are described in part 1.

# *OH, Carbonyl, Epoxide and Propene Formation in the Ozone-Isoprene Reaction*

The initial product of the isoprene / $O_3$ reaction is an energy-rich addition complex, a molozonide, where a 5-membered ring is formed with $O_3$ and with either of isoprene's double bonds:

(1) 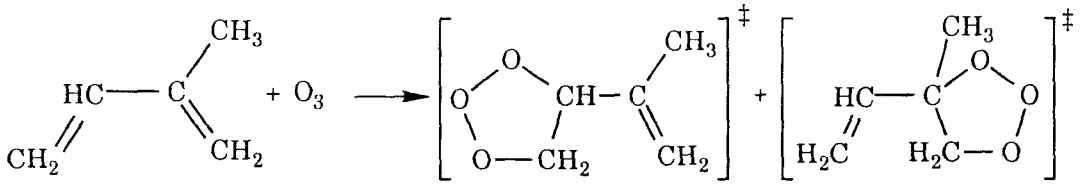

A body of data from mono-alkenes (e.g. 1-butene, trans-2-butene, propene) indicates that the addition complex decomposes, breaking the C-C bond and either one of the O-O bonds, each pathway forming a stable aldehyde or ketone, plus an energy rich Criegee biradical. In the case of the 3,4 addition complex of isoprene, the stable products are methacrolein or formaldehyde:

(2) 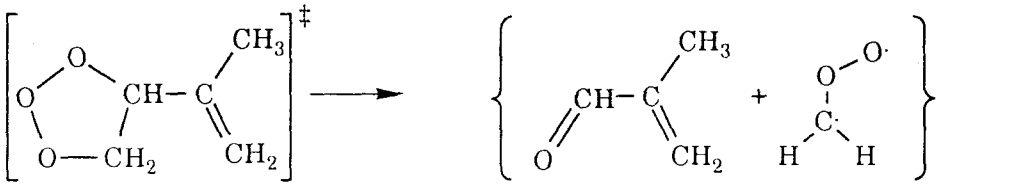

methacrolein Criegee biradical

or, 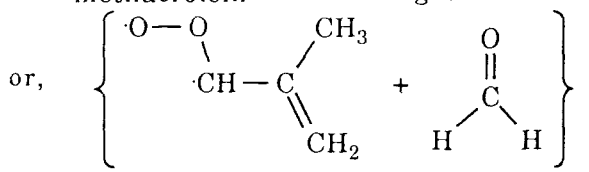

Criegee biradical formaldehyde

The Criegee biradical becomes thermally stabilized or decomposes to form a variety of stable and radical products, including OH, $HO_2$, and $O(^3P)$ (e.g. 2, 11). Recent work by

several groups (2, 3, 4, 5, 11, 12, 13, 14) on the ozone reactions of propene, 2-butene and 2,3-dimethyl 2-butene, has provided conflicting conclusions as to the amounts of these radical products. OH produced by the reaction of ozone with isoprene is both important to smog formation in the atmosphere, and can complicate the standard $O_3$ / hydrocarbon / dark experiment, because much of the hydrocarbon that appears to be reacting with $O_3$ is actually lost via reaction with OH.

To determine the degree of interference in the $O_3$ system from OH reactions, we have carried out two sets of ozone/isoprene experiments: type IO3 contained ozone and isoprene, while type MIO3 contained ozone, isoprene, and methyl cyclohexane, added as an OH tracer and absorber (Table 1). Methyl cyclohexane was chosen because it reacts exclusively with OH, and has a relatively high OH rate constant (relative to other alkanes), while having a sufficiently high vapor pressure to allow introduction of high concentrations into the smog chamber. Both methyl cyclohexane and its oxygenated products elute later from the GC Column than isoprene and most of its products, and hence do not interfere substantially with the isoprene analysis. These experiments allowed us to estimate the amount of OH present in the reaction system.

The product yield curves (product concentration vs. isoprene reacted) for the identified products of the isoprene-ozone reaction, along with the methyl cyclohexane loss data, for experiments IO34 and MIO31 through MIO34 are shown in Figs. 1-5. The same line/symbol combinations for each compound are used throughout these figures. Part of the data from IO32 and IO33 are shown in Figs. 7 and 8, but the complete sets are not shown because these experiments are essentially duplicates of IO34. The results of simulations, discussed in detail below, are included in Figs. 1-5. The mechanism predictions are shown as lines with the same identification as that used for the corresponding product. Methacrolein and methyl vinyl ketone have been observed previously to be products of the

$O_3$-isoprene reaction (2,3). Propene has not been previously observed, but is expected based on the chemistry of other alkenes (see $O_3$-isoprene mechanism, below). Epoxides have been observed in several $O_3$ -alkene systems (11), but do not arise from a well understood pathway. Total yields, on a per molecule reacted basis, ranged from about 62% (IO34) to 79% (MIO33). Fig.6 shows the percent of OH initially reacting with methyl cyclohexane for a given value of R, where R is defined as the methyl cyclohexane/isoprene ratio. The initial condition for each experiment is indicated in Fig. 6. The remainder of the OH reacts with isoprene, hence the results for MIO31 should most closely resemble the experiments without methyl cyclohexane, while in experiment MIO33 the largest portion of the OH was absorbed by the methyl cyclohexane. Fig. 6 was calculated using $k_{methyl\ cyclohexane/OH}=1.04\times10^{-11}$ $cm^3$ $molec^{-1}$ $s^{-1}$, and $k_{isoprene/OH}=1.01\times10^{-10}$ $cm^3$ $molec^{-1}$ $s^{-1}$ (these and other relevant rate constants and their sources are listed in Table 2). Figures 1-5 have increasing amounts of methyl cyclohexane added; in experiment IO34 (Fig. 1), all of the OH which forms reacts with isoprene, and progressively more OH reacts with methyl cyclohexane, reaching a maximum in MIO33 (Fig. 5).

The methyl cyclohexane data (Figs. 1-5) indicate an unanticipated amount of OH in the isoprene-ozone system. As expected, the greater the methyl cyclohexane/ isoprene ratio, the more methyl cyclohexane disappears. There also appears to be a tendency of the methyl cyclohexane reacted vs. isoprene reacted to display upward curvature (increasing slope). This is expected because as the isoprene reacts, the methyl cyclohexane remains nearly constant, hence R increases and the methyl cyclohexane consumes a larger percentage of the OH as each experiment progresses. The noise in the methyl cyclohexane data is a consequence of measuring very small differences; the largest change in the methyl cyclohexane concentration observed was 2.7%.

The slopes and shapes of the product yield curves (Figs. 1-5) expected from the isoprene-$O_3$ system are governed by two separate phenomena. The first is the apparent yield, which in the absence of further reaction with $O_3$ and OH, governs the slope of the lines. The slope of the lines should increase as more methyl cyclohexane is added, e.g. more methacrolein should be produced as the OH is titrated out of the system by the addition of methyl cyclohexane. This assumes that in this $NO_x$-free system the OH-isoprene reaction produces significantly less, if any, methacrolein, methyl vinyl ketone, propene, and epoxides than the $O_3$ reaction. This issue is discussed in some detail below. Figs. 7 and 8 show the complete sets of methacrolein and methyl vinyl ketone data together and allow comparison of the slopes. Both show a clear trend of increasing yield as more methyl cyclohexane is added, consistent with consumption of OH. The second phenomenon that affects the shape of the observed data is the reaction of the products themselves with $O_3$ and OH and $O(^3P)$, causing the yield curves to deflect away from the straight line to form convex downward curves.

The methacrolein data (Fig. 7) indicate a clear, if slight, trend of increasing yield from about 35 to 50% with the addition of methyl cyclohexane. The methyl vinyl ketone data in Fig. 8 show the same trend of increasing apparent yield as OH is removed from the reaction mixture by methyl cyclohexane. The methyl vinyl ketone data (Fig. 8) all appear more curved than the methacrolein data, which may be understood by realizing that the $O_3$ reaction is considerably more important for methyl vinyl ketone; the ratio of $O_3$/OH rate constants is larger by nearly a factor of 7 for methyl vinyl ketone relative to methacrolein (see Table 2).

Data for the minor products 2-ethenyl 2-methyl oxirane, 2-(1-methylethenyl) oxirane, and propene are shown in Figs. 1-5. Several of the data sets have initial zero yields; this is a GC-integrator artifact due to the difficulty in detecting and accurately integrating very

small peaks. All of the curves show distinct deviation from straight lines, indicating significant reaction of these species with $O_3$ and OH subsequent to their formation. This is particularly striking in the propene and 2-(1-methylethenyl) oxirane data. Surprisingly, the 2-ethenyl 2-methyl oxirane curves resemble methacrolein rather than methyl vinyl ketone; e.g. they are rather straight. This is contrary to the expected behavior, as 2-ethenyl 2-methyl oxirane has the same double bond available for attack by $O_3$ and OH as methyl vinyl ketone, not methacrolein.

3-Methyl furan, biacetyl, and methylglyoxal were also observed by both GCMS and FID. 3-Methyl furan accounted for 0.5-1% of the isoprene reacted (data not shown). Methyl glyoxal was not quantified. Trace quantities of biacetyl were also observed.

## *Calculations of Yields from the O3-Isoprene Reaction*

Simulations were carried out varying product spectra from the $O_3$-isoprene reaction and other reactions: 1) to ascertain the importance of the peroxy radicals ($RO_2$ and $HO_2$) formed by the OH-isoprene reaction in the absence of $NO_x$ on OH concentrations in the $O_3$/isoprene system and their effect, if any, on the observed product distribution; 2) to find the OH produced by the $O_3$-isoprene reaction necessary to explain the methyl cyclohexane loss data; 3) to determine the actual product yields from the $O_3$-isoprene reaction itself, taking into account the OH-isoprene reaction, product - $O_3$ and product - OH reactions; and 4) to find the $O(^3P)$ necessary to account for the observed epoxide formation. Simulations were carried out using the mechanism in Table 2, and the computational chemical kinetics scheme, inorganic, and formaldehyde mechanisms of Carter and Atkinson (15). The inorganic portion of the mechanism includes the updates of Atkinson et al. (9). A propene mechanism based on the summary of Atkinson (1) is also included. The products of the

reactions of methacrolein, methyl vinyl ketone, and the two epoxides with $O_3$ and $O(^3P)$, are not included specifically in Table 2. These second generation products are unknown, hence we assumed that they were analogous to the products of isoprene, and assumed the same radical yields and the appropriate hydrocarbon products. As the OH reaction products in the $NO_x$-free system do not affect the OH concentration predicted by the simulation (see below), the OH reactions with product species were all assumed to produce a surrogate peroxy radical (MCHR; see Table 2). These reactions generally have small effects on the outcomes of the simulations as the first generation products do not accumulate to significant concentrations before the termination of the experiments, and the rate constants for their reactions with $O_3$, $O(^3P)$, and OH are smaller than those for isoprene.

### *OH-Isoprene Chemistry in a $NO_x$-Free System*

In the absence of $NO_x$, the OH addition to alkenes results in a suite of alkyl peroxy radicals ($RO_2$). While the chemistry of the species that form in the isoprene-OH reaction has not itself been studied, data for similar but smaller alkyl peroxy radicals, including some that contain secondary and tertiary carbon atoms, are available (1, 16, and references therein). We can therefore make reasonable estimates of the reactions that take place subsequent to the OH-isoprene reaction in the absence of $NO_x$, as in the $O_3$-isoprene experiments. This chemistry is complicated because 6 peroxy radicals are expected from OH addition to isoprene. Four of these result from OH addition to one of the four carbons involved in isoprene's double bonds:

(3) Isoprene + OH ⟶ 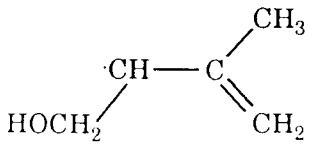 + 3 other isomers

followed by immediate addition of $O_2$ to form ISOH1, 2, 4, and 5:

(4) Isoprene-OH adduct + $O_2$ ⟶ 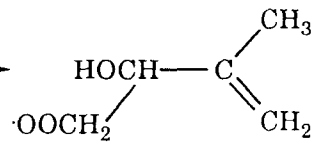

ISOH1

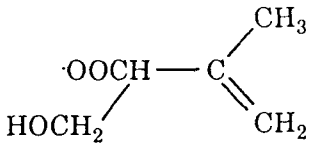

ISOH2

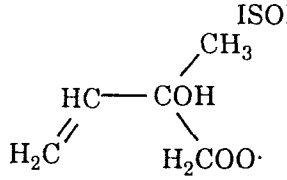

ISOH4

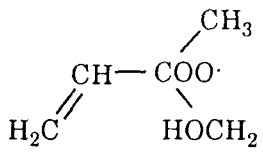

ISOH5

The other two alkyl peroxy radicals are expected to form from addition of $O_2$ to the terminal carbon of the allyl radicals which result from OH addition to the isoprene's 1- or 4- carbons (ISOH3 and 6):

(5) 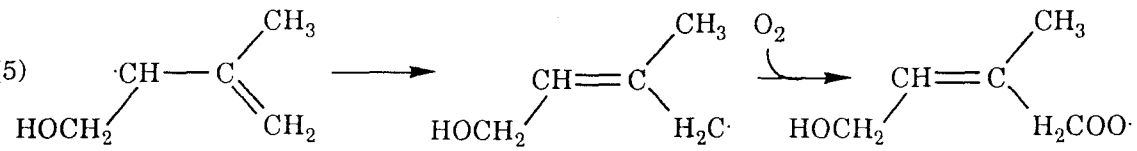

ISOH3

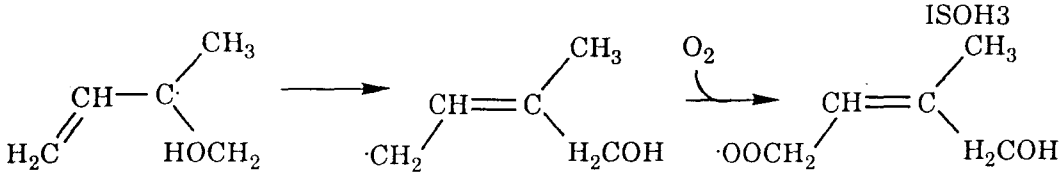

ISOH6

In general these alkyl peroxy radicals react as follows ((1), (16), and references therein):

(6) ISOH1 + ISOH2 ⟶ 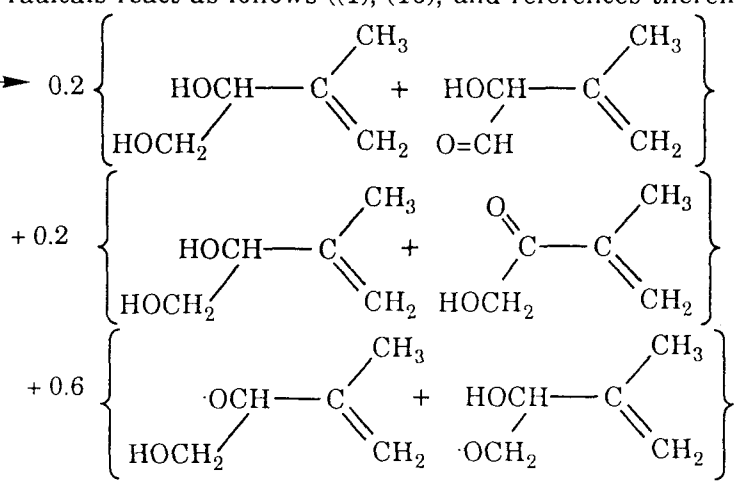

The first two pairs of products are a mixture of dihydroxy and hydroxy carbonyl compounds, and are accounted for in the simulations as DIOH and CAROH, respectively. The final pair of products, the alkoxy radicals, is expected to mostly decompose, to give for example methacrolein, formaldehyde, and $HO_2$, e.g.,

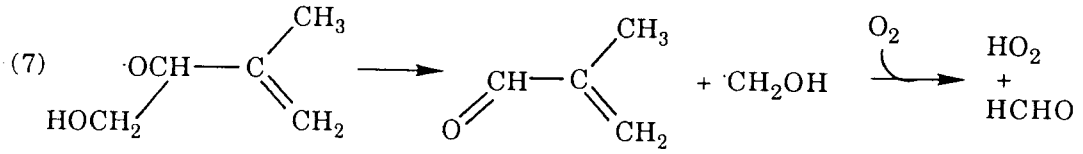


(Methacrolein)

However, it is likely that the small quantities of 3-methyl furan in this system are formed via isomerization of hydroxy alkoxy radicals, followed by a dehydration step. Each of the alkyl peroxy radical permutation reactions is included explicitly in Table 2, except for the self reactions of ISOH2 and 5, which are expected to be negligible because of the very slow combination rates for secondary and tertiary alkyl peroxy radicals. The alkyl peroxy radical combination reactions form 0.6 methacrolein, 0.6 $HO_2$, and 0.6 formaldehyde per ISOH1 or ISOH2 reacted, 0.6 each methyl vinyl ketone, 0.6 $HO_2$, and 0.6 formaldehyde per ISOH4 reacted, and 1.0 each methyl vinyl ketone, 1.0 $HO_2$, and 1.0 formaldehyde per ISOH4 reacted. The remainder of the ISOH1, 2 and 4, as well as all of ISOH3 and ISOH6 result in formation of various dihydroxy and dicarbonyl compounds (1, 16). The alkyl peroxy radicals also react with $HO_2$ to form an organic peroxide:

(8) $RO_2\cdot + HO_2\cdot \rightarrow ROOH + O_2$

This reaction is about an order of magnitude faster than the fastest $RO_2$-$RO_2$ reactions (e.g. reaction 6)(1, 13), hence this is an important sink for both $HO_2$ and $RO_2$. The reactions of the organic peroxides with OH are rather slow (16), however the isoprene-derived organic peroxides will still have a labile double bond. We assumed attack at the double bond, and OH and $O_3$ rate constants that were the average of methacrolein and methyl vinyl ketone rate constants for these reactions. We also assumed the product of the OH-peroxide reaction was the generalized alkyl peroxy radical which does not lead to formation of methacrolein or methyl vinyl ketone, i.e., MCHR (see Table 2). Analogous chemistry was assumed for the methyl cyclohexane - OH reaction products (Table 2). Reactions (6) and (7) and their analogous reactions return an average of 0.54 $HO_2$ molecules per OH reacted. In the absence of $NO_x$, the pathway for conversion of $HO_2$ to OH is:

(9) $HO_2\cdot + O_3 \rightarrow OH\cdot + 2O_2$ ,

however this reaction is fairly slow. Instead, $HO_2$ reacts primarily with the alkyl peroxy radicals and formaldehyde, and to a lesser degree with itself.

Calculations with the above alkyl peroxy radical chemistry indicate that the largest fraction of the $RO_2$ ends up as organic peroxides, with much of the remainder forming dihydroxy and carbonyl hydroxy compounds. The methacrolein and methyl vinyl ketone yields are fairly small; these pathways account for 20% or less of the OH-isoprene reaction, or 8% or less of the total reacted isoprene, and only about half of these reactions result in formation of methacrolein or methyl vinyl ketone. Hence, the $O_3$ reaction must be responsible for the majority of the methacrolein and methyl vinyl ketone observed, and the apparent increase in yields of these compounds with addition of methyl cyclohexane and subsequent OH scavenging, can be understood (Figs. 7 and 8).

## *OH Radical Yield*

Simulations with the mechanism in Table 2 indicate that OH formation in this reaction system does not result from secondary reactions. Both the alkyl peroxy radical reactions (6 and 7) and reaction (9) are too slow to produce significant quantities of OH. Even if, for example, the products of reaction (4) were incorrect and this reaction led instead to quantitative production of the OH radical, reaction (4) would have only a minor (e.g. less than 1%) effect on the predicted OH concentrations. Further, reaction (9) is too slow to convert $HO_2$ effectively to OH; tripling the $HO_2$ produced in the initial $O_3$/isoprene (reaction (1)) increases the OH concentrations by only a few percent. Further, the simulations indicate that because reaction (9) is slow, OH formation in the system is essentially independent of two orders of magnitude variation in the $O_3$ concentration. This is important in the batch reactor - smog chamber in which reactive compounds such as

isoprene and ozone cannot be perfectly mixed, hence concentration gradients of both $O_3$ and isoprene occur.

All of the available evidence indicates that the OH that forms in the $NO_x$-free $O_3$-isoprene system can come only from the $O_3$-isoprene reaction itself, or some hitherto undiscovered OH generation pathway. Simulations revealed that 0.68 ± 0.15 molecule of OH produced per isoprene reacted necessary to explain the methyl cyclohexane loss observed. The mechanism predictions are shown with the data in Figs. 1-5. This OH yield means that in the $O_3$/isoprene system, in the absence of added alkane, about 41% of the isoprene reacts with OH. Niki et al. (2) oxidized tetramethyl ethylene with $O_3$, and concluded that this reaction also produced copious quantities of OH, about 0.7 OH per $O_3$ - tetramethylethylene reacted, consistent with our results. It is impossible to infer anything about the $HO_2$ produced by the $O_3$-isoprene reaction based on methyl cyclohexane loss, because of the slow rate of conversion of $HO_2$ to OH (reaction (9)).

## *Epoxide Formation from the Ozone-Isoprene Reaction*

Epoxides have been observed before in small concentrations from many ozone-alkene reactions, including those of ethene and trans-2-butene (11). It is clear from the analysis above that $O(^3P)$ is not introduced into the chamber from the ozone generator. Initially we assumed that the epoxides (2-ethenyl 2-methyl oxirane and 2-(1-methylethenyl) oxirane) that formed in these ozone experiments resulted from a direct rearrangement of the molozonide:

(10)

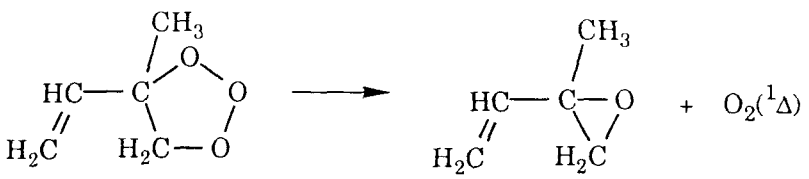


(2-ethenyl 2-methyl oxirane)

This reaction has been observed in the liquid phase (17) and is thermochemically reasonable (18). However, experimental evidence points to direct production of $O(^3P)$ from the Criegee biradical, which then reacts with isoprene to form the epoxides, as proposed by Herron et al. (19);

(11)

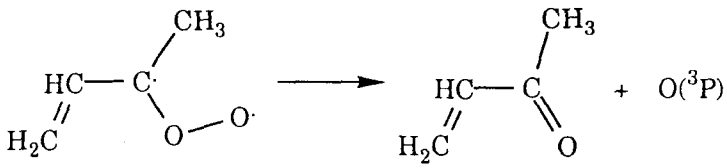

(methyl vinyl ketone)

Strong evidence in support of this mechanism in the $O_3$ oxidation of trans-dichloroethylene has been provided by Niki et al. (20) who inferred about a 20% yield of $O(^3P)$ via this mechanism. It has been implicated to occur to some degree (0-20%) in the tetramethylethylene system as well (2,13), and to a small degree (<5%) from the $O_3$ reaction with trans-2-butene (14).

In separate experiments (discussed in Part 1), we measured the stable and radical products of the $O(^3P)$ reaction with isoprene. A summary of the products is included in Table 3; 84% of the reacted isoprene can be accounted for by the sum of the two epoxides. For the ozone experiments, the observed ratio of 2-(1-methylethenyl) oxirane to 2-ethenyl 2-methyl oxirane is 0.32±.05, matching the ratio measured for the $O(^3P)$ reaction, 0.33±.03. The vast majority of $O_3$ attack takes place on isoprene's unsubstituted double bond, as evidenced by the dominance of methacrolein over methyl vinyl ketone as the major product of the isoprene-$O_3$ reaction by a factor of 2.7, as well as the ratio of the rate constants of the reactions of methacrolein and methyl vinyl ketone with $O_3$ (3.8). Clearly, isoprene's unsubstituted double bond is the favored point of $O_3$ attack by about a factor of 3. If the oxides resulted directly from the breakdown of the molozonide (reaction 10), much more 2-(1-methylethenyl) oxirane than 2-ethenyl 2-methyl oxirane would be expected; just the

opposite of what is observed. Further, unknown 1, which appears to be characteristic of the $O(^3P)$ reaction with isoprene, is also observed in the $O_3$ system.

$O_2$ competes effectively with isoprene for $O(^3P)$, so that the amount of isoprene reacting with $O(^3P)$ rather than $O_3$ in this system is rather small; about 4.7%, however, the $O(^3P)$ yield from the $O_3$ reaction necessary to account for the inferred $O(^3P)$ concentration in the system is large. Calculations indicate that 45 ± 20% of the isoprene that reacts with $O_3$ (with OH taken into account) must produce one $O(^3P)$ to explain the observed epoxide formation. Simulations of the 2-ethenyl 2-methyl oxirane and 2-(1-methylethenyl) oxirane formation are also included in Figs. 1-5. It should be noted that the uncertainty in the $O(^3P)$ yield arises from the dependance of this number on the $O(^3P)$/isoprene rate constant, which was estimated based on the isoprene/OH rate constant (see Table 2, and Part 1). This yield (0.45) is higher than other reported $O(^3P)$ yields that ranged from 5-20% (above). The uncertainties for all of the $O(^3P)$ yields are fairly large, however, and previous reports of $O(^3P)$ yields may have been complicated by OH reactions in those systems, suppressing the apparent $O(^3P)$ yields.

## *Carbonyl Yields*

The apparent yield of methacrolein (Fig. 7) in the absence of methyl cyclohexane is about 37%, calculated on a per molecule reacted isoprene basis, increasing to about 52% upon the addition of large quantities of methyl cyclohexane. Kamens et al. (6) and Niki et al. (7) measured methacrolein in the simple $O_3$-isoprene system and found a methacrolein yield of 41% and >33% respectively, in good agreement with our value of 37%, indicating that, if anything our data slightly underestimate the actual yields. Similarly, the methyl vinyl ketone yield is 17% in the absence of methyl cyclohexane, rising to about 22% (Fig. 8) with the addition of large quantities of methyl cyclohexane, in good agreement with that of Kamens et al.,18% and Niki et al., >13%. The yields observed in the experiments with

large concentrations of methyl cyclohexane should approach the true yields, but as some OH reacted with isoprene even in experiment MIO33, the true yields may be higher than any of these values. The observation that methacrolein and methyl vinyl ketone yields increase as OH is removed is further consistent with the simulation result that the isoprene-OH reaction in the absence of $NO_x$ itself leads to the formation of relatively small quantities of methacrolein or methyl vinyl ketone (via reactions 3-8).

Simulated methacrolein and methyl vinyl ketone concentrations that include the losses of these species to OH and $O_3$ and $O(^3P)$ as they are formed, as well as the proportions of isoprene reacting with OH and $O_3$, are shown in Figs. 1-5. Simulations indicate that the methacrolein yield from the $O_3$-isoprene reaction is 67 ± 9%. For methyl vinyl ketone, the yield is 26 ± 6%. A propene yield of 7 ± 3% fits the data nicely. The reported uncertainties reflect a combination of experimental uncertainties that range from 5% (methacrolein) to 30% (propene) with an estimated calculation error of 10-20%, which accounts for the uncertainties in the rate constants for each compound, combined with the small uncertainties in the reaction temperatures and those that are inherent in the numerical analysis. The yields summarized in Table 3 represent the actual yields necessary to account for the carbonyls, epoxides, and other products that were observed as well as the methyl cyclohexane reacted. The calculated yields of methacrolein, methyl vinyl ketone, and propene are all significantly higher than those observed even in the experiments with added methyl cyclohexane. This arises from two superimposed phenomena: the presence of OH in the system and the reactions of the products themselves with ozone and OH. For example, in the absence of the OH-isoprene reaction, the calculated yields necessary to explain the 0.37 and 0.17 methacrolein and methyl vinyl ketone observed yields would be about 0.53 and 0.21, respectively, due purely to reaction of these compounds with $O_3$ and/or OH. Consequently, the calculated yields are highly sensitive to the uncertainties in the rate constants listed in Table 1. While these results may not necessarily be

mechanistically accurate, e.g. OH may not in fact come directly from the $O_3$-isoprene reaction, they do represent an accurate parameterization of the product distribution of the ozone-isoprene reaction.

## *Ozone-Isoprene Oxidation Mechanism*

Despite extensive mechanistic work on the breakup of the ozonide (2, 3, 6, 7, 11, 12, 13, 14, 18, 19) a mechanism has yet to be developed that can satisfactorily explain the large quantities of OH that clearly form in the $O_3$-alkene systems, the formation of carbonyls (methacrolein and methyl vinyl ketone), propene, and epoxides (2-ethenyl 2-methyl oxirane and 2-(1-methylethenyl) oxirane). In an effort to construct a mechanism that accounts for all of the available data, we propose the following mechanism for the ozone oxidation of isoprene:

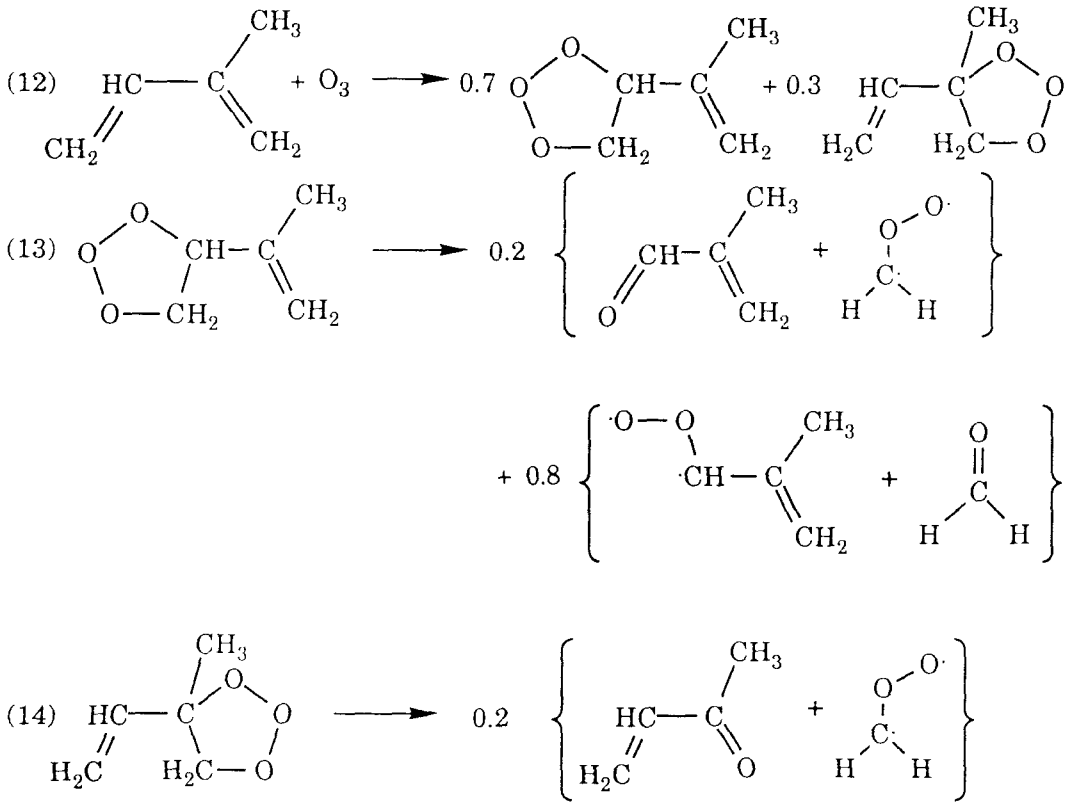

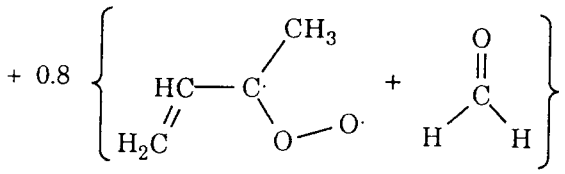

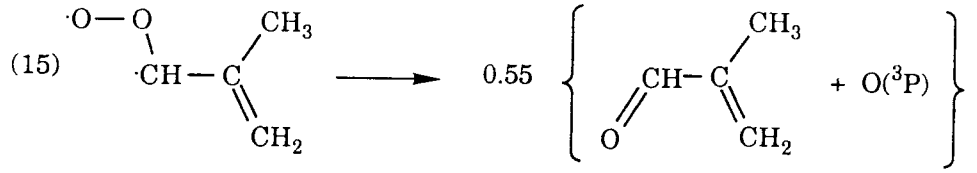

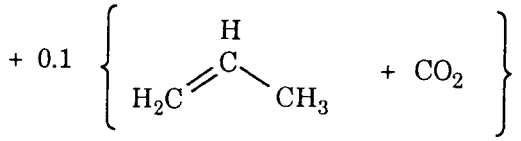

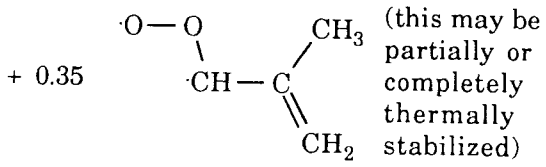


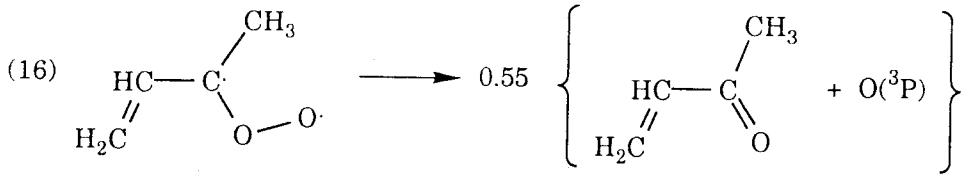

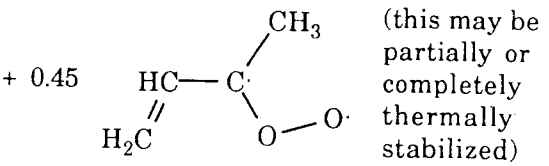


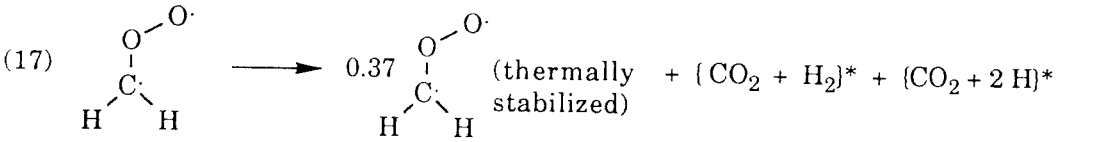


* Coefficient unspecified

This mechanism assumes that the initial $O_3$ attack occurs primarily at the unsubstituted double bond. The ratio is inferred from the yields of methacrolein and methyl vinyl

ketone, and is nearly equal to that predicted by the rate constants of the methacrolein and methyl vinyl ketone reactions with $O_3$. The molozonides have generally been assumed to form equal quantities of the C1 and C4 Criegee (reactions 2, 14 and 15)(1 and references therein), in the absence of information to the contrary. The larger Criegees are expected to be more stable, hence the molozonide might be expected to decompose favoring the C4 Criegee plus formaldehyde. Further, Kamens et al. (6) and Niki et al. (7) measured the formaldehyde yield from the ozone-isoprene reaction, and found 90±5% and 85%, respectively, uncorrected for OH. Niki et al. (7) used isotopically labeled ozone and determined that about 69% of this formaldehyde arose from reactions of $O_3$ itself, rather than secondary chemistry. It appears that the formaldehyde yield from the $O_3$ -isoprene reaction, even in the absence of OH correction, exceeds 50%, consistent with our hypothesis that isoprene's molozonides decompose in favor of the C4 Criegee plus formaldehyde. Hence we have arbitrarily assumed that this pathway is 80%, and the C1 Criegee plus C4 carbonyl 20% (reactions 14 &15). The sources of formaldehyde are the $O_3$ reaction itself, the methacrolein and methyl vinyl ketone-$O_3$ reactions, and the reactions of the alkyl peroxy radicals. Whether the OH initiated alkyl peroxy radical reactions produce labelled formaldehyde is unclear, although it should be at least partially unlabeled. Our simulations with the assumption of an 80% yield from the $O_3$-isoprene reaction in fact underpredicted the formaldehyde observations, showing 50 to 60% formaldehyde yields (depending on the amount of isoprene reacted), with about 80% arising from the $O_3$-isoprene reaction, 18-20% from the alkyl peroxy radical reactions, and 0.5-3% from $O_3$ reactions with the carbonyls. To account for the $O(^3P)$ that reacts to form the epoxides, we have assumed that 55% of the C4 Criegees break down to form carbonyl plus $O(^3P)$ (reactions 17 and 18). This gives a total of 0.45 $O(^3P)$ per isoprene reacted, but only 0.45 methacrolein and 0.19 methyl vinyl ketone. The remainder of the Criegee biradicals form propene, react to provide a source of OH, or become collisionally stabilized and react via the rather slow Criegee reactions (reactions 33-37, Table 2). This mechanism accounts

for the observed yields of methacrolein, methyl vinyl ketone, and propene, as well as 0.35 $O(^3P)$, 0.42-0.6 OH, if we assume reaction (19), below. The OH formation still needs to be accounted for.

Several groups have suggested OH may come from Criegee intermediates via abstraction of the ß-hydrogen atom and intermediate formation of a hydroperoxide, e.g.:

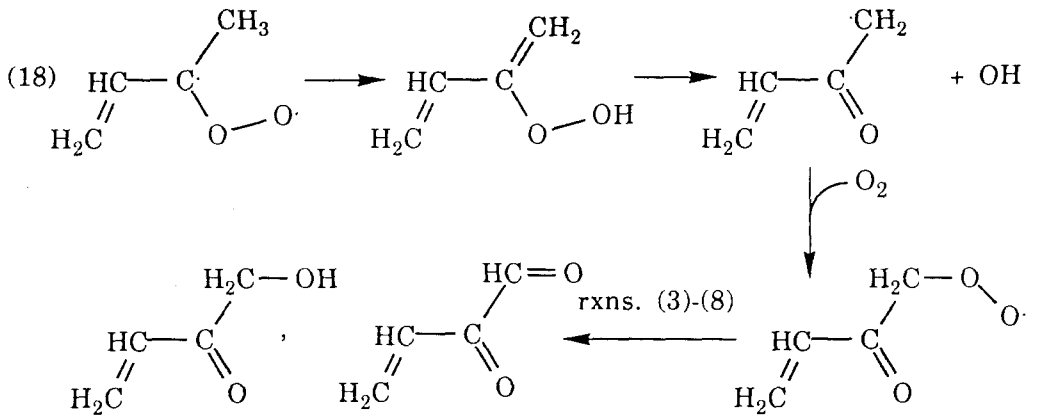


However, this fails to explain OH formation in the isoprene system because 1) an H atom is available for the peroxide formation for only one of isoprene's Criegee intermediates (shown above), and 2) it produces only one OH per reaction; hence 60% of the isoprene must go through the pathway that begins with $O_3$ attack on the substituted double bond. The substituted double bond is clearly the less favored point of $O_3$ attack, as evidenced by: 1) the methacrolein and methyl vinyl ketone rate constants (Table 2), and 2) the dominance of methacrolein over methyl vinyl ketone as the major product of the isoprene-$O_3$ reaction. Further, we have found 100 ± 18% of the products are carbonyls plus propene, none of which could be formed via reaction 18.

We propose two sources of OH; a small amount, probably only a few percent, from the C1 Criegee via the decomposition channel producing HCO and OH (7, 14), and reaction 19:

(19) 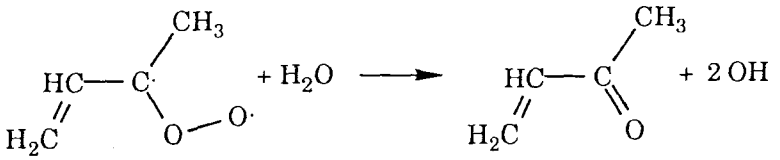

Several lines of evidence support this pathway. It is the only pathway that is consistent with all of our other data; e.g., predicting (i) the observed yields of methacrolein, methyl vinyl ketone, epoxides, propene (this work) and formaldehyde (6,7), and (ii) predicting the concentrations of OH that have been observed (this work, 2). To be thermochemically plausible, the biradical must be in its initial excited state; otherwise the reaction is overall slightly uphill (~8 kcal/mol). Reaction 19 is a bimolecular reaction; Niki et al. (2) have indicated that these biradicals may have to be thermally stabilized in order to undergo bimolecular reactions, however this would make the reaction thermodynamically unfavorable. Several groups have indirectly measured stabilized biradical yields, and seem to have observed decreases for substituted double bonds; e.g. Hatakeyama (12) found ethene, propene and trans-2-butene yielded 39, 25.4, and 18.5 percent stabilized biradical respectively, and Niki et al. (2) found 25-30% for 2,3-dimethyl 2-butene. Further, several studies have provided evidence that the reaction of the thermally stabilized biradicals with $H_2O$ may give an organic acid plus $H_2O$ (21, 22, 23). Despite observations of decreasing stabilized biradicals with increasing carbon number, the large biradicals should be more able to survive until they undergo collisional destabilization than smaller ones. Perhaps the above reaction explains why they have not been observed.

An alternate mechanism for OH formation is the thermodynamically favorable reaction of the Criegee biradicals with $HO_2$:

(20) 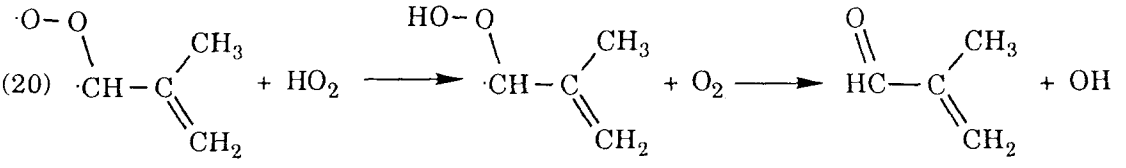

This pathway however both depends on large quantities of $HO_2$ , and produces only one OH per reaction. Using this reaction together with the mechanism in Table 2, we were unable to account for more than about 25% of the OH observed, regardless of the rate constant assumed. While this reaction may well occur, when combined with the other chemistry of this system, it cannot account for the OH observed.

# *Conclusions*

The ozone-isoprene reaction appears on the surface like any other ozone-alkene reaction, producing close to 50% carbonyls, and some propene, as expected from the decomposing Criegee biradical. Addition of methyl cyclohexane to the reaction, in combination with careful consideration of the oxygenated products, including the epoxides, reveals a different picture of the free radical and carbonyl production in the system. The OH yield is nearly 70%, and the yield of $O(^3P)$ about 45%, while the carbonyls plus propene total 100%. The epoxides form from the secondary reaction of $O(^3P)$ with isoprene. The yields of $O(^3P)$ and OH are probably not restricted to isoprene. While OH formation has been fairly well characterized for ethene, and seems to be minimal, this result cannot be extrapolated to larger alkenes. In addition to our finding, an OH yield of 70% was observed for tetramethylethylene (2). Significant quantities of OH have also been observed for propene (3,4), isobutene (3), and as well from the much larger terpenes (5). Clearly for alkenes $C_3$ and larger, OH formation becomes very important, although the mechanism of its formation remains unclear. Epoxides, tracers for $O(^3P)$ formation, have been observed in many systems, including ethene and trans-2-butene (11). It is very likely that $O(^3P)$ formation has been largely overlooked, but occurs in all ozone reactions with alkenes, large or small. Because of both the interference from OH and $O(^3P)$, and the reactions of products with $O_3$ and OH, the carbonyl yields for isoprene are higher than they appear in

the standard ozone-alkene experiments. Measured carbonyl yields in previous studies from most alkene-$O_3$ reactions probably suffer from the same artifacts, and are in fact much higher than generally believed. Our results, combined with the formaldehyde measurements of Kamens et al. (6) and Niki et al. (7), indicate that non-symmetric molozonides do not decompose 50% each way, but instead favor the $C_4$ Criegee plus formaldehyde. The large quantities of OH and $O(^3P)$ make the $O_3$ reaction more important both in smog chamber studies and in the atmosphere.

# *Acknowledgments*

This work was supported by National Science Foundation Grant ATM-9003186. One of the authors (S.E.P.) gratefully acknowledges the support of a Dissertation Fellowship from the American Association of University Women. The authors also appreciate helpful discussions with R. Atkinson and W.P.L. Carter of the University of California at Riverside.

# *References*

(1) Atkinson, R. *Atmospheric Environment* **24A**, 1 (1990).

(2) Niki, H., P.D. Maker, C.M. Savage, L.P. Breitenbach, and M. D. Hurley *J. Amer. Chem. Soc.* **91:**941 (1987).

(3) Herron, J.T., and R.E. Huie *Int'l J. Chemical Kinetics* **10**, 1019 (1978).

(4) Japar, S.M., C.H. Wu, and H. Niki *J. Phys. Chem.* **80**, 2057 (1976).

(5) Atkinson, R., D. Hasegawa, and S.M Aschmann *Int'l J. Chemical Kinetics* **22**, 871 (1990).

(6) Kamens, R. M., M. W. Gery, H. E. Jeffries, M. Jackson, E. I. Cole *Int'l J. Chemical Kinetics* **14**, 955 (1982).

(7) Niki, H., P.D. Maker, C.M. Savage, and L.P. Breitenbach *Environ. Sci. Technol.* **17**, 312a-322a (1983).

(8) Pandis, S.N., S.E. Paulson, R.C. Flagan, and J.H. Seinfeld *Atmospheric Environ.* **25a**, 997 (1991).

(9) Smith, D. and N. G. Adams, Studies of Ion-Ion Recombination using Flowing Afterglow Plasmas, In: The Physics of Ion-Ion and Electron-Ion Collisions, Eds. F. Brouillard and J. W. McGowan, Plenum Press (1983).

(10) Atkinson, R., D.L. Baulch, R.A. Cox, R.F. Hampson Jr., J.A.Kerr, and J. Troe *Int'l J. Chemical Kinetics* **21,** 115 (1989).

(11) Martinez, R.I., J. T. Herron and R. E. Huie *J. Amer. Chem. Soc.* **103,** 3807(1981).

(12) Hatakeyama, S., H. Kobayashi, and H. Akimoto *J. Phys. Chem.* **88**, 4736 (1984).

(13) Martinez, R.I., and J. T. Herron *J. Phys. Chem.* **91**, 946 (1987).

(14) Martinez, R.I., and J. T. Herron *J. Phys. Chem.* **92,** 4644 (1988).

(15) Carter, W., and R. Atkinson, Development and implementation of an up-to-date photochemical mechanism for use in airshed modeling, Summary final report, Calif. Air Resources Board,(1988).

(16) Madronich, S. and J. G. Calvert *J. Geophys. Res.* **95**, 5697 (1990).

(17) Criegee, R. *Agnew. Chem. internat. Edit.* **14**, 745 (1975).

(18) Harding, L. B. and W. A. Goddard III *J. Amer. Chem. Soc.* **100:23**, 7180 (1978).

(19) Herron, J. T., R.I. Martinez, and R.E. Huie *Int'l J. Chemical Kinetics* **14**, 201 (1982).

(20) Niki, H., P.D. Maker, C.M. Savage, and L.P. Breitenbach, and R.I. Martinez *J. Phys. Chem* **88**, 766-769 (1983).

(21) Cox, R.A., and S.A. Penkett, *J. Chem. Soc. Farad. Trans. I* **68**, 1735 (1972).

(22) Calvert, J.G., F. Su, J.W. Bottenheim, and O.P. Strauss *Atmos. Environ.* **12**, 197 (1978).

(23) Hatakeyama, S., H. Bandow, M. Okuda, and H. Akimoto *J. Phys. Chem.* **85**, 2249 (1981).

(24) Atkinson, R., S.M. Aschmann, A. M. Winer and J.N. Pitts *Int'l J. Chemical Kinetics* **13,** 1133 (1981).

(25) Atkinson R. *Chemical Rev.* **19**, 799 (1985).

*Table 1.*

*Summary of Initial Conditions*

| Expt.* | Initial Concentration (ppm) | | |
|---|---|---|---|
| | Isoprene | Methyl cyclohexane | R(see text) |
| IO32 | 9.98 | 0 | 0 |
| IO33 | 11.05 | 0 | 0 |
| IO34 | 11.34 | 0 | 0 |
| MIO31 | 14.08 | 13.81 | 0.981 |
| MIO32 | 14.04 | 123.8 | 8.82 |
| MIO33 | 13.01 | 225 | 17.3 |
| MIO34 | 16.71 | 104.7 | 6.27 |

*Experiments are numbered as follows: hydrocarbon(s) (1 letter each), primary oxidant (up to 3 letters) and a number differentiating experiments of a given type.

## *Table 2.*

## *Ozone and OH - Isoprene Chemistry in a NOx -Free System*

| Rate constant at 298 K | Activation energy (K) | Reactants | Products | Reference for rate constant | Reference for product spectrum |
|---|---|---|---|---|---|
| 1) 1.43E-17 | 2013 | isoprene + $O_3$ → | 0.67 methacrolein + 0.26 methyl vinyl ketone + 0.45 O + 0.68 OH + 0.07 propene + 0.07 $CO_2$ + 0.074 CHO2 + 0.03 CAO2 + 0.03 CVO2 + 0.8 HCHO + 0.19 CO + 0.06 $HO_2$ | 1,a | |
| 2) 1.01E-10 | -410 | isoprene + OH → | 0.126 ISOH1 + 0.194 ISOH2 + 0.1 ISOH3 + 0.174 ISOH4 + 0.268 ISOH5 + 0.138 ISOH6 | 1,a | |
| 3) 5.8E-11 | | isoprene + O → | 0.63 2-ethenyl 2-methyl oxirane + 0.22 2-(1-methylethenyl) oxirane + 0.085 I3PR + 0.12 UKNOWN 1 | b,a | |
| 4) 2.E-13 | | ISOH1 + ISOH1 → | 1.2 methacrolein + 0.4 DIOH + 1.2 HCHO + 0.4 CAROH + 1.2 $HO_2$ | 16,16 | |
| 5) 2.53E-14 | | ISOH1 + ISOH2 → | 1.2 methacrolein + 0.4 DIOH + 1.2 HCHO + 0.4 CAROH + 1.2 $HO_2$ | 16,16 | |
| 6) 2.E-13 | | ISOH1 + ISOH3 → | 0.6 methacrolein + 1.2 $HO_2$ + 0.4 DIOH + 1.0 CAROH+ 0.6 HCHO | 16,16 | |
| 7) 2.53E-14 | | ISOH2 + ISOH3 → | 0.6 methacrolein + 1.2 $HO_2$ + 0.4 DIOH + 1.0 CAROH + 0.6 HCHO | 16,16 | |
| 8) 2.E-13 | | ISOH1 + ISOH4 → | 0.6 methacrolein + 1.2 $HO_2$ + 0.4 DIOH + 0.4 CAROH + 1.2 HCHO + 0.6 methyl vinyl ketone | 16,16 | |
| 9) 4.9E-15 | | ISOH1 + ISOH5 → | 0.9 methacrolein + 1.8 HO2. + 0.1 DIOH + 0.1 CAROH + 1.8 HCHO + 0.9 methyl vinyl ketone | 16,16 | |

| Rate constant at 298 K | Activation energy (K) | Reactants | Products | Reference for rate constant | Reference for product spectrum |
|---|---|---|---|---|---|
| 10) 2.E-13 | | ISOH1 + ISOH6 → | 0.6 methacrolein + 1.2 HO2. + 0.4 DIOH + 1.0 CAROH + 0.6 HCHO | 16,16 | |
| 11) 2.53E-14 | | ISOH2 + ISOH4 → | 0.6 methacrolein + 1.2 HO2. + 0.4 DIOH + 0.4 CAROH + 0.6 HCHO + 0.6 methyl vinyl ketone | 16,16 | |
| 12) 3.1E-16 | | ISOH2 + ISOH5 → | 0.9 methacrolein + 1.8 $HO_2$ + 0.2 DIOH + 0.1 CAROH + 1.8 HCHO + 0.9 methyl vinyl ketone | 16,16 | |
| 13) 2.52E-14 | | ISOH2 + ISOH6 → | 0.6 methacrolein + 0.4 DIOH + 1.2 HCHO + 0.4 CAROH + 1.2 $HO_2$ + 0.6 methyl vinyl ketone | 16,16 | |
| 14) 2.E-13 | | ISOH3 + ISOH3 → | 0.4 DIOH + 1.2 HCHO + 1.6 CAROH + 1.2 $HO_2$ | 16,16 | |
| 15) 2.E-13 | | ISOH3 + ISOH4 → | 0.6 methyl vinyl ketone + 1.2 HO2. + 0.4 DIOH + 1.0 CAROH + 0.6 HCHO | 16,16 | |
| 16) 3.1E-16 | | ISOH3 + ISOH5 → | 0.9 methyl vinyl ketone + 1.8 HO2. + 1.9 HCHO + 0.1 DIOH + 1.0 CAROH | 16,16 | |
| 17) 2.E-13 | | ISOH3 + ISOH6 → | 0.4 DIOH + 1.2 $HO_2$ + 1.2 HCHO + 1.6 CAROH | 16,16 | |
| 18) 2.E-13 | | ISOH4 + ISOH4 → | 1.2 methyl vinyl ketone + 0.4 DIOH + 1.2 $HO_2$ + 1.2 HCHO + 0.4 CAROH | 16,16 | |
| 19) 2.E-13 | | ISOH4 + ISOH5 → | 1.8 methyl vinyl ketone + 1.8 $HO_2$ + 1.8 HCHO + 0.1 DIOH + 0.1 CAROH | 16,16 | |
| 20) 2.1E-13 | | ISOH4 + ISOH6 → | 0.6 methyl vinyl ketone + 1.2 $HO_2$ + 1.2 HCHO + 0.4 DIOH + 1.0 CAROH | 16,16 | |
| 21) 4.9E-15 | | ISOH5 + ISOH6 → | 0.9 methyl vinyl ketone + 0.1 DIOH + 1.8 $HO_2$ + 1.8 HCHO + 1.0 CAROH | 16,16 | |

| Rate constant at 298 K | Activation energy (K) | Reactants | Products | Reference for rate constant | Reference for product spectrum |
|---|---|---|---|---|---|
| 22) 2.E-13 | | ISOH6 + ISOH6 → | 0.4 DIOH + 1.2 $HO_2$ + 1.2 HCHO + 1.6 CAROH | | 16,16 |
| 23) 8.E-16 | | MCHR + MCHR → | 1.2 $HO_2$ | | 16,c |
| 24) 3.E-14 | | MCHR + ISOH1 → | 1.2 $HO_2$ + 0.6 methacrolein + 0.6 HCHO + 0.2 DIOH + 0.2 CAROH | | 16,c |
| 25) 3.E-14 | | MCHR + ISOH2 → | 1.2 $HO_2$ + 0.6 methacrolein + 0.6 HCHO + 0.2 DIOH + 0.2 CAROH | | 16,c |
| 26) 3.E-14 | | MCHR + ISOH3 → | 1.2 $HO_2$ + 0.5 DIOH + 0.5 CAROH | | 16,c |
| 27) 3.E-14 | | MCHR + ISOH4 → | 1.2 $HO_2$ + 0.6 methyl vinyl ketone + 0.6 HCHO + 0.2 DIOH + 0.2 CAROH | | 16,c |
| 28) 3.E-14 | | MCHR + ISOH6 → | 1.2 $HO_2$ + 0.5 DIOH + 0.5 CAROH | | 16,c |
| 29) 3.E-12 | 900 | ISOH1, ISOH2, ISOH3, ISOH4, ISOH5, ISOH6 + HO2. = | PERO | | 16,c |
| 30) 3.E-12 | 900 | MCHR+$HO_2$ → | | | 16,c |
| 31) 2.E-11 | | PERO + HO. → | MCHR | | d,c |
| 32) 8.E-18 | | PERO + $O_3$ → | 0.6 HO. + 0.4 O + 0.7 HCHO | | d,e |
| 33) 1.36E-14 | | CVO2 + HCHO → | OZID | | 1,1 |
| 34) 1.36E-14 | | CVO2 + methacrolein → | OZID | | 1,1 |
| 35) 4.E-18 | | CAO2 + $H_2O$ → | ACRAC | | 1,1 |
| 36) 1.36E-14 | | CAO2 + HCHO → | OZID | | 1,1 |
| 37) 1.36E-14 | | CAO2 + methacrolein → | OZID | | 1,1 |
| 38) 4.06E-18 | | methyl vinyl ketone + $O_3$ → | | | 24,e |
| 39) 1.88E-11 | | methyl vinyl ketone + OH → | ISOH1 | | 1,11 |
| 40) 3.1E-12 | | methyl vinyl ketone + O → | | | b,e |
| 41) 1.08E-18 | | methacrolein + $O_3$ → | | | 24,e |
| 42) 7.9E-12 | | methacrolein + O → | 0.9 OX + 0.1 ISOH1 | | b,a |

| Rate constant at 298 K | Activation energy (K) | Reactants | Products | Reference for rate constant | Reference for product spectrum |
|---|---|---|---|---|---|
| 43) 3.1E-12 | | 2-ethenyl 2-methyl oxirane + O → | | | g,e |
| 44) 7.9E-12 | | 2-(1-methylethenyl) oxirane + O → | | | g,e |
| 45) 1.88E-11 | | 2-ethenyl 2-methyl oxirane + OH → ISOH1 | | | g,f |
| 46) 3.35E-11 | | 2-(1-methylethenyl) oxirane + OH → ISOH1 | | | g,f |
| 47) 1.04e-11 | | MCH + OH → MCHR | | | 1,1 |

a) This work.

b) Estimated from correlations between the rate constants of OH and $O(^3P)$ developed by Atkinson (25).

c) MCHR, the alkyl peroxy radical derived from the OH-methyl cyclohexane reaction was assumed to be entirely secondary peroxy radical. Its products are dominated by alcohols and ketones; little formaldehyde is expected. See also text.

d) Average of methacrolein and methyl vinyl ketone rate constants; see also text.

d) Products unknown/assumed to be exactly analogous to the products of isoprene; same radical yields and the appropriate hydrocarbon products. The hydrocarbon products of these reactions are expected to have a negligible effect on any simulation carried out with the mechanism (see text).

e) The products were lumped with the isoprene-OH products.

f) These rate constants were assumed to equal the values for methyl vinyl ketone (2-ethenyl 2-methyl oxirane) and methacrolein (2-(1-methylethenyl) oxirane). Products were also assumed to react in the fashion of the appropriate methacrolein and methyl vinyl ketone derived radicals.

| | |
|---|---|
| ISOH1-ISOH6 | see text |
| O | $O(^3P)$ |
| CHO2 | $H_2C{\cdot}O{-}O{\cdot}$ |
| CVO2 | $CH_2{=}C{-}C{\cdot}(CH_3)O{-}O{\cdot}$ |
| CAO2 | $\cdot O{-}O{-}C{\cdot}H{-}C(CH_3){=}CH_2$ |
| I3PR | $CH_2{=}C{-}CO{\cdot}(CH_3){-}CH_2O{-}O{\cdot}$ + other free radical products (see text, part 1) |
| DIOH | generalized dihydroxy compound; see text |
| CAROH | generalized hydroxycarbonyl compound; see text |
| PERO | generalized organic peroxide |
| OZID | Criegee biradical-aldehyde adduct |

*Table 3.*

*Summary of Product Yields*

| Reaction | Product | Yield (% of Isoprene reacted leading to product) |
|---|---|---|
| $O_3$ + Isoprene | Methacrolein | 67.±9 |
| | Methyl vinyl ketone | 26.±6 |
| | Propene | 7.0±3 |
| | Hydroxyl Radical | 68.±15 |
| | Ground State Oxygen | 45.±20 |
| total ($C_3$ and $C_4$ products of isoprene) | | 100.± 10 |
| $O_3$ + methacrolein, methyl vinyl ketone | Methyl glyoxal | observed but not quantified |
| Alkyl peroxy radical reactions | 3-Methyl Furan | 1. ± .5 |
| Unknown | Biacetyl | trace |
| $O(^3P)$ + Isoprene* | 2-ethenyl 2-methyl oxirane | 63.± 8 |
| | 2-(1-Methylethenyl) oxirane | 22.± 3 |
| | unknown 1 | 11.± 4 |
| | unknown 2 | 1.0± .5 |
| | 2,2 methylbutenal | 1.7± .8 |
| | Organic Radicals | 8.± 3 |
| Total | | 96.8-105.3 |

*See part 1 for a discussion of experiments leading to these yields.

Figure 1. Product yields from experiment IO34; the symbols are data for each product as indicated; the lines of the same pattern are simulation results for the corresponding product. Note that 2-ethenyl 2-methyl oxirane and 2-(1-methylethenyl) oxirane are plotted with respect to the right-hand axis.

Figure 2. Product yields from experiment MIO31; the symbols are data for each product as indicated; the lines of the same pattern are simulation results for the corresponding product. Note that 2-ethenyl 2-methyl oxirane is plotted with respect to the right-hand axis.

Figure 3. Product yields from experiment MIO34; the symbols are data for each product as indicated; the lines of the same pattern are simulation results for the corresponding product. Note that 2-ethenyl 2-methyl oxirane is plotted with respect to the right-hand axis.

Figure 4. Product yields from experiment MIO32; the symbols are data for each product as indicated; the lines of the same pattern are simulation results for the corresponding product. Note that 2-ethenyl 2-methyl oxirane and 2-(1-methylethenyl) oxirane are plotted with respect to the right-hand axis.

Figure 5. Product yields from experiment MIO33; the symbols are data for each product as indicated; the lines of the same pattern are simulation results for the corresponding product. Note that reacted methyl cyclohexane is plotted with respect to the right-hand axis.

Figure 6. The percent of OH which reacts with methyl cyclohexane rather than isoprene for a given ratio of methyl cyclohexane/isoprene. The initial state of each experiment is indicated in the figure. This percentage increases during the course of each experiment.

Figure 7. Methacrolein formed vs. isoprene reacted for all seven experiments.

Figure 8. Methyl vinyl ketone formed vs. isoprene reacted for all seven experiments.

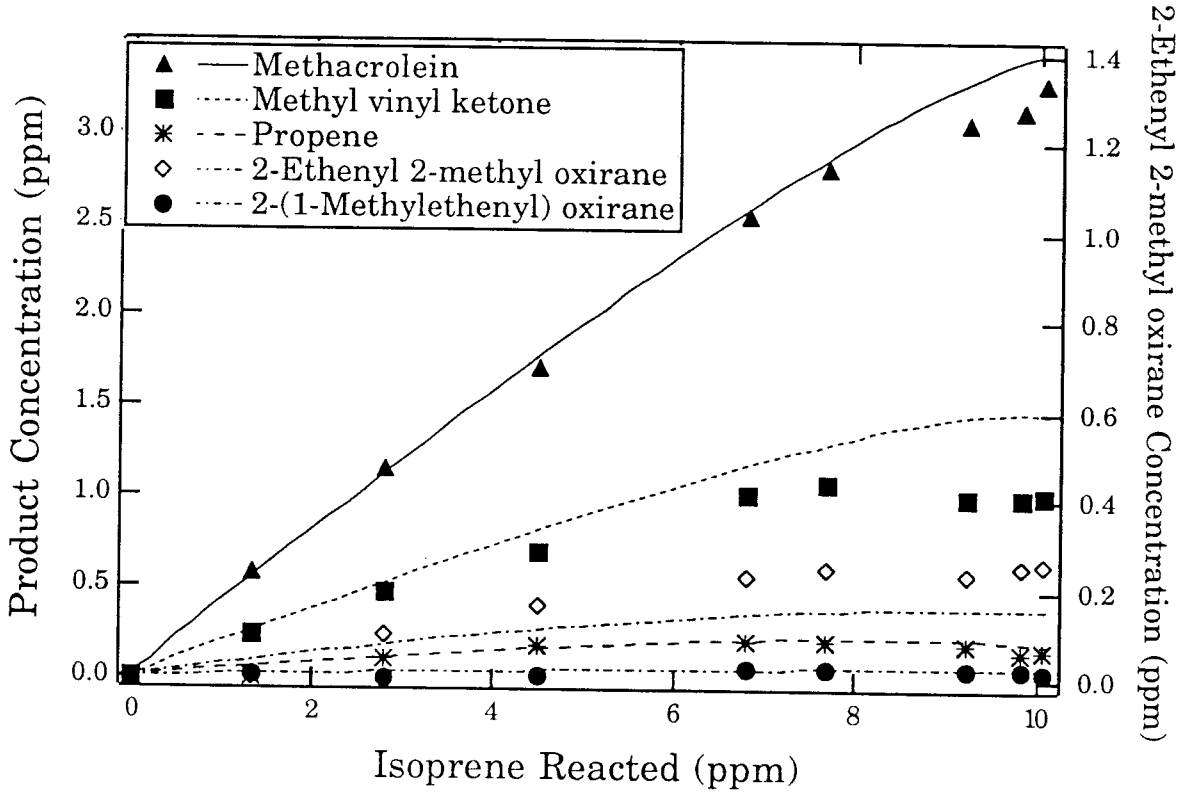
Methacrolein
Methyl vinyl ketone
Propene
2-Ethenyl 2-methyl oxirane
2-(1-Methylethenyl) oxirane
Product Concentration (ppm)
2-Ethenyl 2-methyl oxirane Concentration (ppm)
Isoprene Reacted (ppm)
0.0
0.5
1.0
1.5
2.0
2.5
3.0
0.2
0.4
0.6
0.8
1.2
1.4
0
2
4
6
8
10

Figure 1.

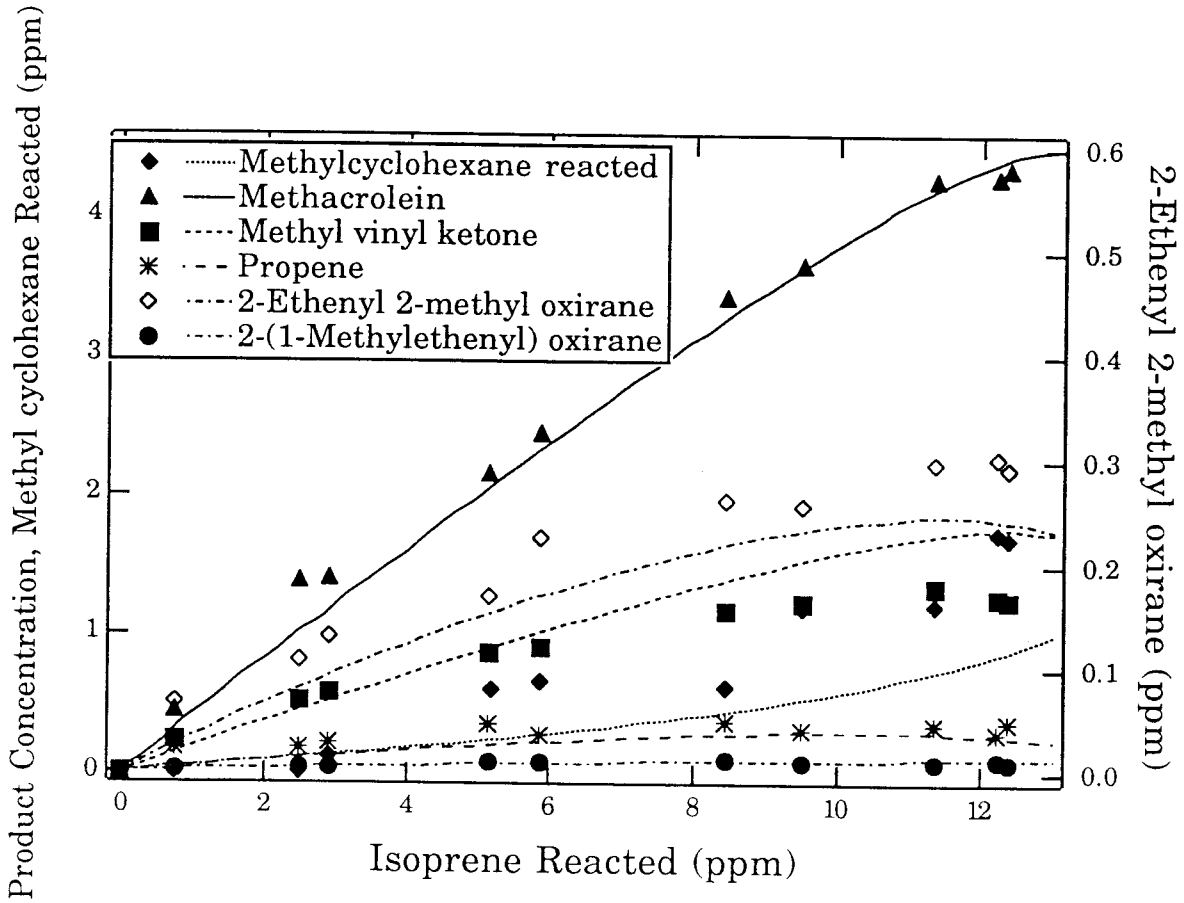
Methylcyclohexane reacted
Methacrolein
Methyl vinyl ketone
Propene
2-Ethenyl 2-methyl oxirane
2-(1-Methylethenyl) oxirane
Product Concentration, Methyl cyclohexane Reacted (ppm)
2-Ethenyl 2-methyl oxirane (ppm)
Isoprene Reacted (ppm)
0
1
2
3
4
0.0
0.1
0.2
0.3
0.4
0.5
0.6
0
2
4
6
8
10
12

Figure 2.

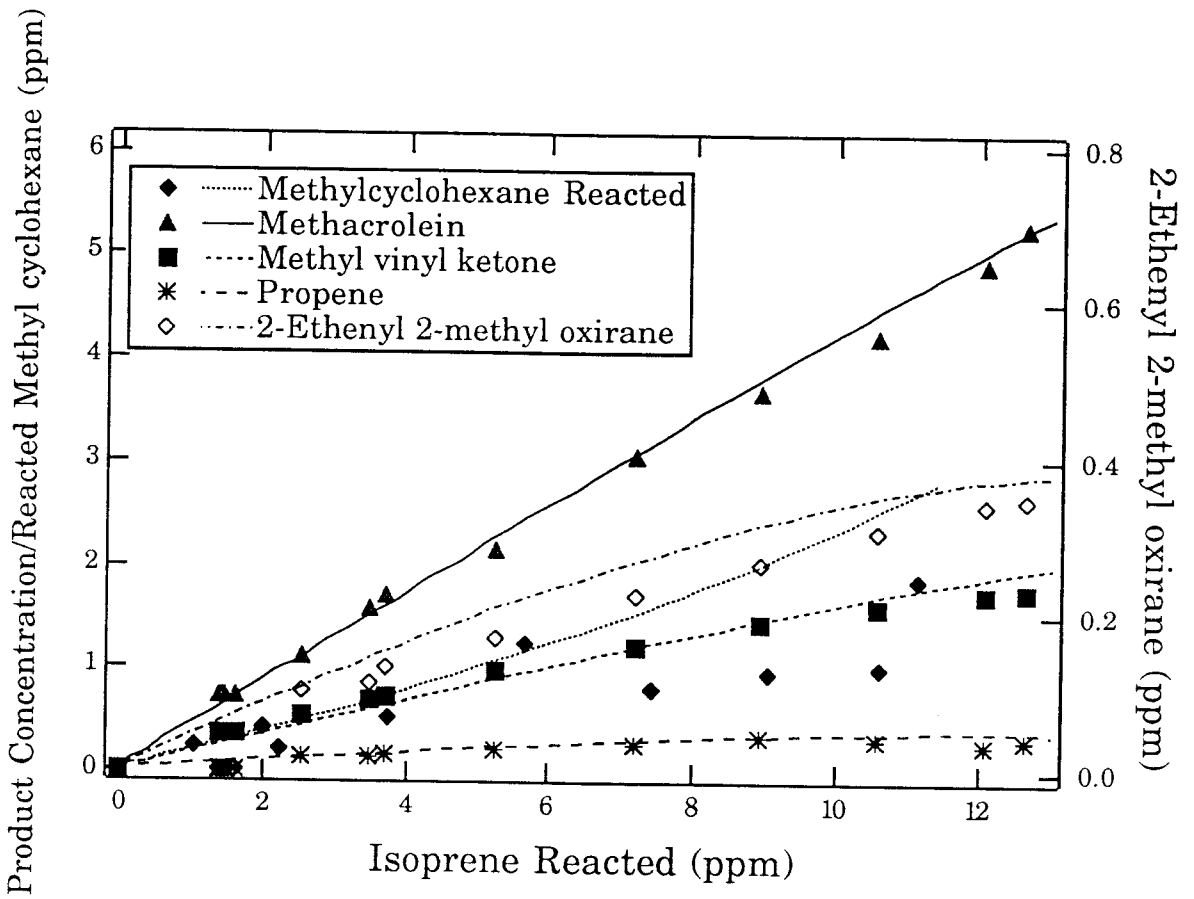
Product Concentration/Reacted Methyl cyclohexane (ppm)
2-Ethenyl 2-methyl oxirane (ppm)
Isoprene Reacted (ppm)
Methylcyclohexane Reacted
Methacrolein
Methyl vinyl ketone
Propene
2-Ethenyl 2-methyl oxirane
0
1
2
3
4
5
6
0.0
0.2
0.4
0.6
0.8
0
2
4
6
8
10
12

Figure 3.

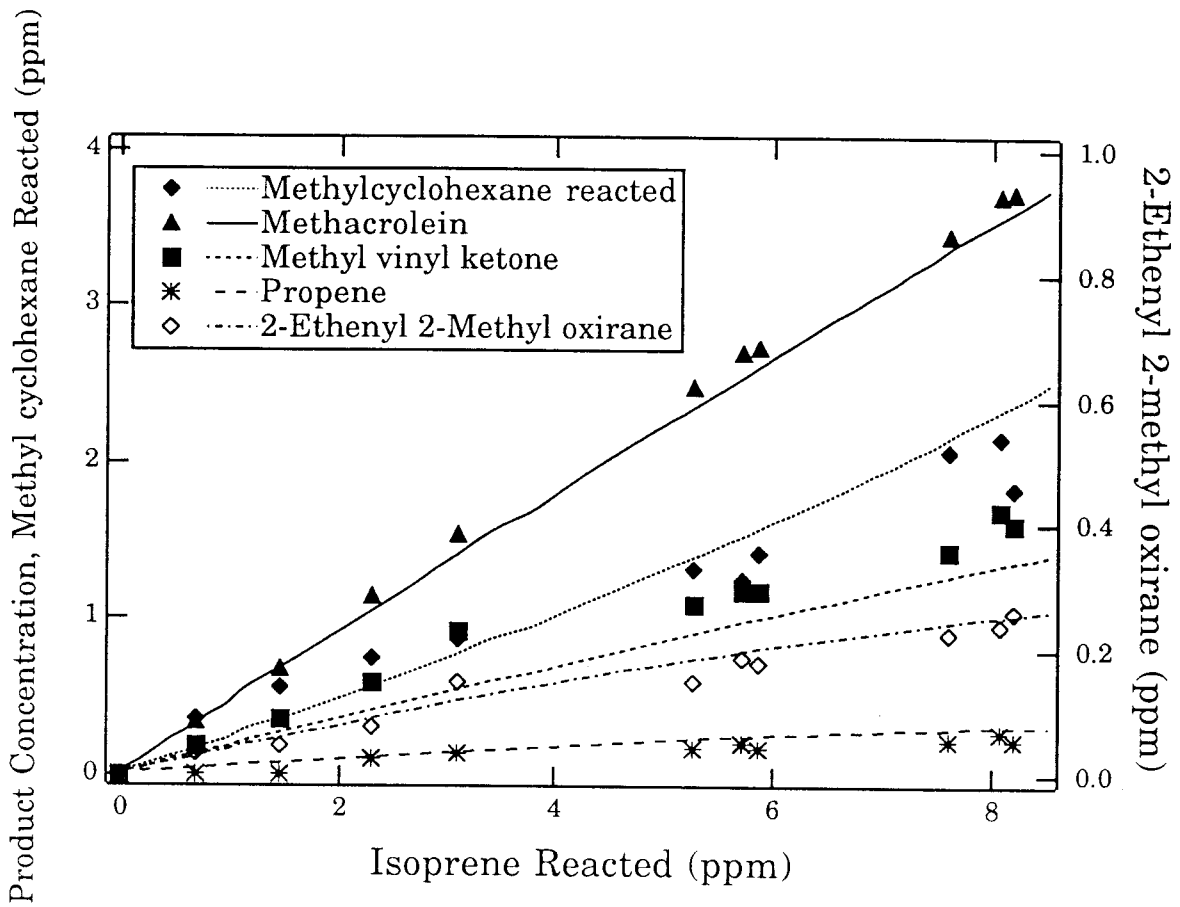
Product Concentration, Methyl cyclohexane Reacted (ppm)
2-Ethenyl 2-methyl oxirane (ppm)
Isoprene Reacted (ppm)
Methylcyclohexane reacted
Methacrolein
Methyl vinyl ketone
Propene
2-Ethenyl 2-Methyl oxirane
0
1
2
3
4
0.0
0.2
0.4
0.6
0.8
1.0
0
2
4
6
8

Figure 4.

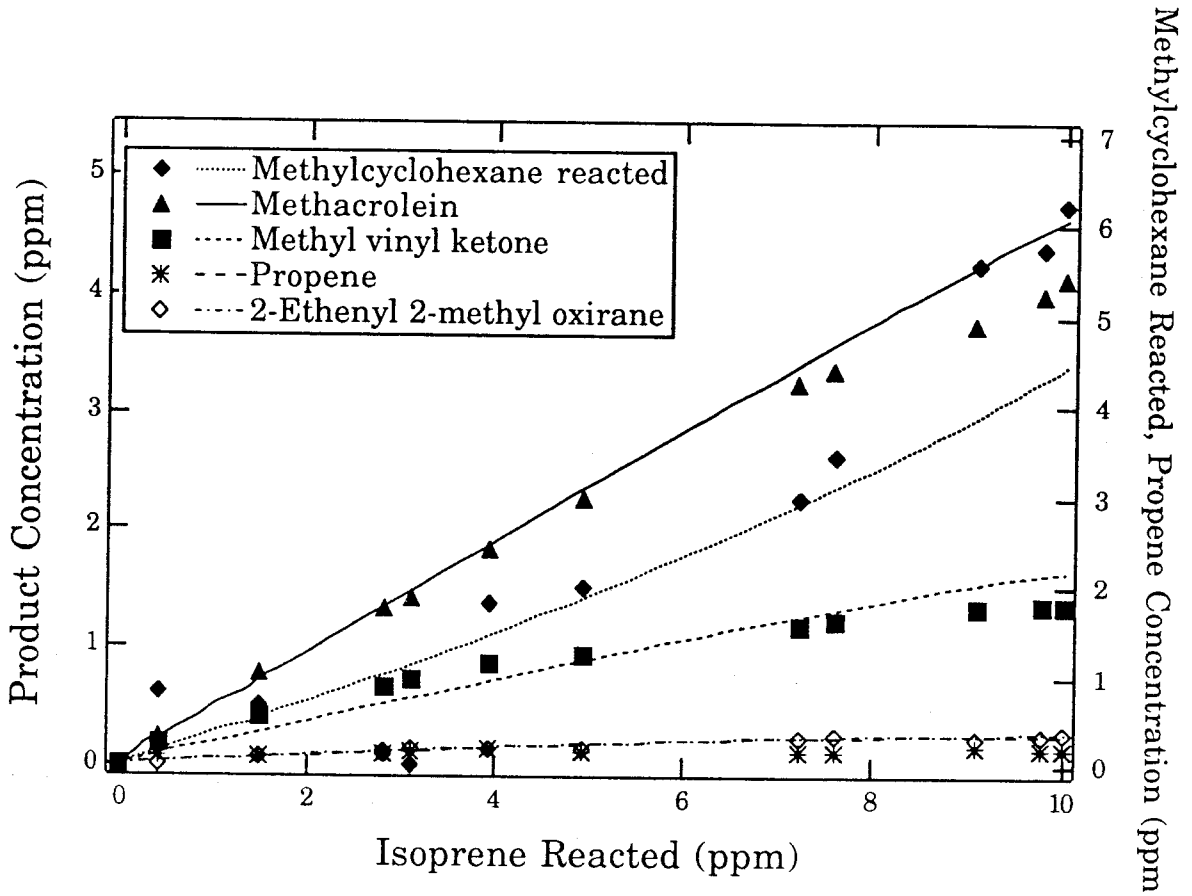
Methylcyclohexane reacted
Methacrolein
Methyl vinyl ketone
Propene
2-Ethenyl 2-methyl oxirane
Product Concentration (ppm)
Methylcyclohexane Reacted, Propene Concentration (ppm)
Isoprene Reacted (ppm)
0
1
2
3
4
5
6
7
8
10

Figure 5.

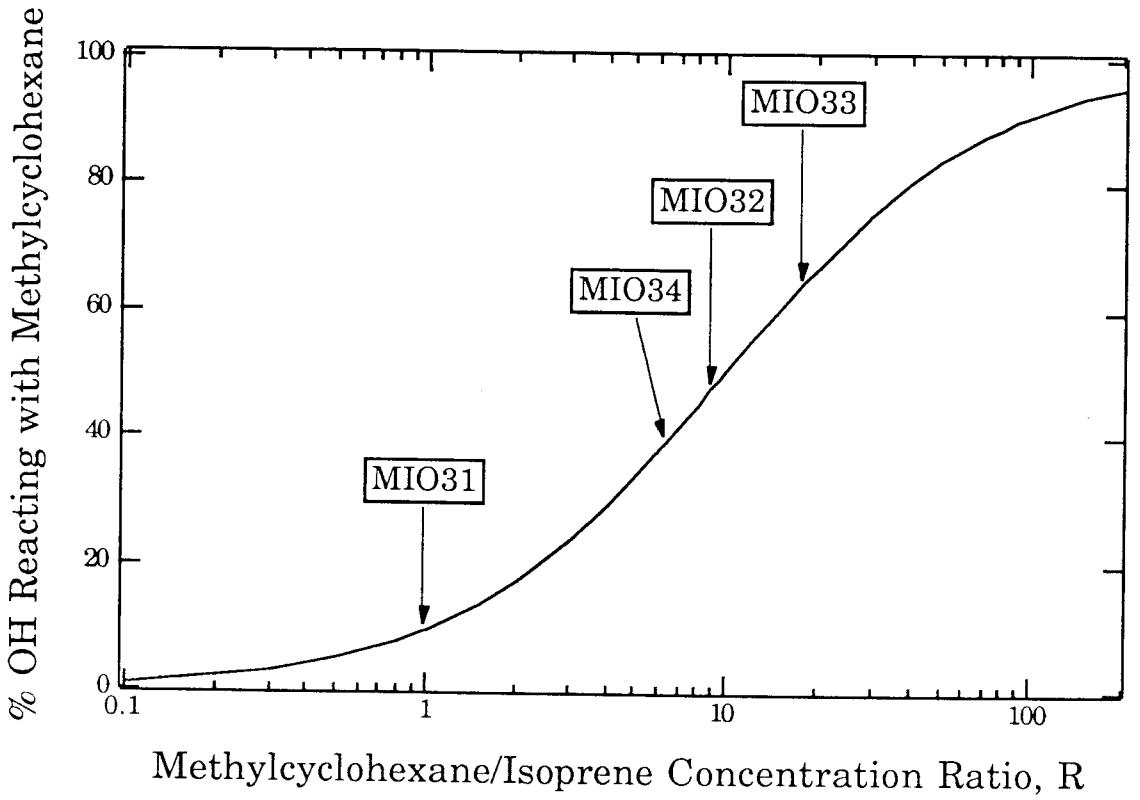
% OH Reacting with Methylcyclohexane
100
80
60
40
20
0
0.1
1
10
100
MIO31
MIO34
MIO32
MIO33
Methylcyclohexane/Isoprene Concentration Ratio, R

Figure 6.

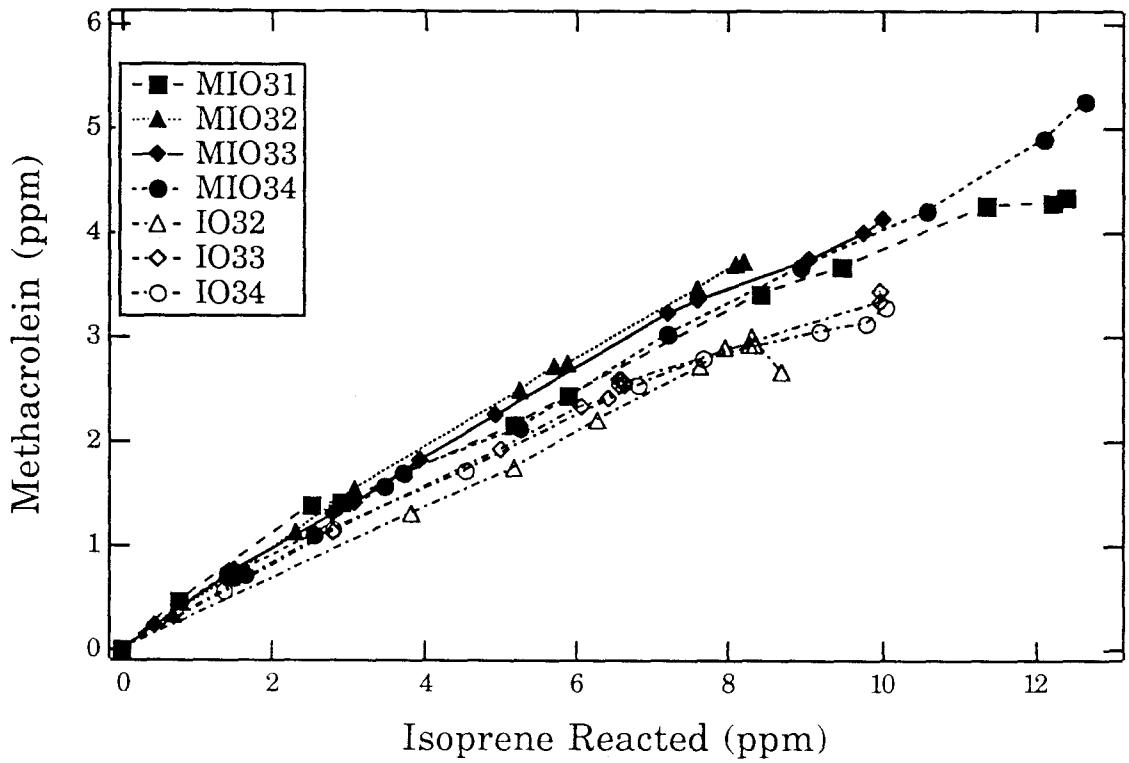
MIO31
MIO32
MIO33
MIO34
IO32
IO33
IO34
Methacrolein (ppm)
Isoprene Reacted (ppm)
0
1
2
3
4
5
6
0
2
4
6
8
10
12

Figure 7.

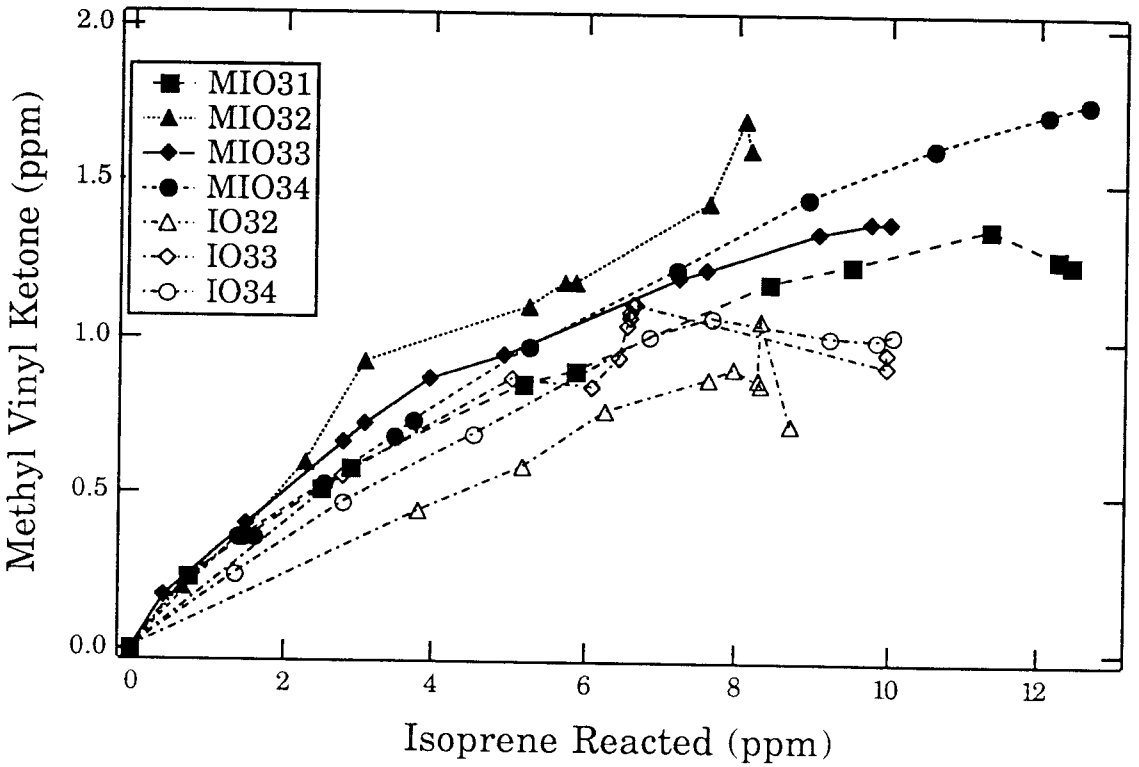
MIO31
MIO32
MIO33
MIO34
IO32
IO33
IO34
Methyl Vinyl Ketone (ppm)
Isoprene Reacted (ppm)
0.0
0.5
1.0
1.5
2.0
0
2
4
6
8
10
12

Figure 8.

# CHAPTER 4

# Development and Evaluation of a Photooxidation Mechanism for Isoprene

## *Introduction*

Implicated in both urban and rural ozone formation (Trainer et al. 1987, Stillman et al. 1990, Chameides et al. 1988), and shown to be a key species in the planetary boundary layer (Jacob and Wofsy 1988), isoprene plays an important role in atmospheric chemistry. Isoprene and the terpenes, a series of isomeric dimers of isoprene, comprise a hydrocarbon source that is estimated to be comparable in magnitude to the anthropogenic emissions (Lamb et al. 1987). We have constructed a mechanism for the atmospheric photooxidation of isoprene that includes the latest kinetic and mechanistic information available. Recent results from the laboratories at Caltech and the U. C. Riverside (UCR) include explicit identification of 66% of the products of the OH-isoprene reaction as methacrolein, methyl vinyl ketone, and 3-methyl furan (Paulson et al. 1991a, Tuazon and Atkinson 1990), which, when combined with the results for formaldehyde, alkyl nitrates, and the unidentified portion of the products from Tuazon and Atkinson (1990a), essentially account for the complete product spectrum from the OH reaction with isoprene. Also, the $O_3$ -isoprene reaction product spectrum has been completely revised, showing significant radical yields and much higher carbonyl product yields (Paulson et al. 1991b) than

previous studies have had to assume for lack of experimental results. We also include in the mechanism the first experimental results for the $O(^3P)$ reaction with isoprene (Paulson et al. 1991a). The $NO_3$-isoprene reaction is updated based on the recent work of Barnes et al. (1990). The recent results of product studies for the methacrolein and methyl vinyl ketone reactions with OH are also included (Tuazon and Atkinson 1989, 1990b). Those aspects of the isoprene oxidation mechanism still unknown are approximated and the contribution resulting from the uncertainties in these features is assessed. The predictions of the mechanism are compared to smog chamber results of runs on isoprene and its major products methacrolein and methyl vinyl ketone carried out both at Caltech and UCR, which include a wide range of conditions. Simulations of a few of the experiments conducted at the University of North Carolina are also included for comparison purposes. Finally, we include the predictions of the Carbon Bond IV mechanism (Gery et al. 1989) for the Caltech experiments.

# *Mechanism Development*

The complete isoprene photooxidation mechanism is summarized in Table 1. We have included the initial reactions of isoprene with OH, $O_3$, $O(^3P)$, and $NO_3$. The mechanism also includes the reactions of each of the products and many of the secondary products of the initial reactions of isoprene.

## *OH-Isoprene Reaction*

OH adds to isoprene's double bonds, favoring the trisubstituted bond. The branching ratio may be inferred from the ratio of methyl vinyl ketone to methacrolein formed, observed by Paulson et al. (1992a), Tuazon and Atkinson (1990), and Gu et al. (1985); about 1.4. OH addition is assumed to take place at the terminal carbon 60% of the time. OH addition to the terminal carbon of either double bond forms a compound with allylic resonance, hence for

these adducts the facile addition of $O_2$ may take place at either of two carbons. This results in the formation of six peroxy radicals:

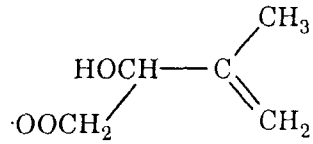

ISOH1

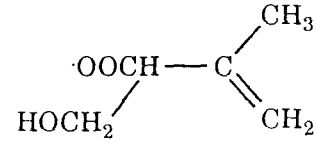

ISOH2

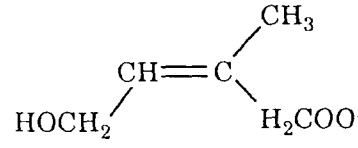

ISOH3

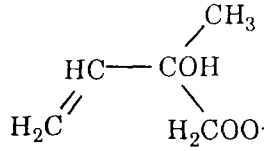

ISOH4

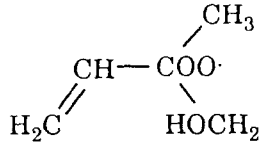

ISOH5

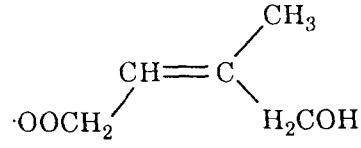

ISOH6

Note that peroxy radicals ISOH3 and ISOH6 have cis- and trans-isomers that form with equal probability. The alkyl peroxy radicals react with NO, $HO_2$, or $RO_2$, depending on conditions. Reaction with NO, the dominant pathway during most of our experiments, results in ß-hydroxy alkoxy radicals (ISOH1, 2, 4, and 5), or δ-hydroxy alkoxy radicals (ISOH3 and ISOH6). The ß-hydroxy alkoxy radicals decompose, producing methacrolein or methyl vinyl ketone as appropriate, as well as formaldehyde, and $HO_2$:

(1)

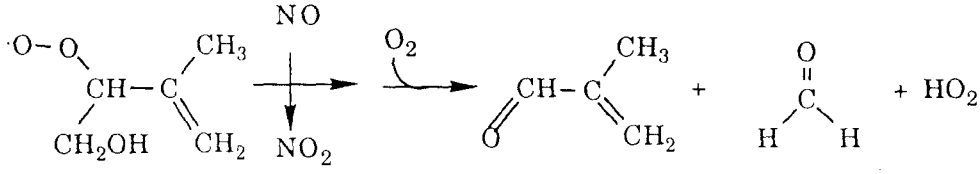

(Methacrolein) (Formaldehyde)

A portion of ISOH4 is also thought to form 3-methyl furan, as follows:

(2)

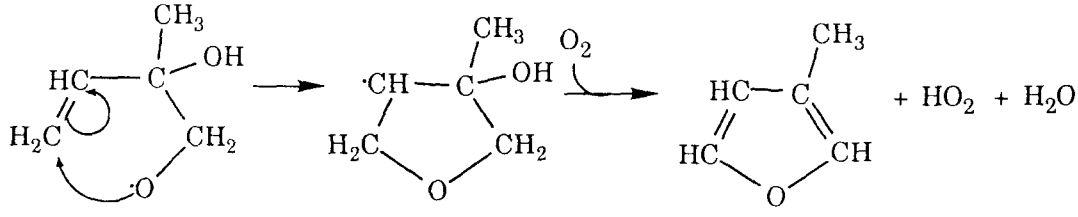

The remaining two alkyl peroxy radicals (ISOH3 and ISOH6) form seven products. Most of these are formed via isomerization involving a six-membered ring transition state, since facile decomposition pathways are not available to these compounds. For example, the cis- form of ISOH3 reacts as follows:

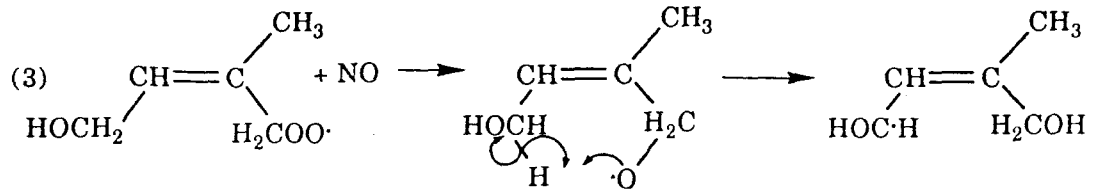

The resulting α-hydroxy alkoxy radical has allylic resonance, and hence may react either via abstraction of a hydrogen atom from the α-hydroxy alkoxy radical resonance form, or via addition of $O_2$ to the β-hydroxy alkyl radical:

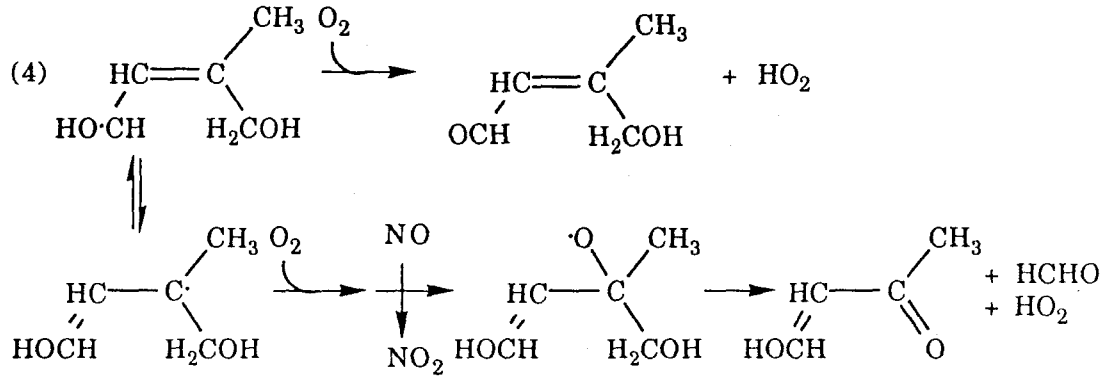

Both the cis- and trans-isomers of radical ISOH6 undergo reactions (1) and (2), leading to the formation of four products, each with equal probability:

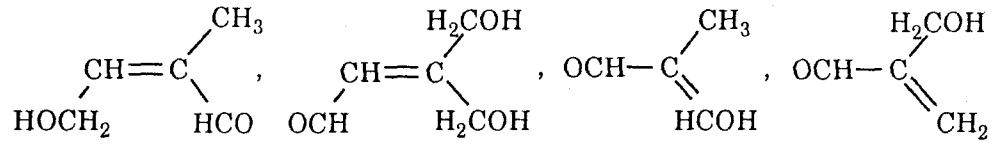

The trans-isomer of radical ISOH3 cannot undergo isomerization and hence reacts with $O_2$, forming the seventh product:

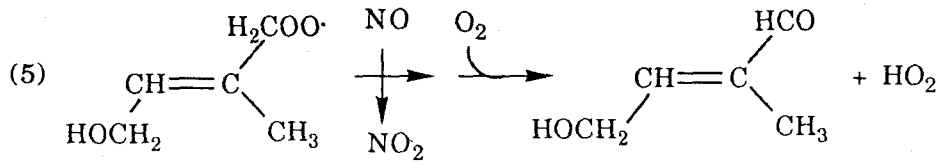

This chemistry is completely consistent with the results of Paulson et al. (1991a), as well as the updated results of Tuazon and Atkinson (1990), in accounting for the carbonyl and 3-methyl furan yields. That these experimental studies were unable to individually identify the other products is also consistent with this mechanism; the collection of products from ISOH3 and ISOH6 are formed in yields of 6% or less each, and are compounds that tend to stick to surfaces, particularly GC columns, hence they should be difficult to detect. These

products, six of which are mono-unsaturated hydroxy aldehydes, are lumped into one species for modeling purposes, IALD1, for which rate constants and products are weighted to account for the component species.

The alkyl nitrate yield from the reactions of the alkyl peroxy radicals with NO is a critical parameter. The observation of Tuazon and Atkinson (1990) of an alkyl nitrate yield from isoprene was 0.14±0.05 (they reported 12%, and with the correction discussed by Paulson et al. (1991a), this becomes 14%). For the current mechanism, we have used a nitrate yield of 0.12 per NO-peroxy radical reaction, however because of additional NO to $NO_2$ conversions that take place in some of the reactions of ISOH3 and ISOH6 (e.g. reaction 3), the assumption of 12% gives an effective yield of 0.13. We have assumed an alkyl nitrate yield of 0.05 for the peroxy radicals that result from the OH reactions with methacrolein and methyl vinyl ketone, and 0.12 for IALD1 as this is a collection of 5-carbon compounds.

## *$O_3$ -Isoprene Reaction*

The $O_3$-isoprene reaction mechanism used here represents the most significant improvement of this mechanism over previous work. The results of Paulson et al. (1991b) clearly show substantial free radical formation in the form of $O(^3P)$ and OH from the $O_3$ - isoprene reaction, as well as much larger carbonyl yields than had been estimated in previous mechanisms (Lloyd et al. 1984, Killus and Whitten 1984, Gery et al. 1989). We have used the mechanism derived in Paulson et al. (1991b), but have reduced somewhat the radical yields so that they fall within the bounds of the uncertainties expressed by that work, and produce better simulations of the chamber runs discussed in this work.

We use the observations of Paulson et al. (1991a) to account for the reaction of $O(^3P)$ with isoprene. The rate constant of the $O(^3P)$-isoprene reaction was estimated using the correlations developed by Atkinson (1985) for the relationship between OH and $O(^3P)$

reaction rates. Although this correlation is very good, the uncertainty for this rate constant is about a factor of 2. We have assumed that the minor decomposition pathway of the $O(^3P)$-isoprene adduct proceeds as follows:

(6)

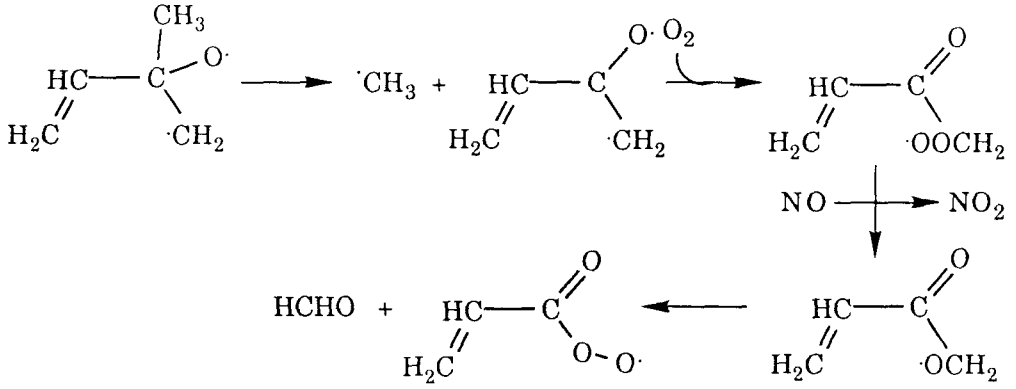


In the mechanism we have lumped the vinylacetylperoxy radical with the similar compound that forms from methacrolein, allowing it to form peroxy acetyl nitrate (PAN) analogs.

## *$NO_3$ -Isoprene Reaction*

The $NO_3$ -isoprene reaction is assumed to proceed via addition to one of the double bonds. Barnes et al. (1990) provided evidence for substantial carbonyl nitrate formation from the reaction of $NO_3$ with a series of alkenes, as well as a decomposition channel that accounts for roughly 10% of the reactants. For the $NO_3$ reaction with isoprene, Barnes et al. (1990) made a rough estimate of the carbonyl nitrate yield of 80%, and observed small quantities of methacrolein, but reported that this compound was below their detection limit and could not be accurately quantified. The $NO_3$ portion of the isoprene mechanism remains fairly uncertain. To be consistent with the results of Barnes et al. (1990), we have assumed that $NO_3$ adds to isoprene in a fashion analogous to OH, and that the nitrate adducts react with $O_2$ to form carbonyl nitrates if they have an available hydrogen (6a), and decompose only if there is no available hydrogen (this is the case for only one of the 6 adduct isomers; 6b):

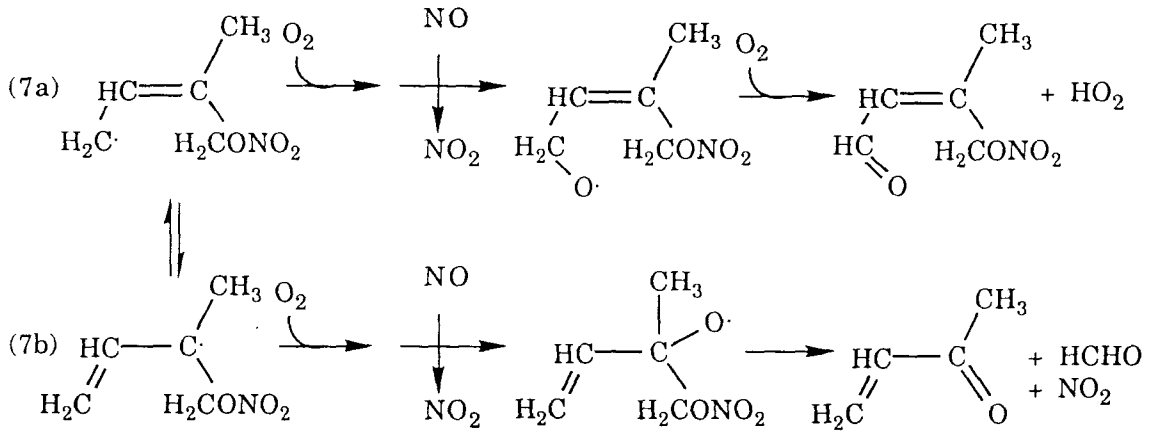

On the surface, this mechanism seems quite inconsistent with the behavior of the analogous ß-*hydroxy* alkoxy radicals (that result from OH addition to isoprene, above, reaction (1)) which decomposes before it can react with $O_2$. This may be rationalized as a result of additional stabilization of the ß-nitrato alkoxy radical from interaction between the alkoxy radical and the nitrate group. This model for the $NO_3$ reaction produces about 90% carbonyl nitrates, and 10% decomposition products.

## *Reactions of the First-Generation Products of Isoprene Photooxidation*

The product spectra for the methacrolein and methyl vinyl ketone reactions with OH have been recently been derived by Tuazon and Atkinson (1990b, 1989). The reactions of these carbonyls with $O_3$ represent fairly uncharted territory, as recent work has indicated significant quantities of OH and $O(^3P)$ formation from $O_3$ reactions with isoprene, propene, tetramethylethylene, isobutene, and terpenes, and these radical yields appear to vary by a factor of 2 or more depending on the parent hydrocarbon (Paulson et al. 1991b, Niki et al. 1987, Japar et al. 1976, Herron and Huie 1978, Atkinson et al. 1990). Carter (1991) ran simulations of methacrolein/$NO_x$, and methyl vinyl ketone/$NO_x$ chamber experiments that were carried out at UCR, and found the optimal combination of the photolysis rates and the OH yield from the $O_3$ reactions for both of these carbonyls; hence we have included these photolysis rates and yields in our mechanism. We have

additionally assumed 80% yields of the methylglyoxal and formaldehyde from the $O_3$ reactions with methacrolein and methyl vinyl ketone. Finally, we assume 20% yields of $O(^3P)$ from each of the reactions. Reactions of these compounds with $NO_3$ are ignored. Reaction with $O(^3P)$ is assumed to proceed with 15% decomposition.

The reaction and rate constant of the lumped product IALD1 is weighted for its component series of hydroxy methyl 2-butenals and 1,1,4 hydroxy butenals. 41% of the OH reaction is expected to abstract the aldehydic hydrogen and subsequently form PAN analogs, with the remainder of the OH reaction occurring by addition to the double bond followed by reaction with NO and decomposition. The double bonds that are already hydroxylated are assumed to react directly with $O_2$, e.g.:

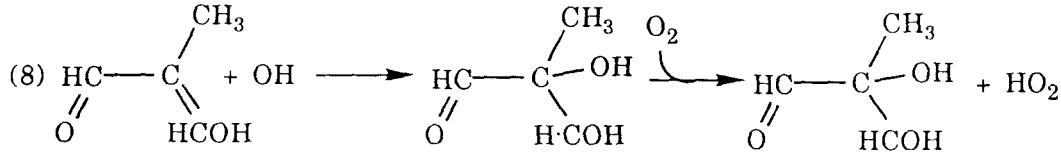


The reactions of OH and $O_3$ with the alkyl nitrates that form in the reactions of the alkyl peroxy radicals with NO are also included in our mechanism. The OH reaction is assumed to liberate $NO_2$ , e.g.:

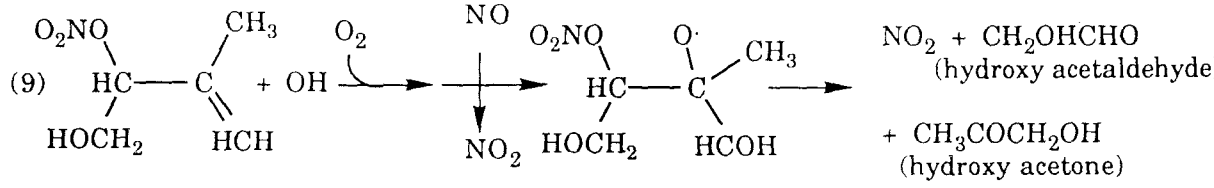


However, a mechanism for the release of $NO_2$ from the $O_3$ reaction is not known, hence we have assumed $NO_2$ release from that reaction is minimal. The reaction of 3-methyl furan with OH, expected to be fast, is also included in the mechanism.

The mechanisms for the reactions of the major secondary products of isoprene oxidation, methyl glyoxal, hydroxy acetaldehyde, hydroxy acetone, and glyoxal, are based on the work of Carter (1988).

# *Evaluation of the Mechanism*

The performance of the mechanism is evaluated by comparison of its predictions to observations from (a) the Caltech smog chamber and (b) the UCR chamber, and (c) the University of North Carolina (UNC) chamber studies carried out in 1982. The Caltech experiments were carried out in conjunction with extensive aerosol measurements that have been reported elsewhere (Pandis et al. 1991). We have used the updated inorganic mechanism recommended in the work of Atkinson et al. (1989).

## *Wall Effects*

Wall effects have long been recognized as important in smog chamber studies (Carter, et al. 1982, Pitts et al. 1984, Leone et al. 1985, Sakamaki and Akimoto 1988, Grosjean 1985). Both adsorption of $O_3$, $NO_2$, $HNO_3$, and HONO, and heterogeneous reactions with the wall of the Teflon chamber have been characterized in the past for the Caltech chamber or similar outdoor chambers, and are included when simulating chamber data. Ozone loss was assumed to be equal to that measured in a chamber used in an earlier study at Caltech (J. Stern and T. Shafer, unpublished data, 1985). We used the wall loss rates for $NO_2$ and $HNO_3$ that were measured in similar smog chambers by Grosjean (1985). Losses of other species to the wall (e.g. isoprene) are expected to be much smaller and were neglected. Leone et al. (1985) derived an expression for initial HONO, that depends on the initial $NO_2$ concentration and the $NO_2$ mixing time, for a Caltech smog chamber; we used this expression to calculate initial HONO concentrations in our simulations of Caltech chamber results. Many studies have found evidence for a heterogeneous reaction between

$NO_2$ and $H_2O$ to give nitrous acid (HONO) (Carter et al. 1982, Pitts et al. 1984, Leone et al. 1985, Sakamaki and Akimoto 1988). Leone et al. (1985) measured this wall reaction for an earlier Caltech chamber, and we have used this rate. Leone et al. also measured 2 ppb formaldehyde in the matrix air. As we did not measure formaldehyde in this study, we have included this result in our simulations. It is important to note that the simulations are most sensitive to the assumed wall effects, particularly HONO formed from the heterogeneous reaction of $NO_2$ when the radical concentrations are low, e.g. before significant $O_3$ concentrations have developed (particularly in low hydrocarbon/$NO_x$ ratio experiments INOXA27 and INOXA29), and after $O_3$ has reached a maximum. Because it acts to reduce the peak $NO_2$ concentration, the heterogeneous formation of HONO tends to reduce the maximum $O_3$ levels predicted by the mechanism slightly for high hydrocarbon/$NO_x$ ratio experiments. Each of the wall effects listed above were increased by a factor of 1.5 to account for the somewhat higher initial surface to volume ratio for these experiments compared to the measurements in other chambers, and the significant deflation of the smog chamber that occurred due to several high volume aerosol instruments that were sampling during these experiments. Our initial volumes were typically 50-55$m^3$, and 30$m^3$ by the end of a run, compared to 60$m^3$ for the above chambers. Except where noted, identical wall effects were used for simulations of all experiments. Finally, we characterized the efficacy of the "bakeout" procedure that we used to clean our chamber between runs. We found that some $O_3$ did form, presumably due to the residual nitric acid and other species that deposited on the walls of the chamber in the previous experiment, as well as trace impurities in the matrix air. $O_3$ was found to form at a rate of about 29, 19, and 11 ppb/hr, on the first, second and third days of baking, respectively. Experiments INOXA25, A27, and A29 were carried out with only one day of baking, while the remaining experiments had two or more days of baking in between. The $NO_x$ -NO signal typically reached 15-25 ppb during bakeouts, although the responsible compounds

are not known. Because this effect is not predicted in the other wall effects discussed above, we have included this small $O_3$ source in our mechanism directly.

## *UV Flux and Temperature*

Our software uses a module that calculates the UV flux as a function of date, time and location. For experiments where clouds were present (INOXS27 and to a minor degree INOX31), the solar flux was adjusted by a factor derived from UV data collected during the experiments. Teflon film attenuates UV radiation by 5-10% (Kelly 1982), and as the Caltech chamber is underlain by a black surface, reflection is expected to be minimal. However Leone et al. found that the UV may be enhanced somewhat in the afternoon hours due to reflection from other nearby surfaces. As these two effects tend to cancel one another, we have used the solar flux calculations without modification. The temperature was adjusted in the simulations every half hour according to the temperature data; the temperature range for each experiment is included in Table 2.

## *Simulations of Caltech Outdoor Smog Chamber Data*

The results of the Caltech chamber experiments, covering a range of conditions including the hydrocarbon/$NO_x$ ratio and initial hydrocarbon concentration, are shown in Figs. 1-4 (refer to Table 2 for the initial conditions of the experiments). Figs. 1a and b show the data and simulation results for INOXA27, which had a very low hydrocarbon/$NO_x$ ratio, as well as a low initial hydrocarbon concentration. These simulation results are fairly independent of the $O_3$ chemistry and completely independent of $NO_3$ chemistry, as very little $O_3$ formed over the course of this experiment. Figs. 2a and b show the results and simulations for experiment INOXA25. This run had an intermediate hydrocarbon/$NO_x$ ratio and an intermediate initial hydrocarbon concentration. Figs. 3a, b and c show the data for experiment INOXO29, including product concentrations, which has a similar hydrocarbon/$NO_x$ ratio as INOXA25, but the initial hydrocarbon concentration is about

four times higher, and the hydrocarbon/$NO_x$ ratio is somewhat higher. The data for experiments INOXS27 and INOXO31 are not shown, but results of the simulations of those data are included in the discussion. Figs. 4a, b and c show the data, including product concentrations for the highest hydrocarbon/$NO_x$ ratio, experiment INOXS30. This experiment was carried out for a period of nearly eight hours. A small secondary $O_3$ peak is observed in this experiment in the region where there is very low available $NO_x$.

The $O_3$ curves observed in the Caltech experiments are qualitatively different from the $O_3$ observed in the UNC experiments; the UNC experiments showed immediate secondary $O_3$ peaks that were not observed in any of our experiments, even though most of the runs had hydrocarbon/$NO_x$ ratios of more than 10, the threshold for this behavior observed in the UNC data. We did observe small secondary peaks in a few of our experiments, however they occurred much later in the runs and did not exceed the initial $O_3$ peak height. The difference in this behavior appears to be largely a result of the difference in the light regimes; UNC began their experiments in the pre-dawn hours, while our chamber was uncovered under full sunlight, typically around noon. While our mechanism (base case; see below), as well as other mechanisms such as Carbon Bond IV (CBM-IV, Gery et al. 1989) predict the secondary $O_3$ peak observed in the UNC experiments, it is much smaller than that observed unless the significant dilution air and initial contaminant concentrations are included.

Figures 1-4 show simulations from the base case mechanism in Table 1, as well as from the mechanism with three different assumptions about the chemistry, and simulations of these experiments by CBM-IV (Gery et al. 1989). These other cases are included to gain an understanding of the sensitivity of the mechanism to key assumptions about the chemistry on areas of uncertainty. The base case, labelled A, is the case that uses the mechanism in Table 1. Case B assumes that the $NO_3$ reaction is a complete $NO_x$ sink, as has been

assumed in several earlier models of isoprene oxidation (Gery et al. 1989, Killus and Whitten 1984). Case C assumes no free radical production from the $O_3$ reaction, except 0.06 $HO_2$; $O(^3P)$ and OH production are removed from the isoprene-$O_3$ reaction, but not the product-$O_3$ reactions. Case D assumes that the mechanism for OH formation from the $O_3$ - isoprene reaction is that of $HO_2$ with a Criegee intermediate; e.g.:

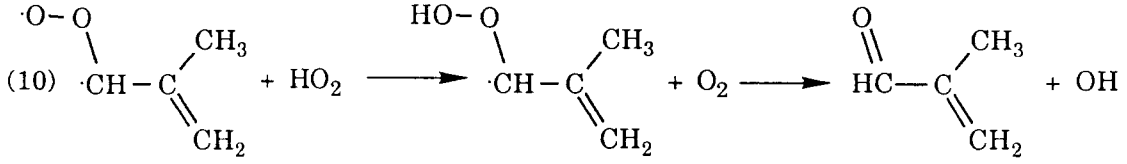


For this we have assumed a Criegee biradical yield of 0.55, and a rate constant for this reaction of $1x10^{-11}$ molecules $cm^{-3}$ $s^{-1}$. Predictions from cases C and D are not included in every plot for visual clarity. Simulations are not plotted for the $NO_X$ -NO curves as these are the sum of several species and hence not illuminating.

Simulations with the base case mechanism predict with reasonable accuracy the initiation of radical formation regardless of the hydrocarbon/$NO_X$ ratio; e.g. the NO curves and the initial portion of the $O_3$ and isoprene curves are in reasonably good agreement with the data. Experiment INOXA27 (Fig. 1) did not develop beyond this phase because of its low hydrocarbon/$NO_X$ ratio; for the other experiments the initial phase of radical formation covers the first 15-90 minutes (Figs. 2-4). The simulations (base case and case B) accurately predict within a few minutes, the observed NO and $O_3$ data for experiments INOXS27, INOXO29, INOXO31 and INOXS30, while they are too slow by about 15 minutes for experiment INOXA25. Case C consistently predicts too slow radical development, and CBM-IV, with much more reactive parameterization of the $O(^3P)$ reaction, but an OH reaction that assumes 1 NO to $NO_2$ conversion per OH reaction but only 0.67 $HO_2$, is slower still. It should be noted that the inorganic portion of CBM-IV is significantly different from the inorganic mechanism used in this work. The chemistry during these initial portions of the experiments is dominated by OH, the reaction next in order of importance is

$O(^3P)$, typically 10%, followed by $O_3$, about half as important as $O(^3P)$. The $NO_3$ reaction is totally negligible until substantial $O_3$ has developed. The performance of the mechanism during the OH dominated periods indicates that the OH chemistry is reasonably accurate. The effects of the modifications to the mechanism may be clearly seen; case B reduces the peak $O_3$ concentration, but has little effect on the speed of radical development, the assumptions for case C slow radical development as well as reducing the peak $O_3$ concentration, and case D both slows and reduces the $O_3$ peak, with a less dramatic effect on the $O_3$ peak height. The maximum $O_3$ reached under a given set of conditions depends on the available $NO_2$, more than any other mechanistic factor.

The $O_3$ simulation curves present a very consistent picture. All of the mechanisms underpredict $O_3$ formation somewhat when the isoprene concentration is very low (e.g. it has largely reacted) and the available $NO_x$ is fairly low. This may be seen particularly in the end of experiments INOXA27 (Fig. 1), INOXA29 (not shown), and the final four hours of INOXS30 (Fig. 4), where our mechanism underpredicts the $O_3$ by 20-40%, and CBM-IV underpredicts by 3-60%. The other cases fall in between. This may indicate that the reactivity of the secondary chemistry, including the chemistry of the methylglyoxal and other carbonyl products is underestimated by the mechanisms.

For the high hydrocarbon/$NO_x$ ratio experiments, the $O_3$ peak itself, which results from isoprene rather than product chemistry, is reasonably represented by our mechanism. The mechanism overpredicts the $O_3$ peak by 23-28% for experiments INOXA25, INOXS27, and INOXS30, and rises to 50% for INOXO29, and 70% for INOXO31. Both of the latter experiments had higher concentrations of both hydrocarbon and $NO_x$. While this is not unreasonable performance, the assumptions of case B led to the most successful predictions of the $O_3$ peak, coming within ±15% of the $O_3$ maximum, again overpredicting the maximum $O_3$ concentration of the high concentration experiments, but accurately

reproducing the moderate concentration experiments. While case C generally fell within a few percent of the $O_3$ peak as well, it predicted much slower $O_3$ formation than was observed. Case D fell between the base case and case C, somewhat slow and somewhat too much $O_3$. CBM-IV tended to underestimate the maximum $O_3$ concentration, from about 20 to 30%, although this is partially a symptom of the slow development of radical concentrations characteristic of this mechanism; $O_3$ will tend to build to higher concentrations if the reactions are fast as there is less time for the processes that destroy $O_3$ to take place. CBM-IV, like the other mechanisms, shifted upward relative tot eh data for the high concentration experiments.

Data on methacrolein, methyl vinyl ketone, and 2-methyl 3-butene oxide concentrations were measured for the higher concentration experiments (INOXS27, S30, O29, and O31). The mechanisms slightly underpredict methacrolein concentrations, by about 15%. The product concentration predictions are included in the figures; it should be kept in mind that the curvature of the simulated product concentrations are largely controlled by the ability of the mechanism to predict the $O_3$ curve. CBM-IV does not form first generation products, hence no simulations are shown for this mechanism. The predicted methyl vinyl ketone concentrations are consistently low by a more significant amount; about 35%. This may indicate that the percent isoprene reacting with OH should be higher, although there are several other potential sources of this discrepancy. It is important to note that, while our mechanism includes a combined yields of these two products from the $O_3$ -isoprene reaction of nearly unity, rather than the previously estimated sum of about 0.5, our mechanism still underpredicts the concentrations of these products. In contrast, predictions of the major epoxide product of the $O(^3P)$ reaction, 2-methyl 3-butene oxide, is in excellent agreement with the data; i.e. within ±5%. This indicates both that the $O(^3P)$ concentration predicted by the mechanism is correct, and that the $O(^3P)$ reactions are indeed important in chamber experiments.

Overall, the mechanism that appears to best predict the data from the Caltech chamber is case B, which includes all of the recent results for OH, $O_3$, and $O(^3P)$ chemistry, but assumes that the $NO_3$ reaction is a complete $NO_x$ sink. The base case is in reasonable agreement as well, although it consistently underpredicts the maximum $O_3$ concentration at low hydrocarbon/$NO_x$ ratios and overpredicts at high hydrocarbon/$NO_x$ ratios. Finally, the peak $O_3$ concentration appears to be less sensitive to the magnitude of the initial hydrocarbon and $NO_x$ concentrations than both our mechanism and the CBM-IV mechanism predict.

# *Conclusions*

A mechanism for the atmospheric photooxidation of isoprene is developed that includes recent developments on each of isoprene's atmospherically important reactions: $O_3$, OH, $O(^3P)$, and $NO_3$. The mechanism is tested against chamber data that include a range of mixtures of these reactions. While it performs reasonably well under conditions where the OH and $O(^3P)$ reactions dominate, it tends to overpredict $O_3$ formation, as well as the speed of development of $O_3$ under conditions where the $O_3$ and $NO_3$ reactions are important. The $NO_3$ reaction is the most uncertain aspect of the isoprene mechanism, and may be responsible for a significant part of this discrepancy. The discrepancy may also arise from the difficulty in extrapolating the results of $O_3$ experimental results, necessarily carried out in the absence of $NO_x$, to conditions that include significant concentrations of $NO_x$.

# *Acknowledgment*

This work was supported by National Science Foundation grant ATM-9003186.

# *References*


Atkinson, R. (1985) Reactions of the OH radical with organic compounds in the atmosphere. *Chemical Rev.* **19**, 799-828.

Atkinson, R., D.L. Baulch, R.A. Cox, R.F. Hampson Jr., J.A.Kerr, and J. Troe (1989) Evaluated Kinetic and photochemical data for atmospheric Chemistry: Supplement III. *Int'l J. Chemical Kinetics* **21:** 115-150.

Barnes, I. , V. Bastian, K. H. Becker, and Z. Tong (1990) Kinetics and products of the reactions of $NO_3$ with monoalkenes, dialkenes, and monoterpenes. *J. Phys. Chem.* **94**, 2413-2419.

Chameides, W.L., R.L. Lindsay, J. Richardson and C.S. Kiang (1988) The role of biogenic hydrocarbons in urban photochemical smog: Atlanta as a case study. *Science* **241**, 1473-1475.

Gardner, E.P., P.D. Sperry, and J.G. Calvert (1987) Photodecomposition of acrolein in $O_2$-$N_2$ mixtures. *J. Phys. Chem.* **91**, 1922-1930.

Gery, M.W., G.Z. Whitten, J.P. Killus, and M.C. Dodge (1989) A photochemical kinetics mechanism for urban and regional scale computer modeling. *J. Geophys. Res.* **94**, 12925-12956.

Grosjean, D. (1985) Wall loss of inorganic compounds in environmental chambers. *Envir. Sci. Tech.* **19**, 1059-1065.

Gu, C.L., C.M. Rynard, D. G. Hendry, T. Mill (1985) Hydroxyl Radical Oxidation of Isoprene. *Envir. Sci. Technol.* **19,** 151-155.

Jacob, D.J., and S.C. Wofsy (1988) Photochemistry of biogenic emissions over the Amazon forest. *J. Geophys. Res.* **93**, 1477-1486.

Kelly, N. (1982) Characterization of fluorocarbon film bags as smog chambers. *Environ. Sci. Technol.* **16**, 763-770.

Killus, P. and G. Z. Whitten (1984) Isoprene: a Photochemical Kinetic Mechanism. *Environ. Sci. Technol.* **18**, 142-148.

Lamb, B., A. Guenter, D. Gay, H. Westburg (1987) A National Inventory of Biogenic Hydrocarbon Emissions. *Atmospheric Environment* **21,** 1695-1705.

Leone, J.A., R.C. Flagan, D. Grosjean, and J.H. Seinfeld (1985) An outdoor smog chamber and modeling study of toluene-$NO_x$ photooxidation. *Int'l J. Chem. Kinet.* **17**, 177-216.

Lloyd, A.C., R. Atkinson, F. W. Lurmann, and B. Nitta (1983) Modeling potential ozone impacts from natural hydrocarbons-I. Development and testing of a chemical mechanism for the $NO_x$-air photooxidations under ambient conditions. *Atmos. Environ.* **17**, 1931-1950.

Niki, H., P.D. Maker, C.M. Savage and J.G. Calvert (1987) Fourier transform infrared study of the kinetics and mechanisms for the Cl-atom and HO-initiated oxidation of glycolaldehyde. *J. Phys. Chem.* **91**, 2174-2178.

Pandis, S.N., S.E. Paulson, R.C. Flagan, and J.H. Seinfeld (1991), Aerosol Formation in the Photooxidation of Isoprene and Beta-Pinene *Atmospheric Environ.* **25a**, 997-1008.

Paulson, S.E., R.C. Flagan and J.H. Seinfeld (1991a) Atmospheric Photooxidation of Isoprene. Part 1: The Reactions of Isoprene with Hydroxyl Radical and Ground State Atomic Oxygen. Submitted to *J. Phys. Chem.*

Paulson, S.E., R.C. Flagan and J.H. Seinfeld (1991b) Atmospheric Photooxidation of Isoprene. Part 2: The Isoprene-Ozone Reaction. Submitted to *J. Phys. Chem.*

Pitts, J.N. Jr, E.S. Sanhueza, R. Atkinson, W.P.L. Carter, A.M. Winer, G.W. Harris and C.N. Plum (1984) *Int'l J. Chem. Kinet.* **16**, 919-927.

Sakamaki, F., and H. Akimoto (1988) HONO formation as unknown radical source in photochemical smog chamber experiments. *Int'l J. Chem. Kinet.* **20**, 111-116.

Stillman, S., J.A. Logan, and S.C. Wofsy (1990) The sensitivity of ozone to nitrogen oxides and hydrocarbons in regional ozone episodes. *J. Geophys. Res.* **95**, 1837-1851.

Trainer, M., E.Y. Hsie, S.A. McKeen, R. Tallamraju, D.D. Parrish, F.C. Fehsenfeld, and S.C. Liu, (1987) Models and observations of natural hydrocarbons on rural ozone. *Nature* **329**, 705.

Tuazon, E.C. and R. Atkinson (1990a) A Product Study of the Gas-Phase Reaction of Isoprene with the OH Radical in the presence of $NO_x$. *Int'l J. Chemical Kinetics* **14**, 1221-1236.

Tuazon, E.C. and R. Atkinson (1990b) A product study of the gas-phase reaction of methacrolein with the OH radical in the presence of $NO_x$. *Int'l J. Chemical Kinetics* **22**, 591-602.

Tuazon, E.C. and R. Atkinson (1989) A product study of the gas-phase reaction of methyl vinyl ketone with the OH radical in the presence of $NO_x$. *Int'l J. Chemical Kinetics* **22**, 1141-1152.

# *Table 1.*
# *Isoprene Oxidation Mechanism*

| rxn #, rate , act. constant energy at 298 K | ref.* , ref.**, | reactants | products |
|---|---|---|---|
| 1) 1.43E-17, 2013 | 1,a | isoprene + O3 → | 0.69 methacrolein + 0.27 methyl vinyl ketone + 0.30 O + 0.55 OH + 0.07 propene + 0.07 CO2 + 0.074 $H_2C{\cdot}O\text{-}O{\cdot}$ + 0.03 $\cdot O\text{-}O\text{-}C{\cdot}H\text{-}C(CH_3)=CH_2$ + 0.03 $CH_2=C\text{-}C{\cdot}(CH_3)O\text{-}O{\cdot}$ + 0.8 HCHO + 0.19 CO + 0.06 $HO_2$ |
| 2) 1.01E-10, -410 | 1,a | isoprene + OH → | 0.126 $.OOCH_2CH(OH)C(CH_3)=CH_2$ + 0.194 $HOCH_2CH(OO.)C(CH_3)=CH_2$ + 0.1 $HOCH_2CH=C(CH_3)CH_2OO.$ + 0.174 $CH_2=CHC(OO.)(CH_3)CH_2OH$ + 0.268 $CH_2=CHC(OH)(CH_3)CH_2OO.$ + 0.138 $.OOCH_2CH=C(CH_3)CH_2OH$ |
| 3) 5.8E-11 | b,a | isoprene + O → | 0.63 2-methyl 3-butene oxide + 0.22 3-methyl 3-butene oxide + 0.085 I3PR + 0.12 unknown 1 |
| 4) 2.E-13 | 16,16 | 2 $.OOCH_2CH(OH)C(CH_3)=CH_2$ → | 1.2 methacrolein + 0.4 dihydroxy cpd + 1.2 HCHO + 0.4 carbonyl hydroxy cpd + 1.2 $HO_2$ |
| 5) 2.53E-14 | 16,16 | $.OOCH_2CH(OH)C(CH_3)=CH_2$ + $HOCH_2CH(OO.)C(CH_3)=CH_2$ → | 1.2 methacrolein + 0.4 dihydroxy cpd + 1.2 HCHO + 0.4 carbonyl hydroxy cpd + 1.2 $HO_2$ |
| 6) 2.E-13 | 16,16 | $.OOCH_2CH(OH)C(CH_3)=CH_2$ + ISOH3 → | 0.6 methacrolein + 1.2 $HO_2$ + 0.4 dihydroxy cpd + 1.0 carbonyl hydroxy cpd + 0.6 HCHO |
| 7) 2.53E-14 | 16,16 | $HOCH_2CH(OO.)C(CH_3)=CH_2$ + ISOH3 → | 0.6 methacrolein + 1.2 HO2. + 0.4 dihydroxy cpd + 1.0 carbonyl hydroxy cpd + 0.6 HCHO |
| 8) 2.E-13 | 16,16 | $.OOCH_2CH(OH)C(CH_3)=CH_2$ + ISOH4 → | 0.6 methacrolein + 1.2 $HO_2$+ 0.4 dihydroxy cpd + 0.4 carbonyl hydroxy cpd + 1.2 HCHO + 0.6 methyl vinyl ketone |

9) 4.9E-15 16,16 $.OOCH_2CH(OH)C(CH_3)=CH_2$ + ISOH5 → 0.9 methacrolein + 1.8 $HO_2$ + 0.1 dihydroxy cpd + 0.1 carbonyl hydroxy cpd + 1.8 HCHO + 0.9 methyl vinyl ketone

10) 2.E-13 16,16 $.OOCH_2CH(OH)C(CH_3)=CH_2$ + ISOH6 → 0.6 methacrolein + 1.2 $HO_2$ + 0.4 dihydroxy cpd + 1.0 carbonyl hydroxy cpd + 0.6 HCHO

11) 2.53E-14 16,16 $HOCH_2CH(OO.)C(CH_3)=CH_2$ + ISOH4 → 0.6 methacrolein + 1.2 $HO_2$ + 0.4 dihydroxy cpd + 0.4 carbonyl hydroxy cpd + 0.6 HCHO + 0.6 methyl vinyl ketone

12) 3.1E-16 16,1 $HOCH_2CH(OO.)C(CH_3)=CH_2$ + ISOH5 → 0.9 methacrolein + 1.8 $HO_2$ + 0.2 dihydroxy cpd + 0.1 carbonyl hydroxy cpd + 1.8 HCHO + 0.9 methyl vinyl ketone

13) 2.52E-14 16,16 $HOCH_2CH(OO.)C(CH_3)=CH_2$ + ISOH6 → 0.6 methacrolein + 0.4 dihydroxy cpd + 1.2 HCHO + 0.4 carbonyl hydroxy cpd + 1.2 $HO_2$ + 0.6 methyl vinyl ketone

14) 2.E-13 16,16 ISOH3 + ISOH3 → 0.4 dihydroxy cpd + 1.2 HCHO + 1.6 carbonyl hydroxy cpd + 1.2 $HO_2$

15) 2.E-13 16,16 ISOH3 + ISOH4 → 0.6 methyl vinyl ketone + 1.2 $HO_2$ + 0.4 dihydroxy cpd + 1.0 carbonyl hydroxy cpd + 0.6 HCHO

16) 3.1E-16 16,16 ISOH3 + ISOH5 → 0.9 methyl vinyl ketone + 1.8 $HO_2$ + 1.9 HCHO + 0.1 dihydroxy cpd + 1.0 carbonyl hydroxy cpd

17) 2.E-13 16,16 ISOH3 + ISOH6 → 0.4 dihydroxy cpd + 1.2 $HO_2$ + 1.2 HCHO + 1.6 carbonyl hydroxy cpd

18) 2.E-13 16,16 ISOH4 + ISOH4 → 1.2 methyl vinyl ketone + 0.4 dihydroxy cpd + 1.2 $HO_2$ + 1.2 HCHO + 0.4 carbonyl hydroxy cpd

19) 2.E-13 16,16 ISOH4 + ISOH5 → 1.8 methyl vinyl ketone + 1.8 $HO_2$ + 1.8 HCHO + 0.1 dihydroxy cpd + 0.1 carbonyl hydroxy cpd

20) 2.1E-13 16,16 ISOH4 + ISOH6 → 0.6 methyl vinyl ketone + 1.2 $HO_2$ + 1.2 HCHO + 0.4 dihydroxy cpd + 1.0 carbonyl hydroxy cpd

21) 4.9E-15 16,16 ISOH5 + ISOH6 → 0.9 methyl vinyl ketone + 0.1 dihydroxy cpd + 1.8 $HO_2$ + 1.8 HCHO

| | |
|---|---|
| | + 1.0 carbonyl hydroxy cpd |
| 22) 2.E-13 | 16,16 ISOH6 + ISOH6 → 0.4 dihydroxy cpd + 1.2 $HO_2$ + 1.2 HCHO |
| | + 1.6 carbonyl hydroxy cpd |
| 23) 8.E-16 | 16,c MCHR + MCHR → 1.2 $HO_2$ |
| 24) 3.E-14 | 16,c MCHR + ISOH1 → 1.2 $HO_2$ + 0.6 methacrolein + 0.6 HCHO |
| | + 0.2 dihydroxy cpd + 0.2 carbonyl hydroxy cpd |
| 25) 3.E-14 | 16,c MCHR + $HOCH_2CH(OO.)C(CH_3)=CH_2$ → 1.2 $HO_2$ + 0.6 |
| | methacrolein + 0.6 HCHO + 0.2 dihydroxy |
| | cpd + 0.2 carbonyl hydroxy cpd |
| 26) 3.E-14 | 16,c MCHR + ISOH3 → 1.2 $HO_2$+ 0.5 dihydroxy cpd + 0.5 |
| | carbonyl hydroxy cpd |
| 27) 3.E-14 | 16,c MCHR + ISOH4 → 1.2 $HO_2$ + 0.6 methyl vinyl ketone + |
| | 0.6 HCHO + 0.2 dihydroxy cpd |
| | + 0.2 carbonyl hydroxy cpd |
| 28) 3.E-14 | 16,c MCHR + ISOH6 → 1.2 $HO_2$+ 0.5 dihydroxy cpd + 0.5 |
| | carbonyl hydroxy cpd |
| 29) 3.E-12 900 | 16,c ISOH1, $HOCH_2CH(OO.)C(CH_3)=CH_2$, ISOH3, ISOH4, ISOH5, |
| | ISOH6 + $HO_2$ → organic peroxide |
| 30) 3.E-12 900 | 16,c MCHR + HO2. → |
| 31) 2.E-11 | d,c organic peroxide + HO. → MCHR |
| 32) 8.E-18 | d,e organic peroxide + O3 = 0.6 HO. + 0.4 O + 0.7 HCHO |
| 33) 1.36E-14 | 1,1 CVO2 + HCHO → OZID |
| 34) 1.36E-14 | 1,1 CVO2 + methacrolein → OZID |
| 35) 4.E-18 | 1,1·O-O-C·H-$C(CH_3)=CH_2$ + H2O → ACRAC |
| 36) 1.36E-14 | 1,1 ·O-O-C·H-$C(CH_3)=CH_2$ + HCHO → OZID |
| 37) 1.36E-14 | 1,1 ·O-O-C·H-$C(CH_3)=CH_2$ + methacrolein → OZID |
| 38) 4.06E-18 | 20,e methyl vinyl ketone + O3 → |
| 39) 1.88E-11 | 1,11 methyl vinyl ketone + OH → ISOH1 |
| 40) 3.1E-12 | b,e methyl vinyl ketone + O → |
| 41) 1.08E-18 | 20,e methacrolein + O3 → |
| 42) 7.9E-12 | b,a methacrolein + O → 0.9 OX + 0.1 ISOH1 |
| 43) 3.1E-12 | g,e 2-methyl 3-butene oxide + O → |
| 44) 7.9E-12 | g,e 3-methyl 3-butene oxide + O → |
| 45) 1.88E-11 | g,f 2-methyl 3-butene oxide + OH → ISOH1 |
| 46) 3.35E-11 | g,f 3-methyl 3-butene oxide + OH → ISOH1 |
| 47) 1.04e-11 | 1,1 MCH + OH → MCHR |

a) Paulson et al., 1991ab.

b) Estimated from correlations between the rate constants of OH and $O(^3P)$ developed by Atkinson (21).

c) MCHR, the alkyl peroxy radical derived from the OH-methyl cyclohexane reaction was assumed to be entirely secondary peroxy radical. Its products are dominated by alcohols and ketones; little formaldehyde is expected. See also text.

d) Average of methacrolein and methyl vinyl ketone rate constants; see also text.

d) Products unknown/assumed to be exactly analogous to the products of isoprene; same radical yields and the appropriate hydrocarbon products. The hydrocarbon products of these reactions are expected to have a negligible effect on any simulation carried out with the mechanism (see text).

e) The products were lumped with the isoprene-OH products.

f) These rate constants were assumed to equal the values for methyl vinyl ketone (2-methyl 3-butene oxide) and methacrolein (3,3-methyl butene oxide). Products were also assumed to react in the fashion of the appropriate methacrolein and methyl vinyl ketone derived radicals.

*Table 2..*
*Summary of Initial Conditions*

| Expt. | Initial Concentration (ppm) | | | | | | | | |
|---|---|---|---|---|---|---|---|---|---|
| | Isoprene | NO (ppm) | $NO_2$ (ppm) | $O_3$ (max) | $HC/NO_x$ | $HONO_i$ (ppb) | Temp | UV | $T_0$(PST) |
| INOXA25 | 1.02 | 0.187 | 0.008 | 0.445 | 26 | 0.3 | no | 6-3 | 12:40 |
| INOXA27 | 0.122 | 0.187 | 0.029 | 0.121 | 2.8 | 0.8 | 29-32 | 6-5 | 11:54 |
| (peak not reached before experiment was terminated) | | | | | | | | | |
| INOXA29 | 0.063 | 0.066 | 0.029 | ~0.350 | 3.32 | 0.9 | 30-33 | 5.5-3.5 | 11:23 |
| (experiment stopped when $O_3$ was 0.331; this experiment also included ~0.05 isopropyl alcohol, of which about 7ppb reacted) | | | | | | | | | |
| INOXS27 | 2.0 | 0.190 | 0.065 | 0.370 | 39.2 | 2 | 34-31 | 5-1.5; very noisy | 12:23 |
| INOXS30 | 2.32 | 0.225 | 0.048 | 0.389 | 42.5 | 1.4 | 24.3-31.7 -30.2 | 1.3-5.2 -1.24 | 8:10 |
| INOXO29 | 4.41 | 0.53 | 0.098 | 0.516 | 35.1 | 3 | 24-28 | 4-2 | 10:52 |
| INOXO31 | 5.59 | 0.960 | 0.300 | 0.601 | 22.2 | 9 | 26-28 | 3.5-1.2; noisy in first 0.5hr | 11:43 |

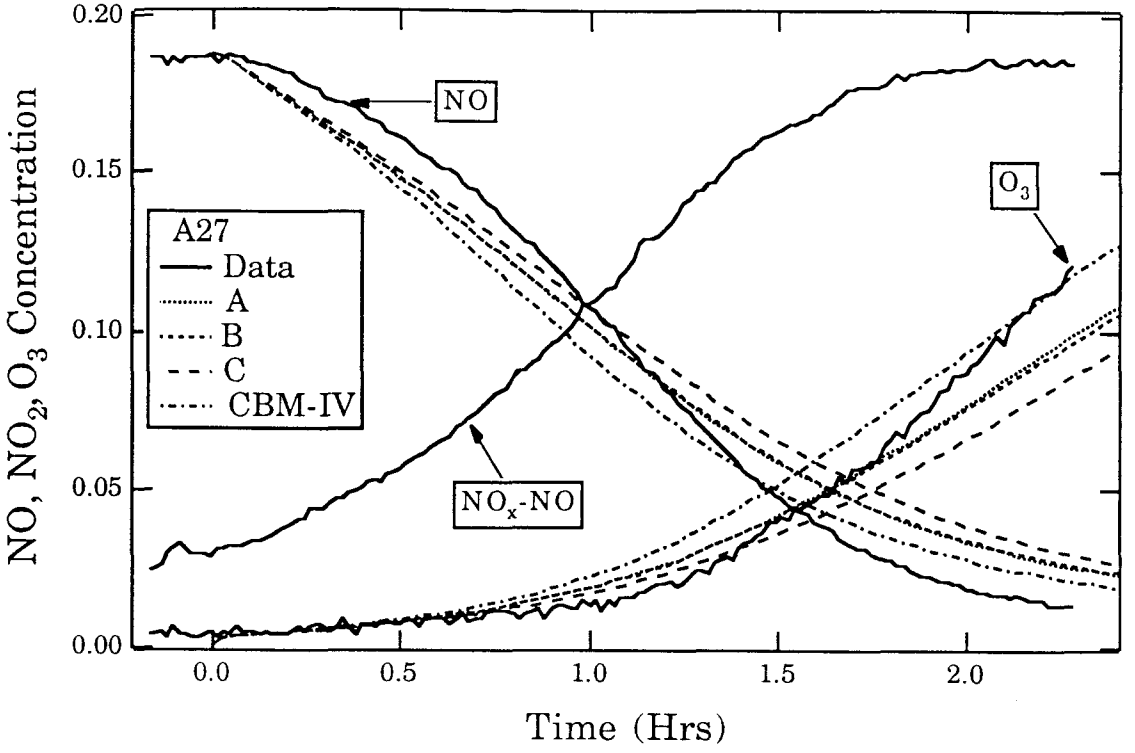


Figure 1a. Run INOXA27, NO and $O_3$ data with simulations.

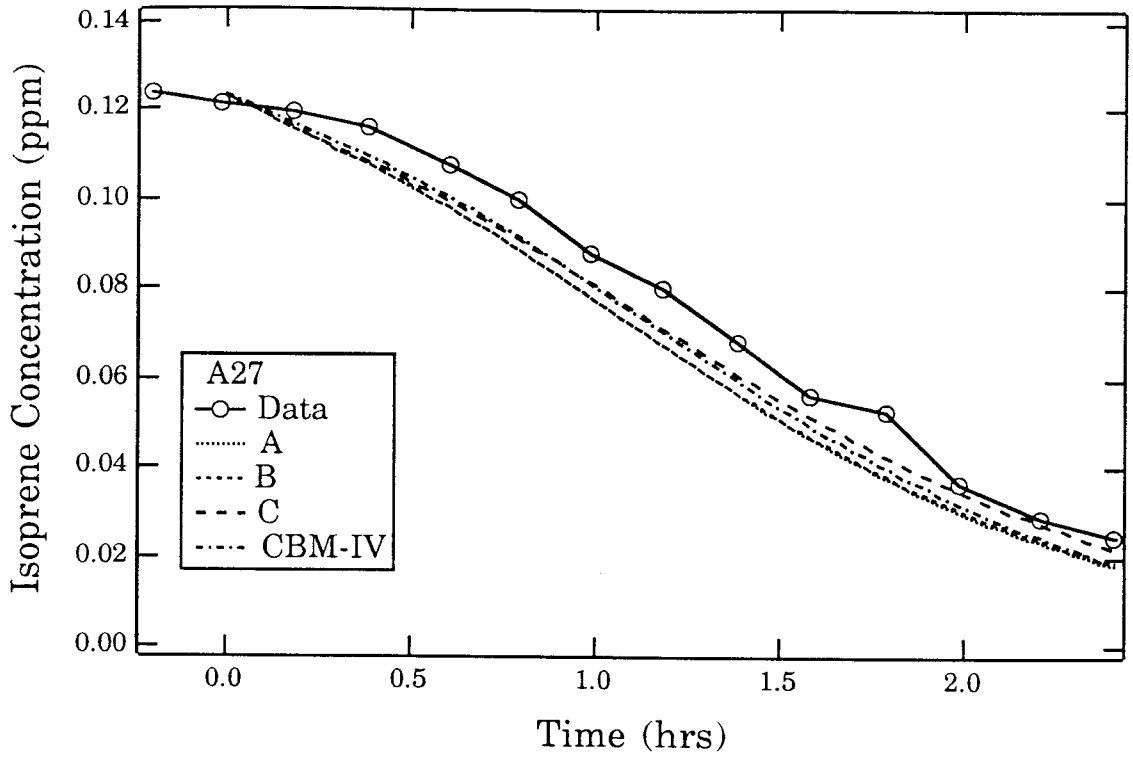


Figure 1b. Run INOXA27, isoprene data with simulations.

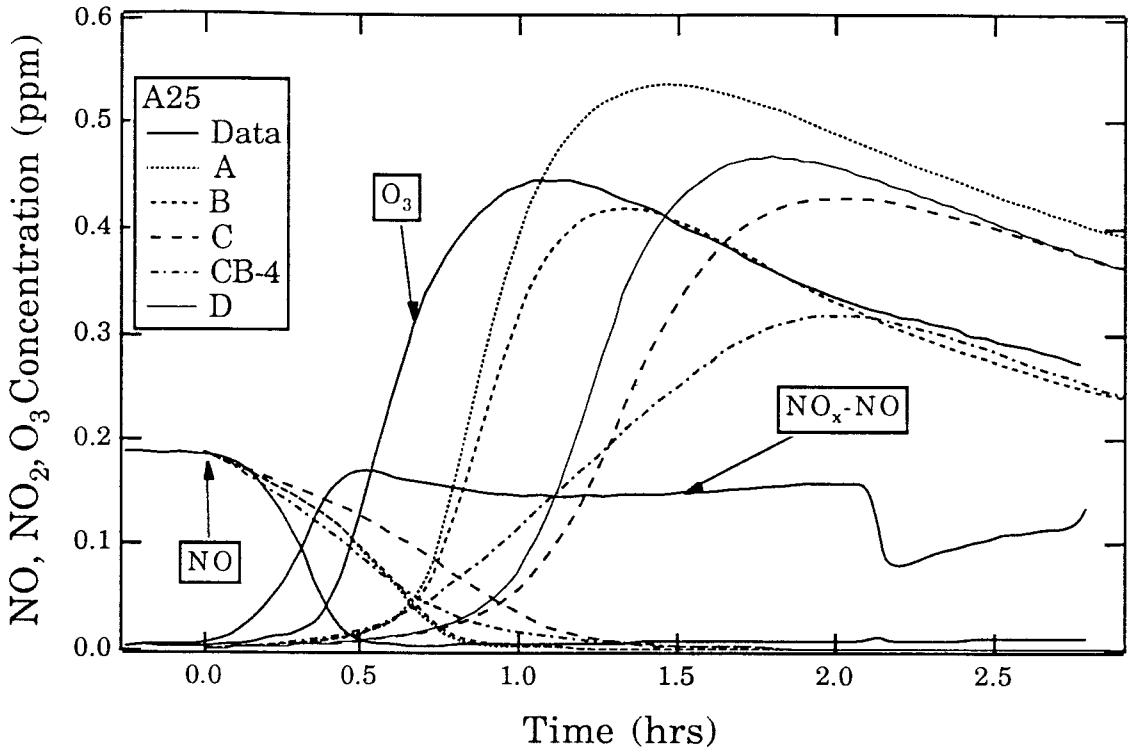


Figure 2a. Run INOXA25, NO and $O_3$ data with simulations.

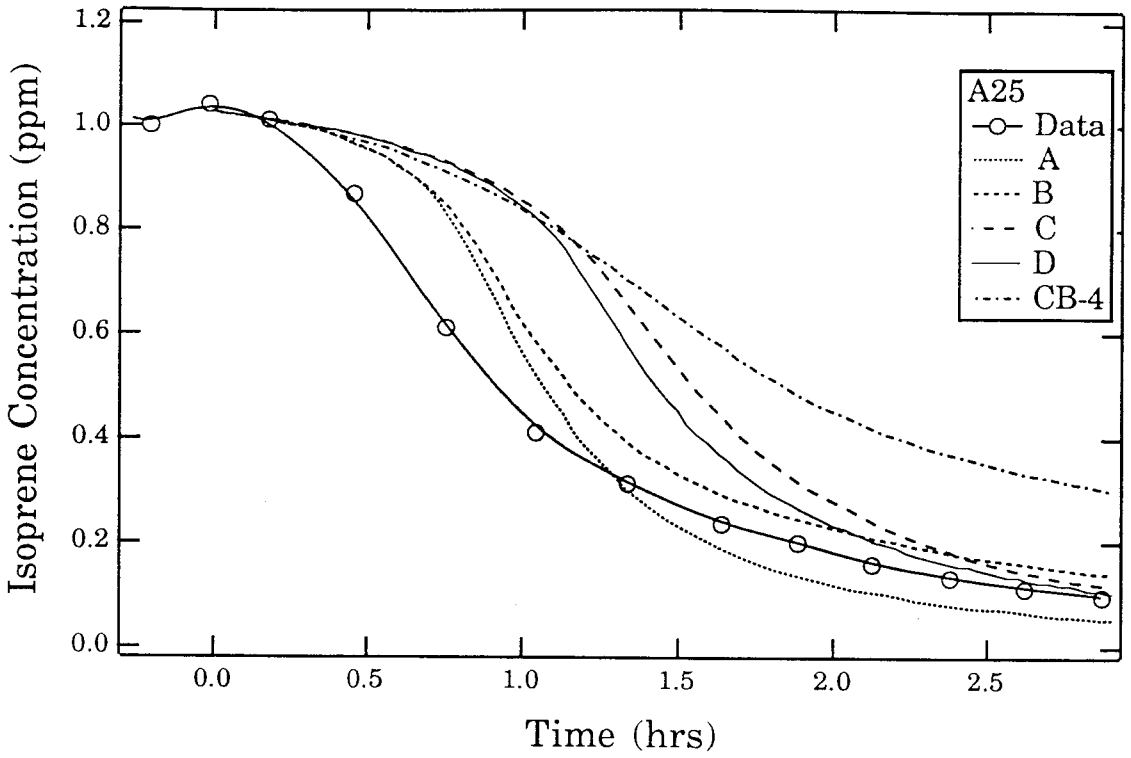


Figure 2b. Run INOXA25, isoprene data with simulations.

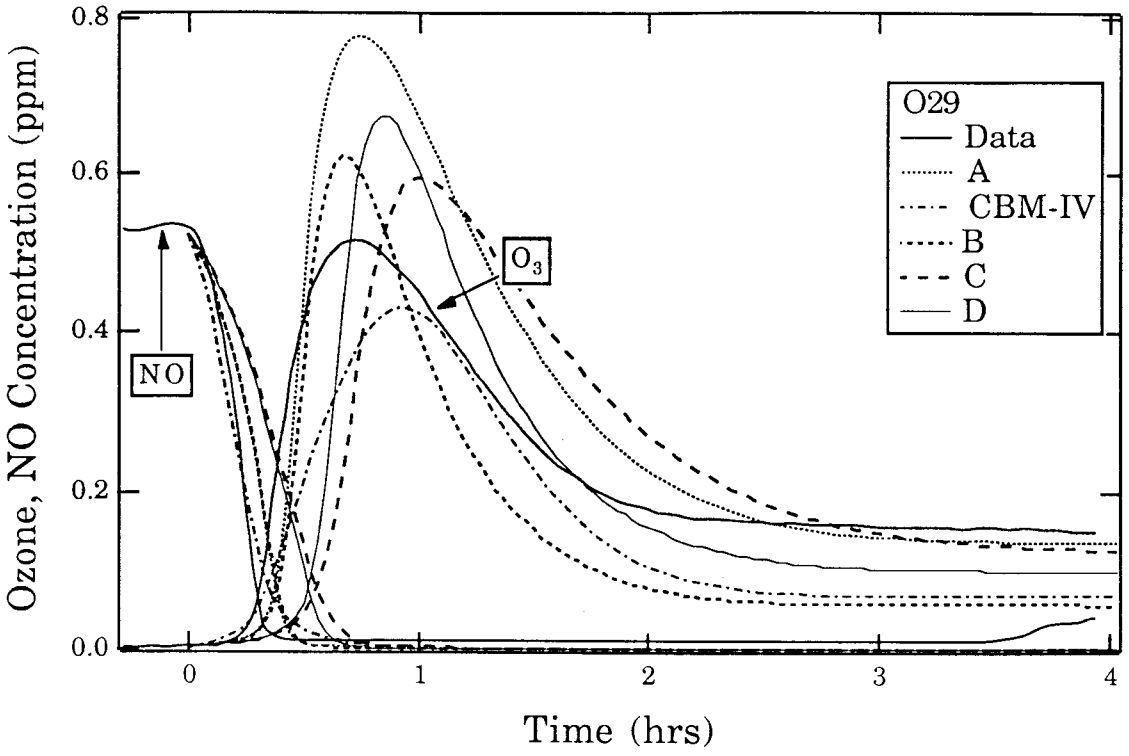


Figure 3a. Run INOXO29, NO and $O_3$ data with simulations.

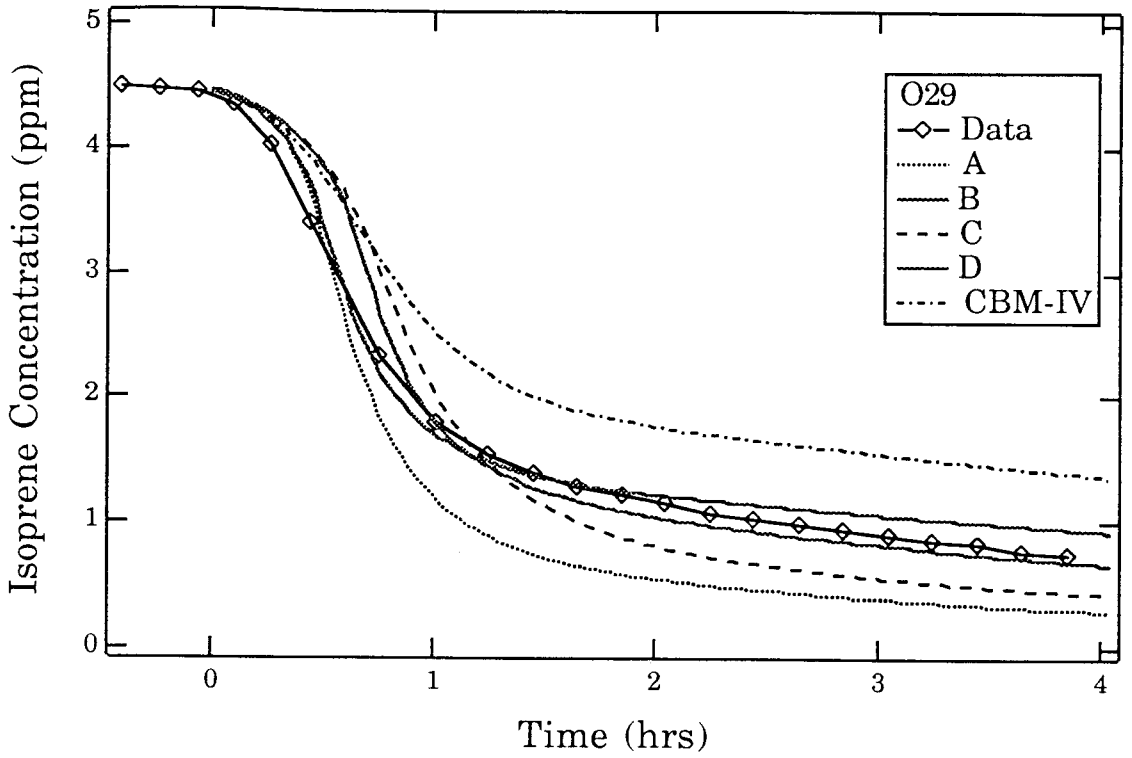


Figure 3b. Run INOXO29, isoprene data with simulations.

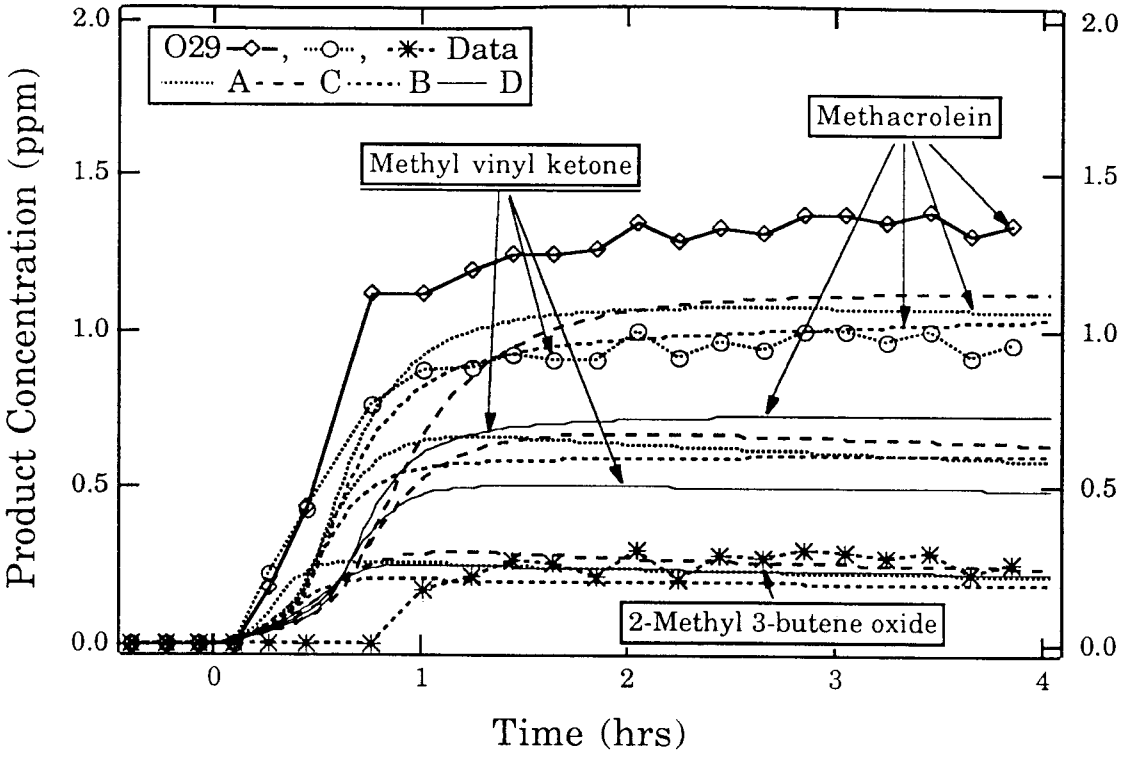


Figure 3c. Run INOXO29, methacrolein, methyl vinyl ketone, and 2-methyl 3-butene oxide data with simulations.

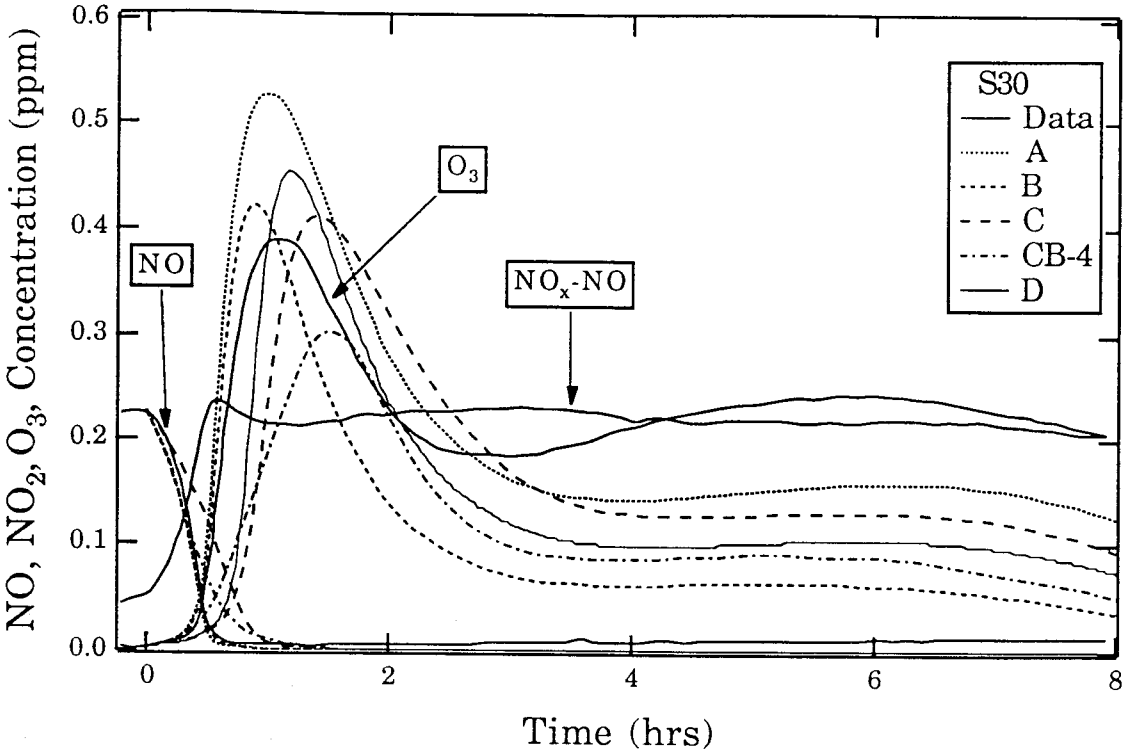


Figure 4a. Run INOXS30, NO and $O_3$ data with simulations.

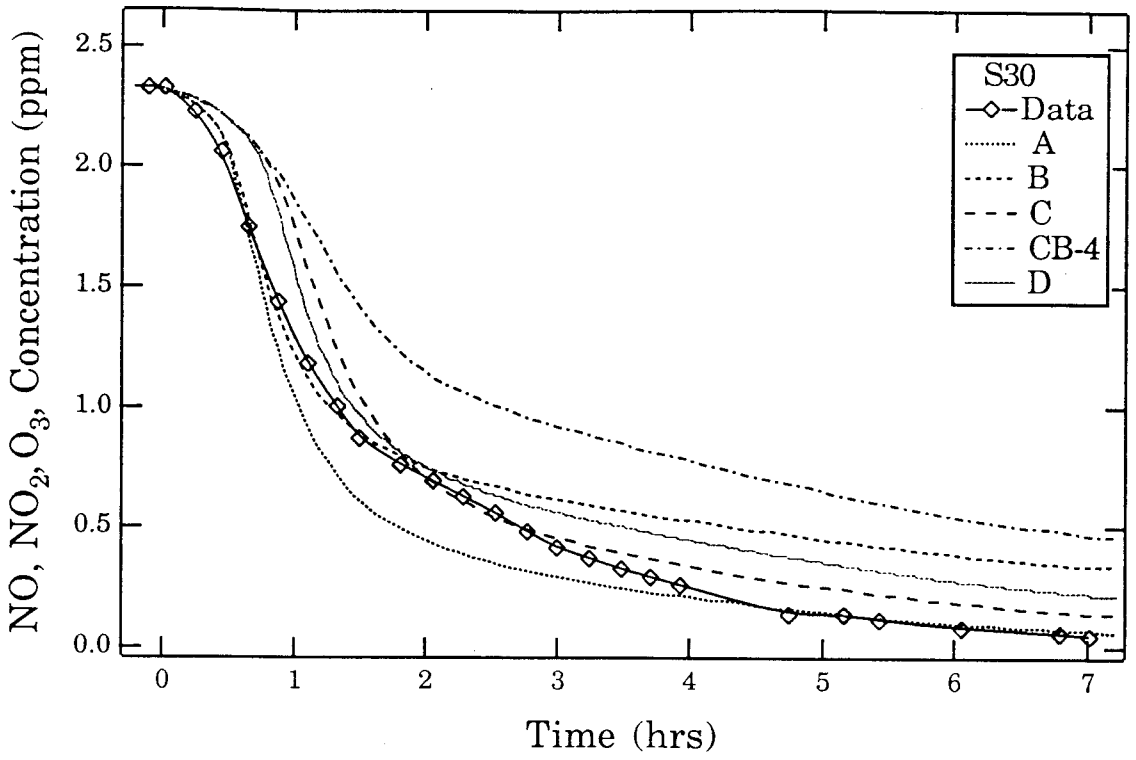


Figure 4b. Run INOXA27, isoprene data with simulations.

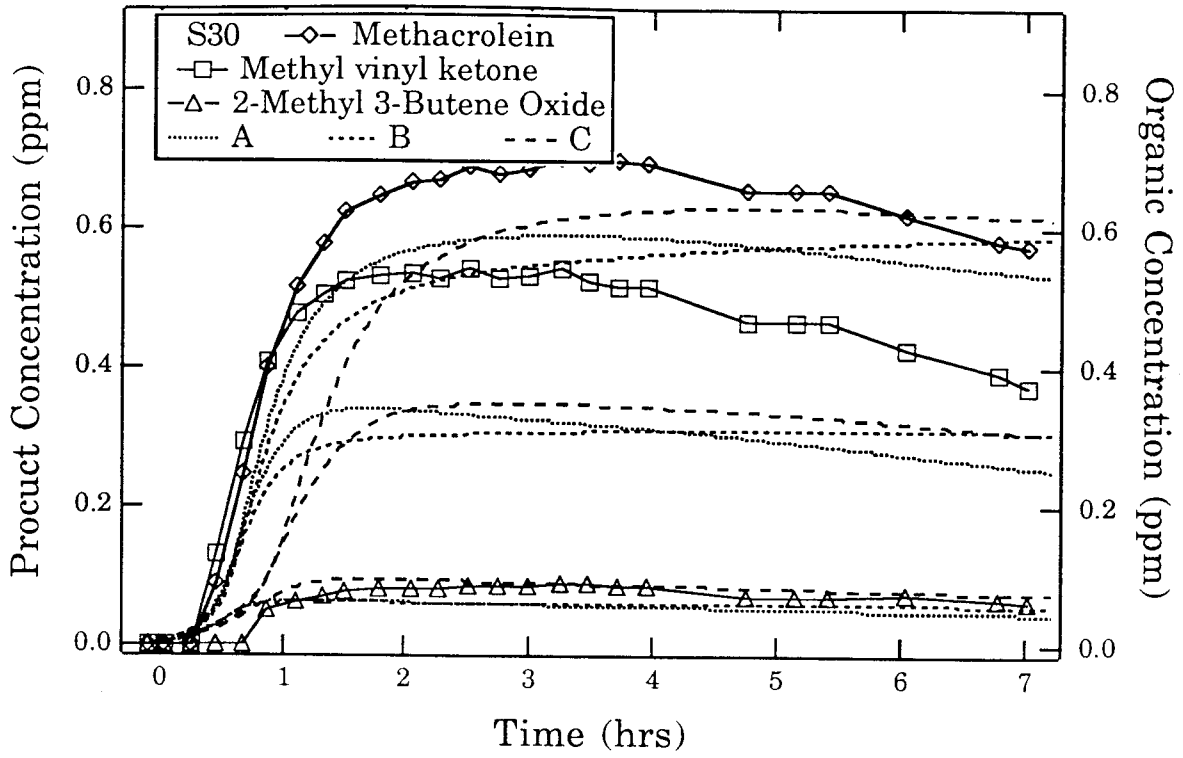


Figure 4c. Run INOXA27, methacrolein, methyl vinyl ketone, and 2-methyl 3-butene oxide.

# CHAPTER 5

# Atmospheric Photochemical Oxidation of 1-Octene: OH, O3, and O($^3$P) Reactions.

Suzanne E. Paulson[a] and John H. Seinfeld[b]

[a]Environmental Engineering Science

[b]Chemical Engineering

California Institute of Technology

Pasadena, CA 91125

Submitted to: *Environmental Science and Technology*

## *Abstract*

The photooxidation chemistry of 1-octene is examined in detail. Formation of OH from the $O_3$ reaction was examined with the use of a tracer/absorber, methyl cyclohexane. The $O_3$ - 1-octene reaction is found to produce, apparently directly, significant quantities of OH, 0.55±0.2 on a per molecule reacted 1-octene basis. Almost 100% of the reacted 1-octene could be accounted for as 80±10% heptanal, 11±6% thermally stabilized Criegee biradical, and about 1% hexane. The OH - 1-octene reaction was found to produce only 15±5% heptanal. The remainder is assumed to result in the formation of alkyl nitrates (33%), and isomerization and eventual formation of multisubstituted products (52%). A separate experiment examining the O($^3$P)-1-octene reaction, showed that the sum of hexyl oxirane and octanal accounted for about 80% of the reacted 1-octene. A photochemical model was developed for 1-octene oxidation, and compared favorably with smog chamber results from $NO/NO_2$/1-octene experiments, prediction ozone maxima within ± 25%.

# *Introduction*

1-Octene is an anthropologically derived contributor to the formation of photochemical smog. 1-Octene itself has been observed at ambient concentrations ranging from 40 ppt to 48 ppb (1). Further, 1-octene is expected undergo photooxidation in a manner which is similar to that of the C-6 and larger 1-alkenes, including, for example, 1-hexene, 1-nonene, and 2-ethyl 1-hexene, which have also been observed in the atmosphere (1,2).

Important questions arise with regard to the photochemical oxidation of the long-chain alkenes (those with a 5-carbon or longer backbone). These compounds may have additional reaction pathways available to them over and beyond those available to the smaller hydrocarbons. For example, it has been proposed that an alkoxy radical (formed from OH addition to the double bond, addition of $O_2$, and subsequent reaction with NO) with a 5 carbon or larger backbone and an available hydrogen atom may undergo isomerization via a 6-membered ring (3, 4, 5, 6). The ozone reaction is at least as uncertain as the OH reaction, as evidenced by Atkinson's (7) summary of ozone-alkene reactions. Of particular interest is the formation of OH radical from the $O_3$ reaction with 1-octene. Recent studies of the $O_3$ reaction with tetramethylethylene and isoprene have revealed about 70% OH yields from these reactions (8, 9). In addition, an earlier study of propene indicated about 30% OH formation from that $O_3$ reaction (10). Several other studies have led the authors to propose OH formation from $O_3$ reactions with isobutene, propene, and several terpenes (11, 12). It is of particular and timely interest to determine the OH yields from additional alkenes. OH production impacts both the effect of alkenes on urban ozone formation and experimental results that have assumed little or no OH formation from the $O_3$ -alkene reaction.

No studies have been carried out to date examining the atmospheric chemistry of 1-octene. In an earlier study in this laboratory, aerosol dynamics and aerosol chemical composition from 1-octene were examined (13, 14). Aerosol formation and oxidation chemistry of 1-heptene by a mixture of OH, $O_3$, and $O(^3P)$ have been examined by Grosjean (15), who identified several aldehyde products (dominated by formaldehyde and hexanal), in addition to small quantities of hexanoic acid.

We have performed a series of smog chamber experiments on the photooxidation of 1-octene using techniques specific for studying OH, $O_3$, $O(^3P)$, and $NO_2$ reactions. We have

focused on the identification and quantification of oxygenated products using GC/FID and GC/MS. We have also used 1-octene-$NO_x$ photooxidation experiments as a tool to refine the overall oxidation mechanism for 1-octene. These results are presented in the order $NO_2$, $O(^3P)$, OH, $O_3$, and the mixed oxidant experiments, so that each section depends only on those that precede it.

# *Experimental System*

The Caltech outdoor smog-chamber facility has been described previously (Pandis et al. 1991 16), and the methods and techniques specific to the methyl nitrite experiments (designed to study the OH reaction), the $O(^3P)$ experiments, $O_3$ experiments and $NO_2$ experiments, as well as the technique for collection and analysis of samples on GC/MS and GC/FID calibrations, are described by Paulson et al. (9, 17), and in more detail in Paulson (18). The initial conditions of the twelve experiments described in this work are summarized in Table 1.

1-Octene used in these experiments was certified 98% pure (Aldrich) and was used without further purification. We were able to detect a slight impurity, amounting to about 1% of the 1-octene signal. GC/MS analysis revealed that this impurity was n-octane. N-octane is relatively unreactive when compared to 1-octene (with an OH rate constant that is slower by a factor of 5; see Table 3); by the end of a typical experiment, during which 90% or more of the 1-octene had reacted, the n-octane remained at 88% of its original signal. While separation of 1-octene and n-octane was not sufficient in some analyses to reliably monitor n-octane, for a few experiments n-octane provides a rough additional check on the OH formed in the system. GC/MS identification of heptanoic acid, 2-ethyl hexanal, and 3-octanone were made by comparison with the National Institute of Standards and Technology library of mass spectral data (19). Identification of hexyl oxiranes, octanal, 2-octanone, and heptanal were made by comparison to standards obtained from Aldrich.

# *Nitrogen Dioxide Reaction*

The $NO_2$ reaction has been found to be slow for mono-alkenes (20), (21). However, the $NO_2$ reaction can be a minor source of interference in experiments that include high concentrations of NO, and consequently $NO_2$, as is the case in methyl nitrite experiments (22). We carried out one experiment (1NO21) to evaluate the importance of this reaction in

the 1-octene system. The experiment involved mixing $NO_2$ and 1-octene in the dark and monitoring for concentration changes. None were observed over the course of the 90 minute experiment. The $NO_2$ and 1-octene signals remained within ± 0.25% and 1.8% ($2\sigma$) of their average values, respectively, with no trend (data not shown). The upper limit for the rate constant for this reaction, calculated by assuming the width of the variation of the data was due to reaction, is $1.2 \times 10^{-21}$ $cm^3$ $molec^{-1}$ $s^{-1}$, hence the $NO_2$ reaction was ignored in the analysis of the other reactions.

## *$O(^3P)$-1-Octene Reaction*

The reaction between $O(^3P)$ and 1-octene, while likely to be of minor importance in the atmosphere, is of significant importance both in the mixed oxidant (1NOX#) and the methyl nitrite (1OH#) experiments (discussed below). Earlier studies of the $O(^3P)$-alkene reaction have shown that this reaction leads to the formation of oxiranes, resulting from direct addition of the $O(^3P)$ atom to the double bond, and aldehydes and/or ketones resulting from a 1,2 hydrogen shift (23). A proportion of many $O(^3P)$-alkene adducts has also been shown to decompose, forming a variety of organic radicals (22, 24). The organic radicals can lead to the formation of OH both in the reaction vessel and in the atmosphere.

We carried out one experiment to examine the reaction between $O(^3P)$ and 1-octene. The chamber was filled with ultra high purity $N_2$, and 1-octene, and $NO_2$ were added, allowed to mix, and the chamber was exposed to sunlight. The 1-octene, $NO_2$, NO, and $O_3$ data appear in Fig. 1, and the organic products are shown in Fig. 2. The summed products, which include octanal, hexyl oxirane, 2-octanone, and heptanal, as well as trace quantities of hexane, 2-ethyl hexanal, and 3-heptanone, account for about 73% of the reacted 1-octene. Octanal and hexyl oxirane, closely related isomers, were not completely separated in any of our analyses, and hence are reported as a sum. As expected, octanal and hexyl oxirane are the dominant products, arising from the following reactions:

(1) 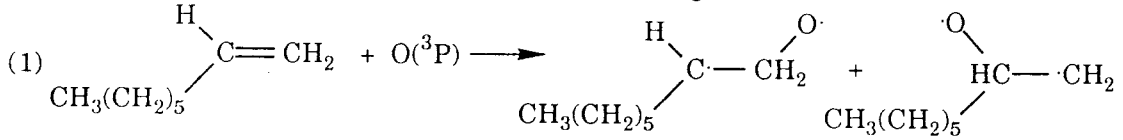

Addition of $O(^3P)$ to the terminal carbon is both less sterically hindered and produces the more stable radical, hence this adduct should be dominant. This adduct can relax or isomerize with a 1,2 hydrogen shift, forming hexyl oxirane and octanal:

(2) 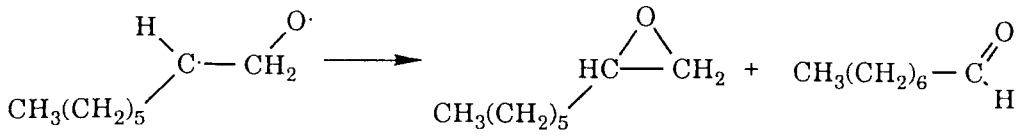

(Hexyl oxirane) (Octanal)

2-Octanone, a much less abundant product, is expected to arise from the other isomer:

(3) 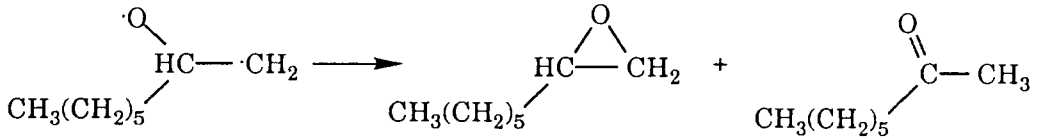

(Hexyl oxirane) (2-Octanone)

There are a number of possible decomposition pathways for the $O(^3P)$-1-octene adduct, many of which can form heptanal along with other products:

(4a) 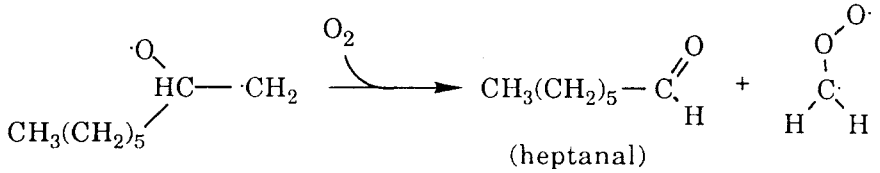

(heptanal)

(4b) 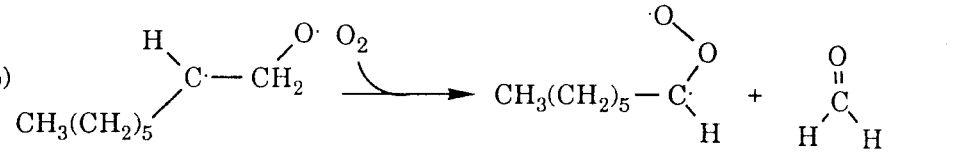

(formaldehyde)

The fate of the biradicals formed in the above reactions is not known.

(4c) 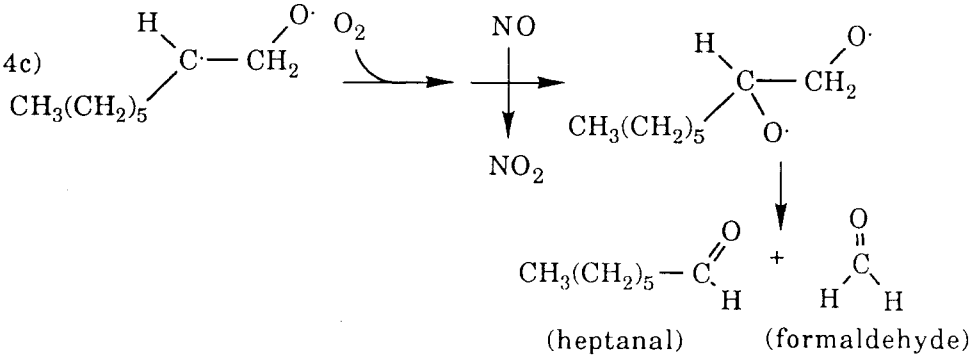

(heptanal) (formaldehyde)

(4d) 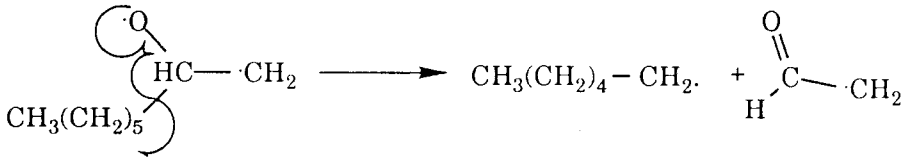

Heptanal also from the OH and $O_3$ reactions. We have used a simplified model of decomposition in simulations (Table 3); we have used a decomposition product that reacts with one NO to produce 0.9 $NO_2$ (with arbitrary 10% organic nitrate formation), plus heptanal and a lumped oxygenated product (indicated as a hydroxy carbonyl compound).

We have assumed that each decomposition leads to two such organic radicals, and that half of these will form heptanal or the lumped oxygenated product.

The source of the minor (1% yield or less) products 2-ethyl hexanal and 3-heptanone remain very unclear. It is possible that they are the products of oxidation reactions of impurities in the 1-octene used in these experiments, although pure liquid samples of 1-octene did not reveal any contaminant peaks other than n-octane.

Simulations of experiment 1O3P1 were carried out using the mechanism in Table 2, and are included in Figs. 1 and 2. The $O(^3P)$-1-octene rate constant was estimated from the $O(^3P)$-OH rate constant correlations developed by Atkinson (25). While the NO and $NO_2$ simulations of this low oxygen system are in good agreement with the data, the $O_3$ formation is very difficult to accurately predict. The observed $O_3$ concentration increases throughout the run (although it does not exceed 3% of the initial $NO_2$ concentration), even after the $NO_2$ concentration has dropped and the NO concentration is several ppm, hence is very difficult to explain. However, the majority of the 1-octene has reacted before the $O_3$ has reached 25ppb. Before we can derive the yields of the observed products of the $O(^3P)$ reaction, we must approximately derive the amount of OH forming in the system. OH can form from the $RO_2/HO_2/NO_x$ reactions resulting from the radical decomposition products (reaction 4 above). Calculations show that OH from the $O_3$ photolysis pathway is minimal, even when the $O_3$ concentration is artificially increased to the observed concentration. The NO and $NO_2$ concentrations are in fact very sensitive to the amount of decomposition initiated $RO_2/HO_2/NO_x$ chemistry that occurs, as this is the dominant pathway for oxidation of NO to $NO_2$. A simulation assuming zero decomposition predicts a maximum NO concentration of 5.45 ppm (the observed maximum was 4.47), and the predicted $NO_2$ concentration decreases to 0.3 ppm after 11 minutes (the observed minimum was 0.87), indicating a process converting NO to $NO_2$ is taking place. The simulations shown in Figs. 1 and 2 were generated assuming an organic radical yield of 0.16, translating into an 0.08 decomposition yield. The combined octanal/hexyl oxirane yield was 0.75, and 2-octanone, 0.055. The heptanal yield from the OH reactions is quite low, about 15% (see below), hence it was necessary to assume some heptanal formation from the $O(^3P)$ reaction, via (4)a, b and c. The heptanal yield that provided the simulations in Figs. 1 and 2 was 0.05. The yields, along with the estimated uncertainties, are listed in Table 2.

## *Hydroxyl Radical Reaction*

If the OH reaction with 1-octene proceeds in the same manner as with its smaller homologues, the reaction is expected to proceed as follows, beginning with OH addition across the double bond (e.g. 7):

(5) 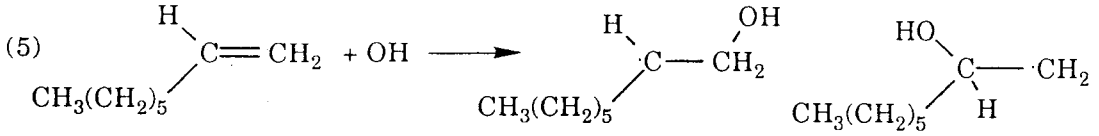

This alkyl radical quickly adds $O_2$, e.g.:

(6) 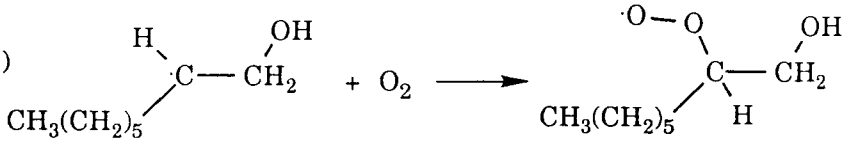

In polluted atmospheres, this alkyl peroxy radical reacts with NO, resulting in partial formation of an alkyl nitrate, an alkoxy radical, and in partial oxidation of NO to $NO_2$:

(7) 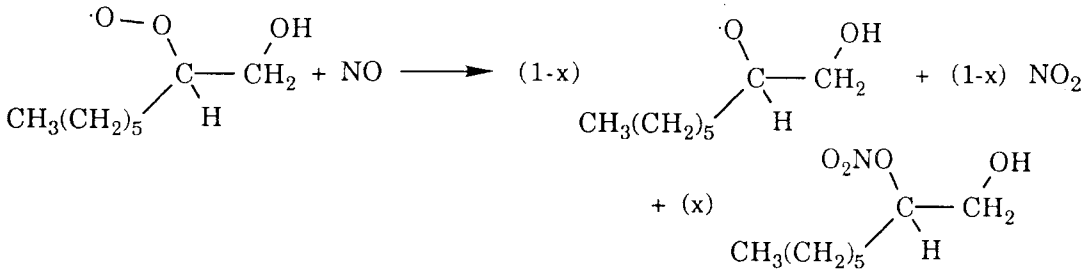

The value of x has not been measured for 1-octene, or any other alkene except isoprene (22), and propene, (26). The value estimated for isoprene (a $C_5$ dialkene) of 0.14±0.05 (see discussion in Paulson et al. (17)) is in agreement with the same size alkane, n-pentane, for which an alkyl nitrate yield of 0.13±0.004 was measured (2- alkyl peroxy radicals (27, 28), indicating that the alkenes may have similar yields as the same size alkanes. The values for propene were 0.017±0.008 and 0.015±0.007 for 2° and 1° alkyl peroxy radicals respectively, compared to 0.042±0.003 and 0.02±0.009 for propane 2° and 1°, respectively. The propene values may have been underestimated, as they were measured in methyl nitrite experiments that may have suffered from some interference from the $O(^3P)$ reaction (see Paulson et al. (17) for discussion). Even so, the 2° propene value may in fact be smaller than its propane counterpart, while the 1° value is in reasonable agreement. The alkyl nitrate yield for n-octane is 0.33 (27), and we have used this value for 1-octene in our simulations. The alkoxy radical may decompose, e.g.:

(8) 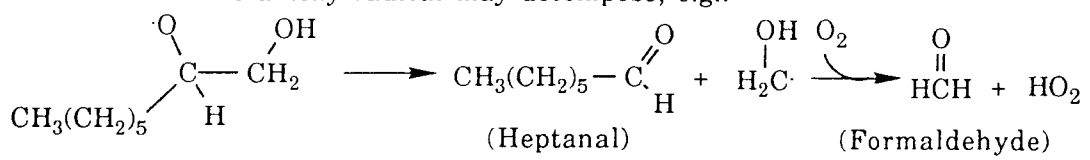

Alternatively, this alkoxy radical may isomerize in the same manner as has been proposed for alkanes (3, 4, 5, 6):

(9)

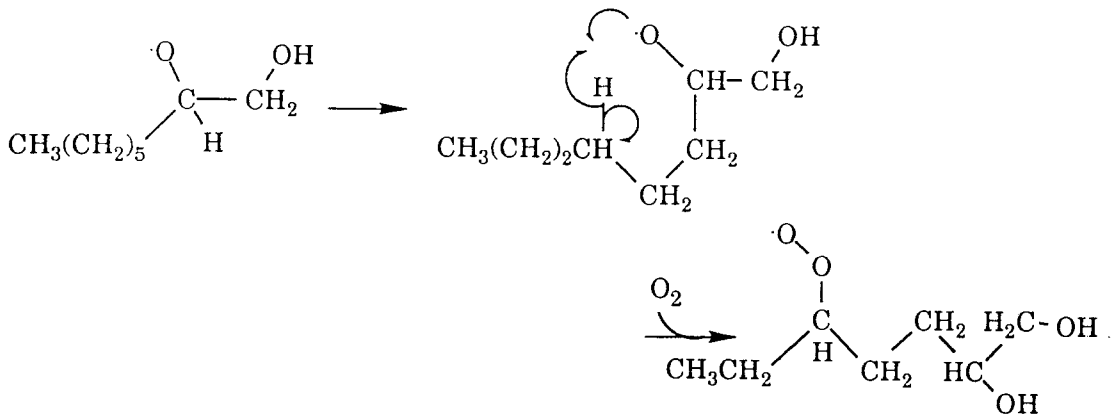

The resulting alkyl peroxy radical, in the presence of NO is expected to form the alkoxy radical with concomitant $NO_2$ production, and partial alkyl nitrate formation. The alkoxy radical is then expected to isomerize again, abstracting the labile 2-carbon hydrogen, and forming the following tri-substitiuted product along with $HO_2$:

(10)

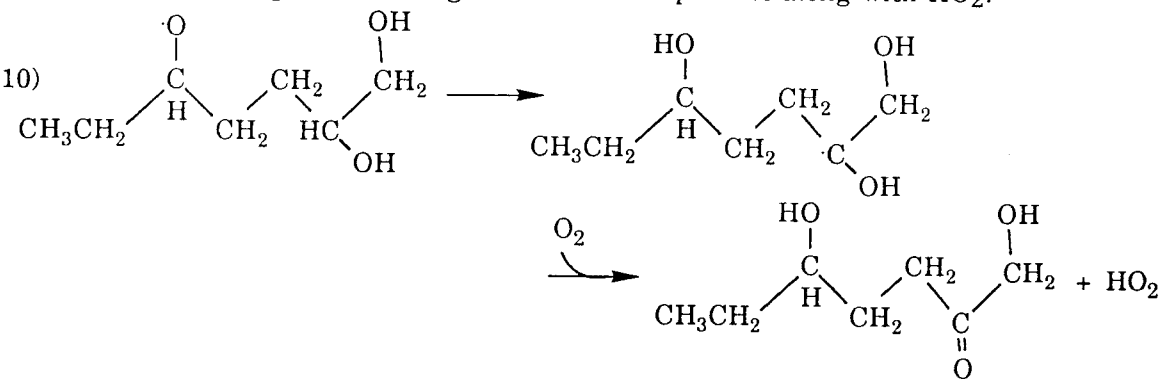

A third alternative reaction pathway is possible for the 1-octene-OH reaction, involving hydrogen abstraction from the alkyl backbone:

(11)

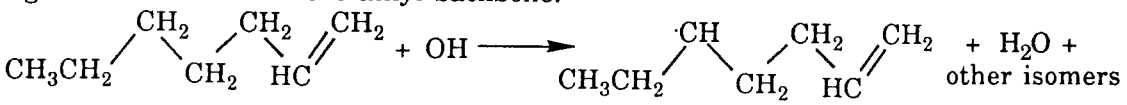

This compound may then isomerize as in reaction (9), react with $NO_2$, or decompose. The H-atom pathway was examined for 1-butene by Atkinson et al. (29), who showed that the extent of hydrogen abstraction from the saturated carbons was less than 5%. If we use a simple kinetic argument to estimate the extent of OH attack on the saturated carbons, we can compare the OH reaction rate of propane, which has the same number of 2° carbons as 1-butene, with the OH reaction rate of 1-butene (2° hydrogens are more labile than 1° hydrogens by a factor of about 6 (30), and predict that H-atom abstraction would account for only about 3.5% of the total reaction of OH, consistent with the Atkinson et al. (29)

findings. The same argument for 1-octene, using n-heptane to estimate the extent of abstraction from the saturated carbons, predicts that about 15% of the OH reaction proceeds through this pathway. The degree to which reactions (8) vs. (9), (10) and (11) occur is explored below.

OH was the dominant oxidant in both the methyl nitrite experiments (1OH1 and 2), and 1NOX1. This latter experiments was designed with a low hydrocarbon/$NO_x$ ratio so that $O_3$ formation would be minimal (Table 1). Major product data from samples concentrated on Tenax and run on a GC/FID for experiments 1OH1, 2, and 1NOX1 are shown with simulated results in Figs. 3, 4, and 5. The final yields of all products are summarized in Table 4. The products include heptanal, hexyl oxirane and octanal, and trace quantities of 2-octanone, as well as hexane, 3-heptanone, and 2-ethyl hexanal in some experiments. Several other small peaks were observed, although none was larger than the heptanal peak, and we were unable to identify their mass spectra. The total yields of identified products were very low; about 22, 16, and 21% for 1OH1, 1OH2, and 1NOX2, respectively. The dominant product is heptanal, an expected product of reaction (8) above. The formation of hexyl oxirane, octanal, and 2-octanone is probably due to $O(^3P)$ formation in the reactor, leading to these products via reactions (2) and (3), above. Small quantities of hexane are expected from the photolysis of heptanal.

Simulations of experiments 1OH1, 2 and 1NOX1 were carried out using the mechanism listed in Table 3. Simulations for 1NOX3, a similar experiment to 1NOX1, are also shown in Fig. 8. We found that good agreement with all three experiments was obtained by assuming that the heptanal yield (via reaction 8) was 0.15. The mechanism was also successful in predicting the hexyl oxirane/octanal concentrations; with the low hydrocarbon/$NO_x$ ratios used in 1NOX2, the OH concentration remains fairly low, hence the $O(^3P)$ reaction is significant.

The final yields from the OH reaction with 1-octene are 0.15±.07 heptanal, which, combined with an assumed alkyl nitrate yield of 0.33, totals 0.48. The remaining products of the 1-octene-OH reaction probably isomerized to form multisubstituted products via reactions (9) and (10), and the similar reactions for the 1-alkoxy radical, or reacted via reaction (11). Some of these products may condense to form aerosol. In an earlier study, we observed that about 3% of the reacted 1-octene was converted to aerosol (Wang et al. 1991a), although those experiments did not make clear whether OH or $O_3$ reactions were responsible for aerosol formation. The low heptanal yield indicates that the 1-octene-OH

reaction may proceed via the following process. 85% of the OH adds across the double bond (reaction 5), and 15% abstracts an H-atom from the backbone (reaction 11). About 33% of each results in formation of organic nitrates, leaving about 57% hydroxy alkoxy radicals, of which about 26% react via channel (8) to produce heptanal, and the remainder react via (9) and (10). The total yields may then be:33% organic nitrate, 10%products from reaction 11, 15% heptanal from reaction 8, and 42% reactions 9 and 10.

# *Ozone Reaction*

Based on results for 1-butene and other alkenes, $O_3$ is expected to add across the double bond (Atkinson 1990 and references therein):

(11) 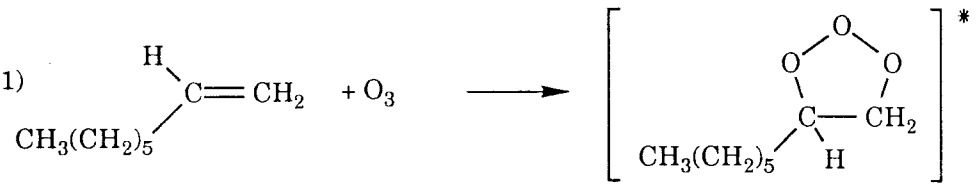

This energetically excited adduct is expected to decompose. Cleavage through the C-C bond and one of the O-O bonds yields two pairs of products: heptanal and the $C_1$ Criegee biradical, and formaldehyde and the $C_7$ Criegee biradical:

(12) 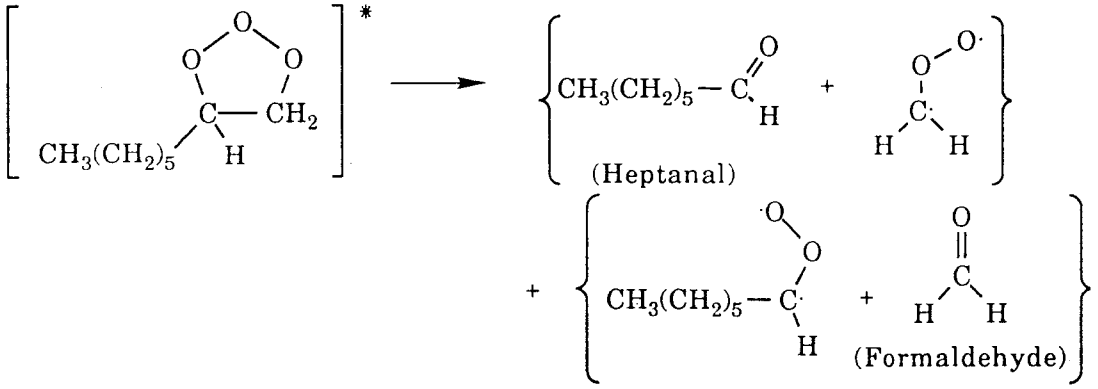

The fate of the $C_7$ Criegee biradical and the ratio of the above two pairs of products are areas of significant uncertainty, particularly for an alkene as large as 1-octene. From results for 1-butene we expect that the $C_7$ Criegee biradical decomposes to form hexane and $CO_2$, or becomes thermally stabilized, and may isomerize to form heptanoic acid (24). From the results for isoprene discussed in Paulson et al. (9), we can expect that the $C_7$ Criegee will result in the formation of OH, more than 50% heptanal, and other species.

Three experiments were carried out to examine the $O_3$ reaction with 1-octene, 1O31&2, and M1O31. The first two experiments involved mixing externally generated $O_3$ with 1-octene in the dark, and the third also included methyl cyclohexane, added to scavenge and track

OH formation from the $O_3$-1-octene reaction. The product concentration data from 1O32 and M1O31, as well as the methyl cyclohexane reacted are shown as a function of 1-octene reacted in Fig. 6. The yield data from the end of experiment 1O31 are shown in Table 4. The reaction of n-octane was also observed in experiment 1O31 (Table 4). As expected from previous studies, significant OH formation is evident. The dominant product species is heptanal, but quantities of heptanoic acid, an unidentified peak, and trace quantities of hexane and 3-heptanone were also observed. The unknown and heptanoic acid eluted from the analytic column in broad peaks, and hence do not develop into integratable peaks until they have reached substantial concentrations. The total product yields, on a per molecule 1-octene reacted basis, were: 43% (1O31), 53% (1O32), and 75% (M1O31). Some of the variation in the total yields results from variation in the detection limits in each of the experiments; that all of the products were not observed in each of the experiments indicates that they did not exceed the detection limits of that experiment; they may still have formed.

Simulations were carried out with the mechanism in Table 3 to determine the OH, carbonyl, and hexane yields needed to explain the data. The mechanism includes chemistry for the alkyl peroxy radicals that form from OH addition to 1-octene; these reactions must be considered as they are potential sources of heptanal and OH. They form and react as follows:

(13) 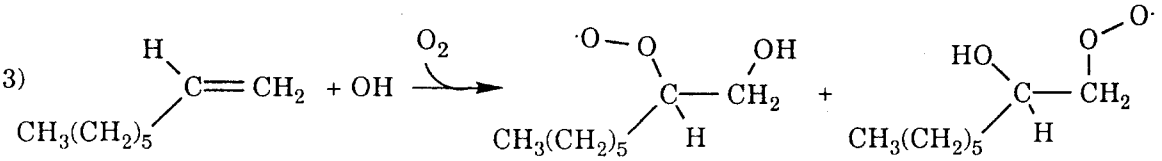

The self reaction of the alkyl peroxy radicals results in the formation of alkoxy radicals, as well as dihydroxy and hydroxy carbonyl compounds (31, 7, and references therein), e.g.,

(14) 2 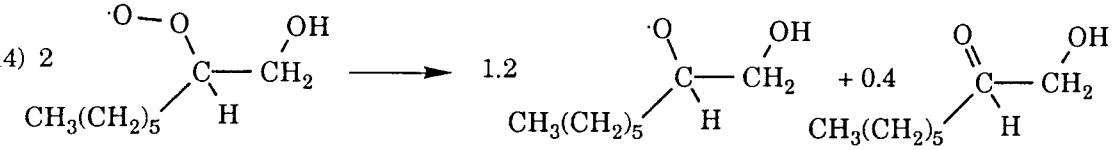

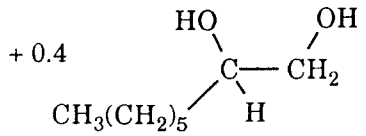

The reactions of the alkoxy radicals are discussed in the OH section above. It appears from analysis of results from the OH reaction that they do not in fact decompose, but instead

largely isomerize. Consistent with the OH experimental results, we assumed a 15% heptanal yield from the alkoxy radical decomposition, with concomitant $HO_2$ and formaldehyde formation. The remaining alkoxy radicals are assumed to form the lumped peroxy radical "MCHR" subsequent to their presumed isomerization (see Table 3). The reaction of the alkyl peroxy radicals with $HO_2$ is at least a factor of 10 faster than the self reactions (see Table 2), and is expected to form an alkyl peroxide:

(15) 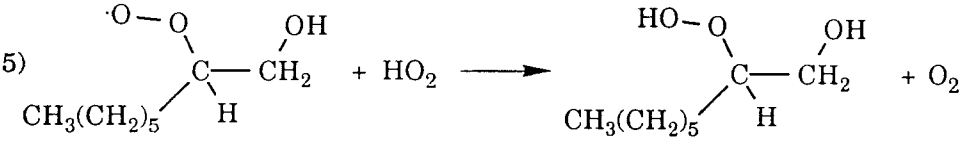

The reaction of methyl peroxide with OH is very slow, hence we have assumed that OH attack will take place on the carbon backbone of these large alkyl peroxides, and thus have assumed an OH rate constant equal to that for hexane. Hence, the OH-alkyl peroxide reaction will form another alkyl peroxy radical, but will not lead to the formation of $HO_2$ or heptanal. The only potential pathway for regeneration of OH from the OH initiated reactions in this $NO_x$ -free system is the reaction:

(16) $HO_2 + O_3 \longrightarrow OH + 2\ O_2$

However, this reaction is relatively slow. Simulations show that the dominant loss pathway for both $HO_2$ and the alkyl peroxides is reaction 15, forming alkyl peroxides and providing no regeneration pathway for $HO_2$ or OH.

To find the OH yield necessary to account for the methyl cyclohexane loss, we ran simulations of experiment M1O31, adjusting the OH yield until it agreed with the data. An OH yield of 0.55 was used to generate the curve shown in Fig. 6. As an independent check on the OH yield, we simulated the impurity n-octane in experiment 1O31, which began at 0.17 ppm and ended at 0.15 ± 0.005 ppm. Simulations of this reaction showed a final n-octane concentration of 0.155, in excellent agreement with the data. The estimated uncertainty for the OH yield, resulting largely from the noise in the methyl cyclohexane data (the maximum change in the methyl cyclohexane signal was 5%) is ± 0.2.

The heptanal yield necessary to account for the concentrations observed (Fig. 6) is 0.8 per molecule of 1-octene reacted. The simulation results for both 1O32 and M1O31 are included in Fig. 6. This yield is higher than the observed yield because it accounts for the 1-octene that reacted with OH rather than $O_3$, and the reaction of heptanal with OH. About 2% of the heptanal that formed came from the alkyl peroxy radical reactions. The hexane yield from the $O_3$-1-octene reaction was rather low; calculations showed that a yield of 0.012 was sufficient to account for the 1O31 data.

Heptanoic acid is expected to form from isomerization of the thermally stabilized $C_7$ Criegee biradical, thought to be facilitated by water (8):

(17) 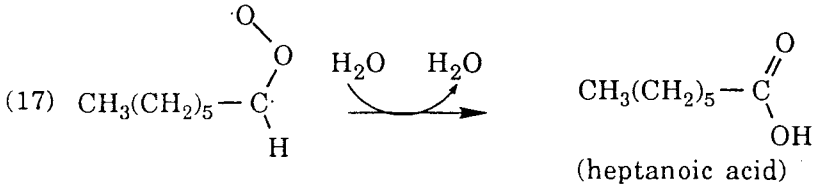

(heptanoic acid)

The heptanoic acid concentration was successfully simulated with a thermally stabilized $C_7$ Criegee biradical yield of 0.1. The estimated uncertainty for this yield is ± 0.06, resulting from the fact that the GC calibration factor for heptanoic acid was estimated.

In summary, we recommend the following yields from the $O_3$-1-octene reaction: 0.80± 0.15 heptanal, 0.012±0.04 hexane, 0.55±0.2 OH and 0.11±0.06 thermally stabilized $C_7$ Criegee biradical. In Paulson et al. (9), we found that the $O(^3P)$ yield from the $O_3$-isoprene reaction was about 0.45. We did not observe evidence for the formation of $O(^3P)$ from the $O_3$ -1-octene reaction, in the form of the known products of the $O(^3P)$-1-octene reaction, which were shown (above) to be octanal, hexyl oxirane, and 2-octanone. However, the rate constant for the $O(^3P)$ reaction with 1-octene is slower than isoprene by a factor of five, hence 1-octene is expected to be much less successful in competing for $O(^3P)$ with $O_2$. Simulations showed that an $O(^3P)$ yield of 0.2 would produce less than 0.04 ppm octanal and hexyl oxirane combined; this is below the detection limit of about 0.06 ppm for these experiments.

We propose the following mechanism for the $O_3$-1-octene reaction. After the initial addition of $O_3$ to the double bond in 1-octene, reaction (11), above, the ozonide decomposes asymmetrically.

(18) 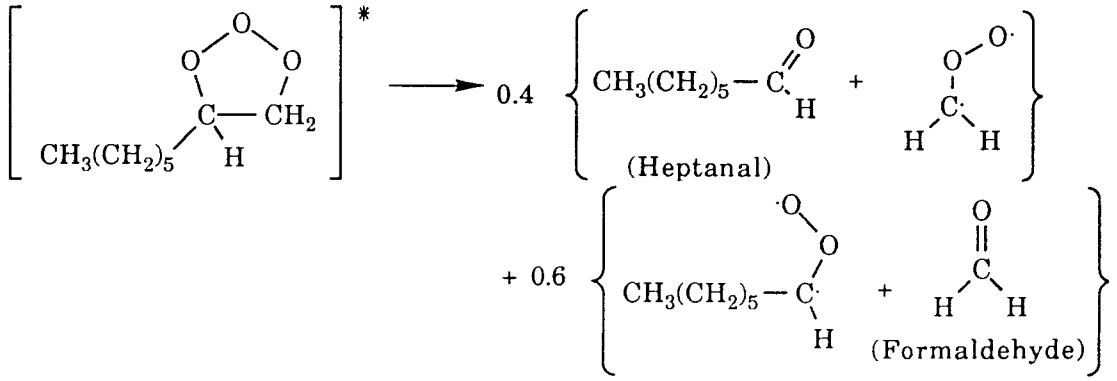


The ratio is rather arbitrary, but since the $C_7$ Criegee biradical is more stable than the $C_1$ Criegee, the formaldehyde/$C_7$ Criegee pair is assumed to dominate. As it appears that the

$C_1$ Criegee does not result in OH formation (7 and references therein), assuming the 0.4/0.6 branching ratio allows room to explain OH formation. The $C_7$ Criegee then breaks down in the following manner:

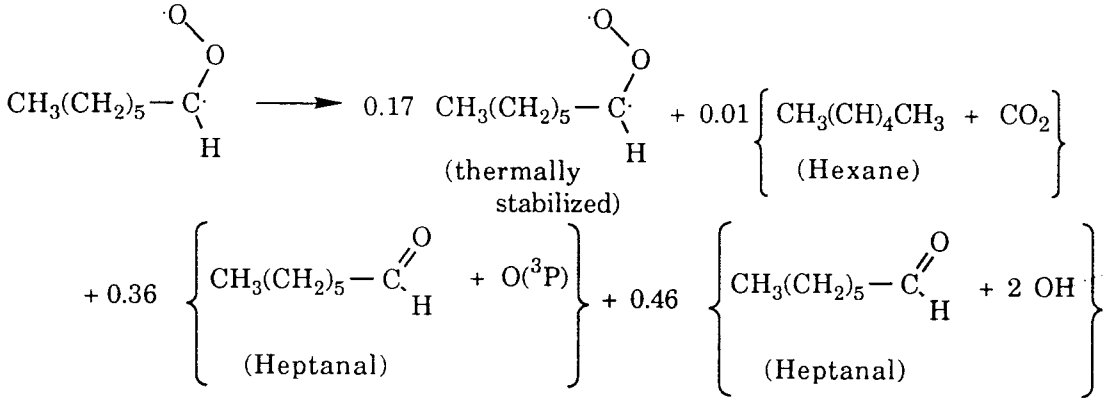


The first two products are derived directly from our observations of heptanoic acid and hexane formation. In Paulson et al. (9), we could only explain OH formation from the well constrained isoprene-$O_3$ reaction by assuming two OH radicals per Criegee biradical that followed that reaction path, hence we assume the same process here. We also observed large quantities of $O(^3P)$ formation from the isoprene-$O_3$ reaction (9), and there is evidence that this pathway is by no means restricted to isoprene; oxirane formation has been observed from the reaction of $O_3$ with ethene, trans 2-butene, and tetramethylethylene (32). While we did not observe oxirane and aldehyde formation in these experiments, simulations showed that the $O(^3P)$ yield would have to exceed about 0.25 to produce observable oxirane and aldehyde under the conditions of these experiments. We have therefore assumed that the remaining $C_7$ Criegee biradical decomposes to give heptanal and $O(^3P)$. The $C_1$ Criegee biradical decomposes or becomes stabilized (7):

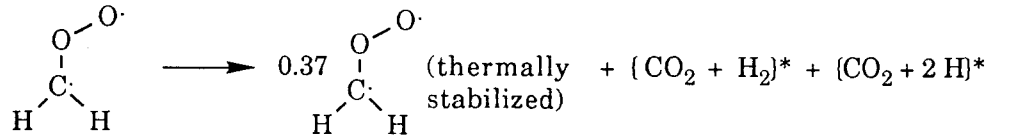


This mechanism produces 0.108 thermally stabilized $C_7$ Criegee biradical, 0.006 hexane, 0.55 OH, 0.21 $O(^3P)$, and 0.79 heptanal. Combined with the additional stabilized biradical from the $C_1$ fragment, the total yield of stabilized biradical is 0.26. This value is consistent with indirect measurements of stabilized biradical yields in other systems. Hatakeyama et al. (33) found ethene, propene and trans-2-butene yielded 39, 25.4, and 18.5 percent stabilized biradical, respectively, and Niki et al. (8) found 25-30% for 2,3-dimethyl 2-butene. The most similar alkene of these is propene, which, like 1-octene, has a mono-

substituted double bond, and which compares favorably with our stabilized biradical yields.

## *Mixed Oxidant Experiments*

In 1-Octene-$NO_x$ experiments OH, $O_3$, and $O(^3P)$ are present, allowing us to evaluate the mechanism for the full photooxidation system. The $NO_x$ experiments can be divided into three sets. 1NOX1 was discussed in the OH section above. 1NOX2-6 are smog simulation runs similar to runs that have been made with many hydrocarbons for mechanism verification purposes. These runs were carried (except for 1NOX3) out as part of a set of experiments designed to study aerosol formation; this aspect is discussed by Wang et al. (13, 14). In the present study, we have run simulations of each of the experiments that involved only 1-octene, $NO_x$ and in some cases small quantities of ammonium sulfate (seed) aerosol. Experiment 1NOX7 was run at a particularly high concentration and includes product data.

The 1-octene, NO, and $O_3$ data for the smog experiments (1NOX2-6), with simulation results are shown in Figs. 7-11. $NO_x$-NO data were not simulated as the instrument response for the organic nitrates was not known. We have used the updated inorganic mechanism recommended in the work of Atkinson et al. (34) in combination with the mechanism in Table 3 to generate the simulations in this work. Simulations using a series of assumptions about the mechanism are compared to the data from 1NOX2 in Fig. 7. The base case, (A) which is detailed in Table 3, makes the following assumptions: from the OH reaction, 15% decomposition via rxn. (8) above, with heptanal formation, 33% organic nitrates, and 52% isomerization and/or H-atom abstraction via rxns. (9) through (11) above. The $O_3$ reaction is assumed to produce 80% heptanal, 45% OH, and 20% $O(^3P)$. From the $O(^3P)$ reaction we assumed an 80% yield for the sum of octanal and hexyl oxirane, 6% 2-octanone, and 8% decomposition (leading to 16% organic radicals). Fig. 7 shows the sensitivity of the prediction to assumptions about the amount of organic nitrate formed (B), the relative importance of reaction (8) vs. reactions (9)-(11) (C), and the amounts of OH (D) and $O(^3P)$ (E) from the $O_3$ reaction. A reduction in organic nitrate formation from 33% to 23% (B) leads to an overestimation of the $O_3$ peak, and a reaction system that is too fast. Curve (C) show the effect of assuming the OH reaction channels 65% through rxn. (8) (forming heptanal), 2% through rxns. (9)-(11), with 33% nitrate formation.

The result is similar to curve (B). Assuming an OH yield from the $O_3$ reaction of 55% rather than 45% produces curve (D), also somewhat fast, and finally, assuming no $O(^3P)$ from the $O_3$ reaction results in some underestimation of the $O_3$ peak.

The mechanism in Table 3 performs well against the chamber data shown in Figs. 7-11. The predicted $O_3$ levels are within 25% of the observed levels, the reaction timing is generally within a few minutes of what is observed. Additionally, the NO, 1-octene, and $O_3$ curves agree with the predictions equally well; these variables do not behave independently. Some consistent disagreement does appear late in the runs, after the $O_3$ has peaked in a regime that can be characterized by low $NO_x$ chemistry. In this portion of the run, the predicted $O_3$ decays faster than the observed $O_3$. This trend has been observed for another alkene (isoprene, 18); whether it is due to the Caltech chamber or uncertainties in the low $NO_x$ chemistry is not known.

Experiment 1NOX7 is included in Figs. 12 and 13, and allows additional testing of the ability of our mechanism to predict the product data. The simulations of this experiment is strongly time shifted, however, the $O_3$ maximum is within 25%, and the magnitude of 1-octene is in good agreement. Heptanal comes within 8%, while the combined hexyl oxirane and octanal signal is underpredicted by about 45%, possibly indicating that the $O(^3P)$/1-octene rate constant may be somewhat faster than estimated. If we instead assume case (C) above, where the OH-1-octene is assumed to react through reaction (8), we find that the model performance is much worse; heptanal is overpredicted by 35%, and the combined hexyl oxirane and octanal signal is underpredicted by about 60%.

# *Summary*

The reactions of 1-octene are in some ways very similar to the those of smaller alkenes, and in others dramatically different. The $NO_2$ reaction is very slow, proceeding at a rate of less than $1.2 \times 10^{-21}$ $cm^3$ $molec^{-1}$ $s^{-1}$. The $O(^3P)$ reaction is similar to that of its smaller homologues; this reaction is dominated by oxirane formation, octanal, and 2-octanone formation. The decomposition pathway, about 8%, is less important than it is for 1-butene, where it accounts for about 20% (24).

The majority of the OH initiated alkoxy radical reaction appears to proceed via a different pathway than the smaller hydrocarbons; the decomposition pathway results in a 15%

heptanal yield. The alkyl nitrate yield from this reaction probably accounts for 33% of the products, leaving 52% unaccounted for by known pathways. The most likely reactions for the remaining alkoxy radicals is an internal isomerization via a six-membered ring combined with some H-atom abstraction from the carbon backbone by OH. Some of these products may enter the aerosol phase, which was shown to account for about 4% of the reacted 1-octene in a previous study (13).

The 1-octene reaction with $O_3$ produces significant quantities of OH, about 0.55 per molecule of 1-octene reacted, as well as about 80% heptanal, 11% thermally stabilized $C_7$ biradical, and 1% hexane, accounting for nearly 100% of the reacted 1-octene. The OH yield is not at all consistent with most $O_3$-alkene studies, but, as discussed in detail in Paulson et al. (9), most previous studies seem to have overlooked OH formation in $O_3$ reaction systems. The OH yield is consistent with those studies that have inferred or measured OH formation (8, 9, 10), and begins to fill out the picture of the quantities of OH that can be expected to form from the alkene family. The heptanal yield is much more than the 50% yield expected from the standard $O_3$-alkene reaction mechanism, and exceeds the rough estimate of hexanal yields from the 1-heptene-$O_3$ reaction reported by Grosjean (15), but this is expected as OH was not accounted for in that study. The observation is consistent with findings for isoprene (9) where carbonyl yields totaled 93%. The decomposition pathway that leads to hexane formation appears to be very minor, at about 1% compared to 6% for 1-butene (24).

The complete mechanism, comprised of the constituent OH, $O(^3P)$, and $O_3$ reactions compares favorably to smog-simulation data. Maximum ozone concentrations are predicted within 25%, as are the timings. The simulations are somewhat improved by assuming that the OH yield from the $O_3$ reaction is 0.45, rather than 0.55, well within the uncertainty of the measurement, and with a 20% yield of $O(^3P)$. .Heptanal formation is in excellent agreement, while the combined hexyl oxirane and octanal signal is underpredicted.

# *Acknowledgements*

This work was supported by National Science Foundation Grant ATM-9003186 and a Dissertation Fellowship from the American Association of University Women.

# *References*


(1) Isidorov, V.A. (1990) Organic Chemistry of the Earth's Atmosphere. Springer-Verlag (Berlin).

(2) Grosjean, D., and K. Fung (1984) *J. Air Poll. Cont. Assoc.* 34:527-543.

(3) Carter, W.P.L., K.R. Darnall, A.C. Lloyd, A.M. Winer, and J.N. Pitts (1976) *Chem. Phys. Lett.* **42**, 22-7.

(4) Baldwin, A.C., J.R. Barker, D.M. Golden, and D.G. Hendry (1977) *J. Phys. Chem.* **81**, 2483-92.

(5) Carter, W.P.L., and R. Atkinson (1985) *J. Atmos. Chem.* **3**, 377-405.

(6) Dobe, S., T. Berces, and F. Marta (1986) *Int'l J. Chemical Kinetics* **18**, 329-44.

(7) Atkinson R., (1990) *Atmospheric Environment* **24A**, 1-41.

(8) Niki, H., P.D. Maker, C.M. Savage, L.P. Breitenbach, and M. D. Hurley (1987) *J. Amer. Chem. Soc.* **91**, 941-6.

(9) Paulson, S.E., R.C. Flagan and J.H. Seinfeld (1991b) *Int'l J. Chem. Kinet.* (in press).

(10)Japar, S.M., C.H. Wu, and H. Niki (1976) *J. Phys. Chem.* **80**, 2057-62.

(11)Herron, J.T., and R.E. Huie (1978) *Int'l J. Chemical Kinetics* **10**, 1019-41.

(12)Atkinson, R., D. Hasegawa, and S.M Aschmann (1990) *Int'l J. Chemical Kinetics* **22**, 871-87.

(13)Wang, S.C., S. E. Paulson, D. Grosjean, R. C. Flagan and J. H. Seinfeld (1991) *Atmospheric Environment* **21** (in press).

(14)Wang, S.C., R. C. Flagan and J. H. Seinfeld (1991) *Atmospheric Environment* **21** (in press).

(15)Grosjean, D. (1984) *Sci. Tot. Envir.* **37:**195-211.

(16)Pandis, S.N., S.E. Paulson, R.C. Flagan, and J.H. Seinfeld (1991) *Atmospheric Environ.* **25a**, 997-1008.

(17)Paulson, S.E., R.C. Flagan and J.H. Seinfeld (1991a) *Int'l J. Chem. Kinet.*(in press).

(18) Paulson, S.E., PhD Thesis, California Institute of Technology, Pasadena, CA (1991)

(19)National Institute of Standards and Technology Mass Spectral Library (1990).

(20)Glasson, W.A. and C.S. Tuesday (1970) *Environ. Sci. Technol.* **4**, 752-61.

(21)Ohta, T., H. Nakagura, S. Suzuki (1986) *Int'l J. Chemical Kinetics* **18**, 1-11 .

(22)Tuazon, E.C. and R. Atkinson (1990) *Int'l J. Chemical Kinetics* **14**, 1221-36.

(23)Cvetanovic, R.J. (1963) *Adv. in Photochem* **1**, 115-82.

(24)Atkinson, R. and A. C. Lloyd (1984) *J. Phys. Chem. Ref. Data* **13**, 315-444.

(25) Atkinson R., *Chemical Rev.* **19**, 799 (1985).

(26) Shepson, P.B., E.O. Edney, T.E. Kleindienst, J. H. Pittman, and G.R. Namie (1985) *Environ. Sci. Technol.* **19**, 849-54.

(27)Atkinson, R., S.M. Aschmann, W.P.L. Carter, A. M. Winer and J.N. Pitts (1982) *J. Phys. Chem.* **86**, 4563-9.

(28) Atkinson, R. , W.P.L. Carter, and A. M. Winer (1983) *J. Phys. Chem.* **87**: 2012-8.

(29)Atkinson, R., E. Tuazon, and W.P.L. Carter (1985) *Int'l J. Chemical Kinetics* **27**, 725-734.

(30) Atkinson, R. *Int'l J. Chemical Kinetics* **19**, 799 (1987).

(31)Madronich, S. and J. G. Calvert (1990) *J. Geophys. Res.* **95**, 5697-715.

(32)Martinez, R.I., J. T. Herron and R. E. Huie (1981) *J. Amer. Chem. Soc.* **92**, 4644-.

(33)Hatakeyama, S., H. Kobayashi, and H. Akimoto (1984) *J. Phys. Chem.* **88**, 4736-9.

(34)Atkinson, R., D.L. Baulch, R.A. Cox, R.F. Hampson Jr., J.A. Kerr, and J. Troe (1989) *Int'l J. Chemical Kinetics* **21**, 115-50.

*Table 1.*

*Summary of Initial Conditions*

| Expt. | Primary Reaction | Initial Concentration (ppm) HC | NO | $NO_2$ | $CH_3ONO$ | Maximum $O_3$ | $HC/NO_x$ Ratio |
|---|---|---|---|---|---|---|---|
| 1NO21 | 1-octene + $NO_2$ | 4.02 | 0.015 | 7.39 | - | - | - |
| 1O3P1 | 1-octene + $O(^3P)$ | 8.25 | 0.062 | 5.5 | - | 0.120 | |
| 1OH1 | 1-octene + OH | 1.50 | 3.49 | 0.51 | 0.6 | 0.014 | - |
| 1OH2 | 1-octene + OH | 1.81 | 4.42 | 1.1 | 1.4 | 0.026 | - |
| 1NOX1 | 1-octene + $NO_x$ | 0.782 | 0.343 | 0.180 | - | 0.005 | 12.0 |
| 1NOX2 | 1-octene + $NO_x$ | 1.59 | 0.166 | 0.075 | - | 0.35 | 52.8 |
| 1NOX3 | 1-octene + $NO_x$ | 0.77 | 0.075 | 0.342 | - | 0.024 | 14.8 |
| 1NOX4 | 1-octene + $NO_x$ | 0.88 | 0.097 | 0.049 | - | 0.28 | 48.2 |
| 1NOX5 | 1-octene + $NO_x$ | 0.56 | 0.134 | 0.021 | - | 0.185[1] | 26.3 |
| 1NOX6 | 1-octene + $NO_x$ | 1.46 | 0.174 | 0.074 | - | 0.292[1] | 47.1 |
| 1NOX7 | 1-octene + $NO_x$ | 20.0 | 1.69 | 1.86 | - | 0.738 | 45.1 |
| 1O31 | 1-octene + $O_3$ | 14.36 | - | - | - | - | - |
| 1O32 | 1-octene + $O_3$ | 14.4 | - | - | - | - | - |
| M1O31 | 1-octene + $O_3$ | 10.94 | - | - | - | - | - |
| + methyl cyclohexane | | 60.9 | | | | | |

[1]Experiment was terminated before ozone had peaked.

*Table 2. Summary of Product Yields*

| Reaction | Product | Yield (% of 1-octene reacted leading to product) |
|---|---|---|
| OH + 1-octene | Heptanal | 15. ± 8 |
| | Organonitrates | 33. ±8 |
| Total | | 48. |
| $O(^3P)$ + 1-octene | Octanal + Hexyl oxirane | 80.± 20 |
| | 2-Octanone | 6.± 3 |
| | Organic Radicals | 8.± 3** |
| Total | | 93. |
| $O_3$ + 1-octene | Heptanal | 80.± 20 |
| | Thermally Stabilized $C_7$ Criegee biradical* | 11. ± 5 |
| | Hydroxyl Radical | 55.± 15 |
| | Unknown | 6. ± 4** |
| | Hexane | 0.8 ± 0.4 |
| Total | | 92. |

* Inferred from the observed heptanoic acid concentration.
** This is not included in the total as its origin is unknown.

## *Table 3. 1-Octene Oxidation Mechanism*

Lumped species (all others are indicated with names or structures)

| | |
|---|---|
| MCHR | Lumped alkyl peroxy radical, mainly secondary and assumed to react as such. |
| HACR1 | Lumped alkyl radical resulting from OH attack on the alkyl backbone of heptanoic acid. |
| HACR2 | Alkyl radical intermediate resulting from reaction of HACR1 with NO. |
| 6R1 | terminal alkyl radical; 6 or 7 carbons. |
| 6R2 | collection of allyl radical products of OH + hexane reaction |
| 6O2 | alkoxy radical form of 6R2 |
| 6AR3 | isomerized 6R2 (an alkyl radical) |
| NCR1 | lumped nitro-alkyl radical |
| RCN1 | lumped nitro-alkyl radical |
| OR | Radical products of the $O(^3P)$-1-octene reaction. |

| Rate constant at 298 K | Activation Energy ($E_a/RT$) (K) | References rate, reaction | Reactants Products[1] |
|---|---|---|---|
| 1) 4.0E-11, | -467 | a, b | 1-octene + OH → 0.7 $CH_3(CH_2)_5CHOO{\cdot}CH_2OH$ + 0.3 $CH_3(CH_2)_5CH(OH)CH_2OO{\cdot}$ |
| 2) 1.7E-17, | 1713 | c, b | 1-octene + $O_3$ → 0.8 HCHO + 0.8 heptanal + 0.11 $H_2C{\cdot}OO{\cdot}$ + 0.11 $CH_3(CH_2)_5C{\cdot}HOO{\cdot}$ + 0.35 CO + 0.33 $CO_2$ + 0.12 $HO_2$ + 0.01 hexane + 0.55 OH + 0.12 $H_2$ + 0.25 $O(^3P)$ |
| 3) 1.1E-11 | | d, b | 1-octene + $O(^3P)$ → 0.77 octanal[2] + 0.17 OR + 0.055 2-octanone + 0.05 heptanal |
| 4) 7.6E-12, | -180 | 6, b | OR + NO → 0.1 organic nitrate + 0.9 $HO_2$ + 0.9 $NO_2$ + 0.9 hydroxy carbonyl cpd. |
| 5) 7.6E-12, | -180 | 6, b | $CH_3(CH_2)_5CHOO{\cdot}CH_2OH$ + NO → 0.33 organic nitrate + 0.67 $NO_2$ + 0.2 $HO_2$ + 0.15 heptanal + 0.2 HCHO + 0.52 $CH_3(CH_2)_5CHO{\cdot}CH_2OH$ |
| 6) 7.6E-12, | -180 | 6, b | $CH_3(CH_2)_5CHO{\cdot}CH_2OH$ + NO → 0.33 organic nitrate + 0.67 $NO_2$ + 0.67 $HO_2$ + 0.67 $CH_3(CH_2)_2CH(OH)(CH_2)_2C(O)CHOH$ |
| 7) 7.6E-12, | -180 | 6, b | $CH_3(CH_2)_5CH(OH)CH_2OO{\cdot}$ + NO → 0.15 heptanal + 0.52 $CH_3(CH_2)_5CH(OH)CH_2O{\cdot}$ + 0.33 organic nitrate + 0.67 $NO_2$ + 0.2 HCHO + 0.2 $HO_2$ |
| 8) 7.6E-12, | -180 | 6, b | $CH_3(CH_2)_5CH(OH)CH_2O{\cdot}$ + NO → 0.33 organic nitrate + 0.67 NO2 + 0.67 $HO_2$ + 0.67 $CH_3(CH_2)_3CH(O)(CH_2)CH(OH)CHO$ |

| Rate constant at 298 K | Activation Energy ($E_a/RT$) (K) | References rate, reaction | Reactants | Products[1] |
|---|---|---|---|---|
| 9) 3.25E-12 | | e, f | organic nitrate + OH → 0.3 hydroxy carbonyl cpd. + 0.3 $NO_2$ + 0.7 NCR1 | |
| 10) 7.6E-12, -180 | | 6, g | NCR1 + NO → 0.3 organic nitrate + 0.7 $NO_2$ + 0.7 hydroxy carbonyl cpd. | |
| 11) 8.E-12 | | e, b | 2-octanone + OH → MCHR | |
| 12) 3.04E-11 | | h, h | heptanal + OH → 0.68 $CH_3(CH_2)_5C(=O)OO\cdot$ + 0.027 $CH_3(CH_2)_4CH\cdot CHO$ + 0.155 $CH_3(CH_2)_3CH\cdot CH_2CHO$ + 0.045 $CH_3(CH_2)_2CH\cdot(CH_2)_2CHO$ + 0.046 $CH_3(CH_2)CH\cdot(CH_2)_3CHO$ + 0.035 $CH_3CH\cdot(CH_2)_4CHO$ | |
| 13) 8.4E-12 | | j, j | $CH_3(CH_2)_5C(=O)OO\cdot$ + $NO_2$ → $CH_3(CH_2)_5C(=O)OONO_2$ | |
| 14) 2.2E16, 26.7 | | j, j | $CH_3(CH_2)_5C(=O)OONO_2$ → $CH_3(CH_2)_5C(=O)OO\cdot$ + $NO_2$ | |
| 15) 7.6E-12, -180 | | 6, j | $CH_3(CH_2)_5C(=O)OO\cdot$ + NO → $CH_3(CH_2)_4CH\cdot$ + $NO_2$ + $CO_2$ | |
| 16) 7.6E-12, -180 | | 6, b | $CH_3(CH_2)_4CH\cdot CHO$ + NO → hexanal + $HO_2$ + $NO_2$ + CO | |
| 17) 7.6E-12, -180 | | 6, b | $CH_3(CH_2)_3CH\cdot CH_2CHO$ + NO → 0.3 organic nitrate + 0.7 $NO_2$ + 0.7 $CH_3(CH_2)_3CHO\cdot CH_2CHO$ | |
| 18) 7.6E-12, -180 | | 6, b | $CH_3(CH_2)_3CHO\cdot CH_2CHO$ + NO → hydroxy carbonyl cpd. + $HO_2$ + $NO_2$ | |
| 19) 7.6E-12, -180 | | 6, b | $CH_3(CH_2)_2CH\cdot(CH_2)_2CHO$ + NO → $CH_3(CH_2)_2CHOH(CH_2)_2C(O)OO\cdot$ + $NO_2$ | |
| 20) 7.6E-12, -180 | | 6, b | $CH_3(CH_2)CH\cdot(CH_2)_3CHO$ + NO → 0.3 organic nitrate + 0.7 $CH_3(CH_2)CHO\cdot(CH_2)_3CHO$ + 0.7 $NO_2$ | |
| 21) 7.6E-12, -180 | | 6, b | $CH_3(CH_2)CHO\cdot(CH_2)_3CHO$ + NO → hydroxy carbonyl cpd. + $NO_2$ + $HO_2$ + CO | |
| 22) 7.6E-12, -180 | | 6, b | $CH_3CH\cdot(CH_2)_4CHO$ + NO → 0.3 organic nitrate + 0.7 $CH_3CHO\cdot(CH_2)_4CHO$ + 0.7 $NO_2$ | |
| 23) 7.6E-12, -180 | | 6, b | $CH_3CHO\cdot(CH_2)_4CHO$ + NO → hydroxy carbonyl cpd. + $NO_2$ + $HO_2$ | |
| 24) 1.9E-4x$J_{NO_2}$ | | j, j | heptanal + h√ → 6R1 + $HO_2$ + CO | |
| 25) 1.6E-5x$J_{NO_2}$ | | j, j | heptanal + h√ → hexane + CO | |
| 26) 1.9E-4x$J_{NO_2}$ | | j, j | octanal + h√ → 6R1 + $HO_2$ + CO | |
| 27) 1.6E-5x$J_{NO_2}$ | | j, j | octanal + h√ → heptane + CO | |
| 28) 7.6E-12, -180 | | 6, b | 6R1 + NO → 0.79 CAROH + 0.79 $NO_2$ + 0.79 $HO_2$ + 0.21 organic nitrate | |

| Rate constant at 298 K | Activation Energy ($E_a$/RT) (K) | References rate, reaction | Reactants | Products[1] |
|---|---|---|---|---|
| 29) 8.4E-12 | | j, j | $CH_3(CH_2)_2CHOH(CH_2)_2C(O)OO\cdot$ + NO2 → | $CH_3(CH_2)_2CHOH(CH_2)_2C(O)OONO_2$ |
| 30) 2.2E16, 26.7 | | j, j | $CH_3(CH_2)_2CHOH(CH_2)_2C(O)OONO_2$ → | $CH_3(CH_2)_2CHOH(CH_2)_2C(O)OO\cdot$ + $NO_2$ |
| 31) 7.6E-12, -180 | | j, j | $CH_3(CH_2)CHOH(CH_2)_2C(O)OO\cdot$ + NO → | propanal + hydroxy carbonyl cpd. + $NO_2$ + $CO_2$ |
| 32) 6.15E-12 | | 15, 24 | heptanoic acid + OH → 0.12 $CH_3(CH_2)_4CH\cdot$ + 0.12 CO | + 0.88 HACR1 |
| 33) 7.6E-12, -180 | | 6, b | HACR1 + NO → | $NO_2$ + HACR2 |
| 34) 7.6E-12, -180 | | 6, b | HACR2 + NO → | substituted heptanoic acid + $NO_2$ + $HO_2$ |
| 35) 7.6E-12, -180 | | 6, b | $CH_3(CH_2)_4CH\cdot$ + NO → | $NO_2$ + $HO_2$ |
| 36) 8.E-16 | | 31, 31 | 2 $CH_3(CH_2)_5CHOO\cdot CH_2OH$ → | 0.2 heptanal + 0.2 $HO_2$ + 0.2 HCHO + 0.4 dihydroxy cpd. + 0.4 hydroxy carbonyl cpd. + $CH_3(CH_2)_5CHOO\cdot CH_2OH$ |
| 37) 2.E-13 | | 31, 31 | $CH_3(CH_2)_5CHOO\cdot CH_2OH$ + $CH_3(CH_2)_5CH(OH)CH_2OO\cdot$ → | 0.2 heptanal + 0.2 $HO_2$ + 0.2 HCHO + 0.4 dihydroxy cpd. + 0.4 hydroxy carbonyl cpd. + $CH_3(CH_2)_5CHOO\cdot CH_2OH$ |
| 38) 2.53E-14 | | 31, 31 | 2 $CH_3(CH_2)_5CH(OH)CH_2OO\cdot$ → | 0.2 heptanal + 0.2 $HO_2$ + 0.2 HCHO + 0.4 dihydroxy cpd. + 0.4 hydroxy carbonyl cpd. + $CH_3(CH_2)_5CH(OH)CH_2OO\cdot$ |
| 39) 2.53E-14 | | 31, 31 | $CH_3(CH_2)_5CH(OH)CH_2OO\cdot$ + MCHR → | 0.12 heptanal + 0.2 $HO_2$ + 0.6 HCHO + 0.7 dihydroxy cpd. + 0.7 hydroxy carbonyl cpd. + 0.5 $CH_3(CH_2)_5CH(OH)CH_2OO\cdot$ |
| 40) 2.53E-14 | | 31, 31 | $CH_3(CH_2)_5CHOO\cdot CH_2OH$ + MCHR → | 0.12 heptanal + 0.2 $HO_2$ + 0.6 HCHO + 0.7 dihydroxy cpd. + 0.7 hydroxy carbonyl cpd. + 0.5 $CH_3(CH_2)_5CHOO\cdot CH_2OH$ |
| 41) 3.E-14 | | 31, b | MCHR + MCHR → | $HO_2$ |
| 42) 3.E-12 | | 31, b | MCHR + $HO_2$ → | peroxide2 |
| 43) 6.E-12 | | k, b | peroxide2 + OH → | OH + MCHR |
| 44) 3.E-12 | | 31, 31 | $CH_3(CH_2)_5CHOO\cdot CH_2OH$ + $HO_2$ → | peroxide |

| Rate constant at 298 K | Activation Energy ($E_a$/RT) (K) | References rate, reaction | Reactants | Products[1] |
|---|---|---|---|---|
| 45) 3.E-12 | | 31, 31 | $CH_3(CH_2)_5CH(OH)CH_2OO\cdot + HO_2$ | → peroxide |
| 46) 5.6E-12 | | k, b | peroxide + OH | → 0.7 $CH_3(CH_2)_5CHOO\cdot CH_2OH$ + 0.3 $CH_3(CH_2)_5CH(OH)CH_2OO\cdot$ |
| 47) 7.036E-12 | | 23, 23 | $CH_3(CH_2)_5C\cdot HOO\cdot + NO$ | → heptanal + $NO_2$ |
| 48) 7.036E-13 | | 23, 23 | $CH_3(CH_2)_5C\cdot HOO\cdot + NO_2$ | → heptanal + $NO_3$ |
| 49) 4.E-18 | | 23, 23 | $CH_3(CH_2)_5C\cdot HOO\cdot + H_2O$ | → heptanoic acid |
| 50) 1.36E-14 | | 23, 23 | $H_2C\cdot OO\cdot$ + heptanal | → ozonide |
| 51) 1.36E-14 | | 23, 23 | $CH_3(CH_2)_5C\cdot HOO\cdot$ + HCHO | → ozonide |
| 52) 1.36E-14 | | 23, 23 | $CH_3(CH_2)_5C\cdot HOO\cdot$ + heptanal | → ozonide |
| 53) 8.68E-12 | | 6, b | n-octane + OH | → MCHR |
| 54) 1.04e-11 | | 6, b | methyl cyclohexane + OH | → MCHR |
| 55) 7.6E-12, -180 | | 6, m | MCHR + NO | → 0.84 dihydroxy cpd. + 0.16 organic nitrate + 0.78 $HO_2$ + 0.84 $NO_2$ |
| 56) 5.6E-12 | | 6, b | Hexane + OH | → MCHR |

---

1. Addition of molecular oxygen to alkyl and acyl radicals is implicit in many reactions.
2. Octanal is used to represent the sum of octanal and hexyl oxirane.

a) Estimated from trend of $C_2$-$C_7$ 1-alkene-OH rate constants, which approach $4.0 \times 10^{-11}$, with an asymptotic trend. The activation energy was assumed to be the same as that for the 1-butene-OH reaction.

b) This work.

c) The rate at 298K for 1-heptene and the activation energy for 1-butene were used.

d) Estimated from correlations between the rate constants of OH and $O(^3P)$ developed by Atkinson (15).

e) Estimated from structure-activity relationships (30), based on the major hydroxy nitrate isomer.

f) Based on the assumption that if OH attacks either the $\alpha$ or $\beta$ carbons, $NO_2$ is lost.

g) Same assumption as above, with the additional assumption that the alkoxy radical isomerizes.

h) Rate constant and branching ratios estimated from structure-activity relationships (Atkinson, 1987 (30)).

j) Analogous to acetaldehyde.

k) As the OH-methyl peroxide reaction is very slow, OH was assumed to attack the backbone, hence the rate constant for hexane was assumed.

m) Based on extensive estimates of the branching ratios, products and rate constants from structure-activity relationships developed by Atkinson (30).

*Table 4. Average Product Yields for Low Concentration Experiments*

| Experiment | Total reacted 1-Octene (ppm) | Heptanal | Hexyl oxirane plus Octanal | 2-Octanone | Hexane | 3-Heptanone | 2-Ethyl hexanal | n-Octane reacted (ppm) |
|---|---|---|---|---|---|---|---|---|
| 1OH1 | 0.85 | .085±.04 | .093±.04 | .015±.01 | .01±.005 | .012±.006 | .009±.04 | .007±.002 |
| 1OH2 | 1.33 | .10±.05 | .043±.02 | .011±.005 | .009±.005 | --- | ---- | --- |
| 1NOX1 | 0.3 | .22±.08 | .07±.03 | .016±.008 | --- | --- | .007±.003 | --- |
| 1O31* | 13.9 | .35±.15 | heptanoic acid: .011±.005 | --- | .005±.03 | .01±.05 | unknown: .027±.015 | .17-.15 =.02 |

*Included here because data was collected only at the end of the experiment.

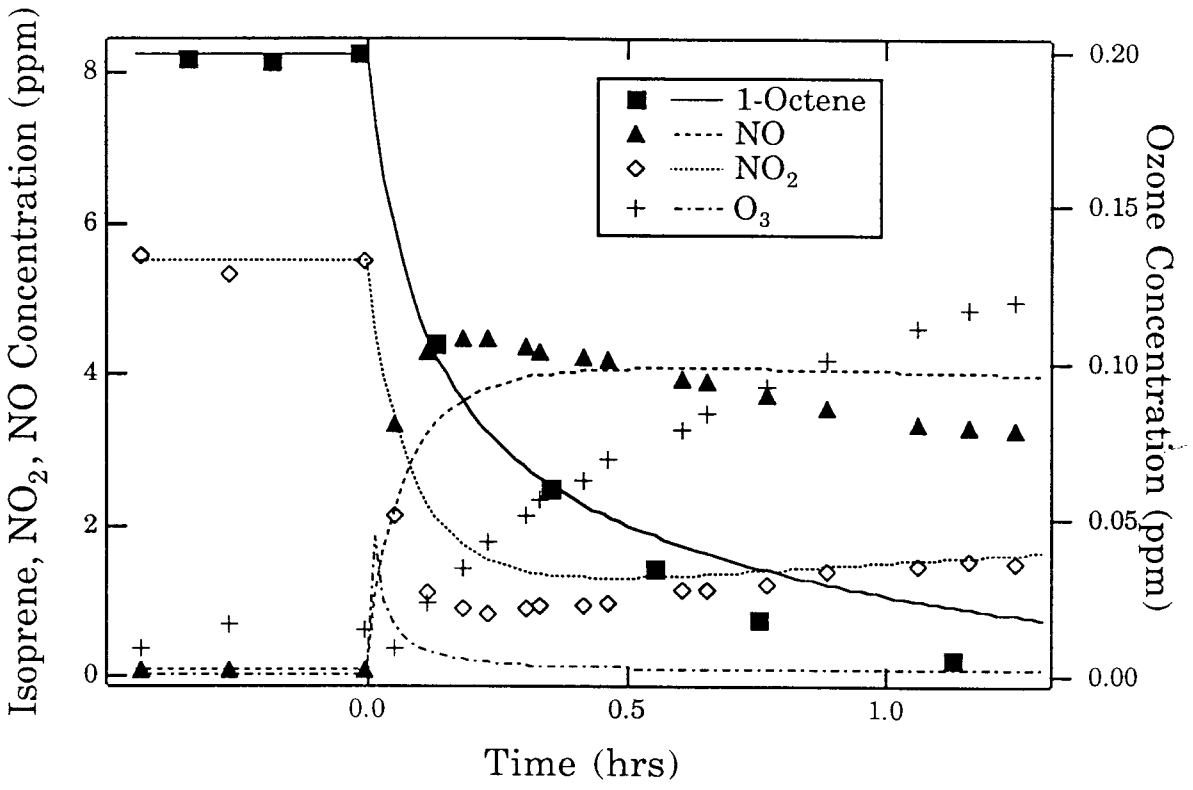


Figure 1. NO, $NO_2$, $O_3$, and 1-octene data and simulations for experiment 1O3P1. Note that $O_3$ is plotted with respect to the right-hand axis.

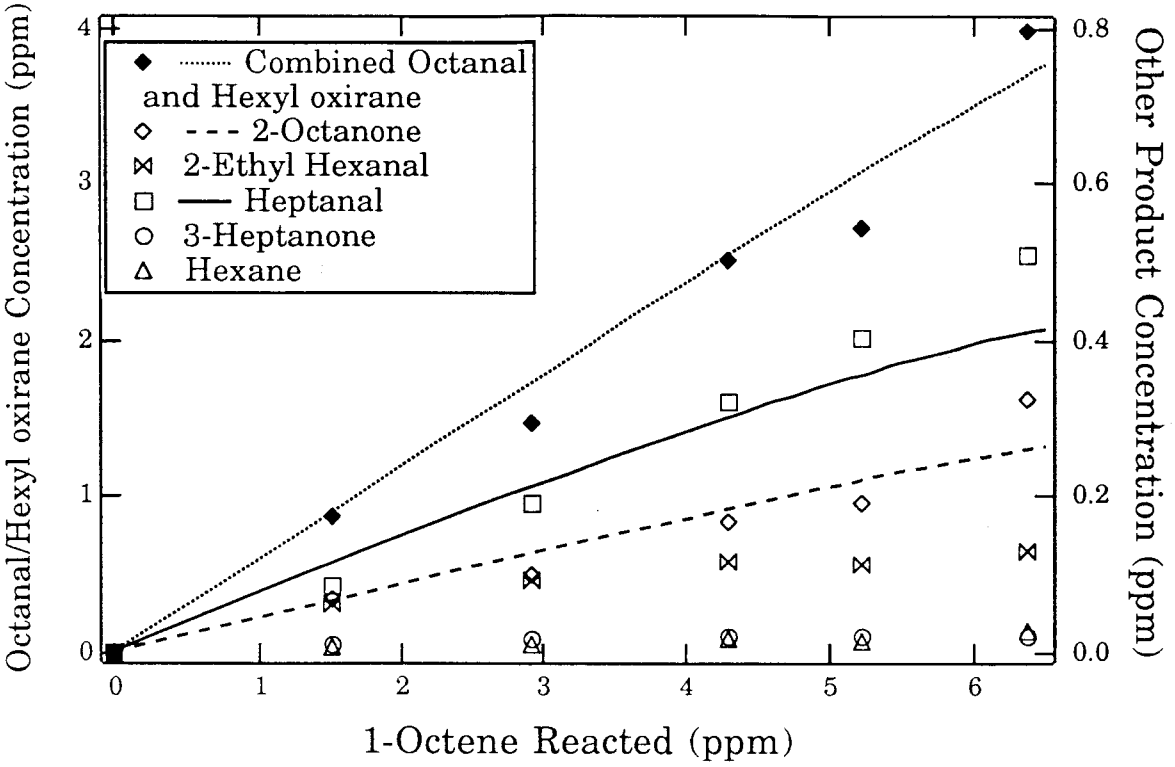


Figure 2. Product concentrations and simulations from experiment 1O3P1. Note that the combined octanal/hexyl oxirane is plotted with respect to the left-hand axis, and the other products with respect to the right-hand axis.

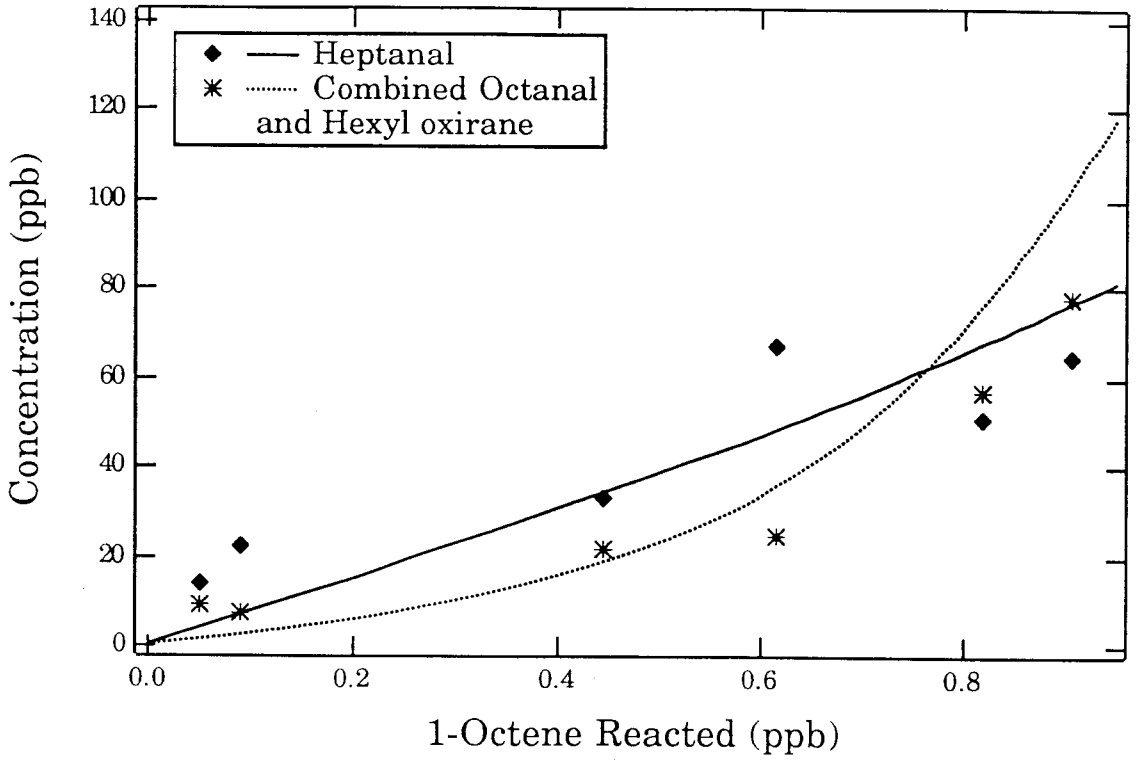


Figure 3. Heptanal and combined octanal and hexyl oxirane vs. 1-octene reacted from experiment 1OH1. Data are shown as symbols and simulations as lines.

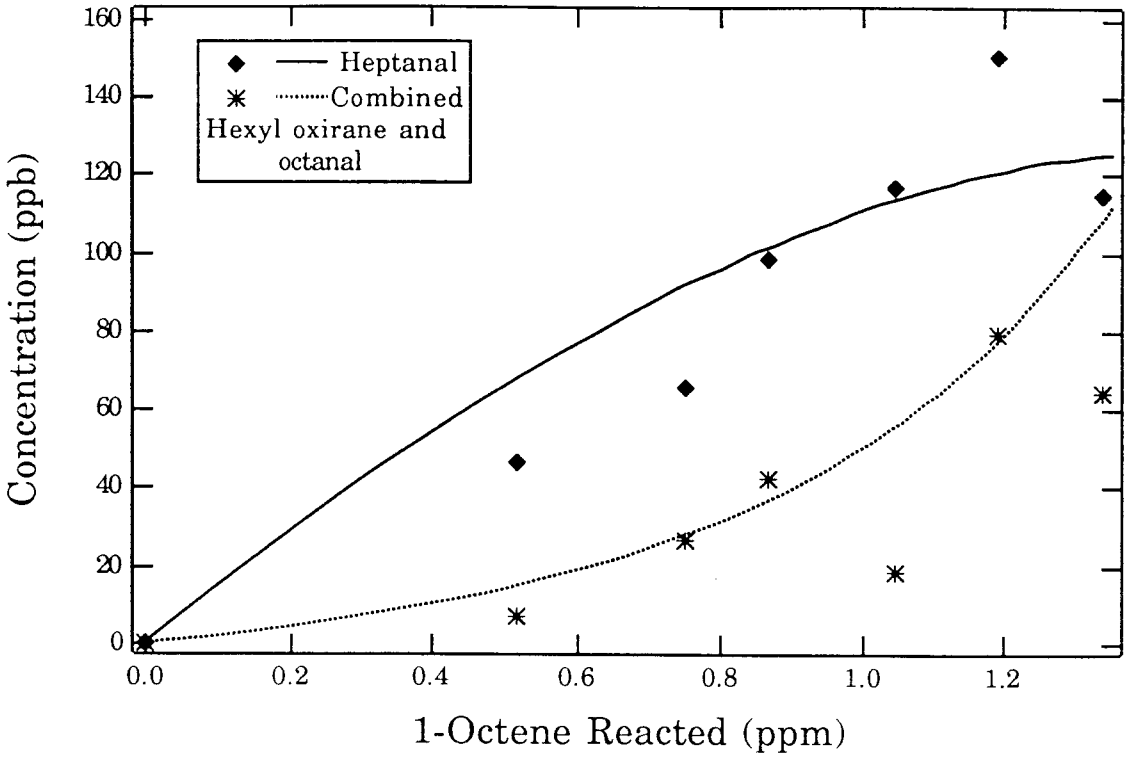


Figure 4. Heptanal and combined octanal and hexyl oxirane vs. 1-octene reacted from experiment 1OH2. Data are shown as symbols and simulations as lines.

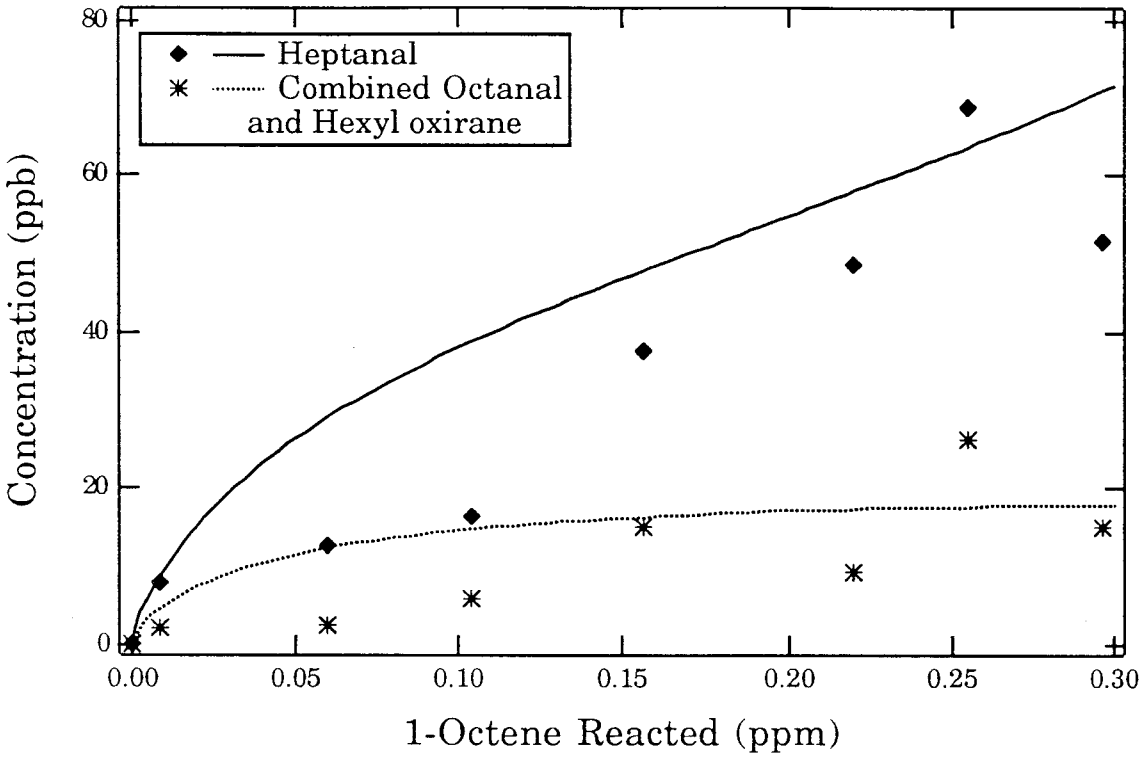


Figure 5. Heptanal and combined octanal and hexyl oxirane vs. 1-octene reacted from experiment 1NOX1. Data are shown as symbols and simulations as lines.

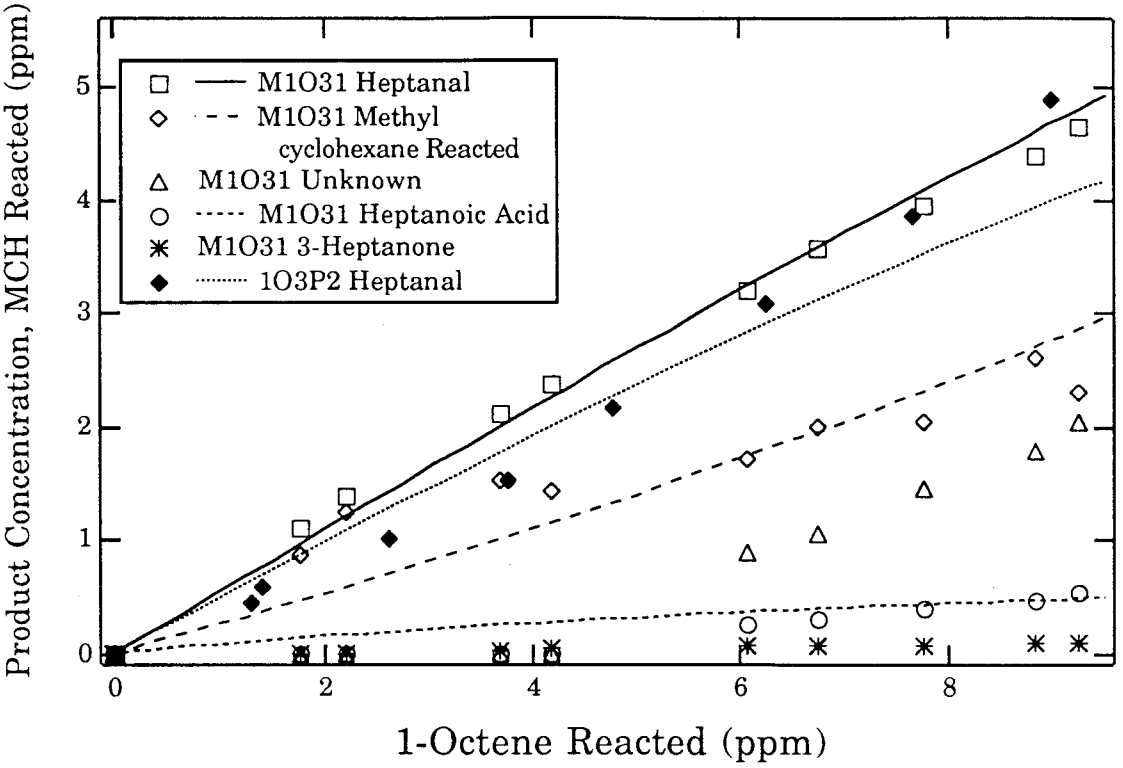


Figure 6. Product concentration and methyl cyclohexane reacted vs. 1-octene reacted for experiments 1O32 and M1O31. Data are indicated with symbols; simulations with lines.

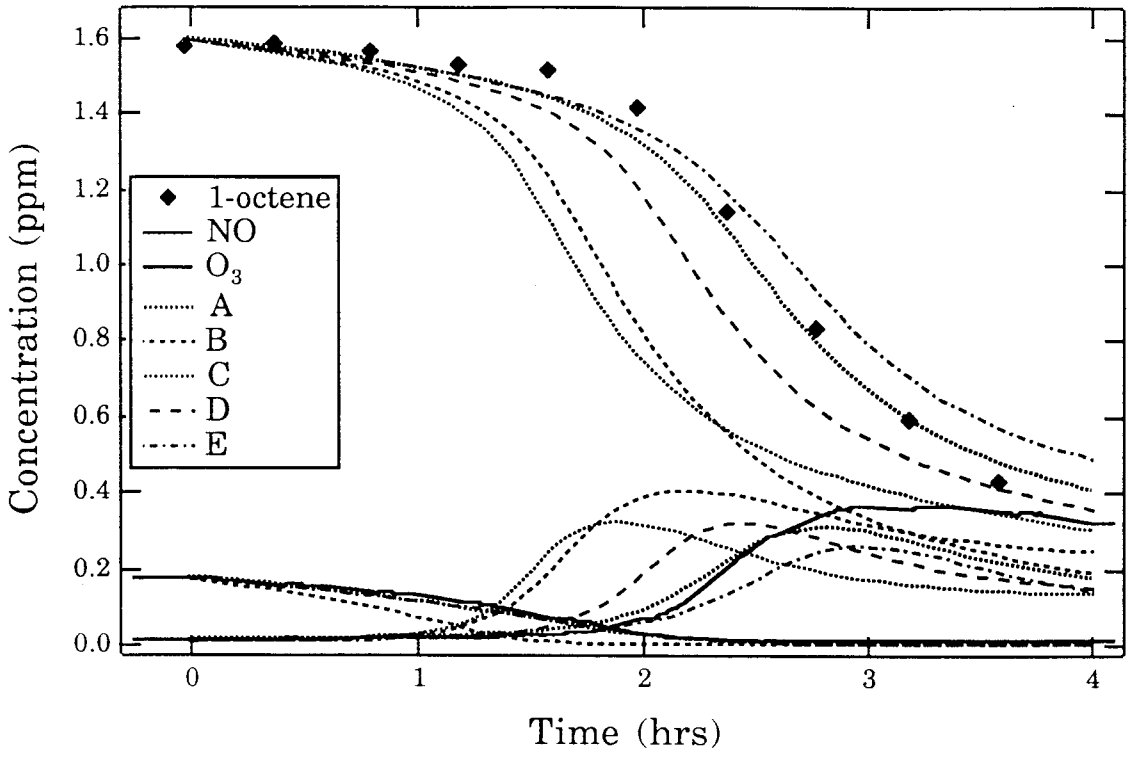


Figure 7. NO, $O_3$, and 1-octene data (symbols and solid lines) and simulations (broken lines) from experiment 1NOX2. The conditions for the simulations are indicated in the text. Some of the simulations for NO have been omitted for clarity.

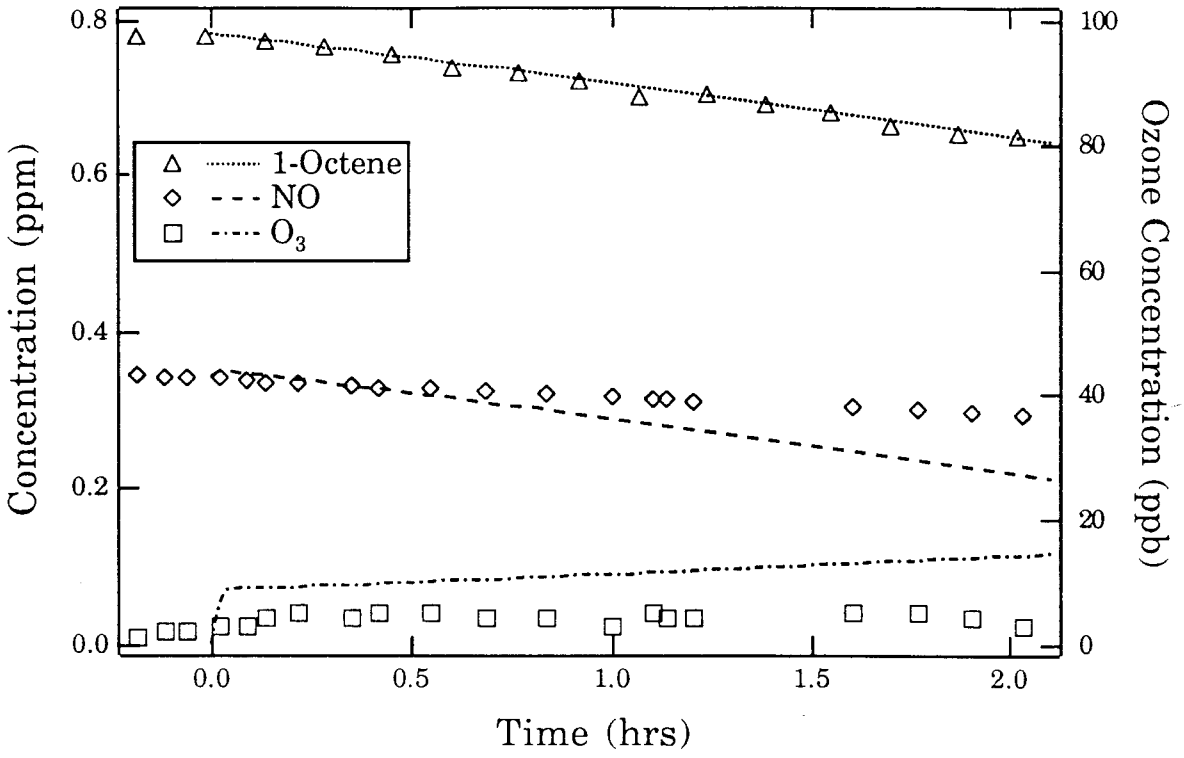


Figure 8. NO, $O_3$, and 1-octene data (symbols) and simulations (lines) from experiment 1NOX3. Note that $O_3$ is plotted with respect to the right-hand axis.

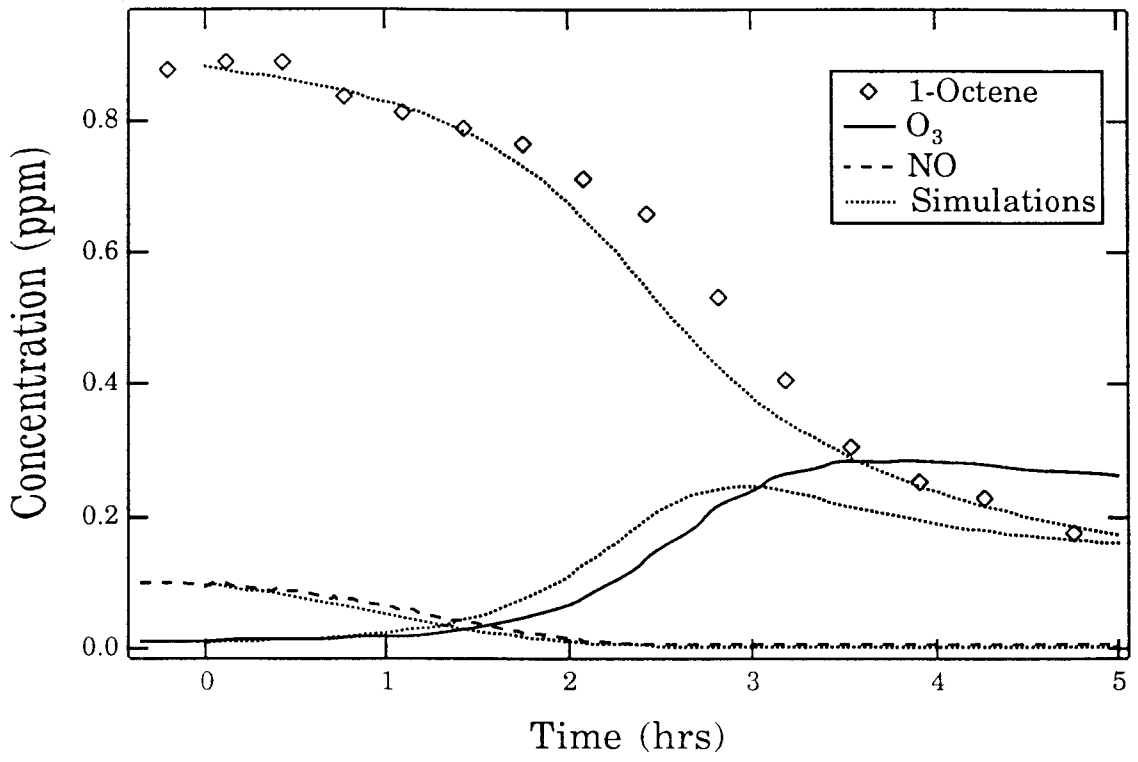


Figure 9. NO, $O_3$, and 1-octene data (solid and dashed lines, and symbols) and simulations (dotted lines) from experiment 1NOX4.

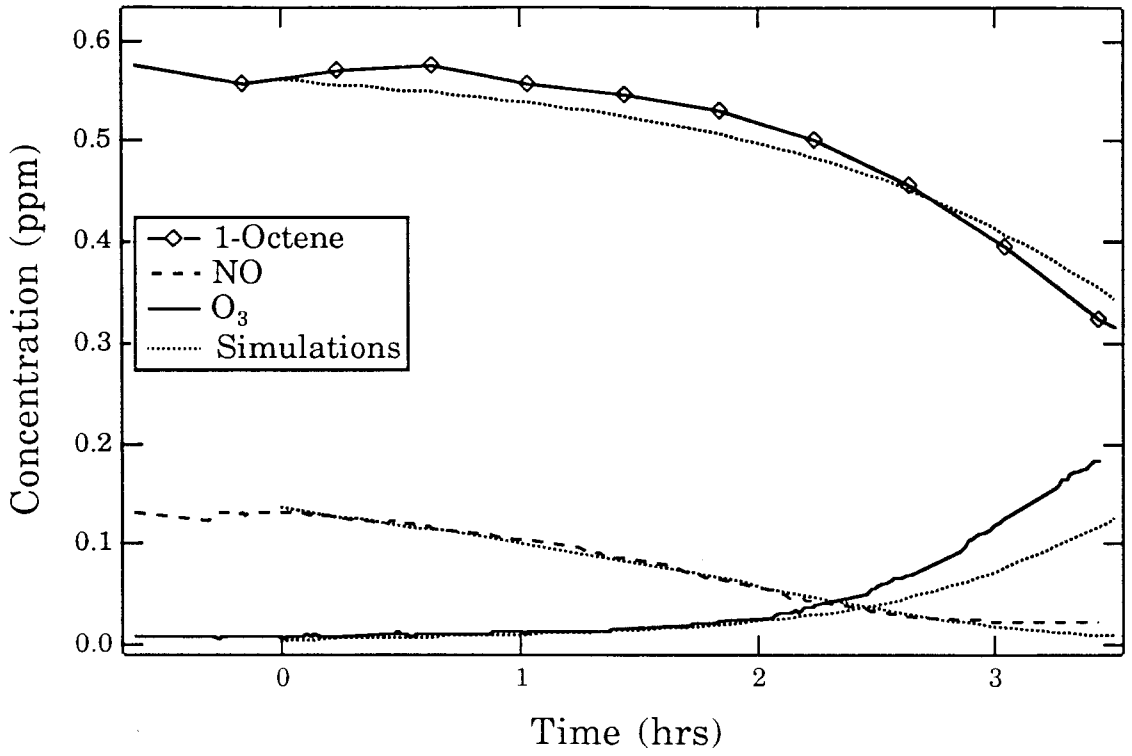


Figure 10. NO, $O_3$, and 1-octene data (symbols) and simulations (lines) from experiment 1NOX5.

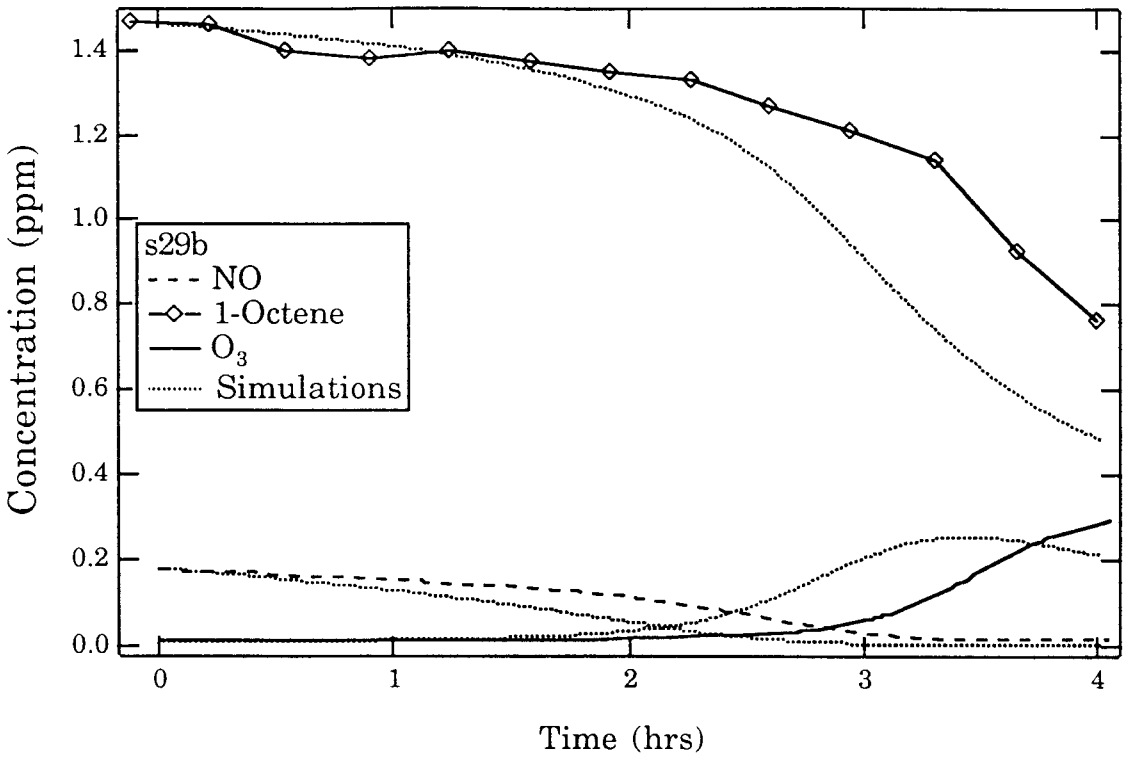


Figure 11. NO, $O_3$, and 1-octene data (symbols) and simulations (lines) from experiment 1NOX6.

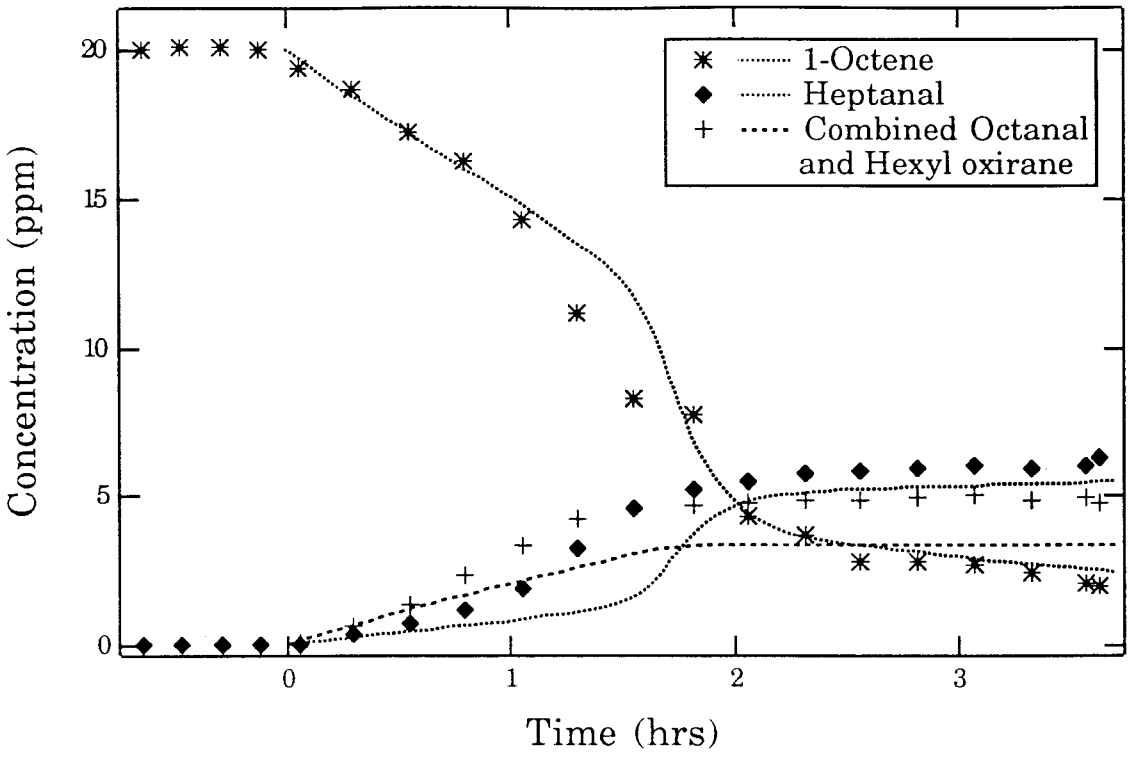


Figure 12. 1-Octene, heptanal, and combined hexyl oxirane and octanal data (symbols) and simulations (lines) from 1NOX7.

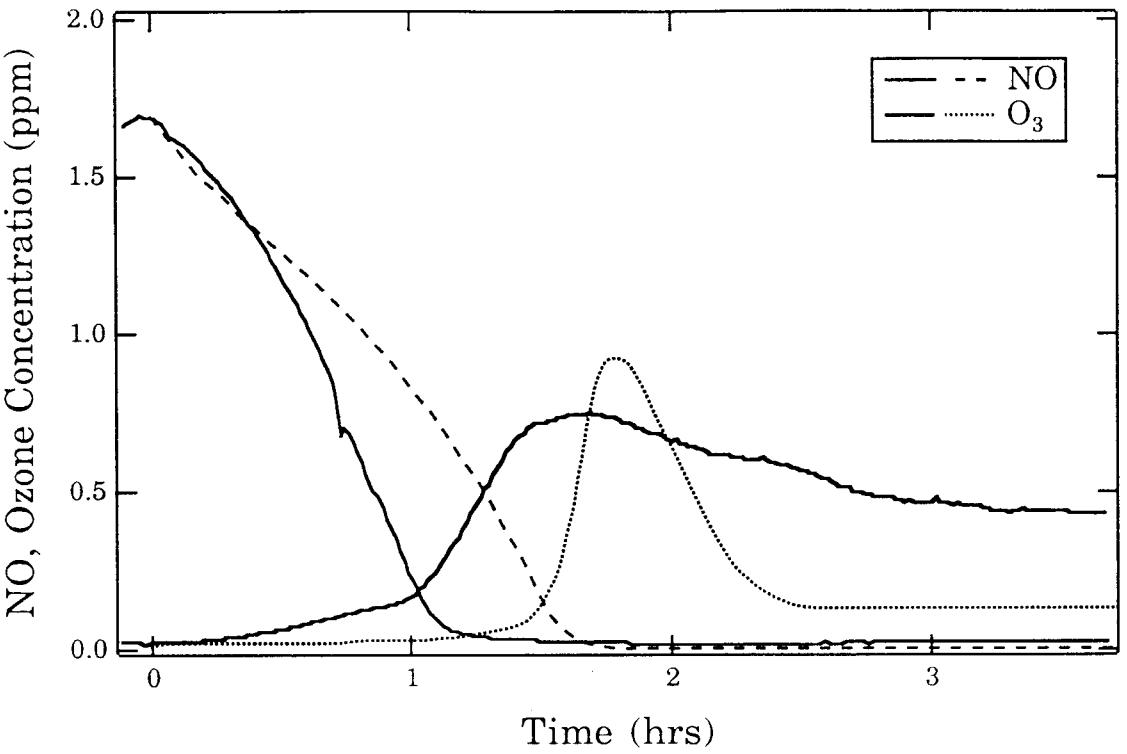


Figure 13. NO, and $O_3$ data (symbols) and simulations (lines) from experiment 1NOX7.

# CHAPTER 6

*Chicken Little was right.*

# Characterization of Photochemical Aerosols From Biogenic Hydrocarbons

S. E. PAULSON, S. N. PANDIS, U. BALTENSPERGER, J. H. SEINFELD, R. C. FLAGAN
Departments of Environmental and Chemical Engineering, California Institute of Technology, Pasadena, CA 91125

E. J. PALEN and D. T. ALLEN
Department of Chemical Engineering, University of California, Los Angeles, CA 90024-1592, USA

C. SCHAFFNER and W. GIGER
Institute for Water Resources and Water Pollution Control (EAWAG), CH-8600 Dubendorf, Switzerland

A. PORTMANN
Institute for Inorganic Chemistry, University of Zurich, Winterthurerstr, 190, CH-8057 Zurich, Switzerland

Published in:
*Journal of Aerosol Science* Volume 21, pp. S245-S249 (1991)

# *Abstract*

An extensive set of outdoor smog chamber experiments was carried out to study aerosol formation by two representative biogenic hydrocarbons; isoprene and ß-pinene. The hydrocarbons, at concentrations ranging from a few ppb to a few ppm, were photooxidized in the presence of NOx. Isoprene was found to produce negligible aerosol at ambient conditions, whereas ß-pinene aerosol carbon yields were as high as 8%, depending strongly on the hydrocarbon to NOx ratio. Aerosol samples subjected to infrared absorption spectroscopy revealed that the dominant aerosol products for both isoprene and ß-pinene are organic nitrates, organic acids, as well as other carbonyls and hydroxy compounds. GCMS of the neutral fraction of the ß-pinene aerosol revealed nopinone and several other compounds with molecular weights ranging from 138-200 amu, indicating mainly mono- and dioxygenated products. The average vapor pressure of the ß-pinene aerosol was estimated to be 37 ± 24 ppt at 31 C. Scanning electron micrographs showed that the particles consist of both liquid droplets and agglomerates of small (40-60 nm) solid particles.

# *Introduction*

Biogenic hydrocarbons are produced by vegetation in quantities comparable to anthropogenic emissions (Lamb *et al.* 1987). Recent aerosol measurements in Southern California showed that a substantial fraction of fine aerosol carbon is modern and suggested that the short-lived but highly reactive biogenic hydrocarbons may be important aerosol precursors (Global Geochemistry Corporation 1989). Monoterpenes, the dominant biogenics from conifers, have been recognized as potential sources of organic aerosol since at least 1960 (Went 1960), but only a few studies have been carried out, almost exclusively using ozone as the oxidant species. Biogenic hydrocarbons are oxidized in both urban and

rural environments by a combination of hydroxyl radical (OH) and ozone (Atkinson 1990). Isoprene and α- and ß-pinene have been found to produce aerosol when allowed to react with ozone; α- and ß-pinene at concentrations of around 20 ppb, while isoprene required much higher concentrations (Kamens *et al.* 1981; 1982, Hatakeyama *et al.* 1989). Studies of the composition of biogenic aerosols are even scarcer. Some condensed products have been identified for α- and ß-pinene, again from reactions with ozone, and at very high (70 to 100 ppm) initial hydrocarbon concentrations of (Hull 1981; Hatakeyama *et al.* 1989). In these studies, the identified compounds for ß-pinene were nopinone (6,6 dimethyl bicyclo(3.1.1)heptan-2one), 3-hydroxy nopinone, and ketopinone (6,6 dimethyl bicyclo(3.1.1)heptan-2,3dione). However, as these experiments were carried out at concentrations 3 to 4 orders of magnitude higher than ambient conditions, they may not be relevant to atmospheric aerosols. Nopinone is also found in the gas phase; it is the dominant stable product from the ozone-ß-pinene reaction, accounting for about 40% of the reacted ß-pinene (Hatakeyama *et al.* 1989).

In view of the limited data, particularly under conditions similar to the atmosphere, which includes both OH and ozone as well as $NO_x$, this study was undertaken to investigate the importance of biogenic hydrocarbons as aerosol precursors. The study focused on isoprene and ß-pinene as representative hydrocarbons. Isoprene is the most abundant compound emitted by deciduous trees and many plants (Lamb 1987), and is exceptionally reactive, leading to efficient ozone production. ß-pinene together with α-pinene make up the largest share of monoterpene emissions (Zimmerman *et al.* 1979, Altshuller 1983).

# *Experimental Description*

The hydrocarbon/$NO_x$ photooxidation experiments took place in the Caltech outdoor smog chamber facility. The smog chamber is a 60 $m^3$ batch reactor constructed of Teflon film.

Initial hydrocarbon concentrations ranged from 70 to 10,000 ppb for isoprene, and 28 to 10,800 ppb for ß-pinene. The $NO_x$, biogenic hydrocarbon, and optional seed $(NH_4)_2SO_4$ aerosol were injected sequentially into the covered chamber, time was allowed for mixing, and then the chamber was exposed to sunlight. The gas-phase parameters measured during the experiments included concentrations of $O_3$ (Dasibi Model 1008-PC), NO and $NO_x$ (Thermo Electron Corp. Model 14D/E), isoprene, ß-pinene and major products (Hewlett-Packard 5890 Capillary Gas Chromatograph), smog chamber temperature, total and UV solar radiation (Eppley Laboratory pyranometer, Model 8-48). The aerosol particle size distribution was monitored using the Scanning Electrical Mobility Spectrometer (SEMS) (Wang and Flagan 1990) for the 0.01-0.2 μm size range and a Royco Model 226 Laser Optical Particle Counter for the 0.12 to 5 μm size range. The Scanning Electrical Mobility Spectrometer consists of a Differential Mobility Analyzer (TSI Model 3071) with a Condensation Nucleus Counter (TSI Model 3071) as a particle detector and gave a 60 data point size distribution per minute. The Fuchs surface of the aerosol particles was measured using the epiphaniometer (Gaggeler *et al.* 1989). Nuclepore filters from the epiphaniometer were coated with Au/Pd and subjected to Scanning Electron Microscopy (SEM) (Phillips SEM 515). Additional aerosol samples were collected once or twice during each experiment on the eight stages of a Hering low pressure impactor. The aerosol deposits on each stage were characterized using infrared spectroscopy (Palen and Allen 1989). The average saturation vapor pressure of the condensing species was measured with a method based on the Tandem Differential Mobility Analyzer (TDMA) technique developed by Rader and McMurry (1986). Aerosol samples for GCMS (Finnigan) analysis were collected on annealed quartz filters and prepared using Soxhlet extraction with $CH_2Cl_2$.

Aerosol samples for GCMS analysis were obtained by withdrawing a sample from the smog chamber through two 47 mm quartz fiber filters (Pallflex, Putnam, CT), in separate

filter holders, using a pump fitted with a 10.6 lpm critical orifice. The sampling tube, filter holders and connections were stainless steel or aluminum, with Teflon gaskets. The filters were annealed at 450 C for one hour to reduce background carbon, and stored in annealed quartz jars with Teflon-lined caps. The sampling tubes and filter holders were ultrasonically cleaned with glass-distilled, ultra clean water, then methanol and finally hexane. Samples were kept frozen while in storage, and shipped to Dübendorf, Switzerland in dry ice for GCMS analysis. The samples were prepared with Soxhlet extraction using methylene chloride, and run on a Finnigan Electron Ionization GCMS (Bremen, West Germany) using a 24 m column, 10% phenyl, 90% methyl poly-siloxane, programmed at 4 C/min from 40 C to 240 C.

## *Characterization of Isoprene and ß-Pinene Aerosols*

The aerosol data from the SEMS and OPC were inverted and the resulting aerosol distributions were integrated to give the aerosol volume $V_a$. The aerosol carbon concentration (ACC) was obtained from the aerosol volume ($V_a$) using the parameterization of Izumi *et al.* (1988): ACC = 0.49 $V_a$, where the constant 0.49 g $cm^{-3}$ represents the aerosol carbon density. The aerosol carbon yield was then calculated by dividing ACC by the loss of the biogenic. The results of the OPC/SEMS were also used to calculate the Fuchs surface of the aerosol particles. This surface was then compared with the measurements of the epiphaniometer and an agreement within 10% was found (Pandis *et al.* 1991). The isoprene aerosol carbon yield remained under 0.8% even for initial concentrations as high as 6 ppm. The reaction of 70 ppb of isoprene in the presence of 400 seed particles $cm^{-3}$ of $(NH_4)_2SO_4$ did not result in the formation of any condensable products, leading to the conclusion that aerosol formation from the isoprene photooxidation is negligible under ambient isoprene concentration levels (0.1-30 ppb). The ß-pinene aerosol carbon yield is as much as 8% and depends strongly on the initial $HC/NO_x$

concentration ratio *r*. A maximum is observed for values of *r* between 10 and 20 ppbC/ppb $NO_x$. Formation of condensable aerosol products was observed for ß-pinene concentrations as low as 20 ppb, and nucleation of new particles for as low as 60 ppb.

Scanning Electron Micrographs showed expected liquid aerosol particles on all filters. In some experiments, these droplets had coalesced, forming a large pool visible by eye and not stable under the electron beam. Filters from all experiments also contained some agglomerates, comprised of small particles of 40-60 nm size (Fig. 1), indicating that a fraction of the aerosol formed consisted of solid material.

An average vapor pressure of the aerosol products of the ß-pinene photooxidation was estimated using the TDMA technique. Particles of diameter 103, 125 and 156 nm were separated from the surrounding organic vapors and evaporated at a temperature of 31 C. Using the diameter change and assuming a molecular weight of 200 g $mole^{-1}$, a density of 1.4 g $cm^{-3}$ and a molecular diffusivity of 0.06 $cm^2$ $s^{-1}$ an average saturation vapor concentration of 0.037 to 0.024 ppb was estimated. Assuming that these condensable species have similar heats of vaporization as the mono-- and dicarboxylic acids studied by Tao and McMurry (1989), their average vapor saturation concentration at 25 C should be roughly 9 ppt.

Analysis of the FTIR spectra of both the ß-pinene and isoprene aerosol indicated a strong organic nitrate absorbances at 1280 $cm^{-1}$, C=O absorbances at roughly 1720-1780 $cm^{-1}$, and richly detailed organic fingerprint region of 900-1400 $cm^{-1}$ (Fig. 2), as well as hydroxyl group absorbances at 3380 $cm^{-1}$. The carbonyl peak contains both alkyl carbonyls and organic acids. By assuming a number of C-H bonds per condensed molecule (6 for isoprene and 14 for ß-pinene) we can estimate the number of nitrate and carbonyl groups per molecule. As expected (Atkinson 1990), ß-pinene appears to have somewhat more

nitrates per molecule than isoprene, at 0.4 and 0.27, ±50% respectively. The carbonyls are more difficult to quantify, as the strength of the carbonyl stretch depends strongly on whether the carbonyl is acid or alkyl. If we assume that the carbonyls are pure acid, we have 1.8 and 1.1 carbonyls per molecule of ß-pinene and isoprene respectively. Assuming purely alkyl carbonyls, we have 6.1 and 4 carbonyls per molecule respectively. Other information (e.g. peaks around 3220 $cm^{-1}$), indicate that the real value is somewhere between these two extremes.

GCMS was carried out for ß-pinene aerosol samples collected at the end of two experiments with 300 and 1800 ppb of initial hydrocarbon. The results indicate that about 11 major species and several more minor ones are able to condense at these concentrations. The relative abundances of the aerosol extract along with their approximate molecular weights are listed in Table 1. Comparisons with mass spectra of authentic samples confirm the presence of nopinone, as well as a likely match for the minor species pinocamphone (2,6,6 trimethyl bicyclo(3.1.1)heptan-3one). Any organic acids in the samples were not derivatized, and hence remained in the GC column, however, nitrates should appear. The highest molecular weight species may be nitrates but we lack data below 50 amu where characteristic nitrate fragments typically occur. The condensed compounds appear in about the same proportions in the aerosol samples from both experiments, and none of the compounds is completely absent from either of the samples. Some variations do appear; compounds 8 and 10 are much more abundant in the higher concentration case, and 2 and 4 in the lower concentration case. Possible factors include differences in $r$ and the quantities of reacted hydrocarbon. The isoprene-derived aerosol was also a mixture of several species with molecular weights ranging from 86 to 154 amu, with most of the compounds at around 112 amu.

*Table 1. Relative Abundances and Molecular Weights of Components of β-Pinene Aerosol Neutral Extract*

| *β-pinene* | *% of compound in neutral aerosol extract* | | | | | | | | | | |
|---|---|---|---|---|---|---|---|---|---|---|---|
| 300 ppb | 11 | 18 | 3 | 7 | 3 | 2 | 8 | 3 | 18 | 2 | 1 |
| 1800 ppb | 12 | 11 | 2 | 2 | 1 | 1 | 11 | 13 | 19 | 14 | 2 |
| estimated MW | 138 | 154 | 152 | 141 | 155 | 168 | 168 | 168 | 168 | 197 | 180 |

# *Conclusions*

The organic aerosols produced in the isoprene and ß-pinene systems are clearly a mixture of several molecular species, even when the biogenic hydrocarbon concentration is low. The species include nitrates, acids, aldehydes, ketones, and alcohols, often with more than one functional group being found on the condensed molecules. Some appear to be sufficiently highly substituted to form solid particles. The relative complexity of the aerosol composition indicates that there are several pathways leading to its formation from the gas phase. In particular, OH and ozone produce different aerosol species, with each providing a variety of possible isomers. In the presence of $NO_x$, organic nitrates are well known to be formed from the reactions of OH, but only in very small quantities from ozone. On the other hand, ozone provides the only pathway for the formations of organic acids (Atkinson 1990). This is dramatically illustrated in Fig. 3, where we observed two nucleation bursts, and calculated the loss due to ozone and OH. The results indicate that each oxidant produced sufficient condensable species to lead to nucleation. The observation that aerosol formation depends on $r$ may be understood by realizing that $r$ controls the relative amounts of OH and ozone reacting with the hydrocarbon, and both OH and ozone lead to aerosol formation by separate pathways.

# *References*

Altshuller, A. P. (1983). Review: Natural volatile organic substances and their effect on air quality in the United States. *Atmos. Environ.*, **17**: 2131-2165.

Atkinson, R. (1990). Gas-phase tropospheric chemistry of organic compounds: a review. *Atmos. Environ.*, **24A**: 1-41.

Gaggeler H. W., U. Baltensperger, M. Emmenegger, D. T. Jost, A. Schmidt-Ott, P. Haller and M.. Hofmann (1989). The epiphaniometer, a new device for continuous aerosol monitoring. *J. Aerosol Sci.*, **20:** 557-564.

Global Geochemistry Corporation (1989). Estimation of contemporary carbon in fine particle aerosols. Final Report to the Coordinating Research Council, Atlanta, GA.

Hatakeyama S., K. Izumi, T. Fukuyama and H. Akimoto (1989). Reactions of ozone with α-pinene and ß-pinene in air: yields of gaseous and particulate products. *J. Geophys. Res.*, **94:** 13013-13024.

Hull, L.A. (1981). Terpene Ozonolysis Products. *Atmospheric Hydrocarbons*, Vol. 2, Ann Arbor Science Publishers, 161-204.

Izumi K., K. Murano, M. Mizuochi and T. Fukuyama (1988). Aerosol formation by the photooxidation of cyclohexene in the presence of nitrogen oxides. *Environ. Sci. Technol.*, **22:** 1207-1214.

Kamens, R. M., H. E. Jeffries, M. W. Gery, R. W. Wiener, K. G. Sexton and G. B. Howe (1981). The impact of α-pinene on urban smog formation: an outdoor smog chamber study. *Atmos. Environ.*, **15:** 969-981.

Kamens, R. M., M. W. Gery, H. E. Jeffries, M. Jackson and E. I. Cole (1982). Ozone-isoprene reactions: product formation and aerosol potential. *Int. J. of Chemical Kinetics*, **14:** 955-975.

Lamb, B., A. Guenther, D. Gay and H. Westberg (1987). A national inventory of biogenic hydrocarbon emissions. *Atmos. Environ.*, **21:** 1695-1705.

Pandis, S. N., U. Baltensperger, J. K. Wolfenbarger and J. H. Seinfeld (1991). Inversion of aerosol data from the epiphaniometer (submitted).

Palen, E. J. and D. T. Allen (1989). Size distributions of organic and inorganic functional groups in ambient Los Angeles aerosol. *Abstracts of the 1989 Annual Meeting of the American Association for Aerosol Research*, 245, Reno, Nevada.

Rader, D. J. and P. H. McMurry (1986). Application of the tandem differential mobility analyzer to studies of droplet growth or evaporation. *J. Aeros. Sci.*, **17:** 771-787.

Tao, Y. and P. H. McMurry (1989). Vapor pressures and surface free-energies of C14-C18 monocarboxylic acids and C5-dicarboxylic and C6-dicarboxylic acids. *Environ. Sci. Technol.*, **23:** 1519-1523.

Wang, S. C. and R. C. Flagan (1990). Scanning Electrical Mobility Spectrometer. *Aerosol Sci. Technol.*, **13:** 230-240.

Went, F. W. (1960). Blue hazes in the atmosphere. *Nature,* **187:** 641-643.

Zimmerman, P. R. (1979). Determination of emission rates of hydrocarbons from indigenous species of vegetation in the Tampa/St. Petersburg Florida area. EPA-904/9-77-028.

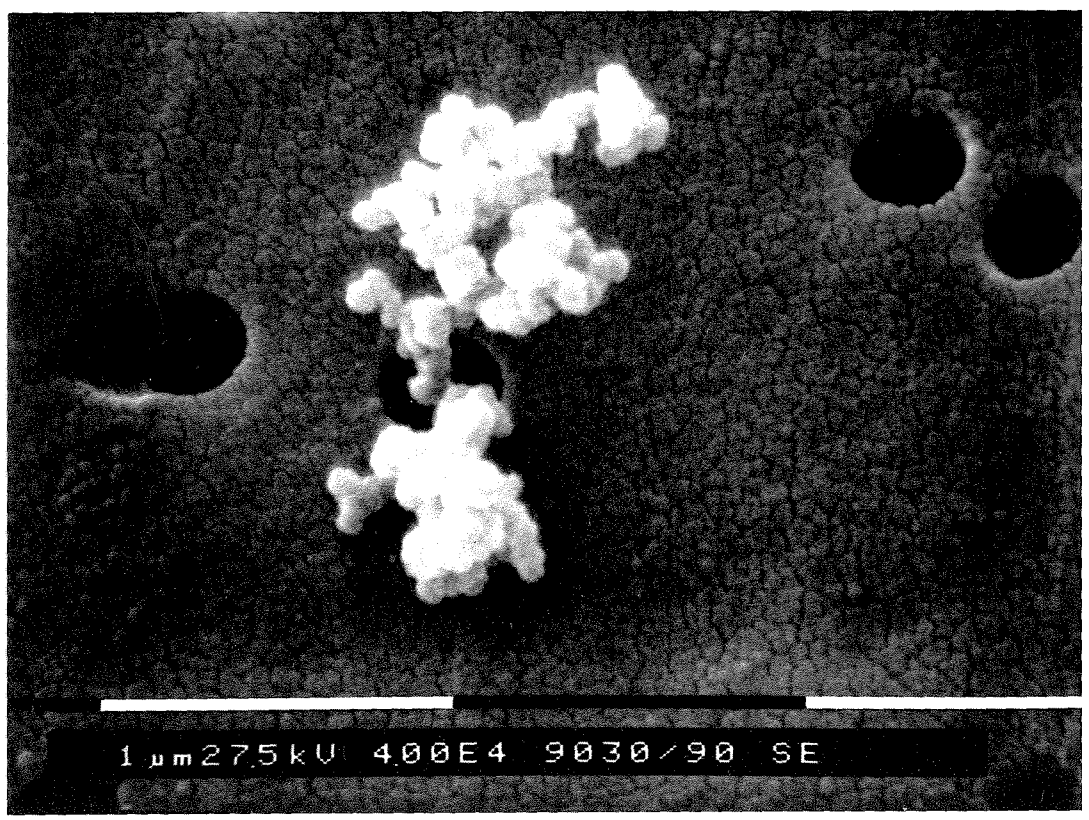


Figure 1. Aerosol particles formed in a smog chamber experiment with an initial isoprene concentration of 4.45 ppm. The white bar represents 1 mm. The black holes are Nucleopore filter pores (0.4 mm diameter).

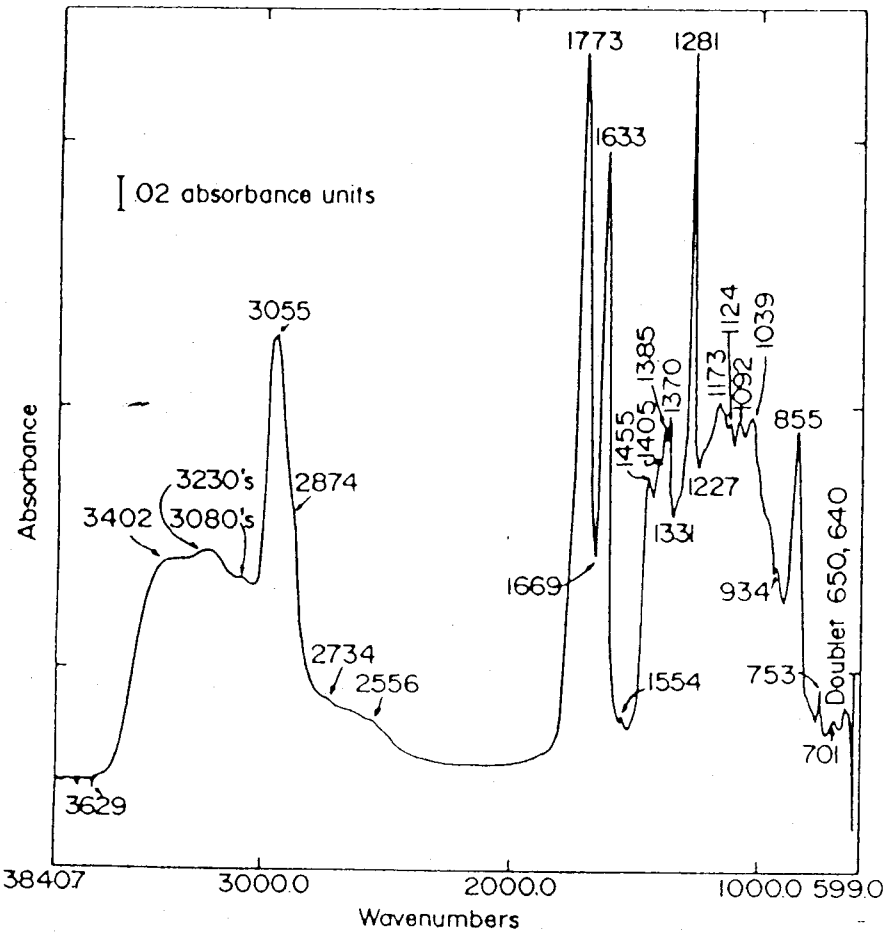


Figure 2. FTIR spectrum of ß-pinene aerosol 1-2 mm size cut from an experiment with 2 ppm initial ß-pinene.

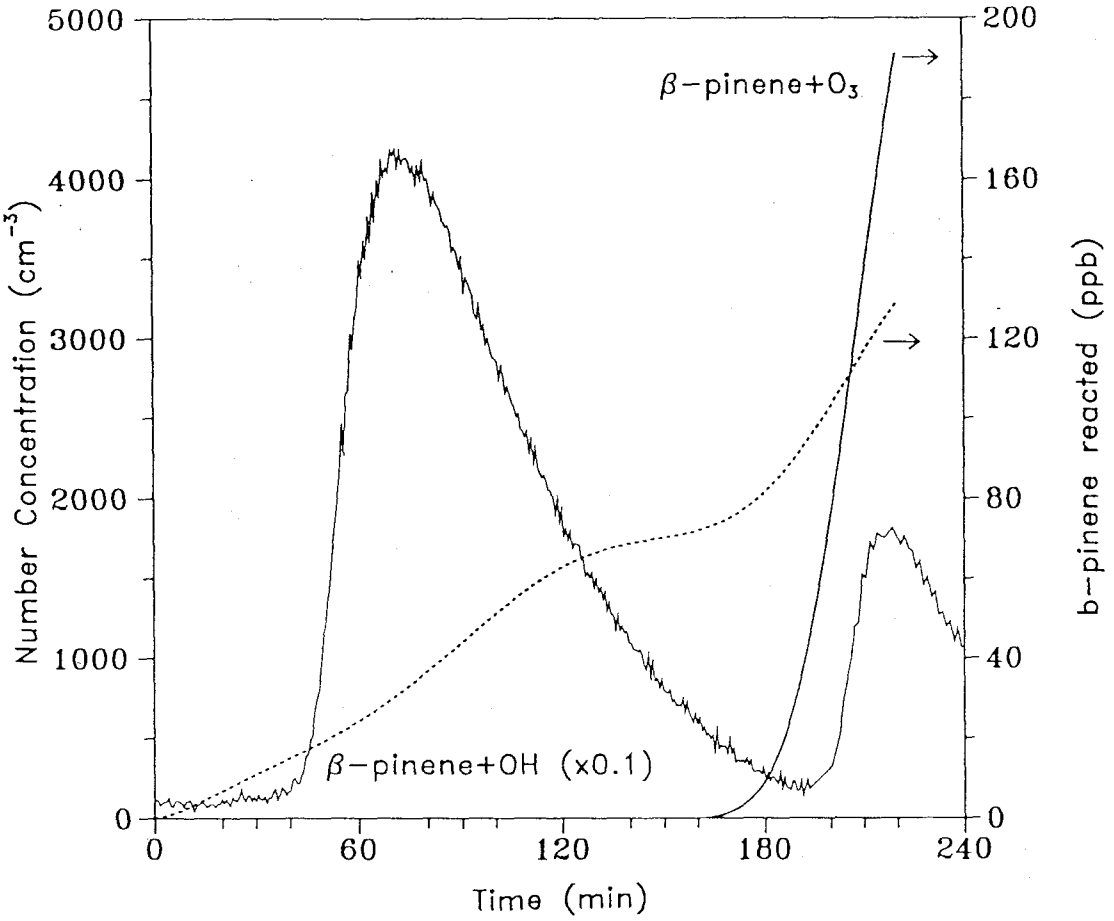


Figure 3. ß-pinene aerosol number concentration (data) and ß-pinene loss due to OH (dotted line) and $O_3$ (solid line). Data are from the same experiment as Fig. 2. ß-pinene reactions were calculated from measured ozone concentrations, and OH was assumed to be responsible for the remaining ß-pinene loss.

# CHAPTER 7

# Summary and Conclusions

*There is a theory that states that if anyone ever figures out how the universe works, it will disappear and be replaced by something more bizarrely inexplicable. There is another theory that states that this has already happened.*

*(abs. from D. Adams-Hitch Hikers Guide to the Galaxy)*

The principal contribution of this thesis is in the provision of an entirely new look at the $O_3$ reactions of alkenes. These reactions are very important in the atmosphere, and it appears that the accepted $O_3$-initiated oxidation mechanism has been very far from the correct mechanism. Little OH formation has been assumed; this radical is typically formed in 50-70% yields. Carbonyl yields are close to 100%; they have been assumed to be around 50%. Production of $O(^3P)$ has been entirely ignored. It is clear that the radical and carbonyl yields need to be evaluated for the full range of atmospherically relevant alkenes.

Another contribution of this thesis is the photooxidation chemistry of 1-octene. This is the first assessment of the chemistry of this compound, and a much more detailed study than has been carried out on a C-5 or larger alkene. From this work, it appears that isomerization will turn out to be a major reaction pathway for the C-5 and larger hydrocarbons.

The work in this thesis also provides the atmospheric community with photochemical oxidation mechanisms for isoprene and 1-octene, mechanisms that are soundly based in detailed experiments and analysis. These mechanisms can be expected to perform under a wider range of conditions than those that have been tuned to a narrow range of chamber experiments.

A series of experiments have carried out on both isoprene and 1-octene under widely varying conditions. The experiments were designed each to examine an individual oxidant; $O_3$, OH, $NO_2$ , or $O(^3P)$. All of these experimental designs, but especially those which have been employed repeatedly in studies of the reactions of these oxidants in the past, suffer from interferences from oxidants other than the one intended; generally another of the above set of four. Some of the sources of interfering oxidants result from the experimental design itself; for example, the formation of $NO_2$ and subsequently $O(^3P)$ in the OH experiments using methyl nitrite results from the necessity to include large quantities of NO to suppress $O_3$ formation. In other experiments the interfering oxidants result directly from the primary reaction itself; this is the case for the $O_3$ experiments in which the $O_3$-alkene reaction produces large quantities of both OH and $O(^3P)$. In the $O(^3P)$ experiments small amounts of organic radical formed in the $O(^3P)$-alkene reaction react with NO, present because $NO_2$ is employed as the $O(^3P)$ source, to eventually form OH. While the interfering reactions make interpretation of the data extremely complicated, and virtually impossible without the use of chemical kinetics modeling, and have often led to misinterpretation of results in past studies, they also offer tremendous avenues for insights into the chemistry.

One of the main contributions of this thesis is the extensive photochemical kinetics modeling carried out. It is a technique that has not been commonly carried out in the kind of detailed mechanistic studies that make up much of this thesis. Simulations are

essential to understanding reaction systems as complicated as gas-phase atmospheric pressure studies, and allow quantification of processes and product yields not attainable with pencil and paper.

Another critical development of this thesis is the application of GCMS to both gas-phase and aerosol chemistry. While the value of GCMS has long been recognized, this represents an expansion to the Caltech arsenal of analytical techniques.

Our results, when combined with those of previous studies allow us to account for virtually 100% of the OH-isoprene products. The hydroxyl radical reaction yields 60.5% carbonyls, 5.1% 3-methyl furan, and 12% organonitrates, leaving 22% of the product not individually identified. These are a collection of multisubstituted products, 2-4% of which condense to the aerosol phase. The OH reaction is difficult to study because of the necessity of including NO, which provides a formation pathway for $O(^3P)$, complicating the analysis of any OH-alkene reaction. This problem is likely to have interfered with previous studies of OH-alkene reaction systems to some degree, independent of the source used for OH, resulting in carbonyl product yields that are low.

While we were not able to determine the products of the $NO_2$-isoprene reaction, we measured its rate constant and found $1.8 \times 10^{-19}$ $cm^3$ $molec^{-1}$ $s^{-1}$.

We have found that the $O(^3P)$-isoprene reaction results in smaller quantities of free radicals than previously believed; only about 8% produces species that results in $HO_2$ formation. Most of the remainder forms epoxides; the epoxide yield, at 84% is about double that expected based on results for 1-butene. The 1,2 hydrogen shifts that appear to be prevalent for 1-butene are minimal if they occur at all; however, the reaction forms 2,2 methyl butenal via an isomerization involving a five-membered ring.

The ozone-isoprene reaction appears on the surface like any other ozone-alkene reaction, producing close to 50% carbonyls, and some propene as expected from the decomposing Criegee biradical. Addition of methyl cyclohexane to the reaction, in combination with careful consideration of the oxygenated products, including the epoxides, reveals a different picture of the free radical and carbonyl production in the system. The OH yield is nearly 70%, and the yield of $O(^3P)$ about 45%, while the carbonyls plus propene total 100%. The epoxides form from the secondary reaction of $O_3$ with isoprene. The yields of $O(^3P)$ and OH are probably not restricted to isoprene. While OH formation has been fairly well characterized for ethene, and seems to be minimal, this result cannot be extrapolated to larger alkenes. It is very likely that $O(^3P)$ formation has been overlooked, but occurs in all ozone reactions with alkenes, large or small. Because of both the interference from OH and $O(^3P)$, and the reactions of products with $O_3$ and OH, the carbonyl yields for isoprene are higher than they appear in the standard ozone-alkene experiments. Measured carbonyl yields from most alkene-$O_3$ reactions probably suffer from the same artifacts, and are in fact much higher than generally believed. Our results, combined with the formaldehyde measurements of Kamens et al. (6) and Niki et al. (7), indicate that non-symmetric molozonides do not decompose 50% each way, but instead favor the $C_4$ Criegee plus formaldehyde. The large quantities of OH and $O(^3P)$ make the $O_3$ reaction more important both in smog chamber studies and in the atmosphere.

A mechanism for the oxidation of isoprene is developed and includes the recent developments on each of isoprene's atmospherically important reactions: $O_3$, OH, $O(^3P)$, and $NO_3$. The mechanism is tested against chamber data that include a range of mixtures of these oxidants. While it performs reasonably well under conditions where the OH and $O(^3P)$ reactions dominate, it tends to overpredict $O_3$ formation, as well as the speed of development of $O_3$ under conditions where the $O_3$ and $NO_3$ reactions are important. The

$NO_3$ reaction is the most uncertain aspect of the isoprene mechanism, and may be responsible for a large part of this discrepancy. The discrepancy may also arise from the difficulty in extrapolating the results of $O_3$ experimental results, necessarily carried out in the absence of $NO_x$, to conditions that include significant concentrations of $NO_x$.

The reactions of 1-octene are in some ways very similar to the those of smaller alkenes, and in others dramatically different. The $NO_2$ reaction is very slow, proceeding at a rate of less than $1.2 \times 10^{-21}$ $cm^3$ $molec^{-1}$ $s^{-1}$. The $O(^3P)$ reaction is similar to its smaller homologues; this reaction is dominated by epoxide formation and octanal and 2-octanone formation. The decomposition pathway, about 7%, is less important than it is for 1-butene, where it accounts for about 20%.

The majority of the OH initiated alkoxy radical reaction appears to proceed via a different pathway than the smaller hydrocarbons; the decomposition pathway accounts for only about 22% of the reactions of this radical. The alkyl nitrate yield from this reaction probably accounts for 33% of the products, leaving 52% unaccounted for by known pathways. The most likely reaction for the remaining alkoxy radicals is an internal isomerization via a six-membered ring. Some of these products may enter the aerosol phase.

The 1-octene reaction with $O_3$, has been shown to produce significant quantities of OH, about 0.55 per molecule of 1-octene reacted, and the products heptanal, 80%, thermally stabilized $C_7$ biradical, 11%, and hexane, 1%, account for nearly 100% of the reaction. The OH yield is not at all consistent with most $O_3$-alkene studies, however most previous studies seem to have overlooked OH formation in the reaction systems. The heptanal yield is much more than the 50% yield expected from the standard $O_3$-alkene reaction mechanism, but is expected once OH is taken into account. The decomposition pathway

that leads to hexane formation appears to be very minor, at about 1% compared to 6% for 1-butene (Atkinson and Lloyd, 1984).

The organic aerosols produced in the isoprene and ß-pinene systems are clearly a mixture of several molecular species, even when the biogenic hydrocarbon concentration is low. The species include nitrates, acids, aldehydes, ketones, and alcohols, often with more than one functional group being found on the condensed molecules. Some appear to be sufficiently highly substituted to form solid particles. The relative complexity of the aerosol composition indicates that there are several pathways leading to its formation from the gas phase. In particular, OH and ozone produce different aerosol species, each providing a variety of possible isomers. In the presence of $NO_x$, organic nitrates are well known to be formed from the reactions of OH, but only in very small quantities from ozone. On the other hand, ozone provides the only pathway for the formations of organic acids.

As result of this thesis, several questions have been answered and others have been raised. The long-chain alkenes and certainly isoprene, especially with respect to urban photochemical oxidation, are much better understood. The understanding of long-chain alkanes and aromatics is still incomplete. Another entire class of hydrocarbons has been thrown into question: the alkenes, small and large alike. The extent and mechanism of the very important free radical production by the $O_3$ reactions with these hydrocarbons is in need of further investigation, to include the full compliment of atmospherically important alkenes.

# APPENDIX 1

# Gas-Phase ß-Pinene Data

*Table A1.*
*Summary of Initial Conditions for ß-Pinene Experiments*

| Expt. # * | Initial Concentration (ppb) HC | NO | $NO_2$ | $O_3$ max. | $HC/NO_x$ |
|---|---|---|---|---|---|
| 6 | 67 | 134 | 71 | 230 | 3.3 |
| 7 | 63 | 135 | 37 | 190 | 3.7 |
| 8 | 129 | 44 | 22 | 185 | 20 |
| 9 | 36 | 33 | 16 | 190 | 7.3 |
| 10 | 28 | 80 | 54 | 35 | 2.1 |
| 11 | 92 | 200 | 1600 | 300 | 0.51 |
| 15 | 340 | 40 | 26 | 100 | 52 |
| 16 | 2060 | 770 | 212 | 350 | 20 |

* These numbers correspond to the experiments reported in Pandis et al. (1991).

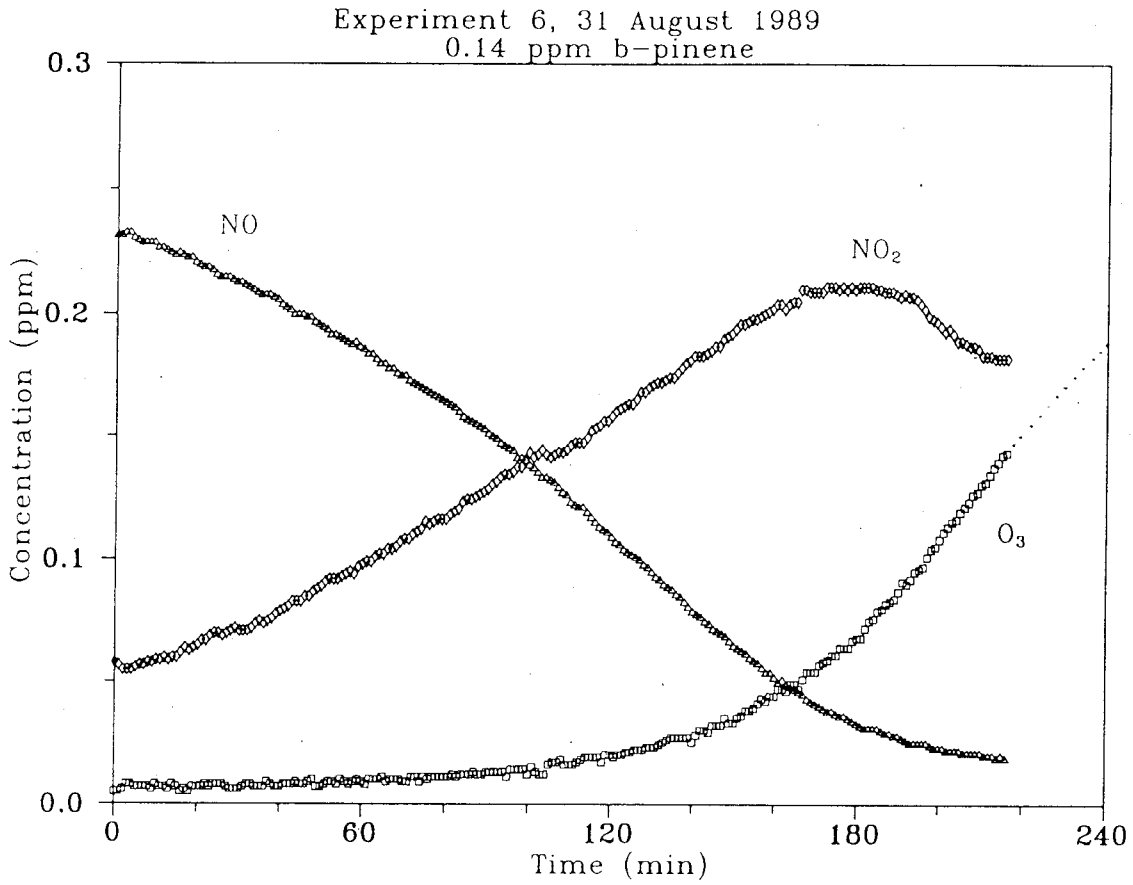


Figure A1.1. NO, $NO_x$ - NO (identified as $NO_2$), and $O_3$ data for experiment 6.

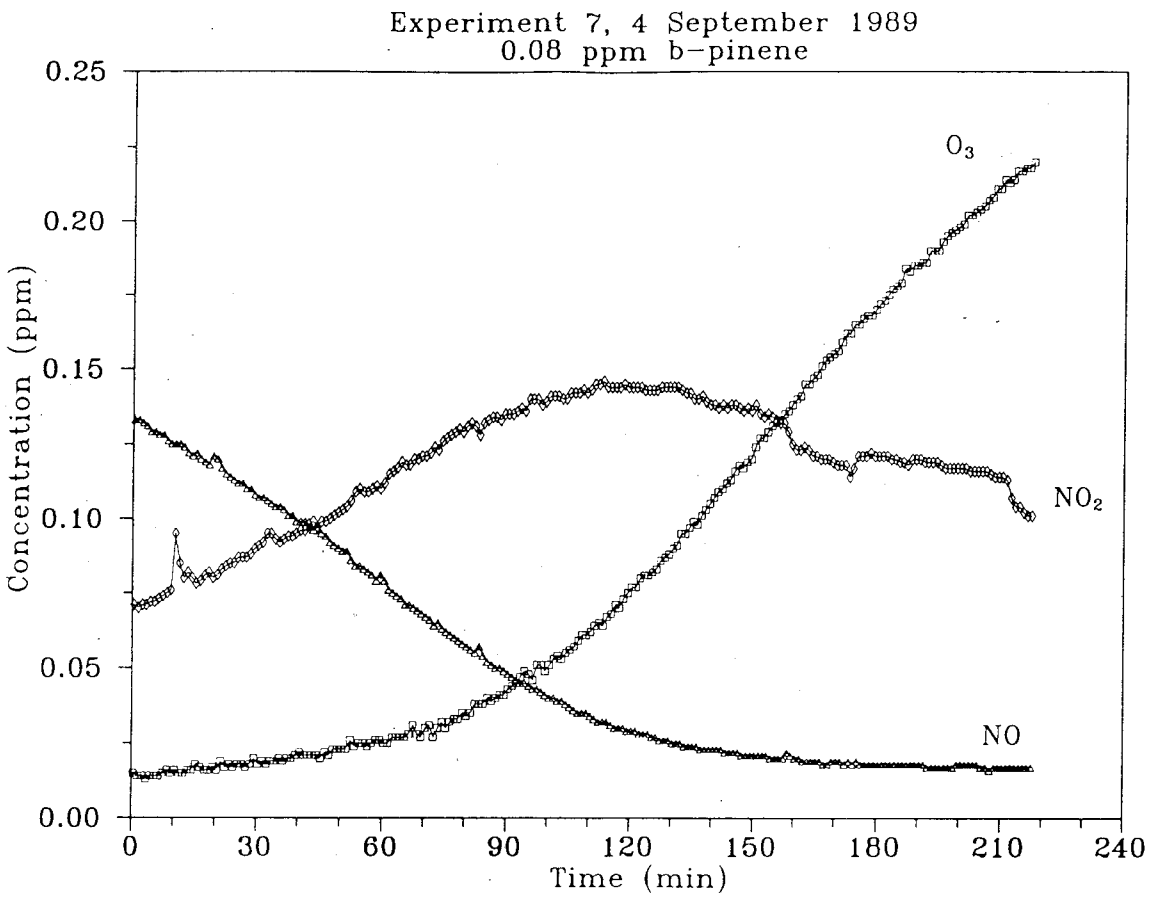


Figure A1.2. NO, $NO_x$ - NO (identified as $NO_2$), and $O_3$ data for experiment 7.

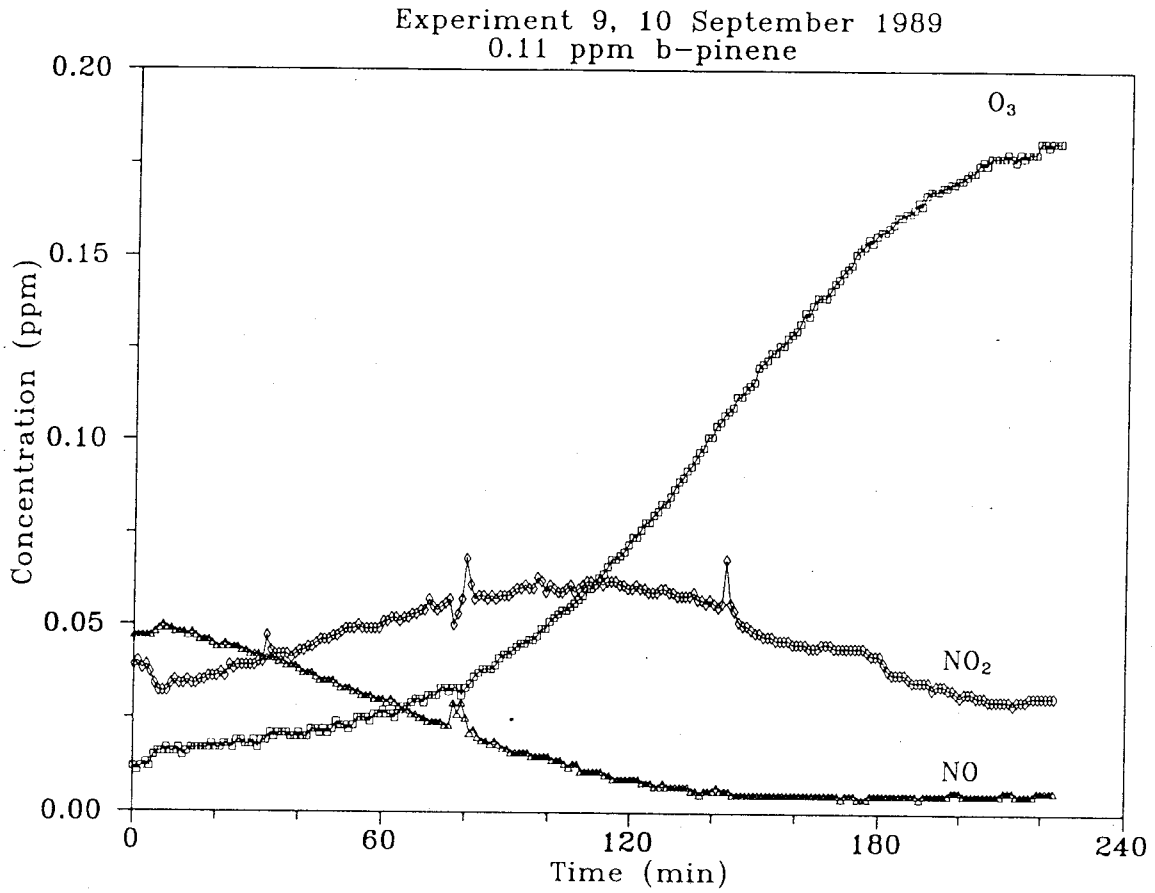


Figure A1.3a. NO, $NO_x$ - NO (identified as $NO_2$), and $O_3$ data for experiment 9.

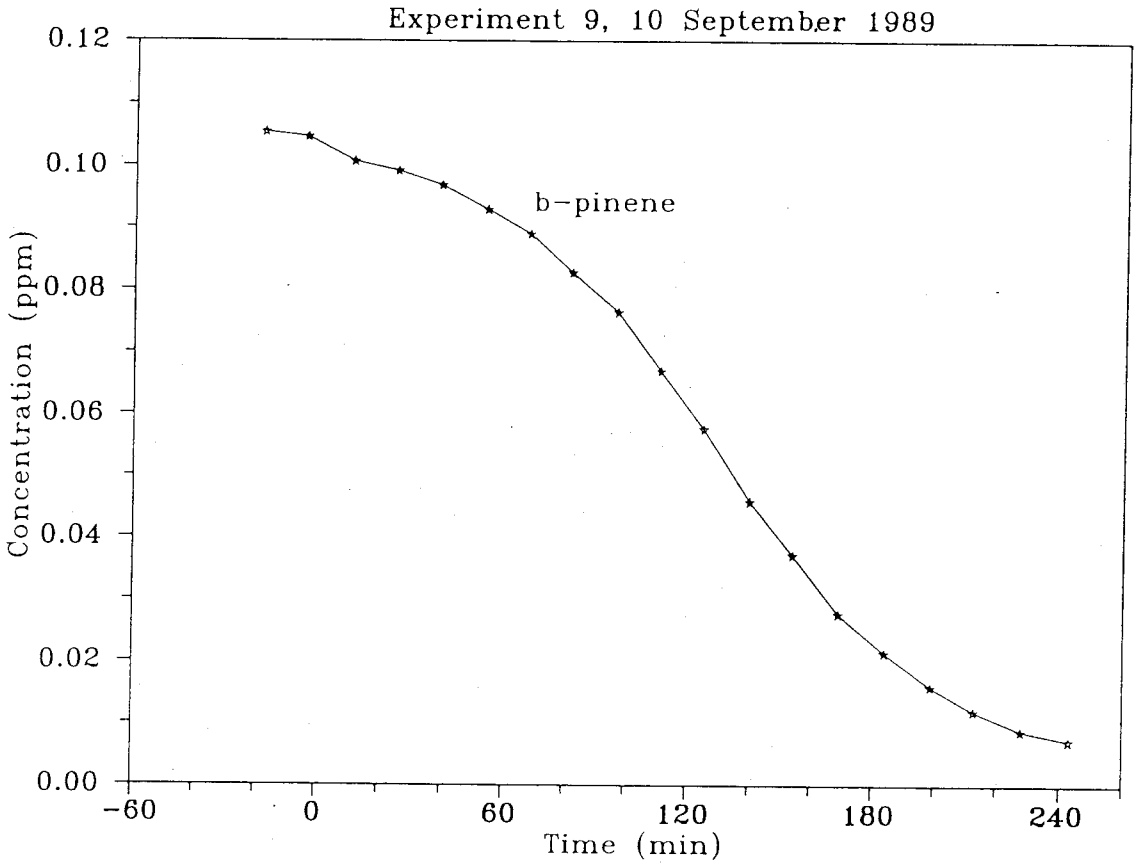


Figure A1.3b. ß-pinene data for experiment 9.

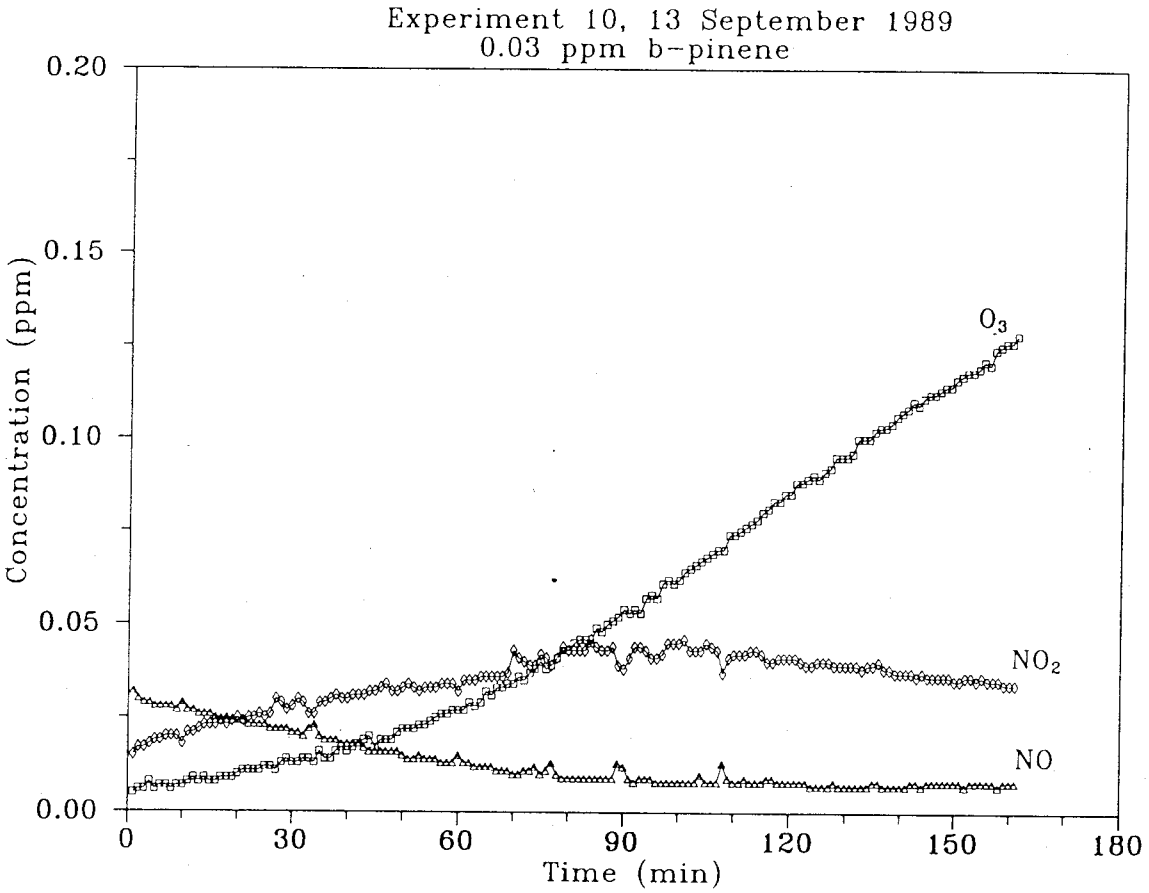


Figure A1.4a. NO, $NO_x$ - NO (identified as $NO_2$), and $O_3$ data for experiment 10.

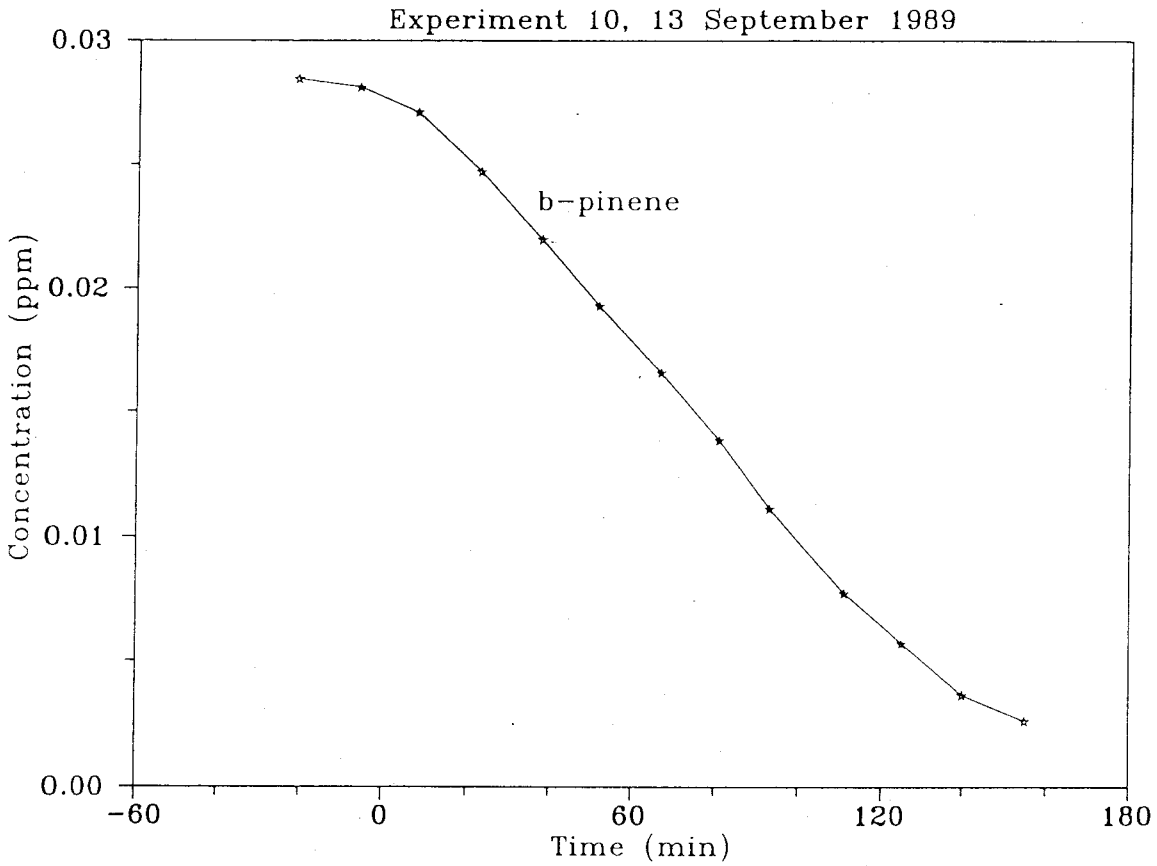


Figure A1.4b. ß-pinene data for experiment 10.

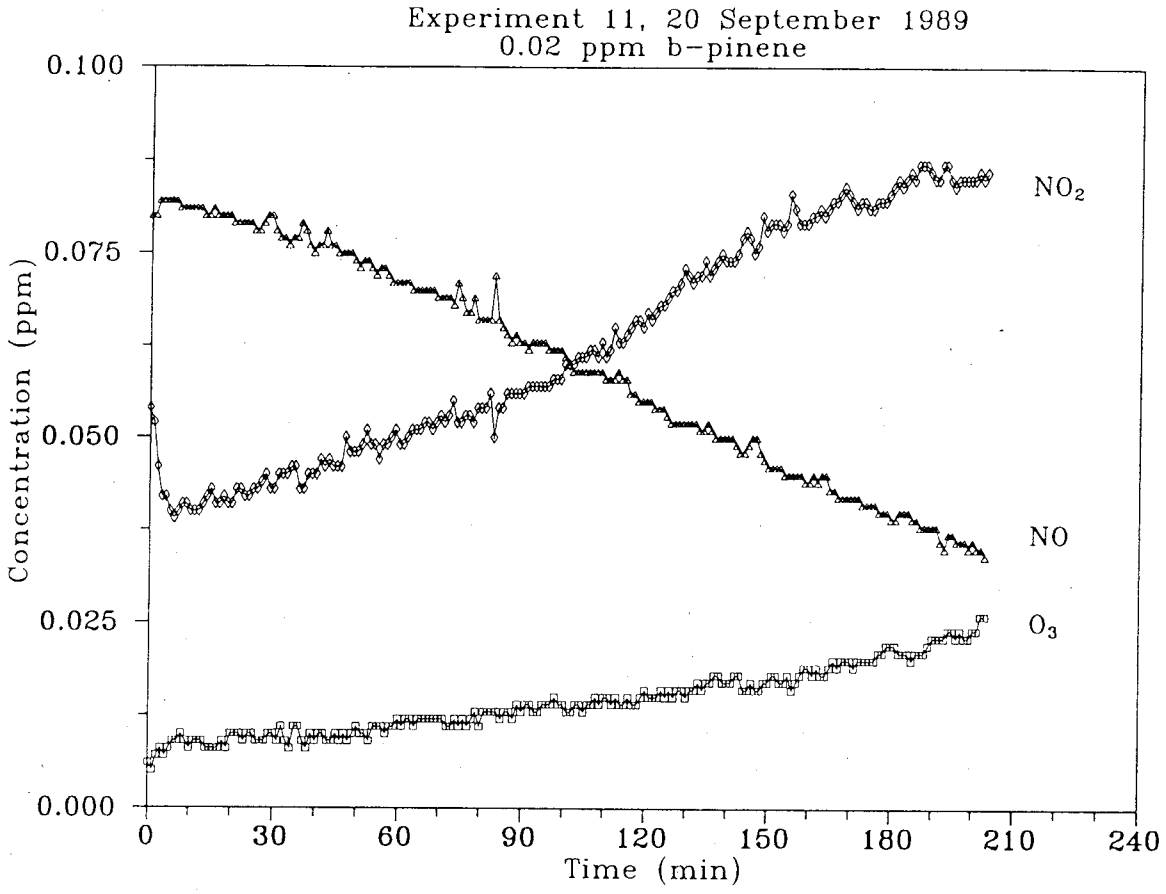


Figure A1.5a. NO, $NO_x$ - NO (identified as $NO_2$), and $O_3$ data for experiment 11.

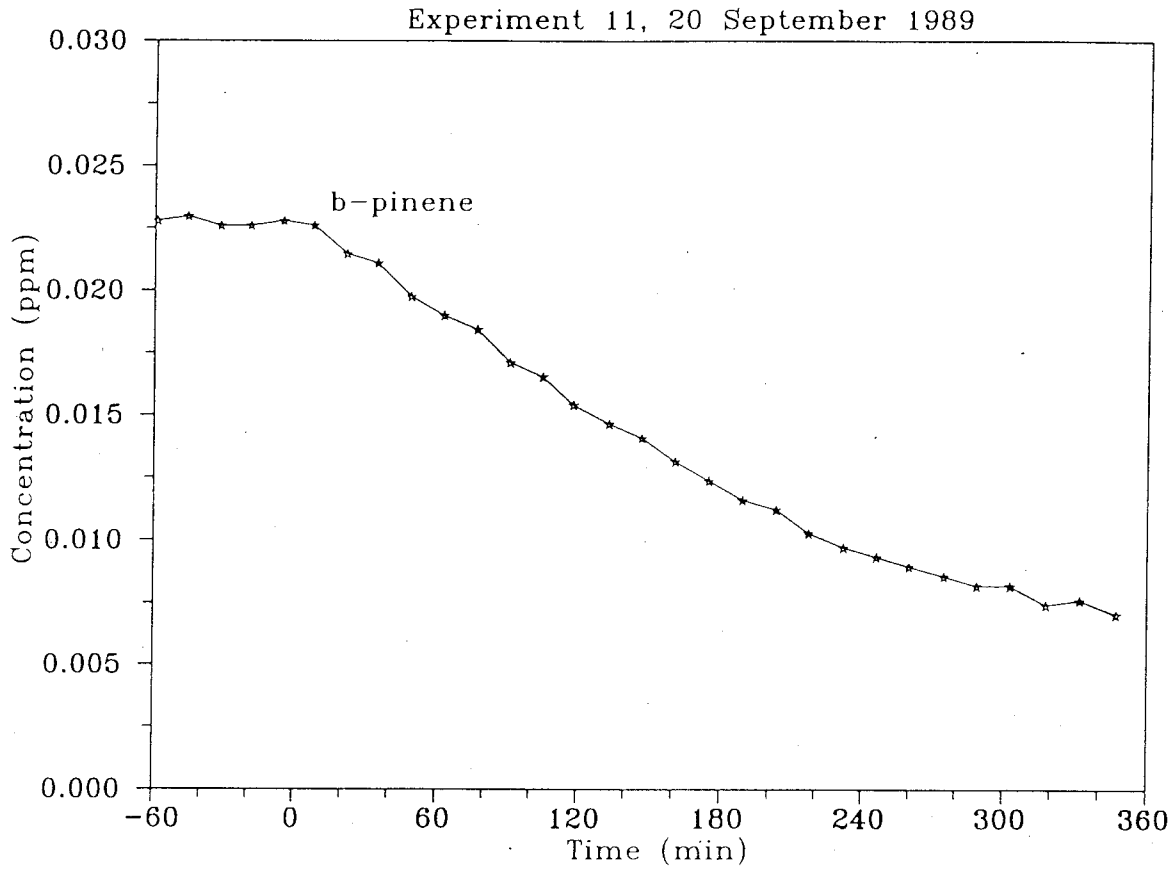


Figure A1.5b. ß-pinene data for experiment 11.

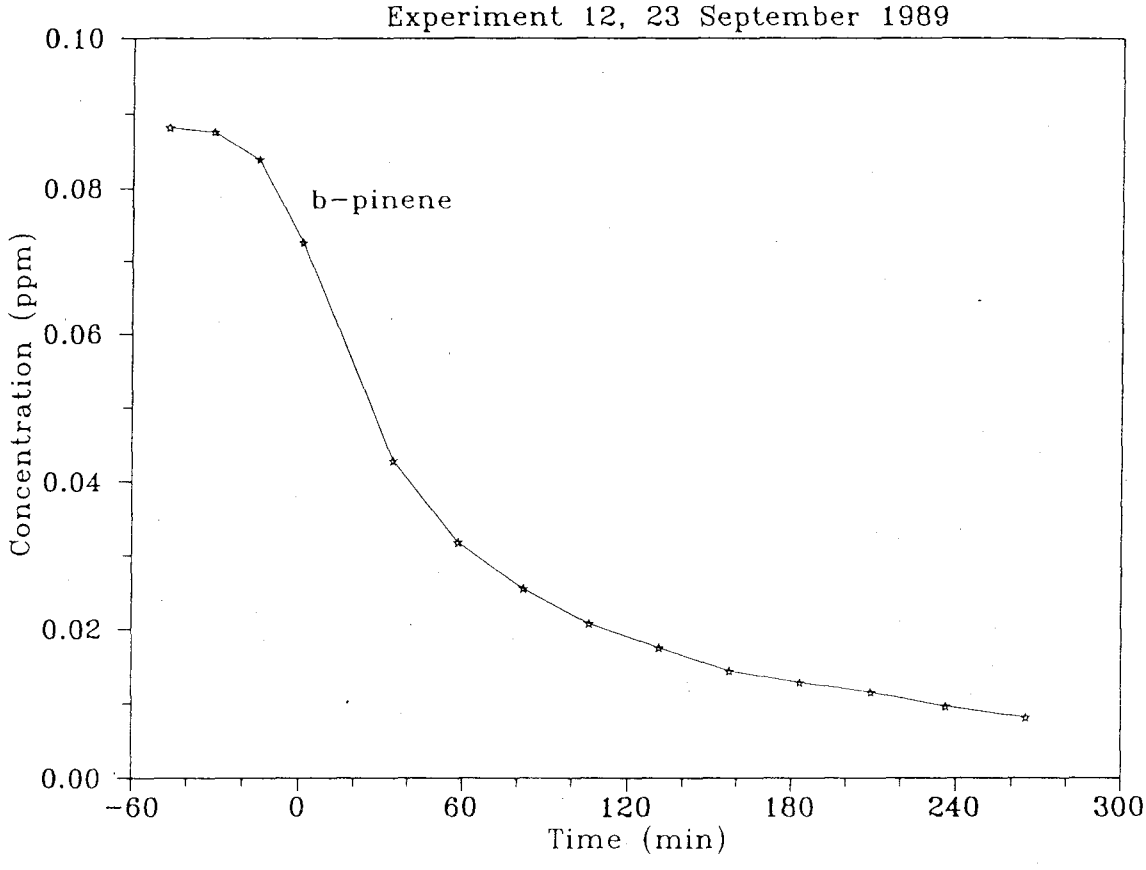


Figure A1.6. ß-pinene data for experiment 12.

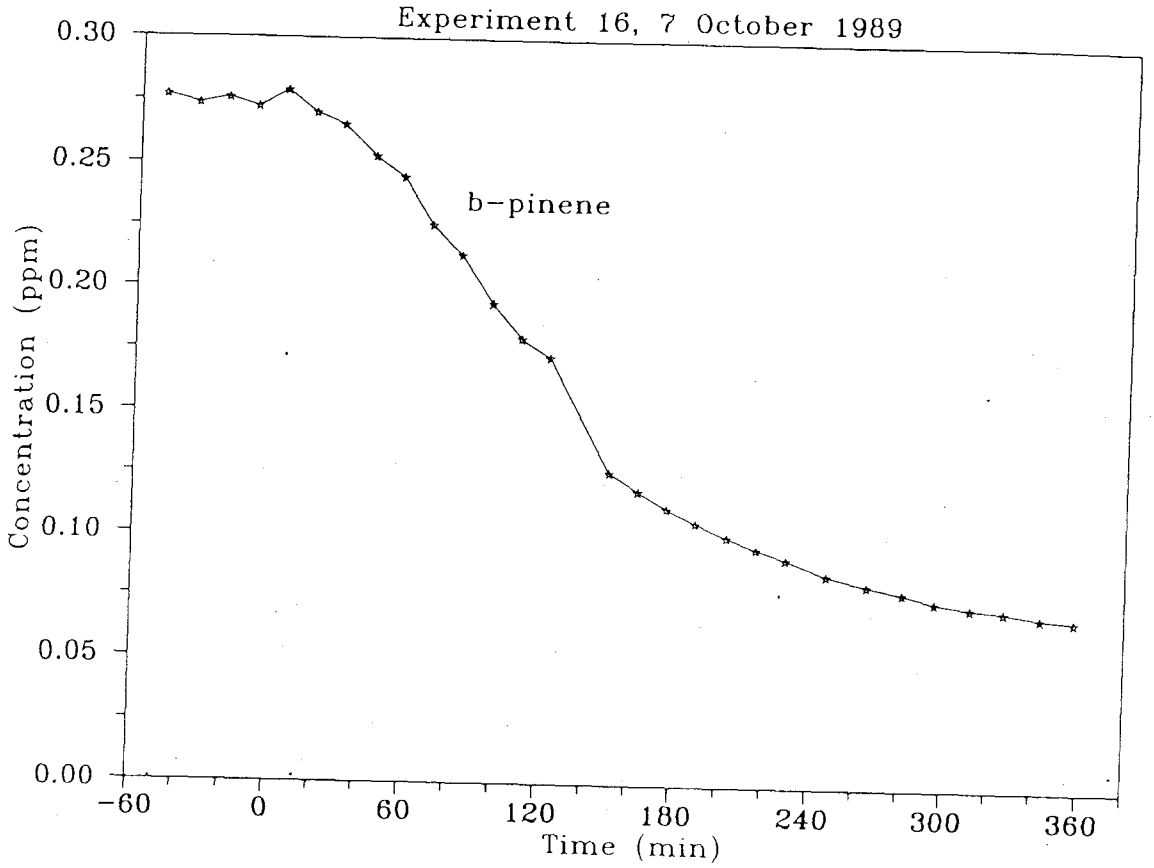


Figure A1.7. ß-pinene data for experiment 16.

# APPENDIX 2

# Description of Cryotrap-Thermal Desorption Unit

Samples for GCMS analysis and FID quantitation were collected on tenax tubes. Samples are obtained by withdrawing air from the smog chamber first through a Teflon sampling line inserted 15 cm into the smog chamber, then an 0.5 micron pore size, 47mm Tfe filter (Millipore) in an aluminum filter holder, the Tenax tube, and finally a pump fitted with a 1 lpm critical orifice. The samples were desorbed and focussed by an instrument built in this laboratory, shown schematically in figure 1, Chapter 2. The instrument consists of a tube desorber, a cryogenic trap which can be heated quickly, a heated six-port valco sampling valve and heated transfer lines. The four heated zones, the Tenax tube, the cryo trap, the transfer lines and the valve are each maintained at constant temperature or ramped by separate temperature controllers, each on separate AC lines.

The six-port valve has 1/8" fittings and is constructed from hastelloy C (for inertness to sulfur oxides), with a 3.5" standoff assembly and manual handle. While 1/16" fittings would have provided more convenient connections, this valve had been previously purchased by Caltech, and has provided leak-free operation when used with the appropriate reducing ferrules. The valve oven and its temperature controller were obtained from Valco; the controller a the separate box that sits above the unit.

The Tenax-packed tubes are constructed from 1/4" nickel tubing (chosen for inertness) packed with 0.8g Tenax, and fitted with pesticide grade glass wool (Alltech) plugs and Teflon-packed valves (Nupro Co.) at each end. The valves allow for easy short-term storage and eliminate sample contamination problems. The sampling tubes are each wound with 100 watt heating cord, which are plugged into the desorption instrument. Heating cords were obtained from C&H surplus electronics (Pasadena). Connection to the transfer lines are made via swage fittings. Temperature ramping of the Tenax traps is accomplished with a CN5051J fast response temperature controller and the solid state relay attached to the back wall of the chassis (Fig. A2.1).

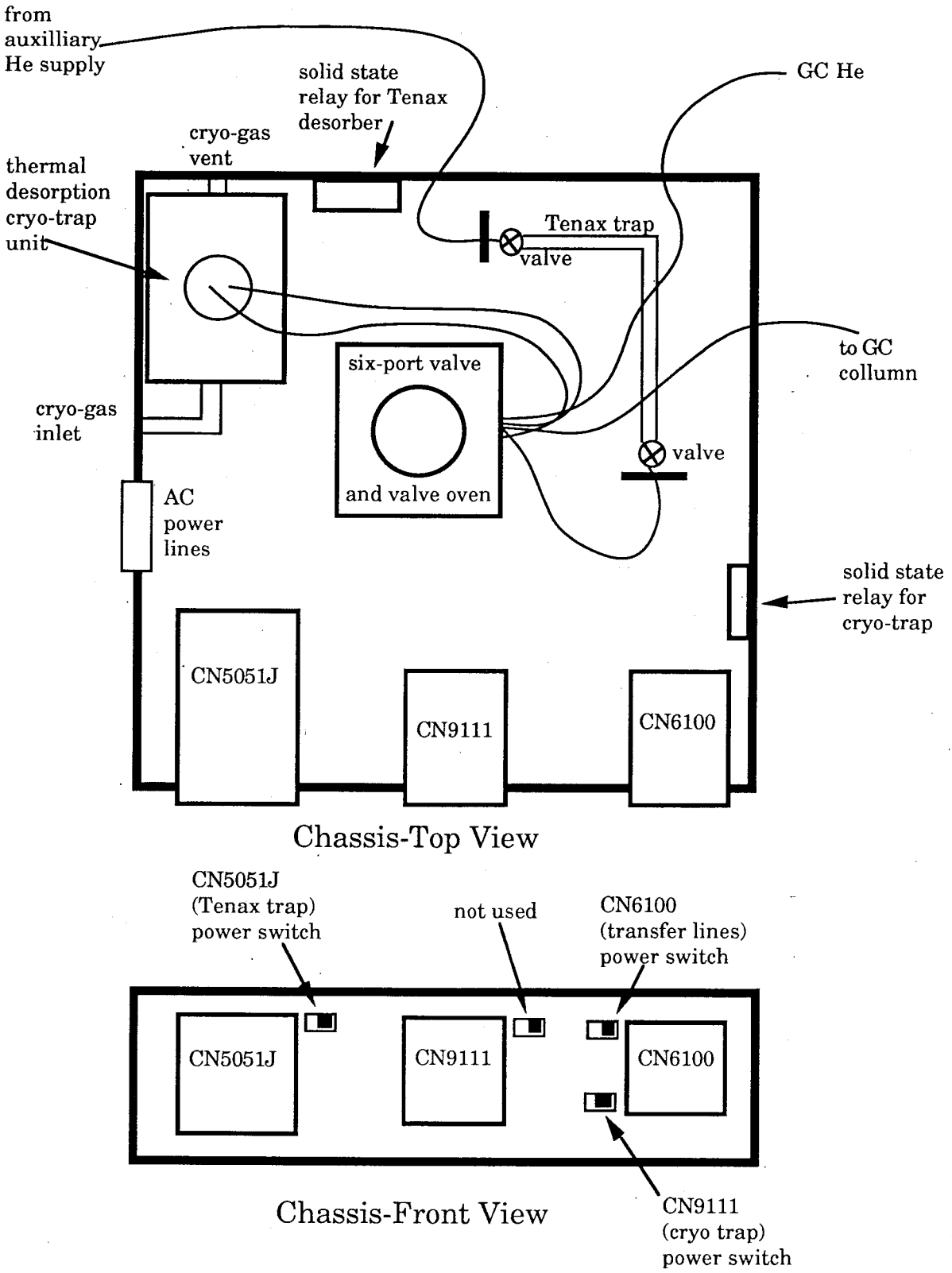


Fig. A2.1. Cryo-trap Thermal Desorption Unit top and front views.

The circuit diagram for the external wiring and modifications is shown in (Fig. A2.2).

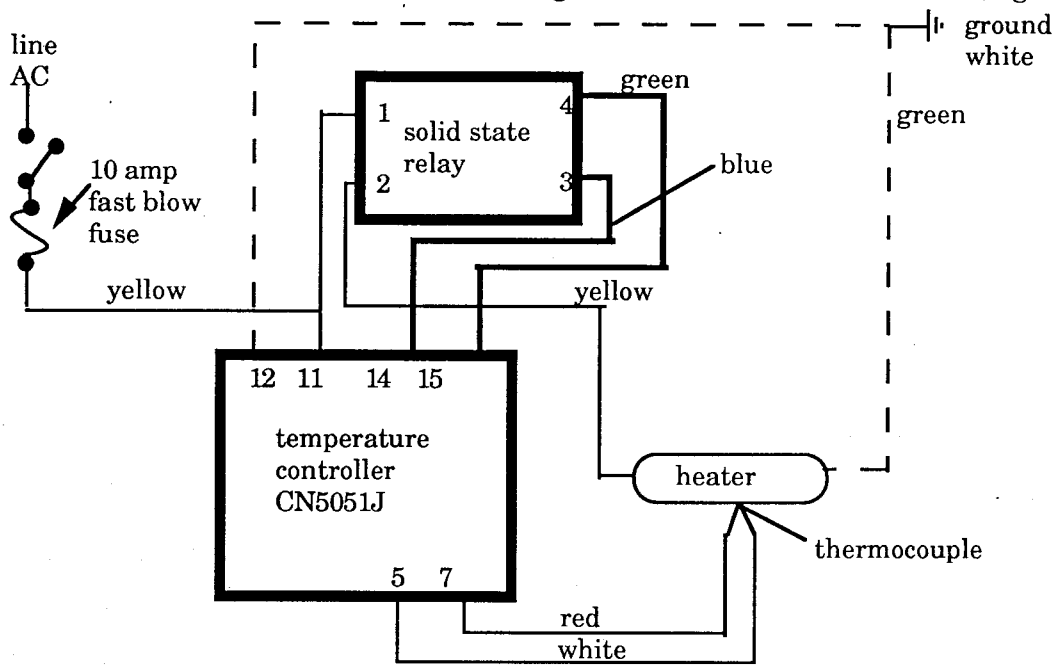


Wiring diagram for CN5051J

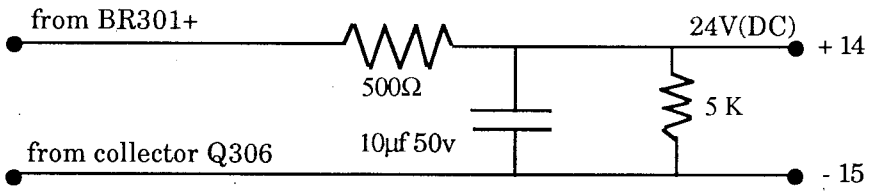


Modification diagram for CN5051J:
mechanical relay in temperature controller has been removed from circuit

Fig. A2.3. External wiring and modification circuit for CN5051J.

Thermocouples for CN5051J, as well as CN6100 and CM9111 were made by spot-welding type K thermocouple wire.

The cryo-trap consists of a 1/16" nickel tube wound around a 200 watt cartridge heater; 3/8" diameter by 1 1/4" long, ceramic core and inconel sheath (Omega Engineering), housed in a silver-soldered brass container with Teflon top, plumbed to the liquid nitrogen dewar. The heater is controlled by a CN9111 temperature controller (Omega Engineering), and must be switched on and off with the labeled switch on the front plate of the chassis; see diagram 1. The controller is wired to the solid-state relay on the right side of the chassis, and then to the cartridge heater (see Fig. A2.3 for circuits).

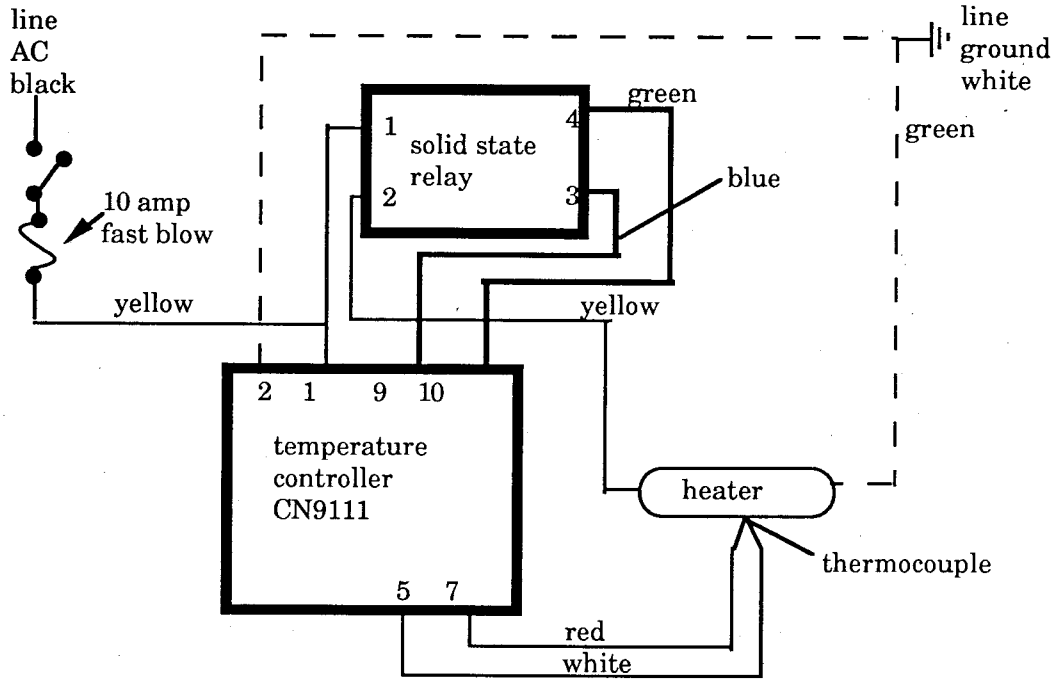


Wiring diagram for CN9111

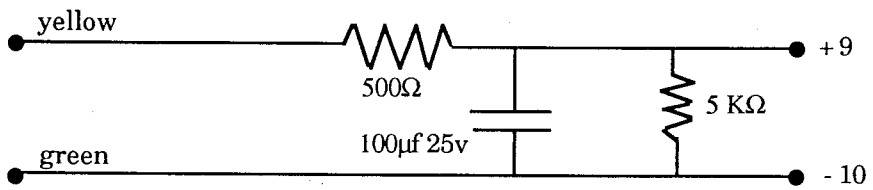


Filter capacitor diagram for CN9111:
trace to mechanical relay cut

Fig. A2.1. External wiring and modification circuit for CN9111.

The brass housing, surrounded by insulation, is cooled by venting gas from an external liquid nitrogen tank. The cooling of the cryo-trap is accomplished by switching a solenoid valve on the liquid nitrogen tank by hand.

Transfer lines connecting the six-port valve, the Tenax trap, and cryo-trap, and the GC are wound with several 100 watt heating cords in series, and maintained at about 80 C with a CN6100 controller (Omega Engineering). The connection from the 1/16" nickel transfer line is made directly from the sampling valve to the GC column with a Valco connector.

Samples, once collected, are introduced to the GC as follows. The sample tube is ramped to 220 C over a period of 3 minutes, and held at 220 C for 2 minutes. This is accomplished by setting JN5051J to 220 C, and switching it on. An auxiliary helium stream carries the desorbing compounds into the cryo-cooled trap (maintained at -120 C). Meanwhile the GC carrier gas (He) is shunted directly into the GC. Once Tenax desorption is complete, the valve is switched so that the carrier gas flows through the cryo-trap and then into the GC. The auxiliary flow is used to further desorb the tenax tube at 250 C for 3 minutes, and allow it to slowly cool, cleaning it for the next use. The cryo-trap is then heated to about 150 C in about 45 seconds, and the trapped compounds are swept onto the GC column. It was found that further focussing was necessary, and this was accomplished by submerging a loop of the column in a cup of liquid nitrogen while the cryo-trap-collumn transfer was taking place. Finally, the column is removed from the liquid nitrogen, and the GC temperature program commenced. This desorber design, while in some ways cumbersome, has several advantages. It allows for a large capacity tenax trap by decoupling the column flow requirements from the tenax desorption requirements, and the external valve on the sample tubes allow easy manipulation of the samples without concern of contamination. Finally, the instrument was built for a fraction of the cost of a commercial desorber.

GCMS (Hewlett Packard model 5980 with mass selective detector) and GC/FID (Hewlett Packard model 5890) analyses were carried out on separate instruments, both equipped with 30m x 0.25mm DB-5 (J&W Scientific) columns. The GCMS was set up to alternately run liquid-phase samples in addition to the gas-phase samples described here, requiring that two columns by plumbed together into the detector. This was accomplished by connecting the two columns 6" upstream of the inlet with a pressfit Y-connector (Unimetrics Co.). The pressfit connector lead to a slight increase in background gasses ($O_2$, $N_2$, Ar, $CO_2$) detected in the GCMS.

# APPENDIX 3

# GC/FID and GC/MS Chromatograms and Mass Spectra

This section contains a series of chromatograms and mass spectra selected from the more than 2000 chromatograms and spectra that support this thesis. They are organized into sections, listed below. Note that only GC/FID data were used for quantitative analyses.

Section 1: Isoprene GC/MS data. Figs. 1-20.

Section 2: Isoprene GC/MS spectral library. Figs. 21-27.

Section 3: 1-Octene GC/MS data. Figs. 28-56.

Section 4: 1-Octene GC/MS spectral library. Figs. 57-66.

Section 5: Isoprene GC/FID sample traces. Figs. 67-72.

Section 6: 1-Octene GC/FID sample traces. Figs. 73-78.

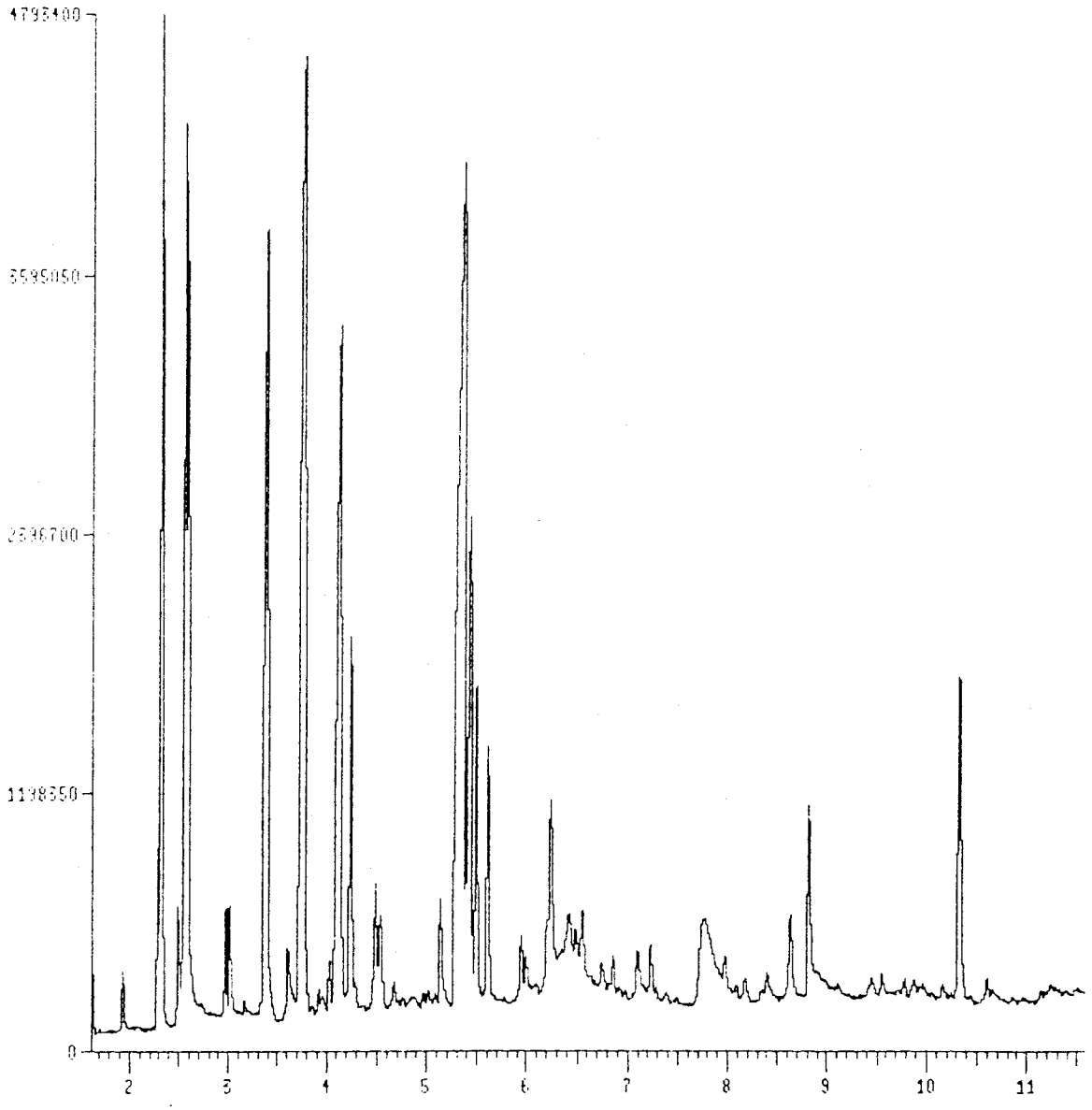


Figure A3.1. Total ion chromatogram from experiment INOXN16. Ordinate: relative units. Abscissa: retention time. Oxidants included $O_3$ , OH, and $O(^3P)$, hence this file contains the complete product spectrum. Order of elution of peaks corresponds to order in FID traces. Data file V3:SP24N16A.D. Mass spectra similarly identified correspond to this chromatogram.

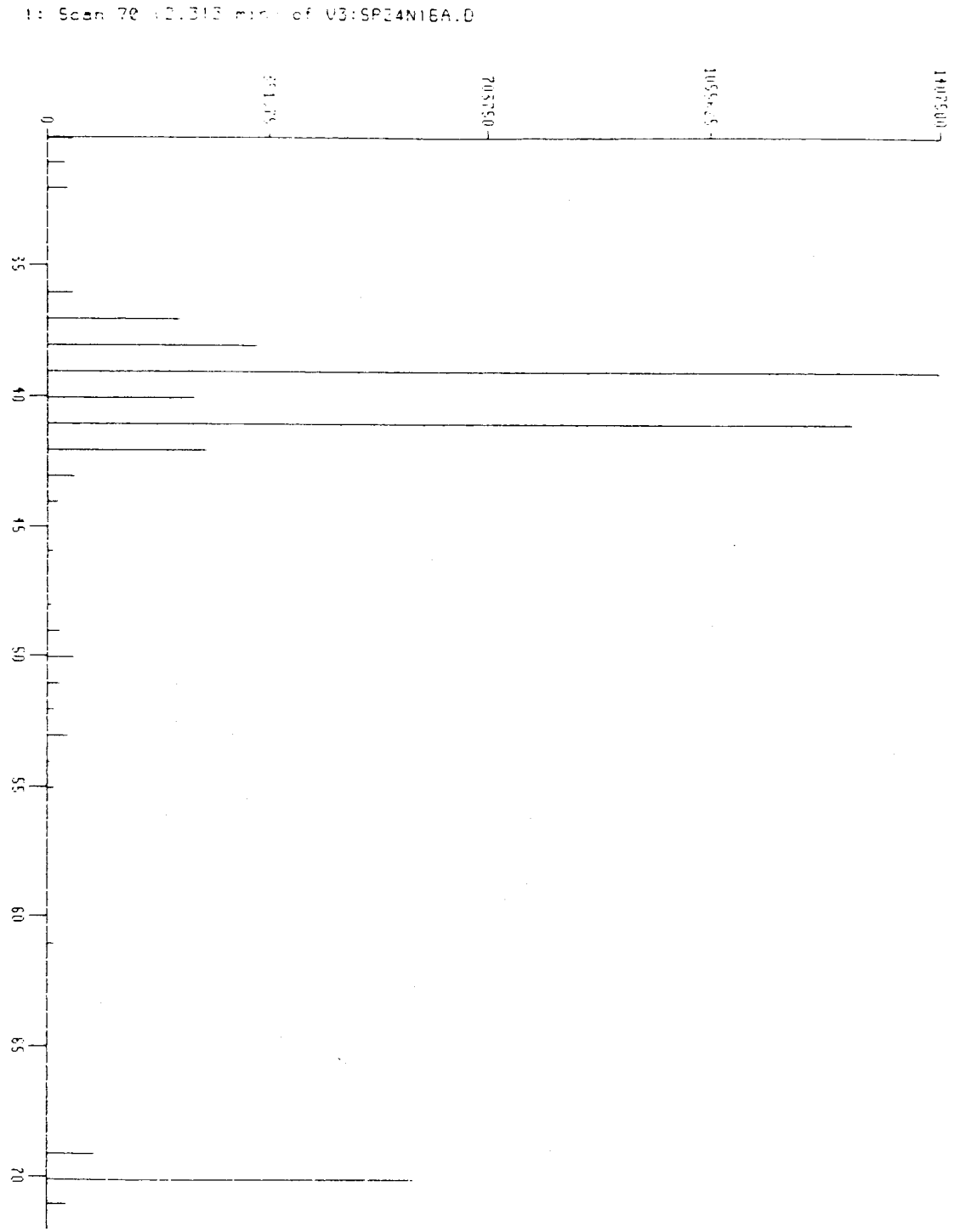


Figure A3.2. Ion current (ordinate) vs mass/charge (amu)(abscissa). File and retention time as indicated. Identified as methacrolein.

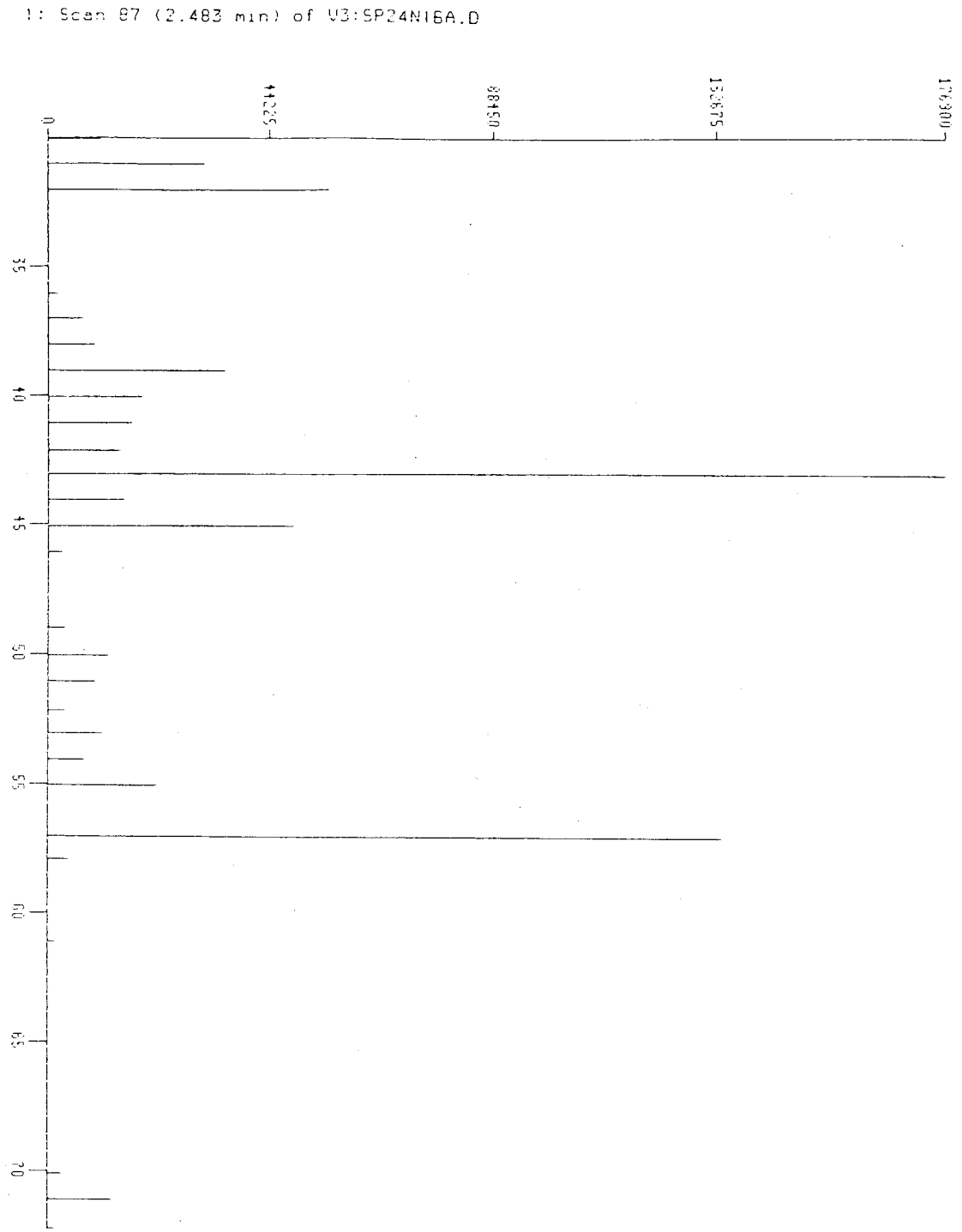


Figure A3.3. Ion current (ordinate) vs mass/charge (amu)(abscissa). File and retention time as indicated. Unidentified.

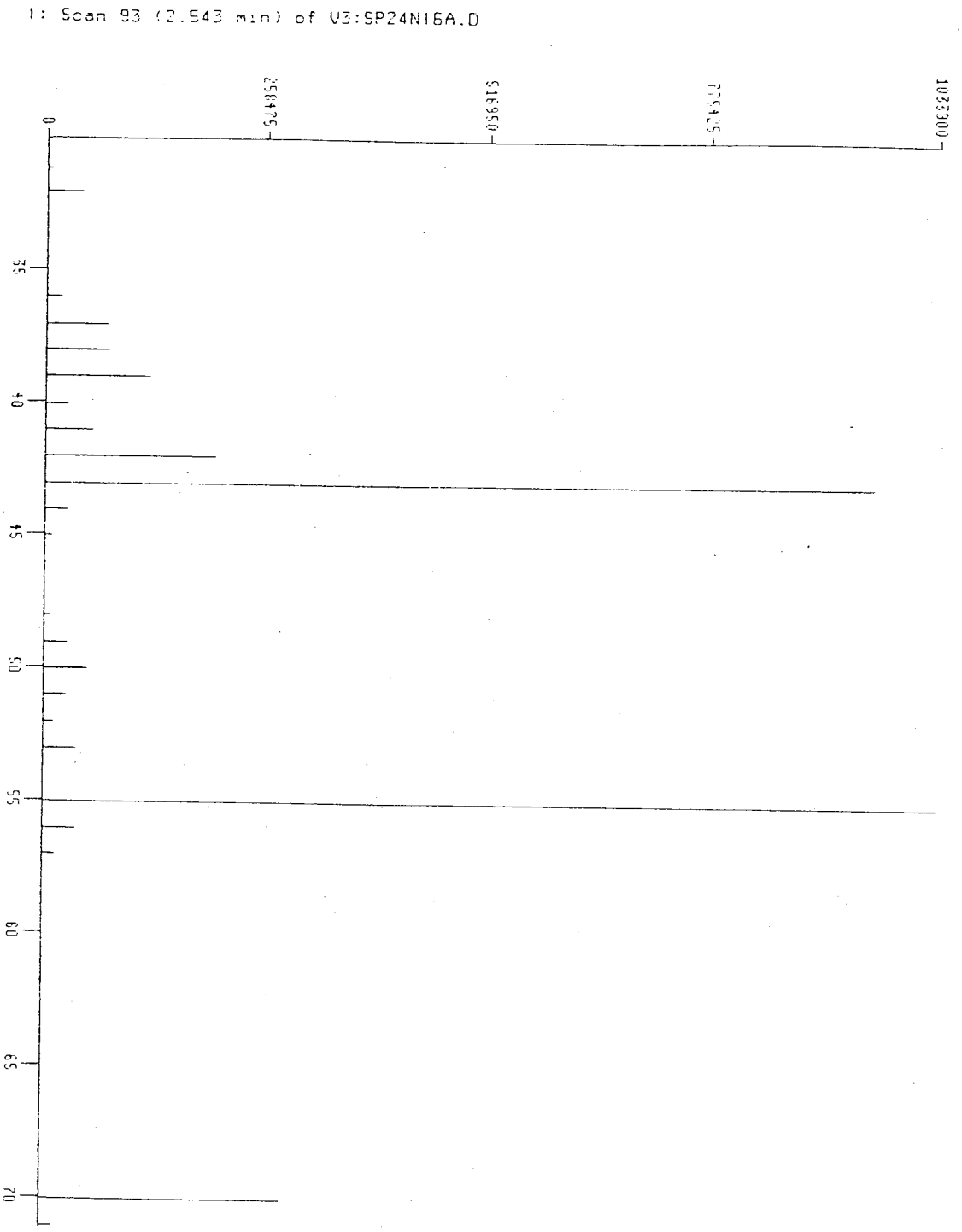


Figure A3.4. Ion current (ordinate) vs mass/charge (amu)(abscissa). File and retention time as indicated. Identified as methyl vinyl ketone.

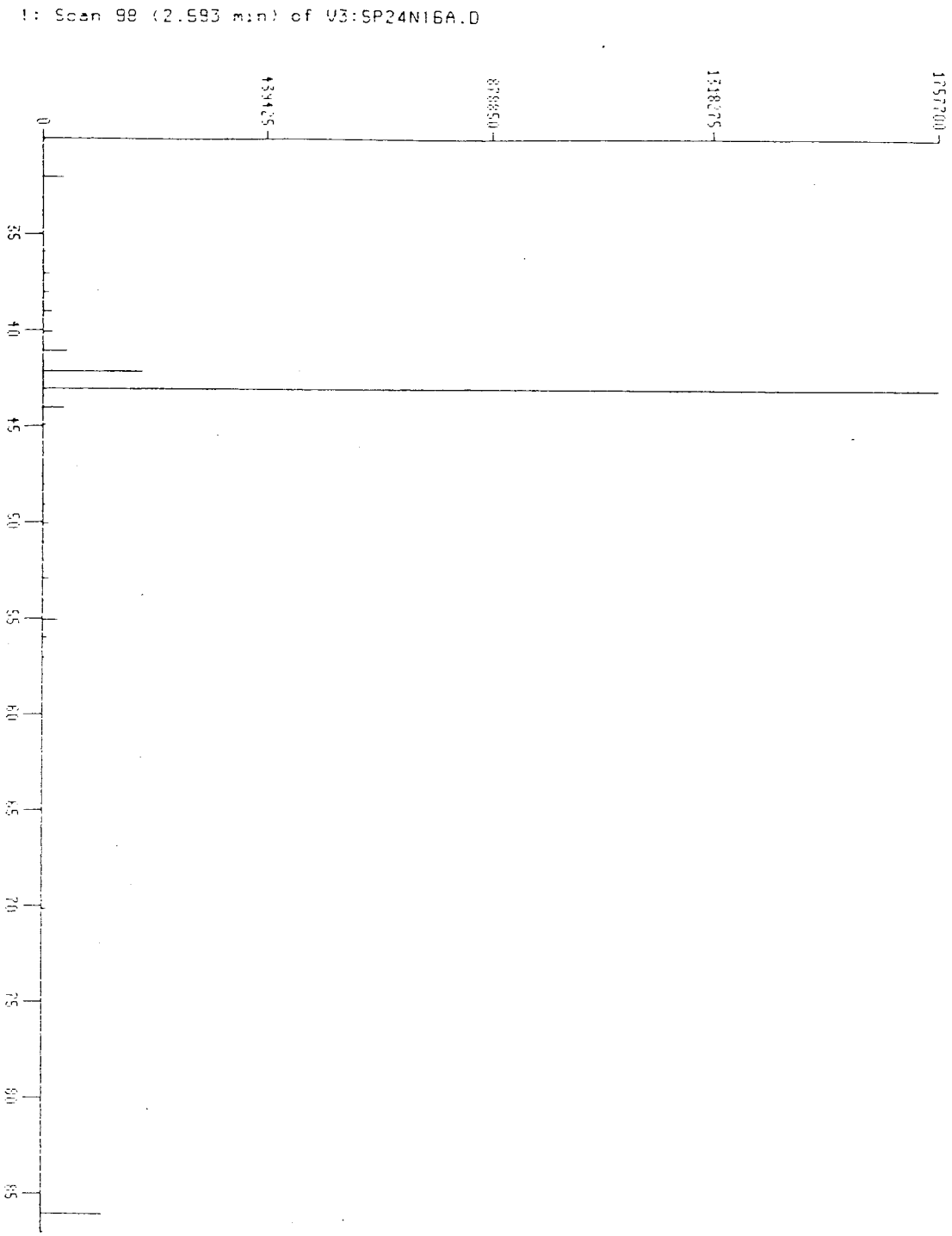


Figure A3.5. Ion current (ordinate) vs mass/charge (amu)(abscissa). File and retention time as indicated. Identified as biacetyl.

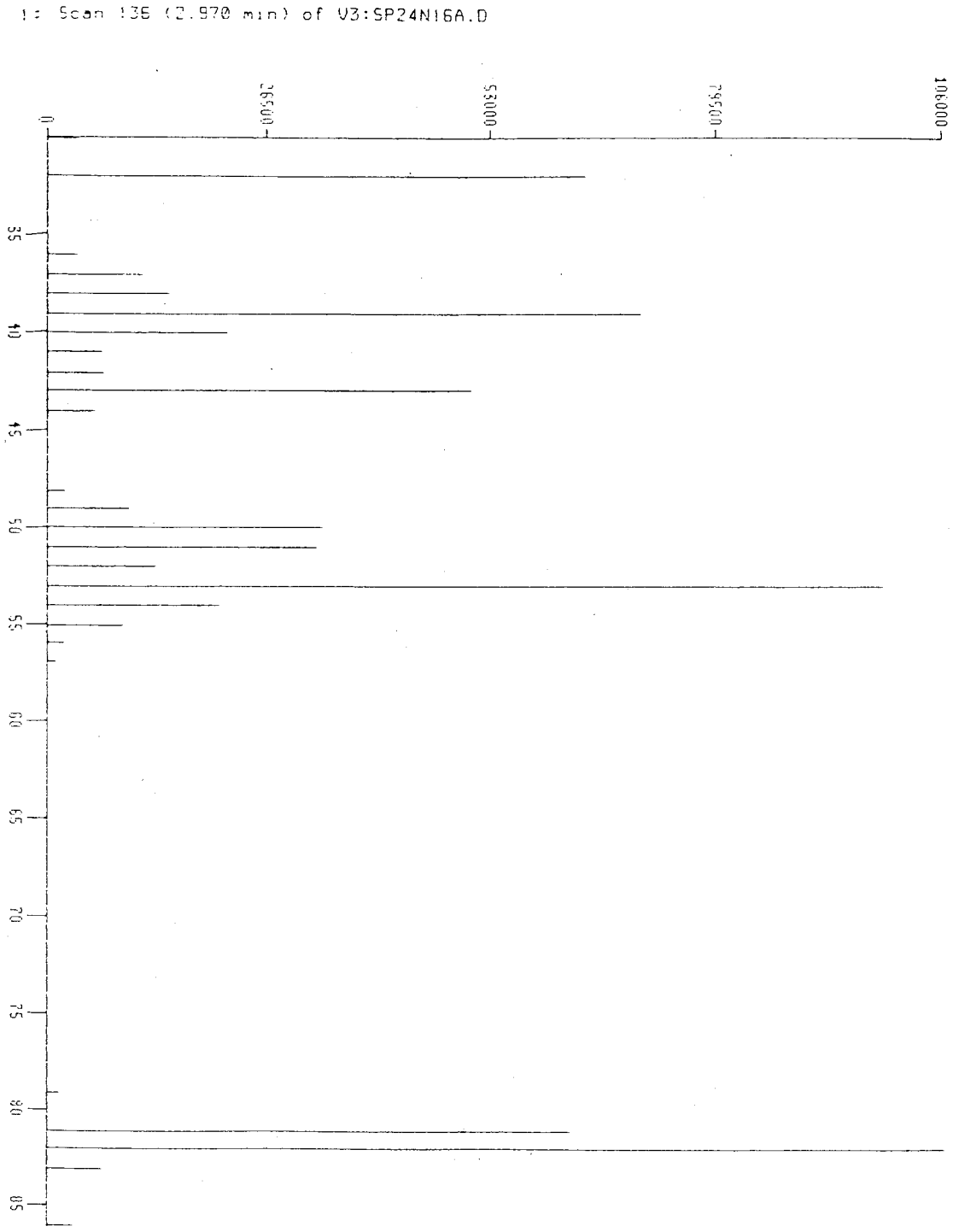


Figure A3.6. Ion current (ordinate) vs mass/charge (amu)(abscissa). File and retention time as indicated. Identified as 3-methyl furan.

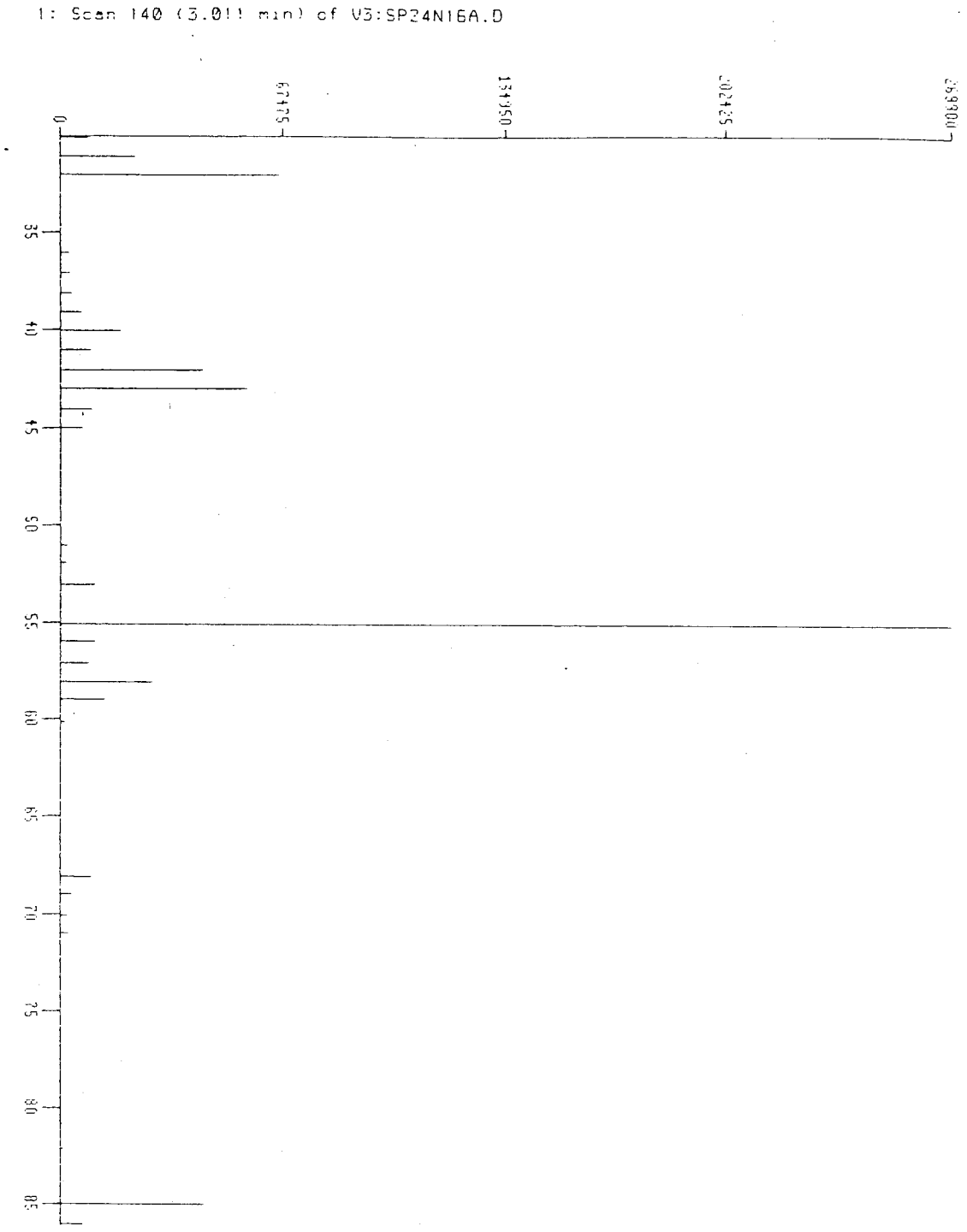


Figure A3.7. Ion current (ordinate) vs mass/charge (amu)(abscissa). File and retention time as indicated. Unidentified.

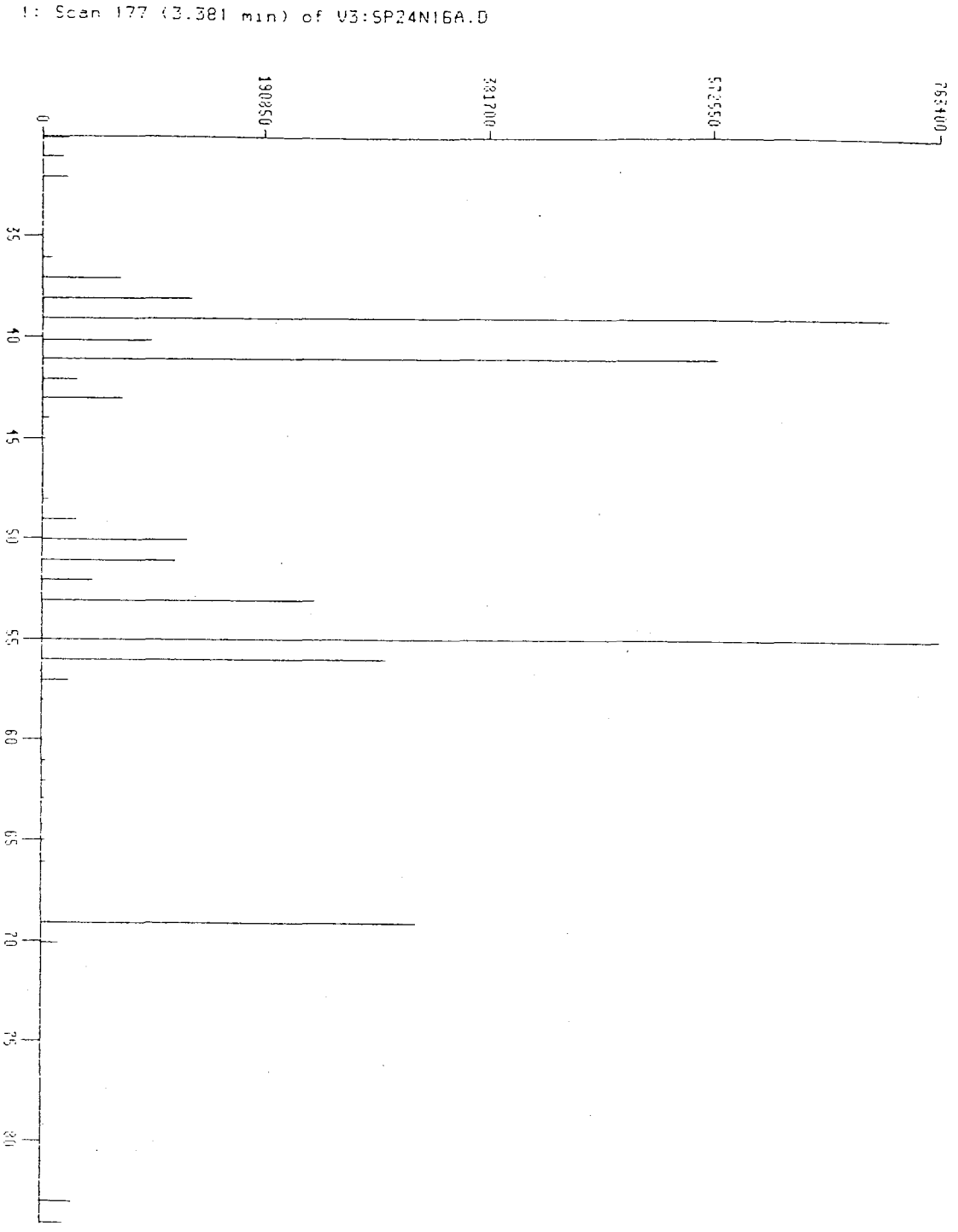


Figure A3.8. Ion current (ordinate) vs mass/charge (amu)(abscissa). File and retention time as indicated. Identified as 2-methyl 3-butene oxide.

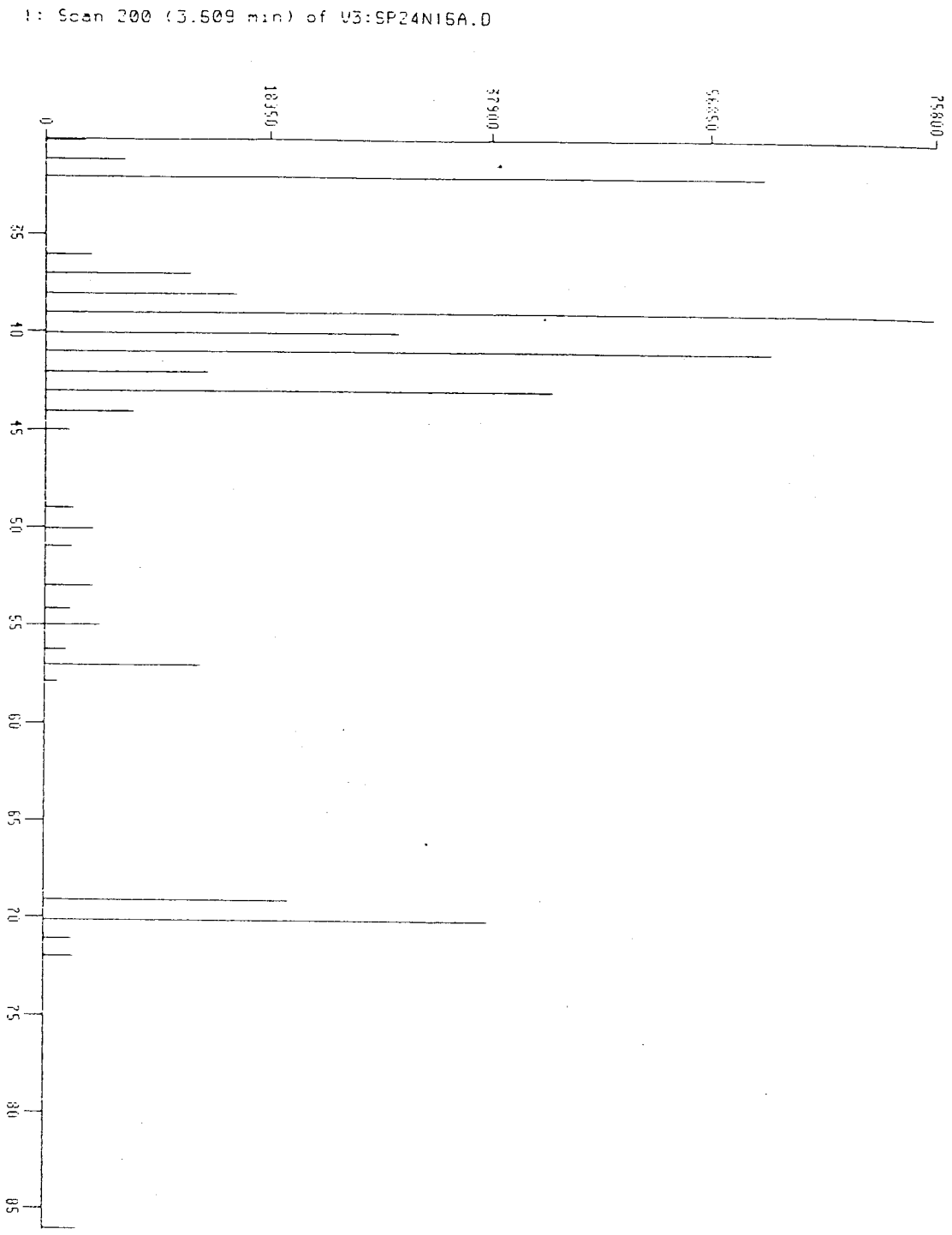


Figure A3.9. Ion current (ordinate) vs mass/charge (amu)(abscissa). File and retention time as indicated. Unidentified.

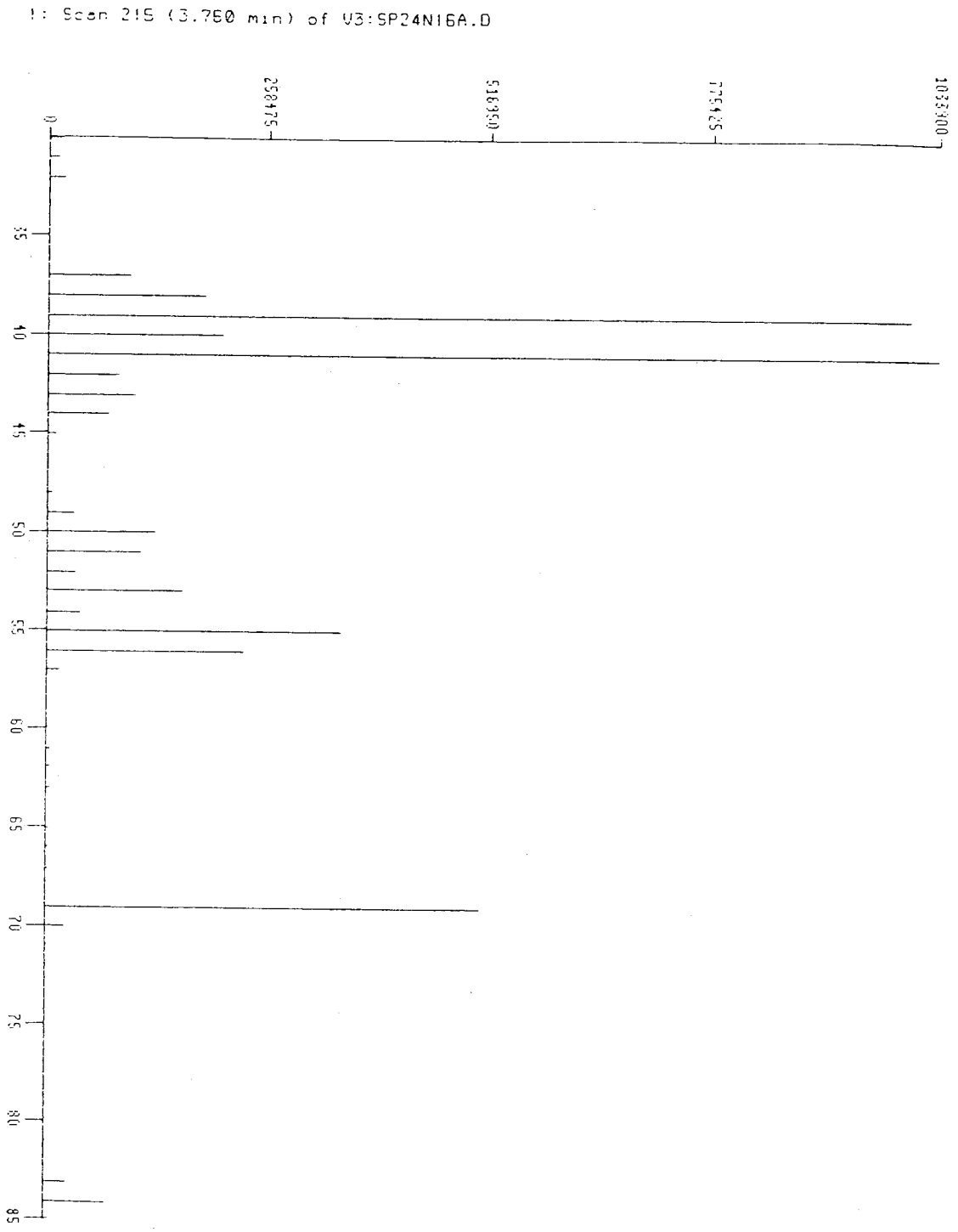


Figure A3.10. Ion current (ordinate) vs mass/charge (amu)(abscissa). File and retention time as indicated. Identified as 3,3-methyl butene oxide.

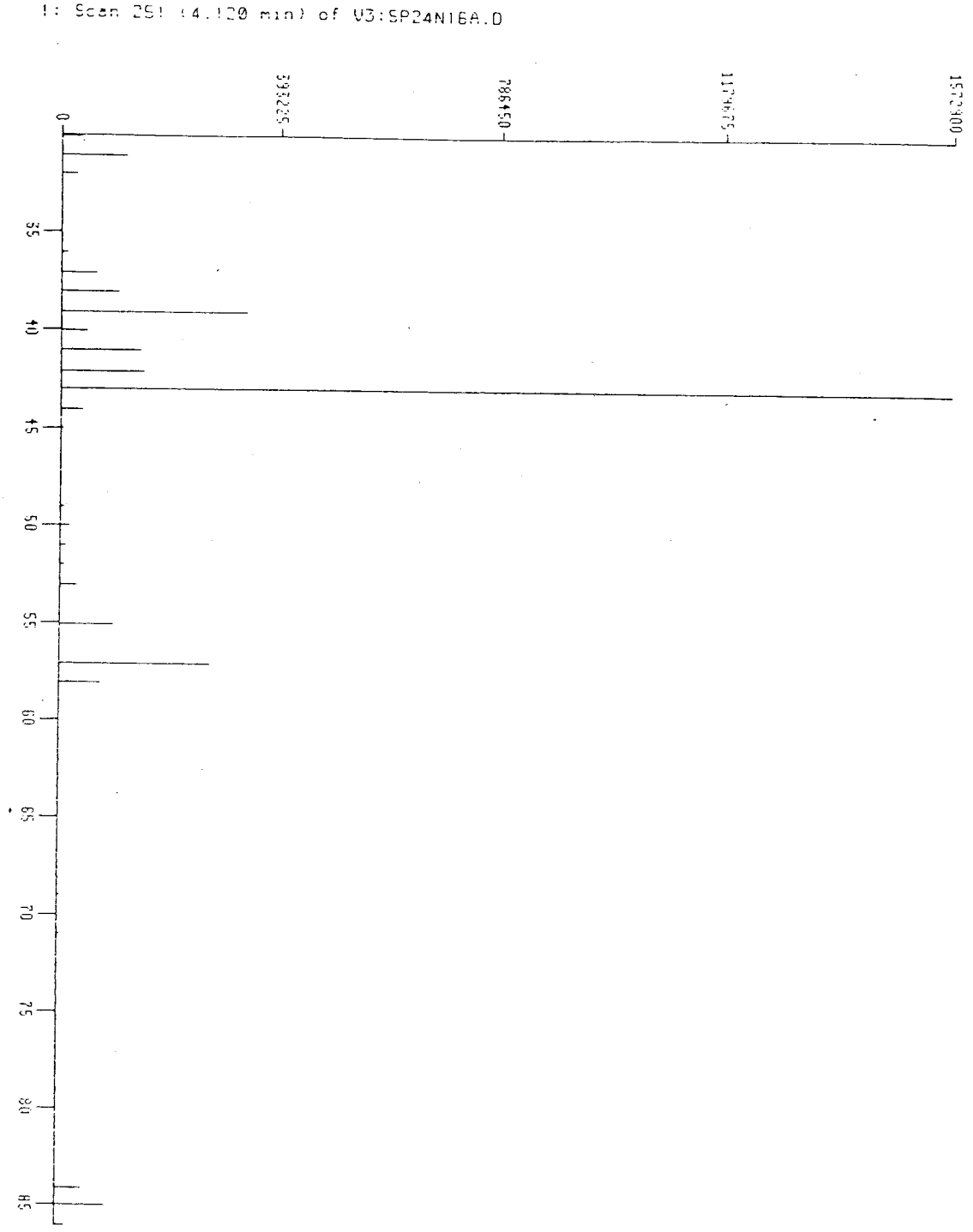


Figure A3.11. Ion current (ordinate) vs mass/charge (amu)(abscissa). File and retention time as indicated. Unidentified.

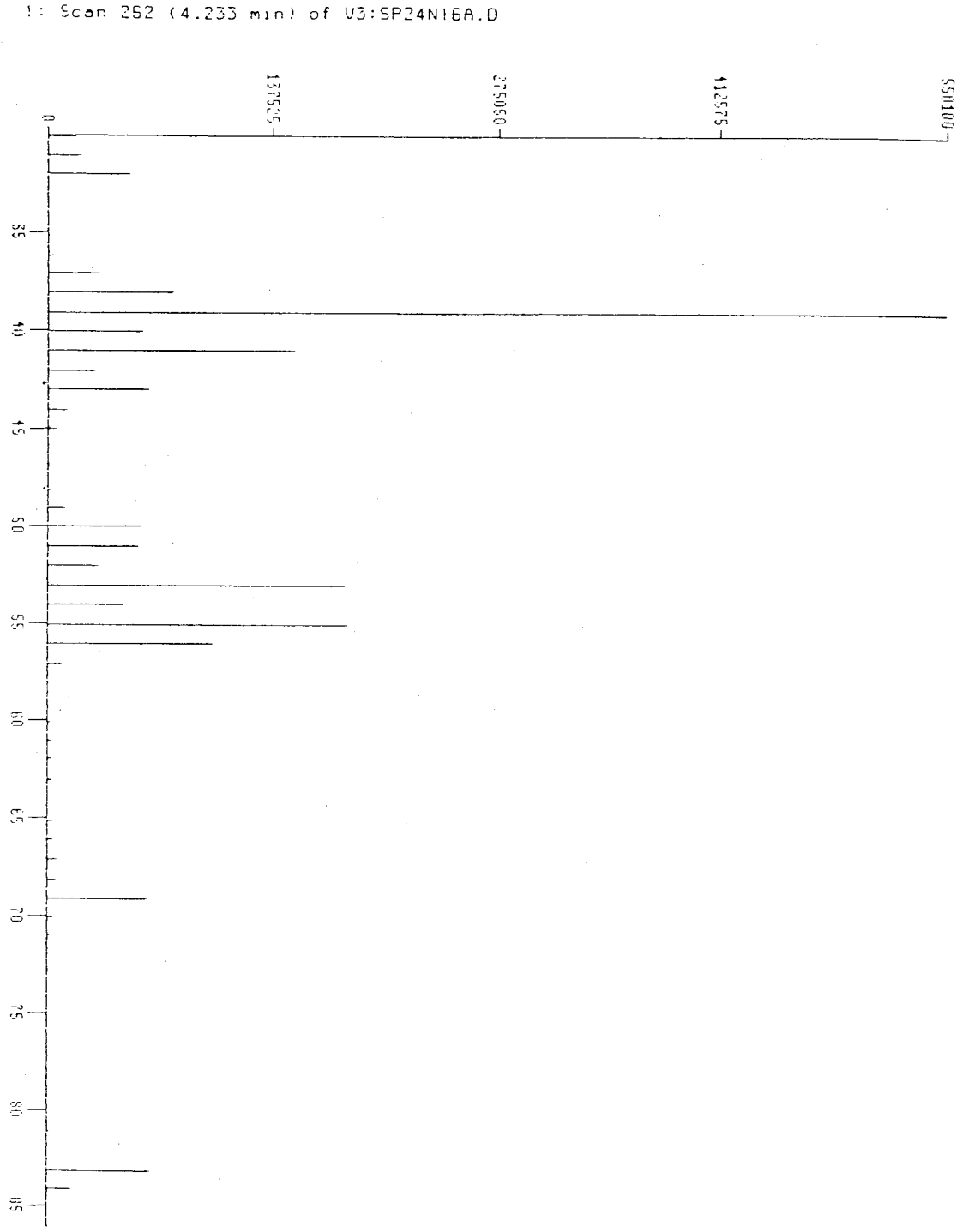


Figure A3.12. Ion current (ordinate) vs mass/charge (amu)(abscissa). File and retention time as indicated. Unidentified.

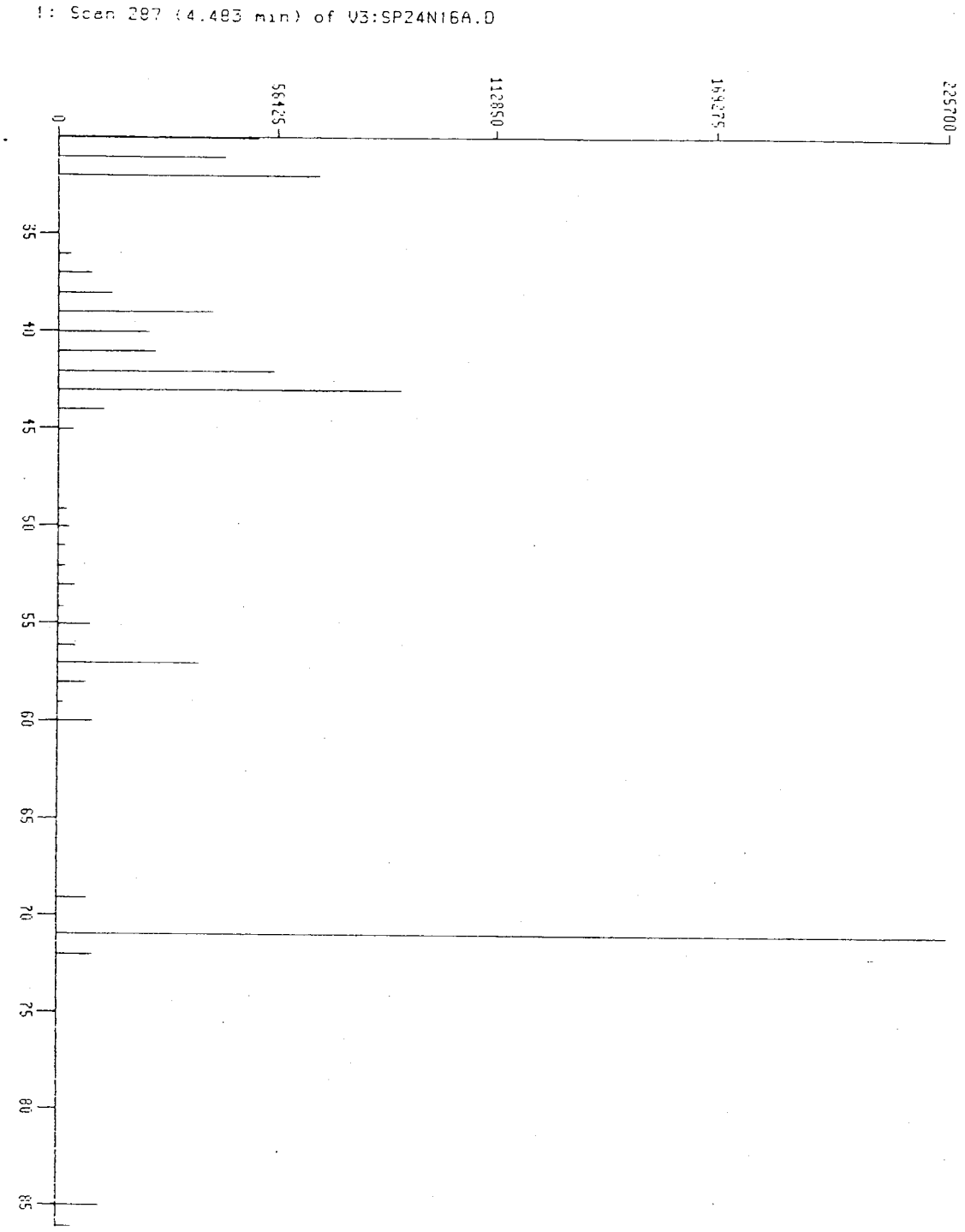


Figure A3.13. Ion current (ordinate) vs mass/charge (amu)(abscissa). File and retention time as indicated. Unidentified.

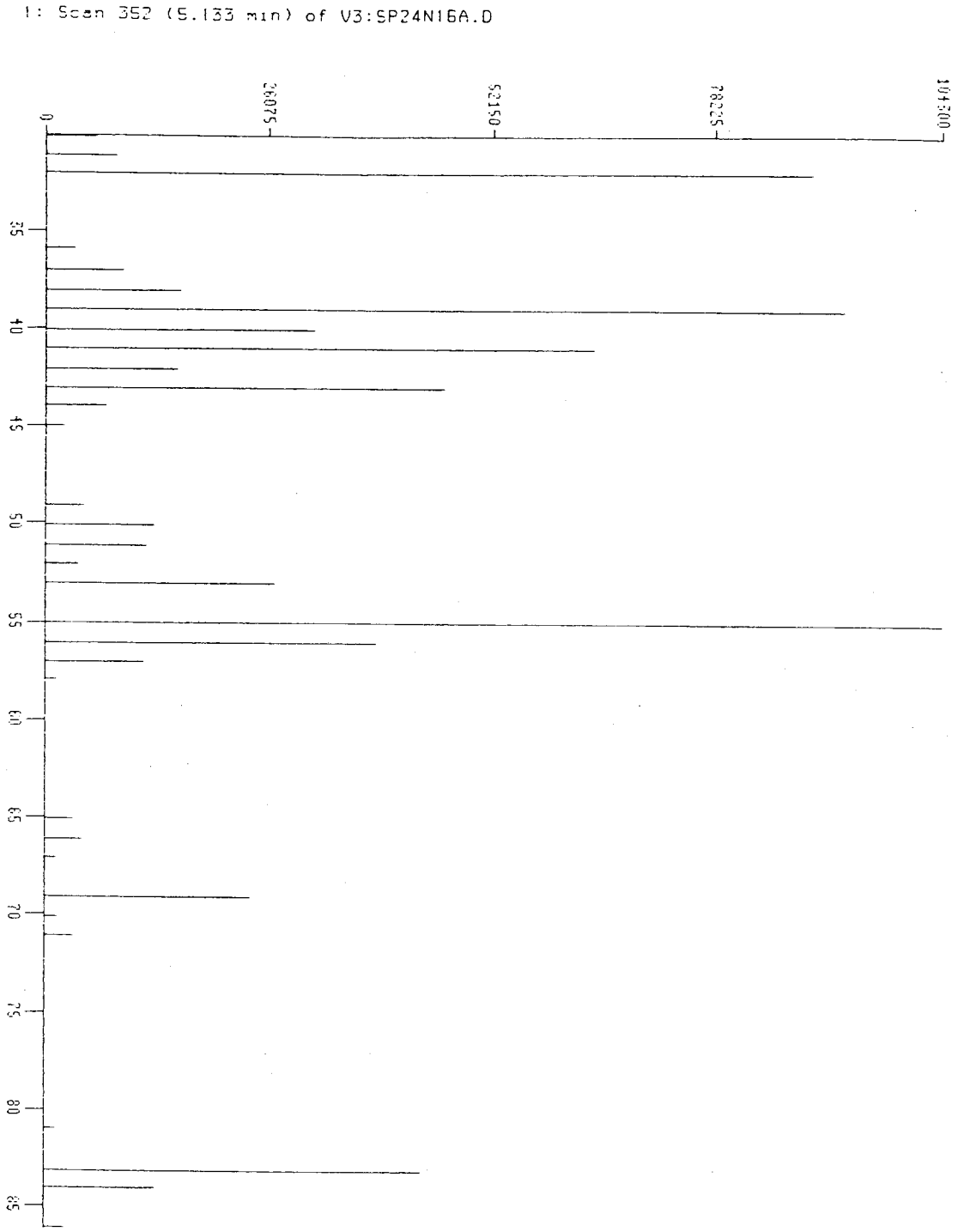


Figure A3.14. Ion current (ordinate) vs mass/charge (amu)(abscissa). File and retention time as indicated. Unidentified.

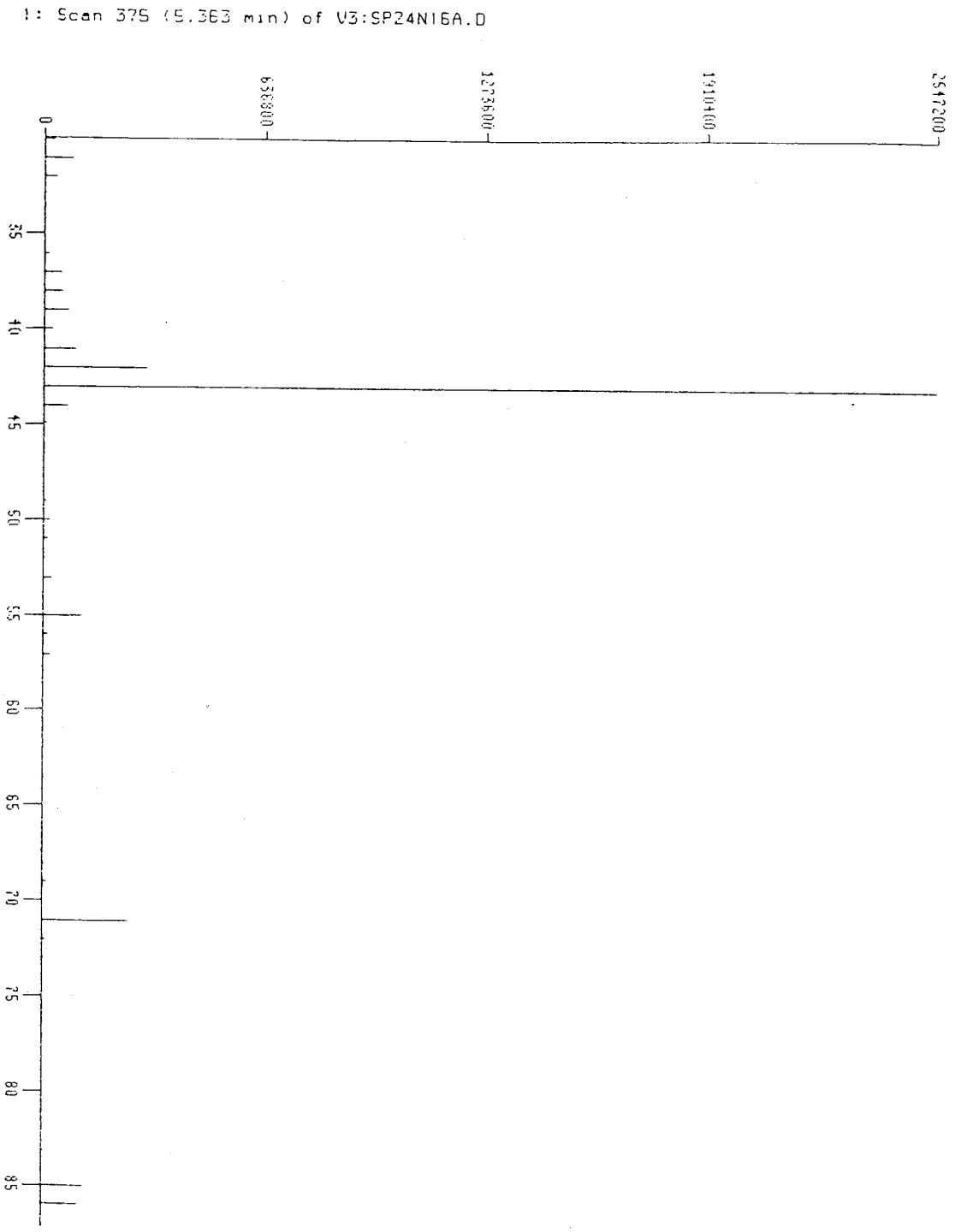


Figure A3.15. Ion current (ordinate) vs mass/charge (amu)(abscissa). File and retention time as indicated. Unidentified.

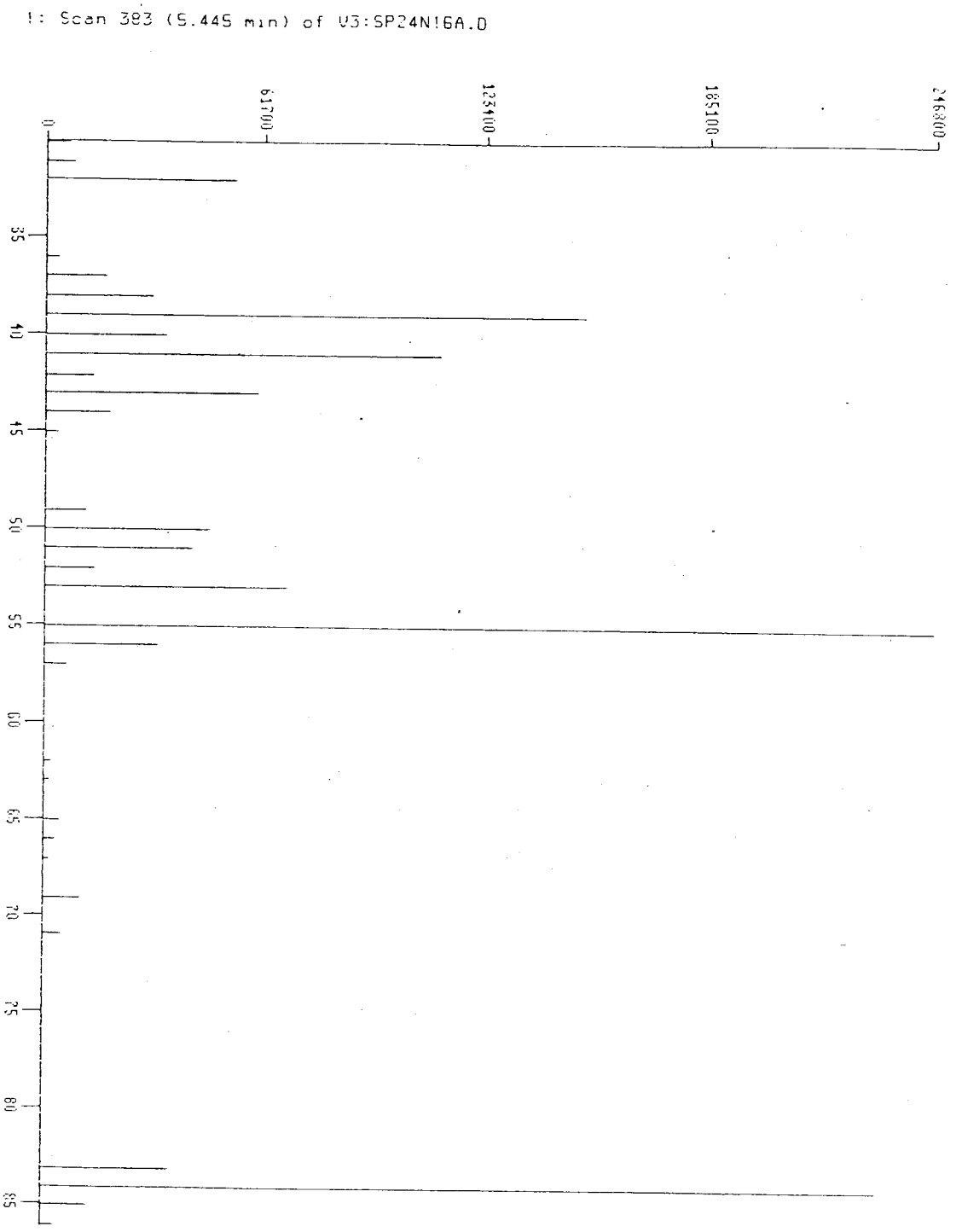


Figure A3.16. Ion current (ordinate) vs mass/charge (amu)(abscissa). File and retention time as indicated. Unidentified.

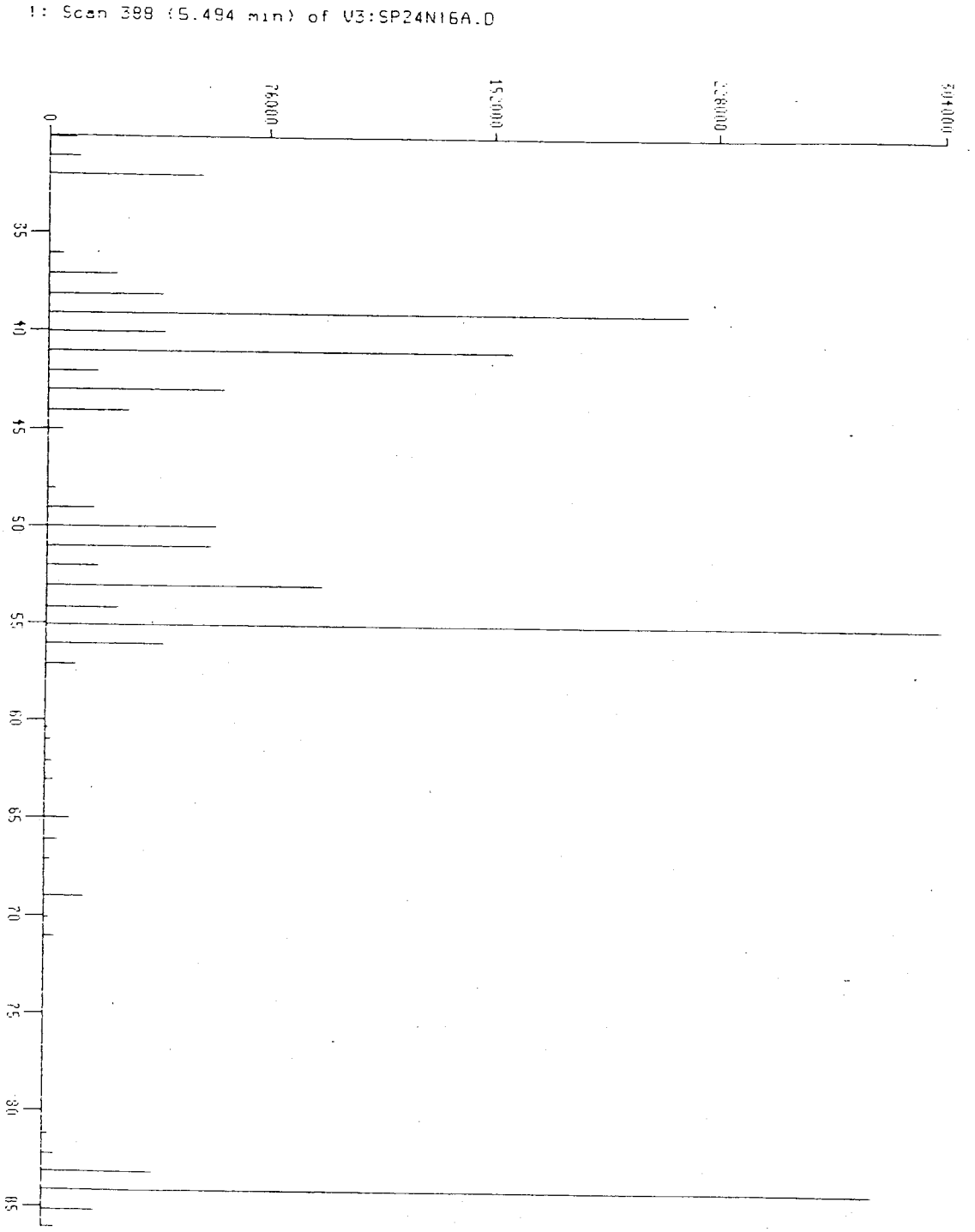


Figure A3.17. Ion current (ordinate) vs mass/charge (amu)(abscissa). File and retention time as indicated. Identified as 2-methyl 2-butenal.

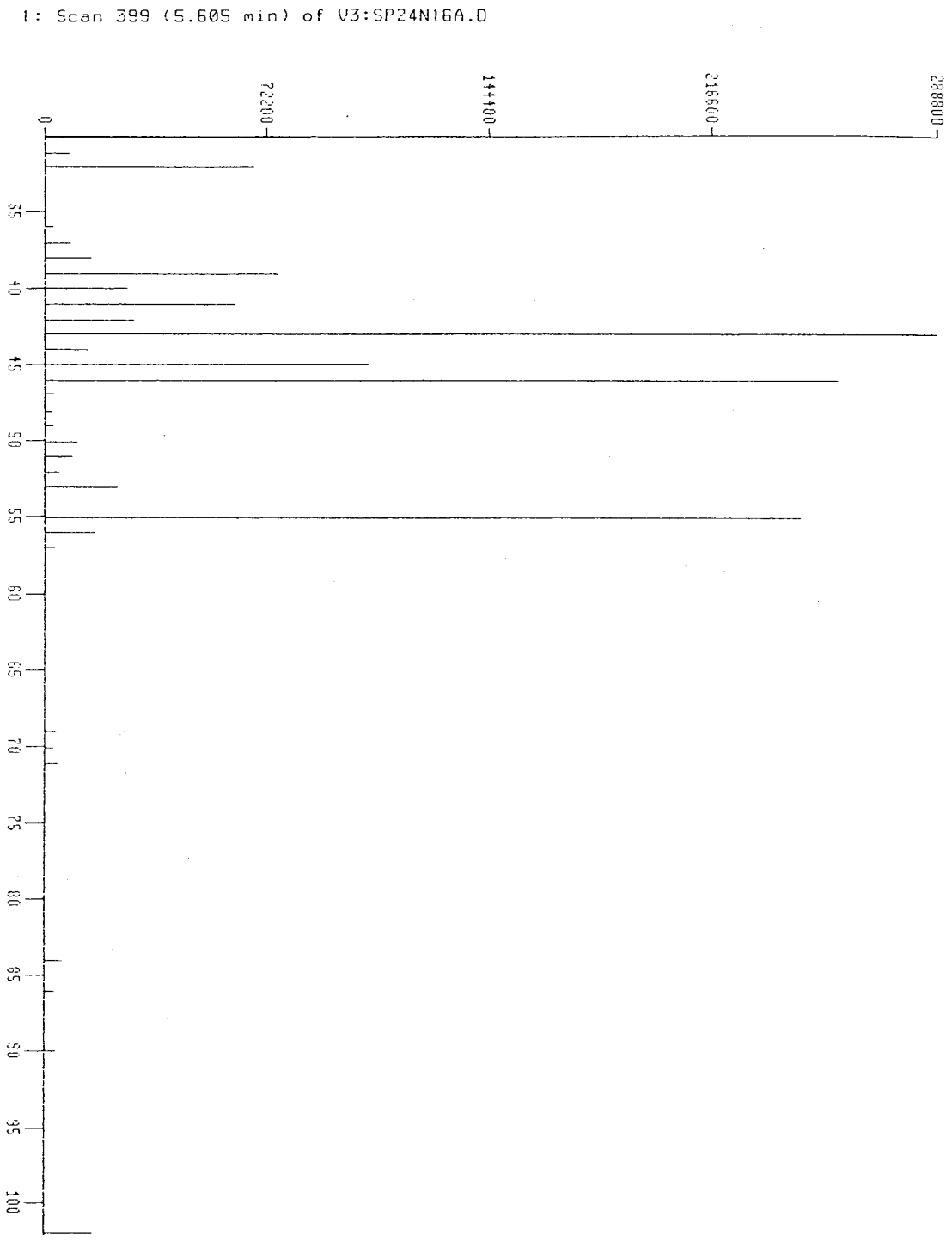


Figure A3.18. Ion current (ordinate) vs mass/charge (amu)(abscissa). File and retention time as indicated. Unidentified; probable nitrate compound.

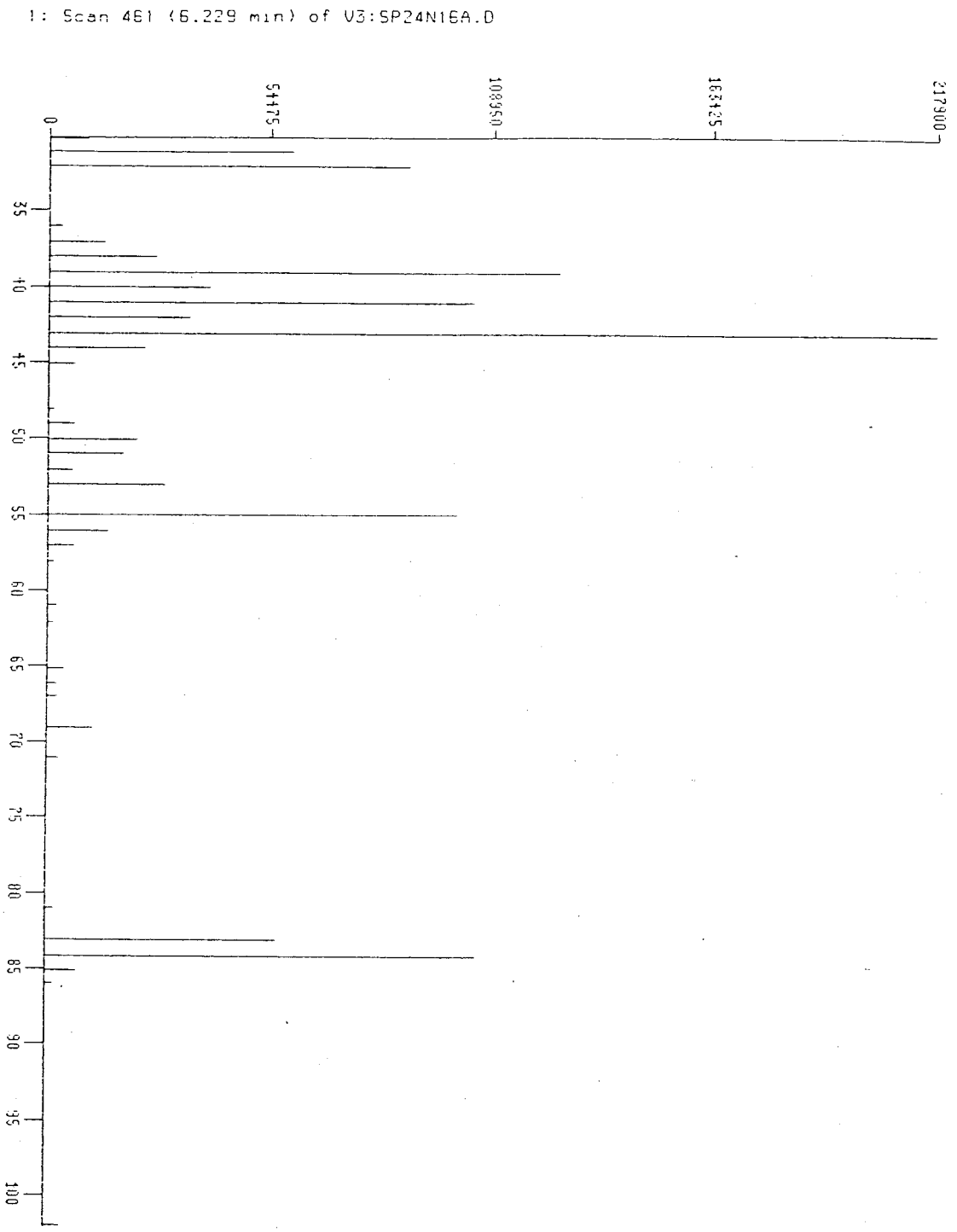


Figure A3.19. Ion current (ordinate) vs mass/charge (amu)(abscissa). File and retention time as indicated. Unidentified.

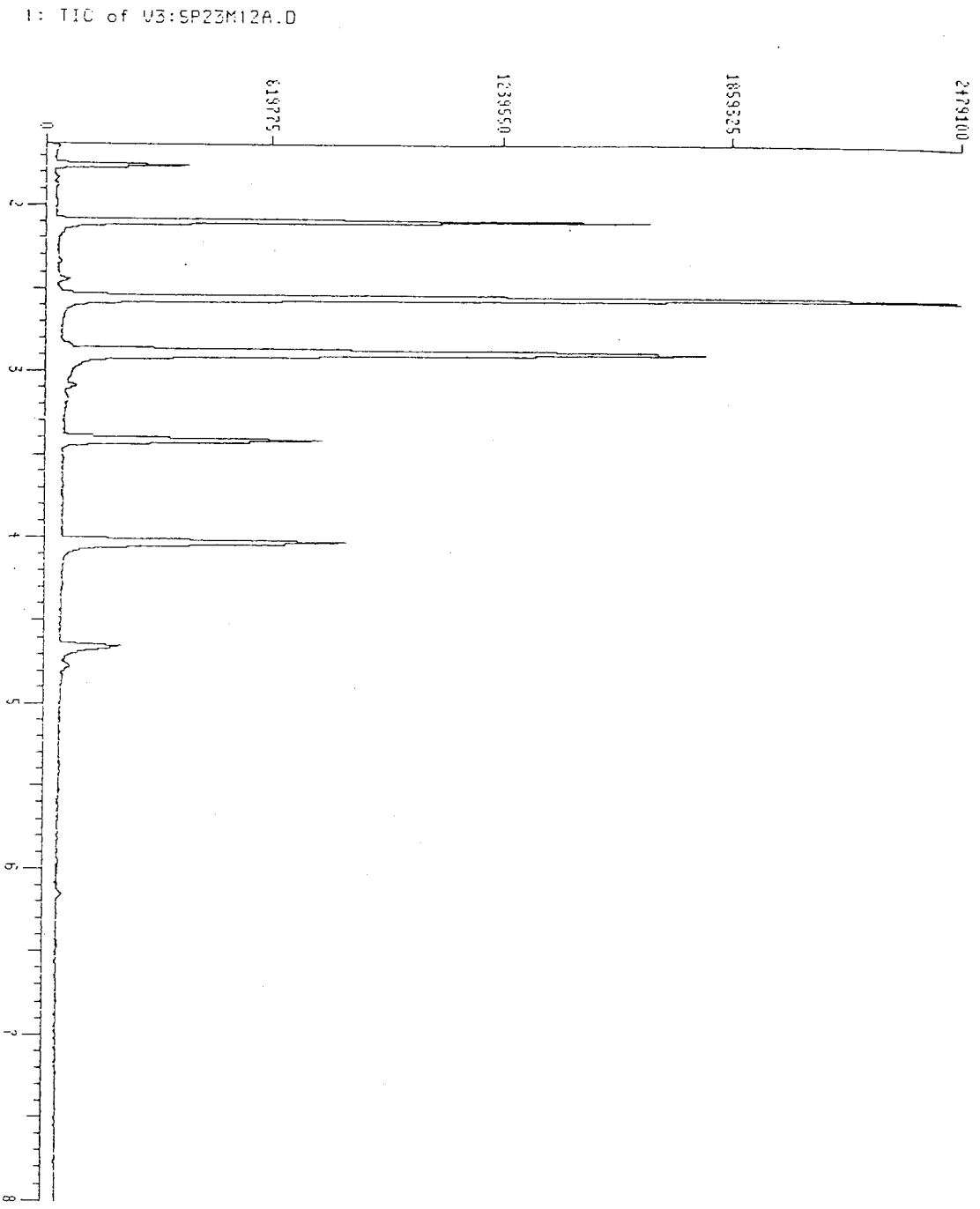


Figure A3.20. Total ion chromatogram from experiment IOH5. Ordinate: relative units. Abscissa: retention time. This is a typical chromatogram. Peaks (beginning with 2.6 mins.) are methacrolein, methyl vinyl ketone, 3-methyl furan (small peak), 2-methyl 3-butene oxide, and 3,3-methyl butene oxide. First two peaks are air. This sample was run 7 months after sample featured in Fig. 1; note that retention times are reproducible.

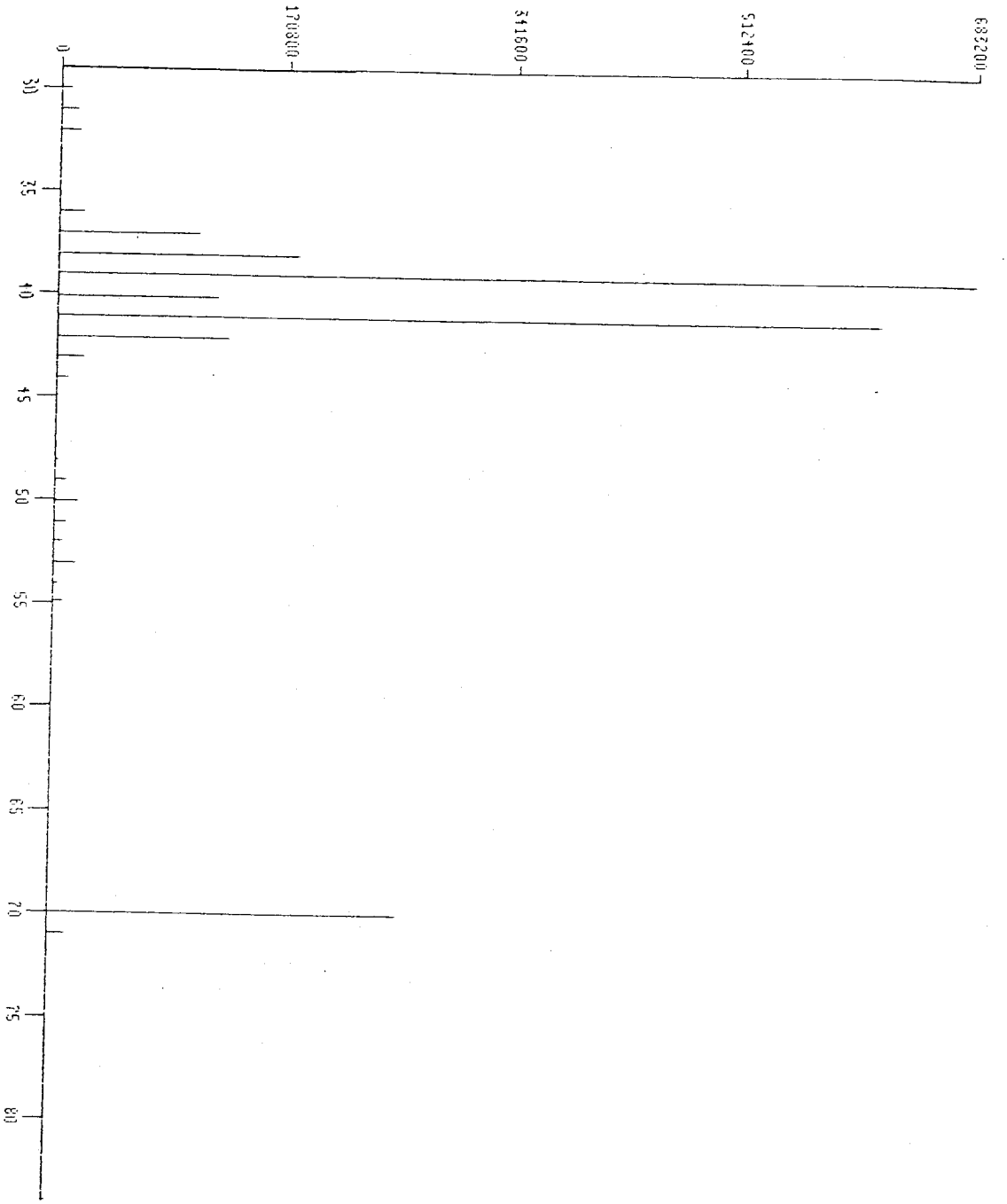


Figure A3.21. Ion current (ordinate) vs mass/charge (amu)(abscissa). Isoprene reference spectrum: methacrolein (standard obtained from Aldrich).

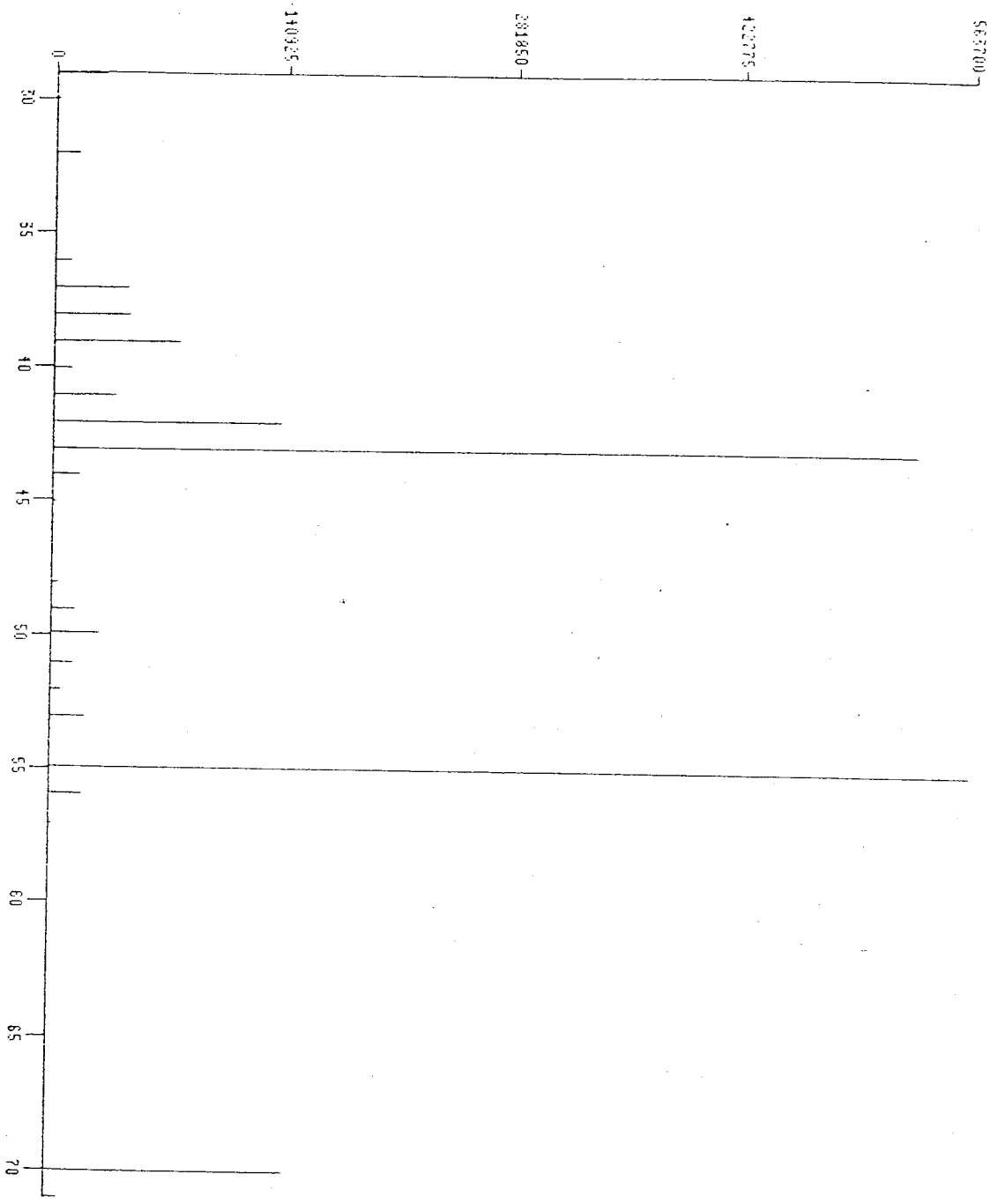


Figure A3.22. Ion current (ordinate) vs mass/charge (amu)(abscissa). Isoprene reference spectrum: methyl vinyl ketone (standard obtained from Aldrich).

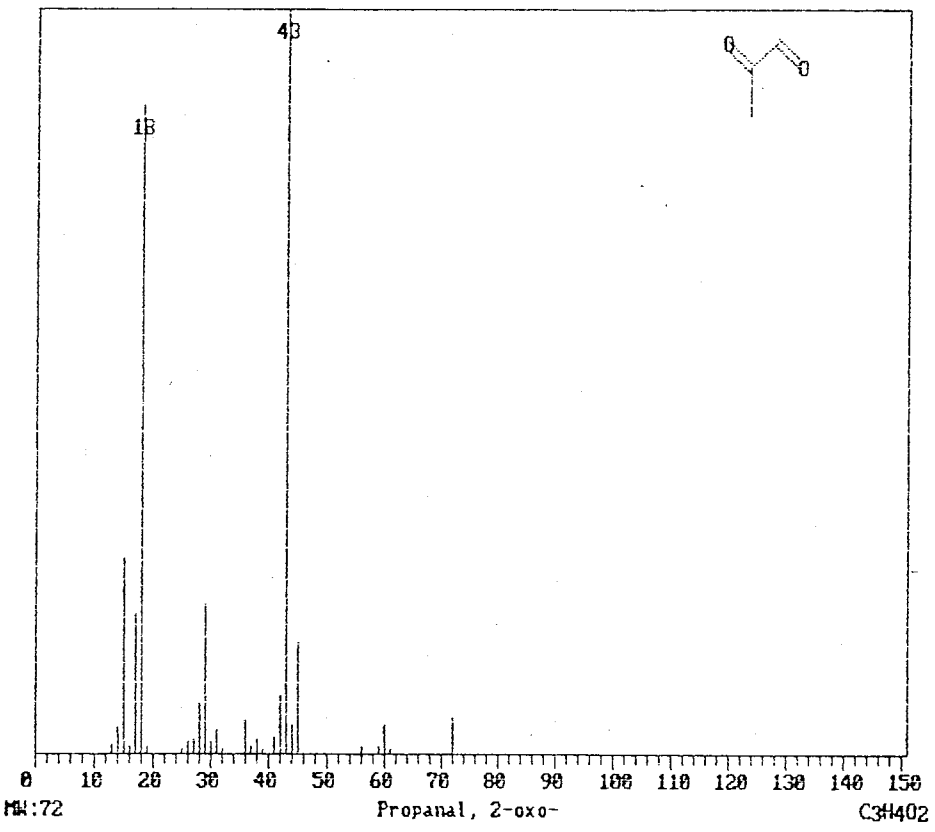


Figure A3.23. Ion current (ordinate) vs mass/charge (amu)(abscissa). Isoprene reference spectrum: methyl glyoxal from National Institute of Standards and Technology Mass Spectral Library (1990).

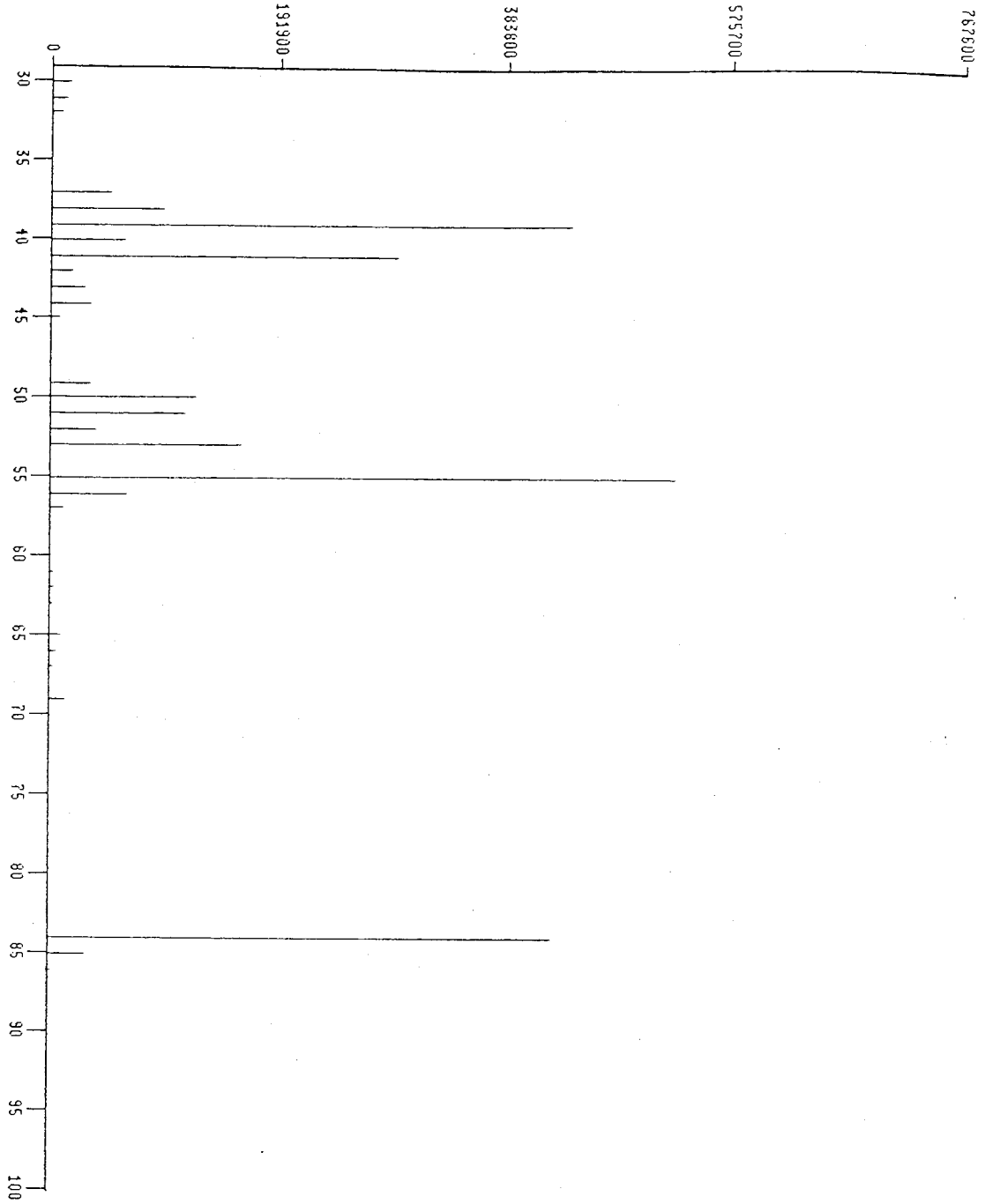


Figure A3.24. Ion current (ordinate) vs mass/charge (amu) (abscissa). Isoprene reference spectrum: 2-methyl 2-butenal (standard obtained from Aldrich).

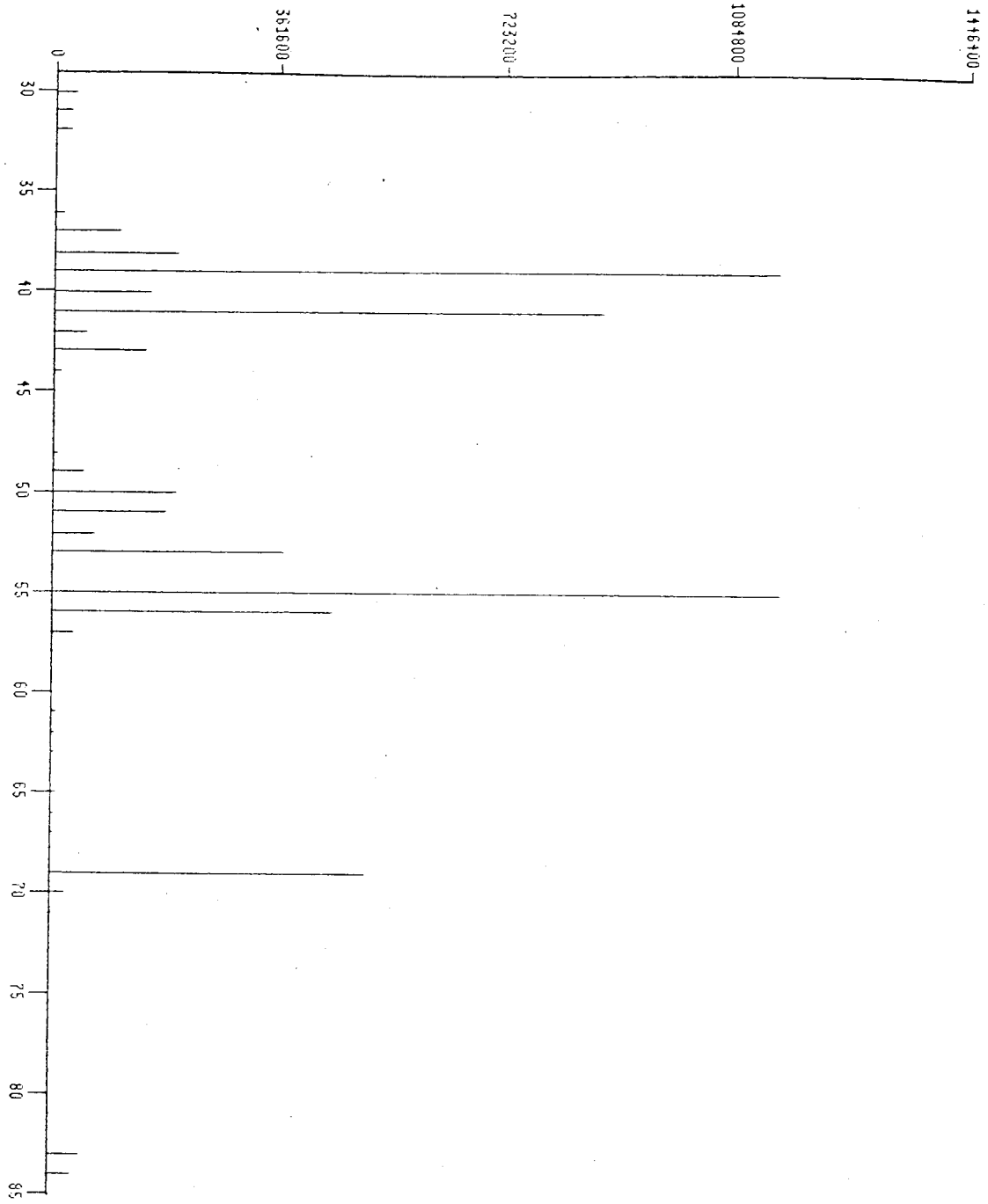


Figure A3.25. Ion current (ordinate) vs mass/charge (amu) (abscissa). Isoprene reference spectrum: 2-methyl 3-butene oxide (standard obtained from Aldrich).

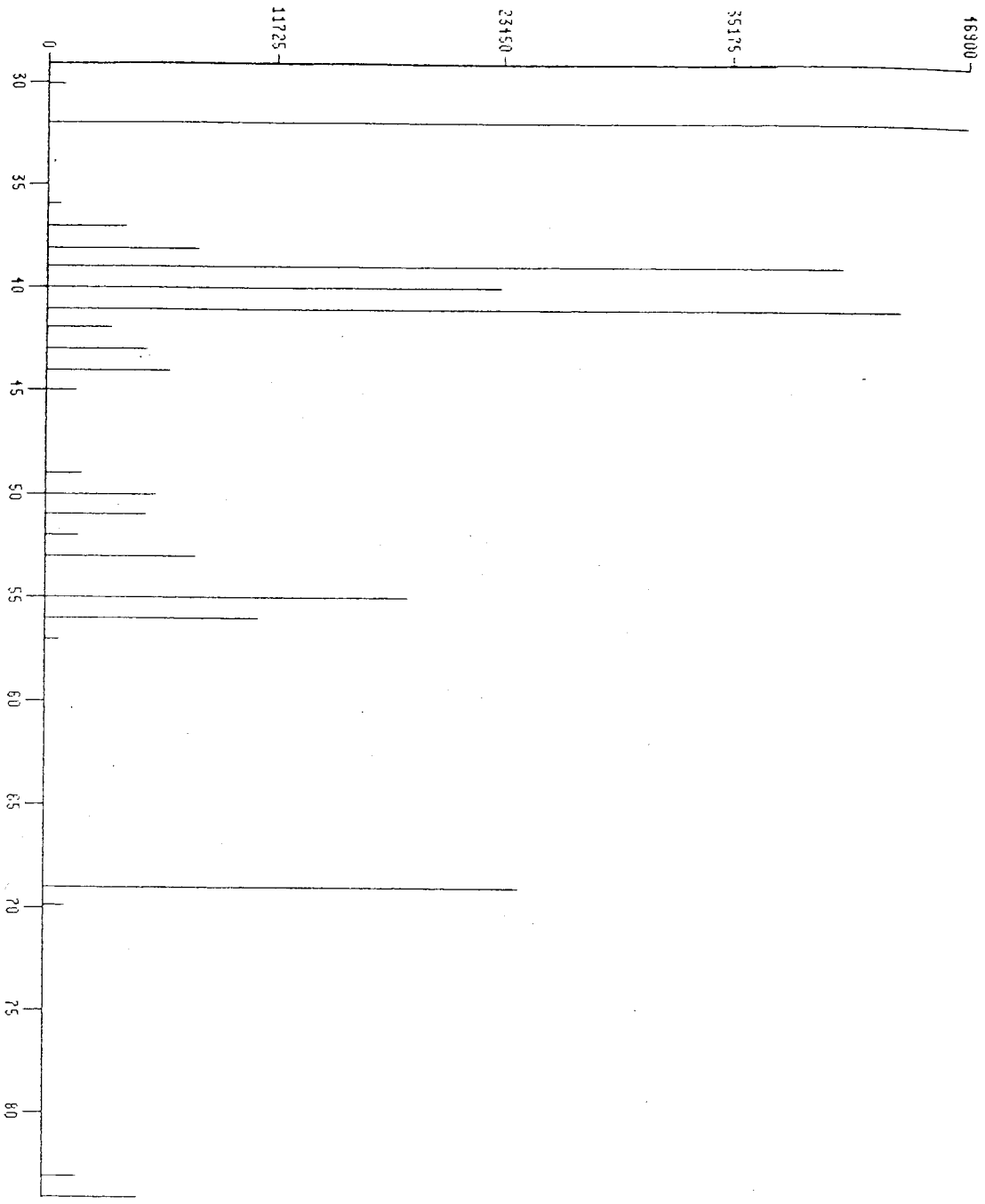


Figure A3.26. Ion current (ordinate) vs mass/charge (amu) (abscissa). Isoprene reference spectrum: 3,3-methyl butene oxide (see note in Chapter 2).

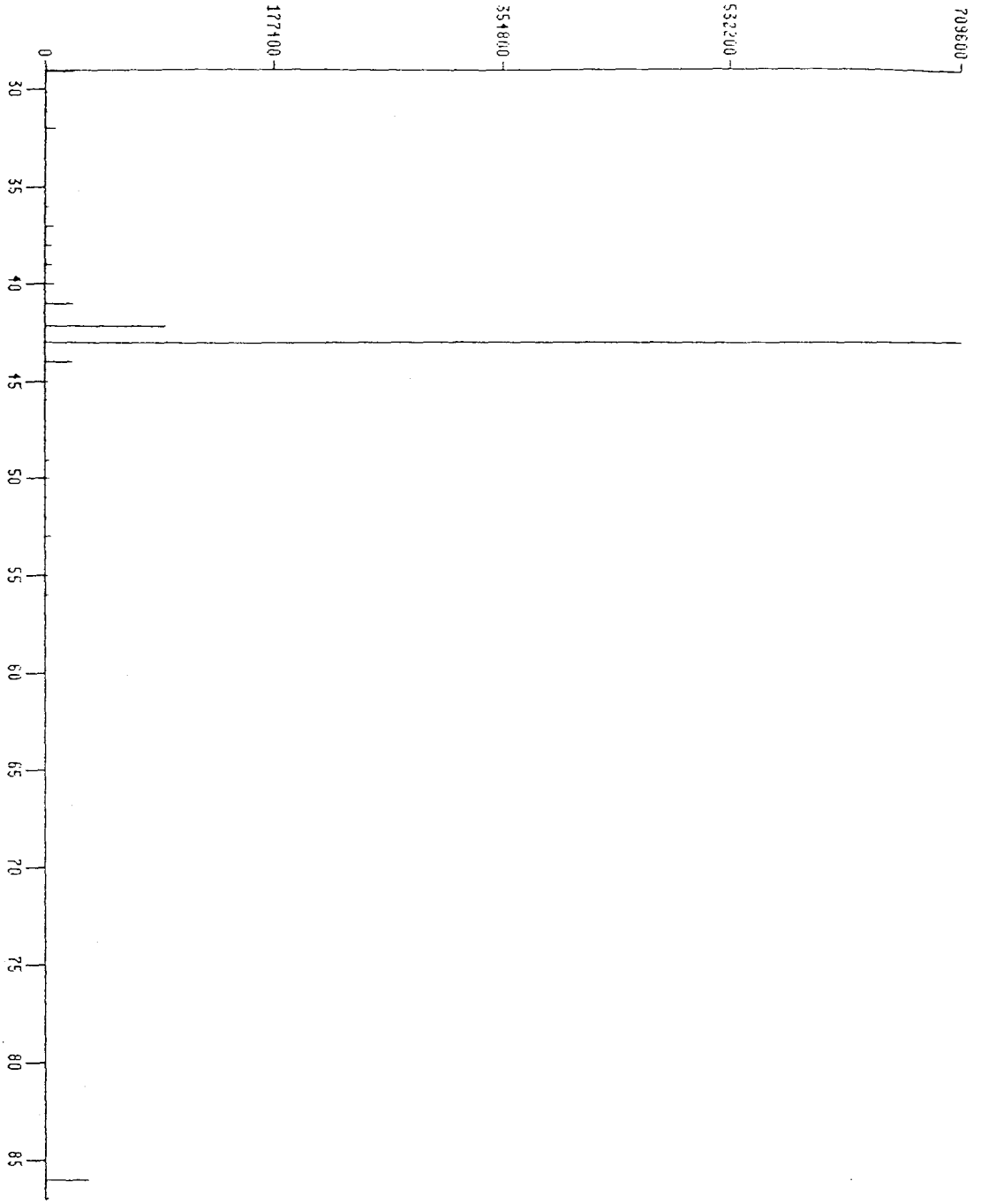


Figure A3.27. Ion current (ordinate) vs mass/charge (amu) (abscissa). Isoprene reference spectrum: biacetyl (standard obtained from Aldrich).

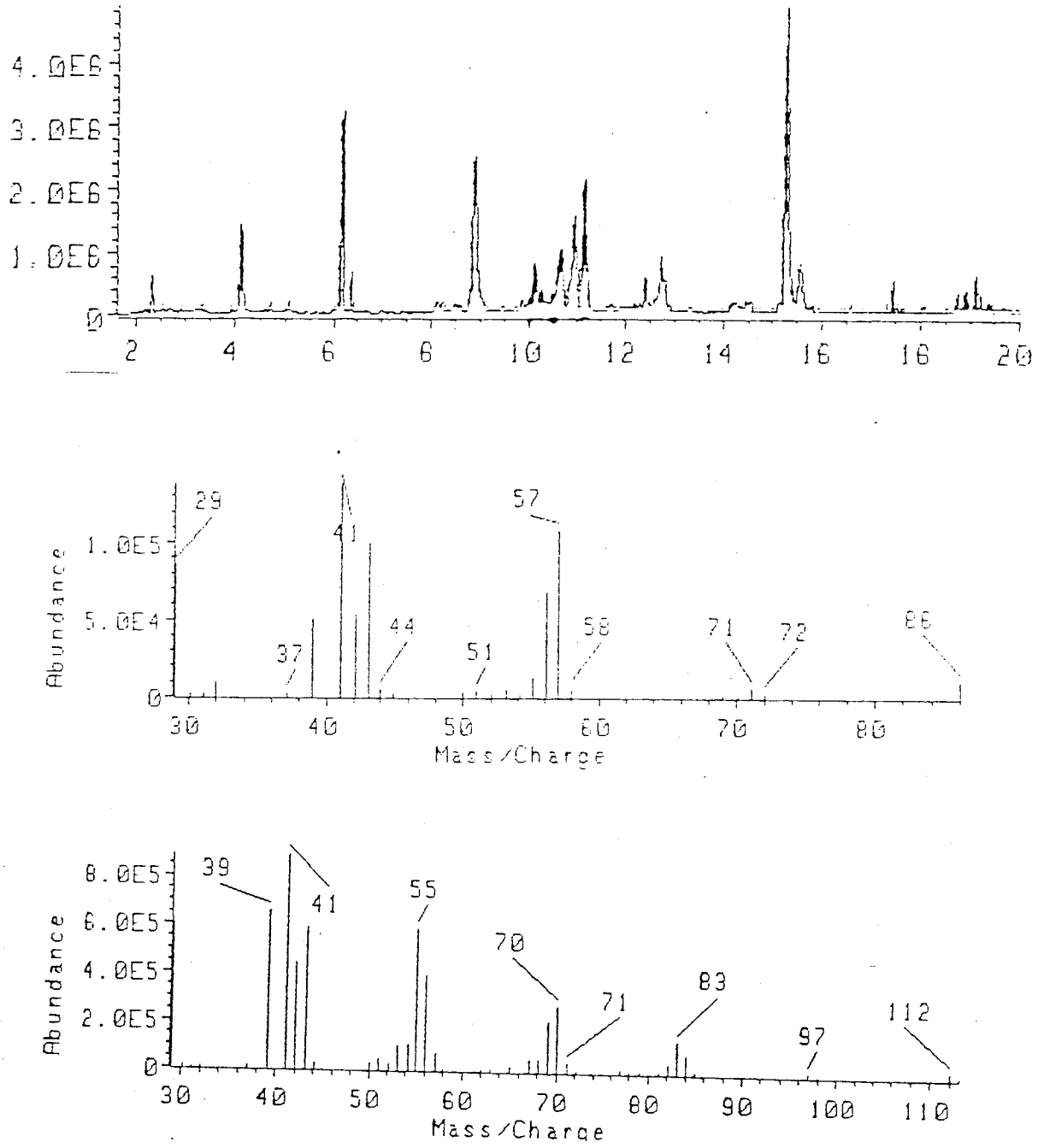


Figure A3.28. (a) Total ion chromatogram of experiment 1O3P1. Ion current (ordinate) vs retention time (abscissa). Order of elution of peaks corresponds to order in FID traces. Note that chromatogram is not quantitative. (b) Scan of 2.337 mins.; identified as hexane, and (c) scan of 6.148 mins.; identified as 1-octene.

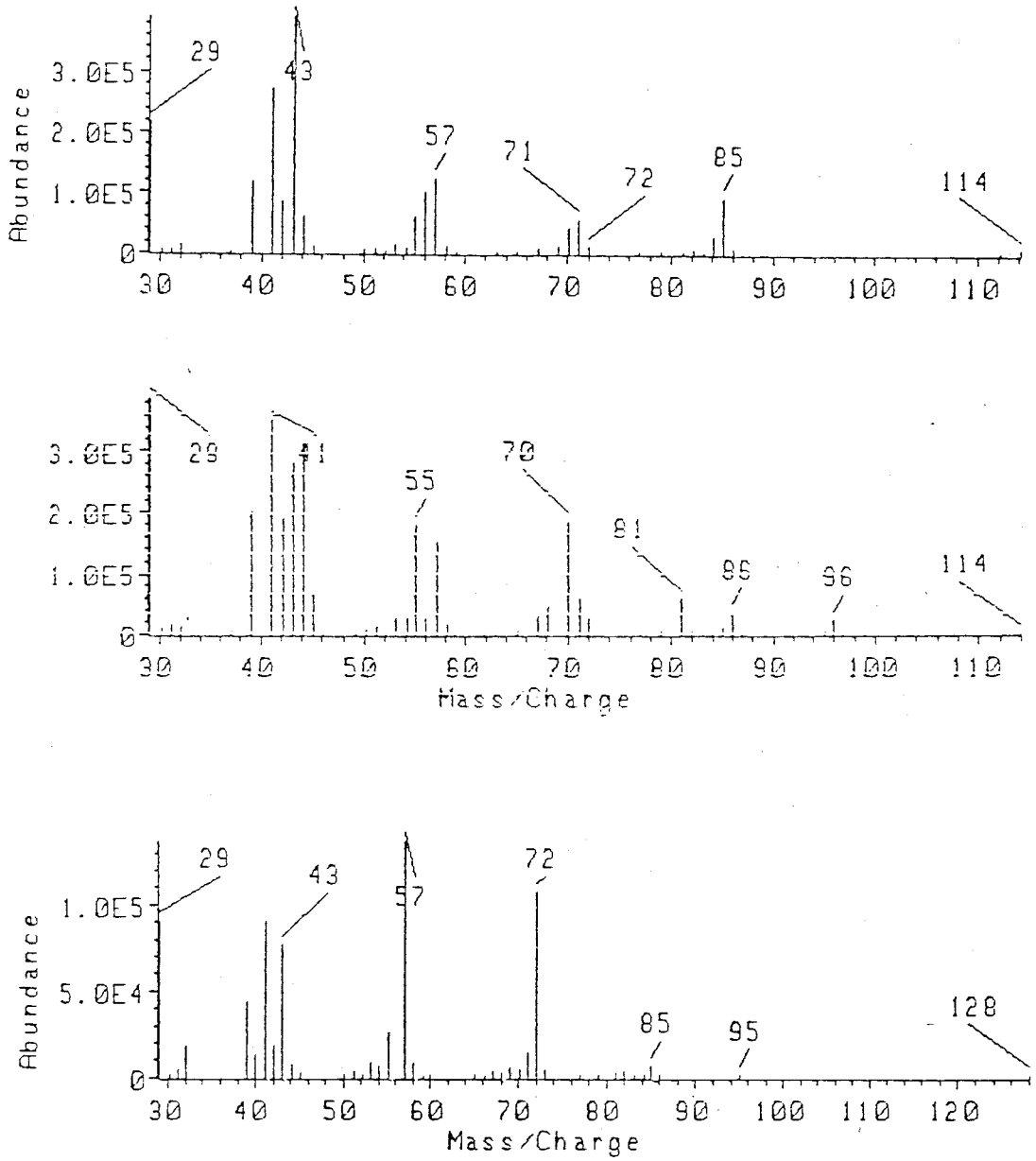


Figure A3.29. (a) Scan of 6.445 mins.; identified as n-octane, (b) Scan of 8.981 mins.; identified as heptanal, and (c) scan of 10.138 mins.; identified as 2-ethyl hexanal.

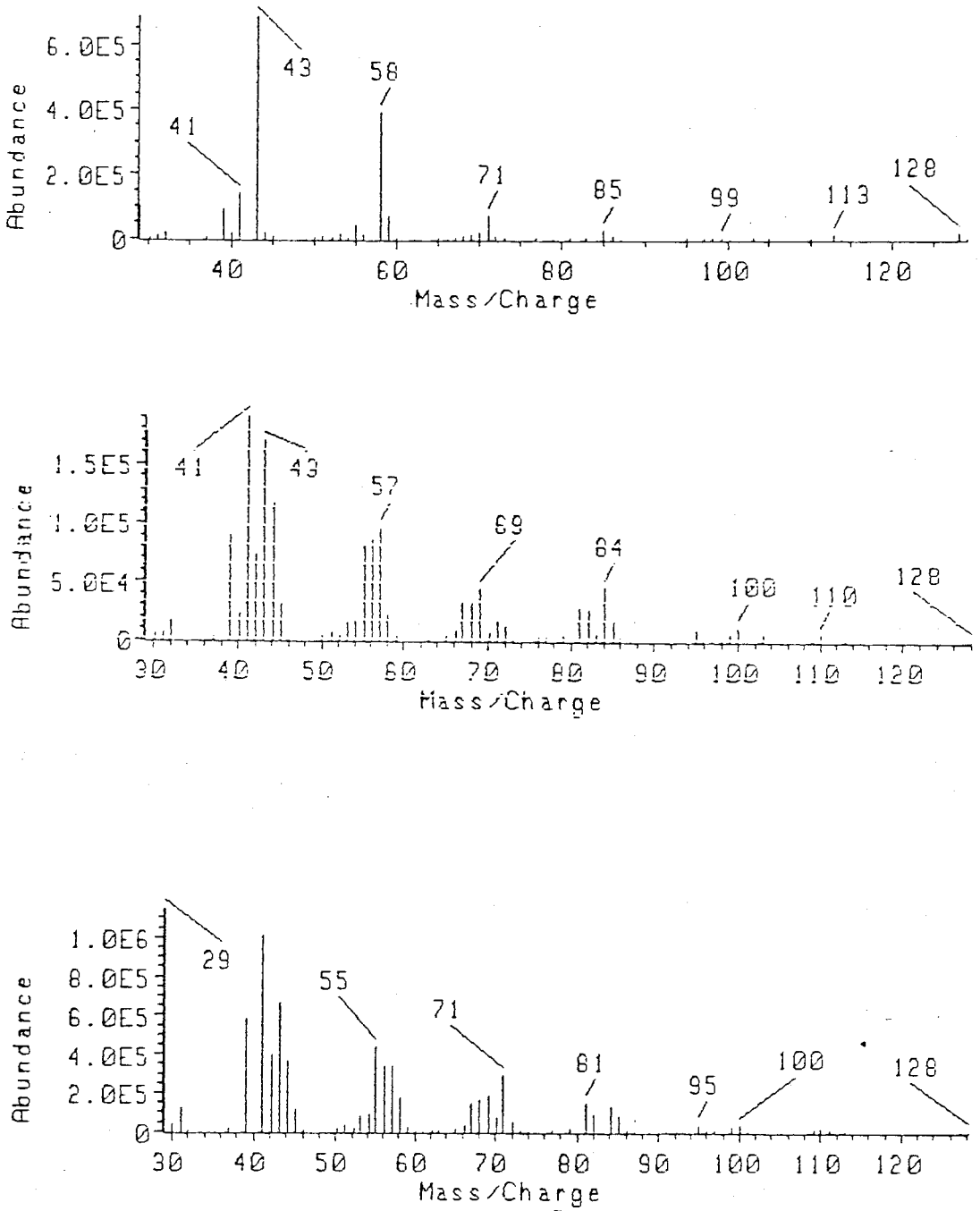


Figure A3.30. (a) Scan of 10.68 mins.; identified as 2-octanone (b) scan of 10.936 mins.; identified as octanal, and (c) scan of 11.241 mins.; identified as 1,2 octyl epoxide.

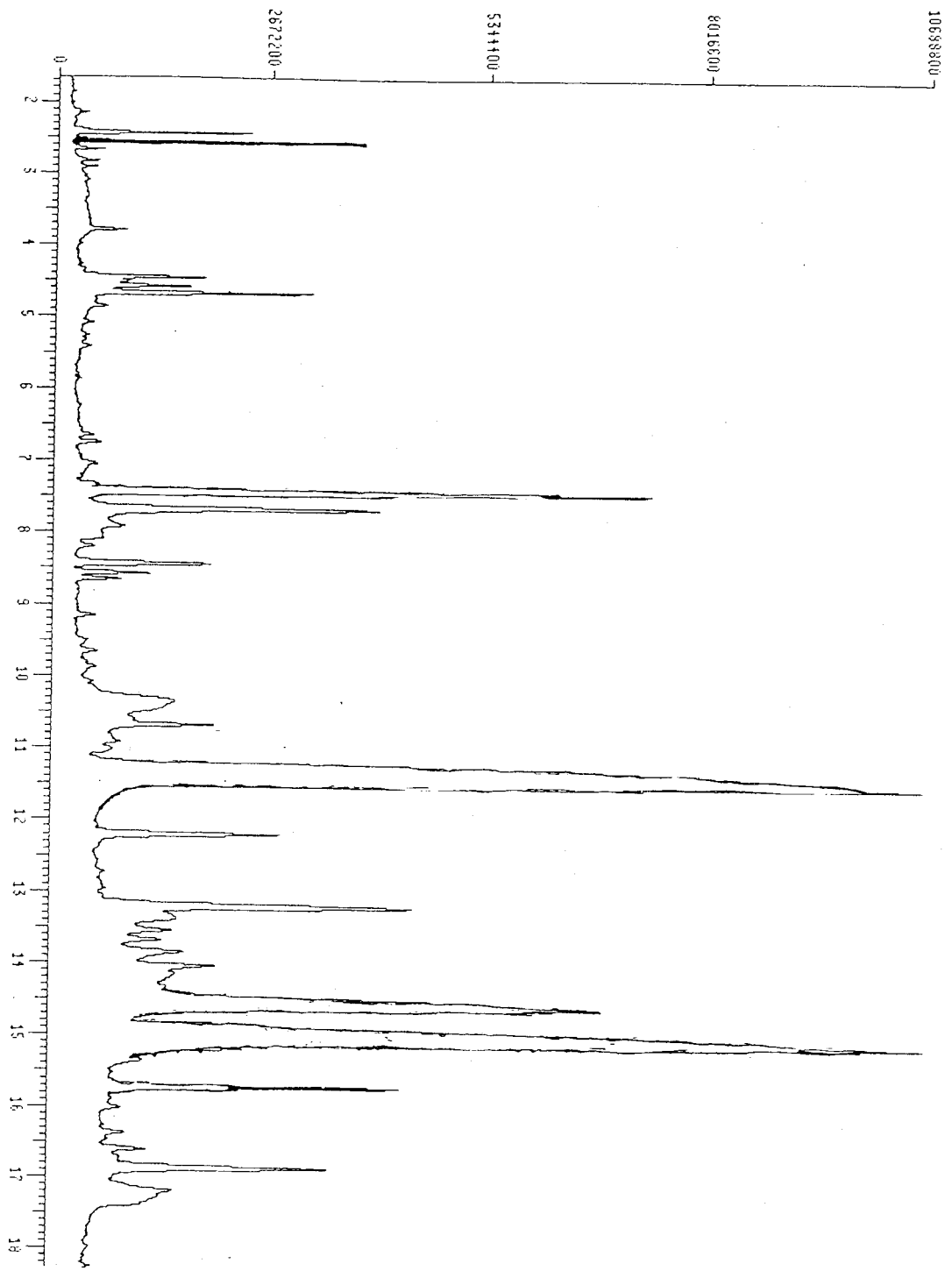


Figure A3.31. Total ion chromatogram from experiment 1NOXN04. Ordinate: relative units. Abscissa: retention time. Oxidants included $O_3$ , OH, and $O(^3P)$, hence this file contains the complete product spectrum. Order of elution of peaks corresponds to order in FID traces. Data file V3:SP04S12B.D. Mass spectra similarly identified correspond to this chromatogram.

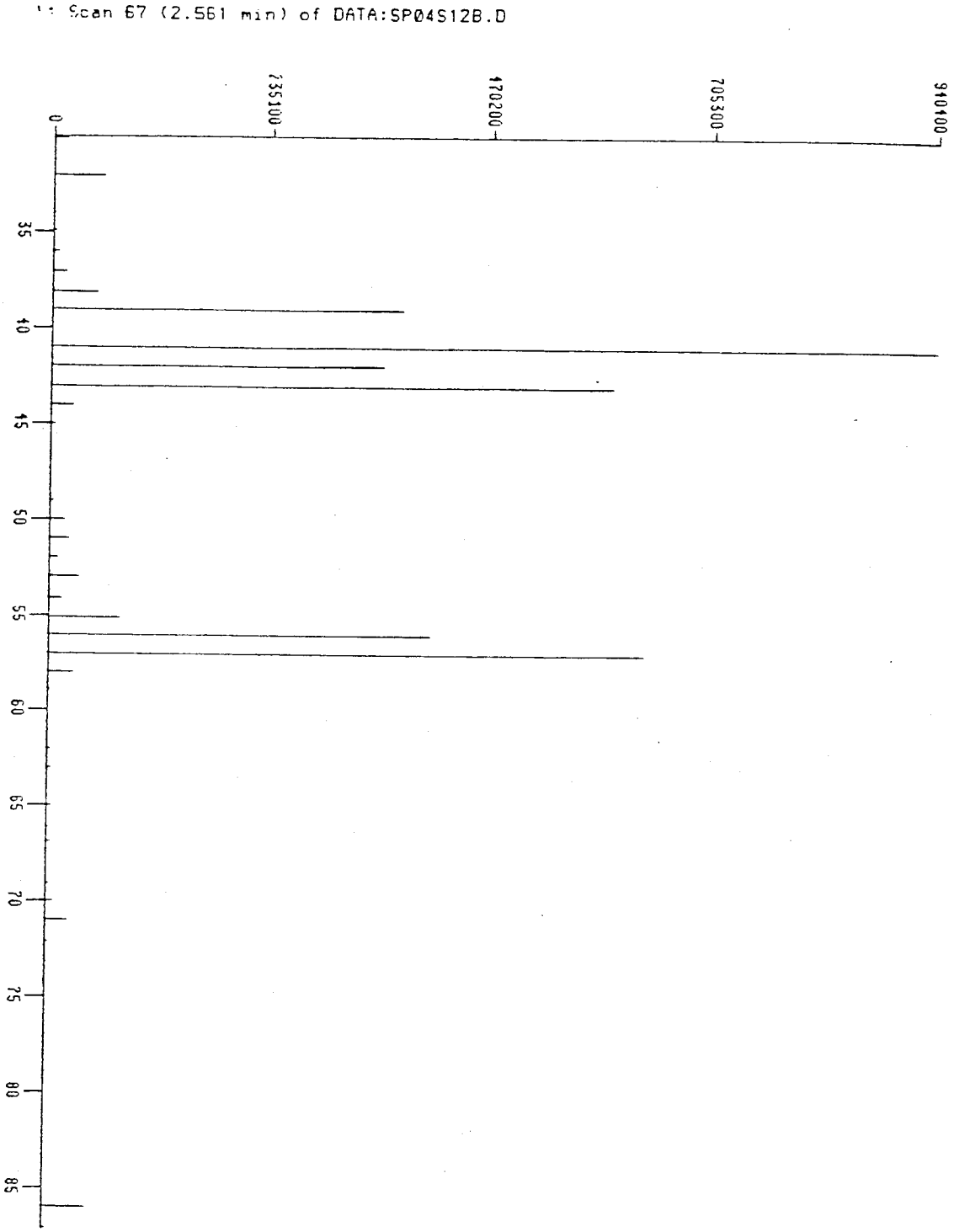


Figure A3.32. Ion current (ordinate) vs mass/charge (amu) (abscissa). File and retention time as indicated. Identified as hexane.

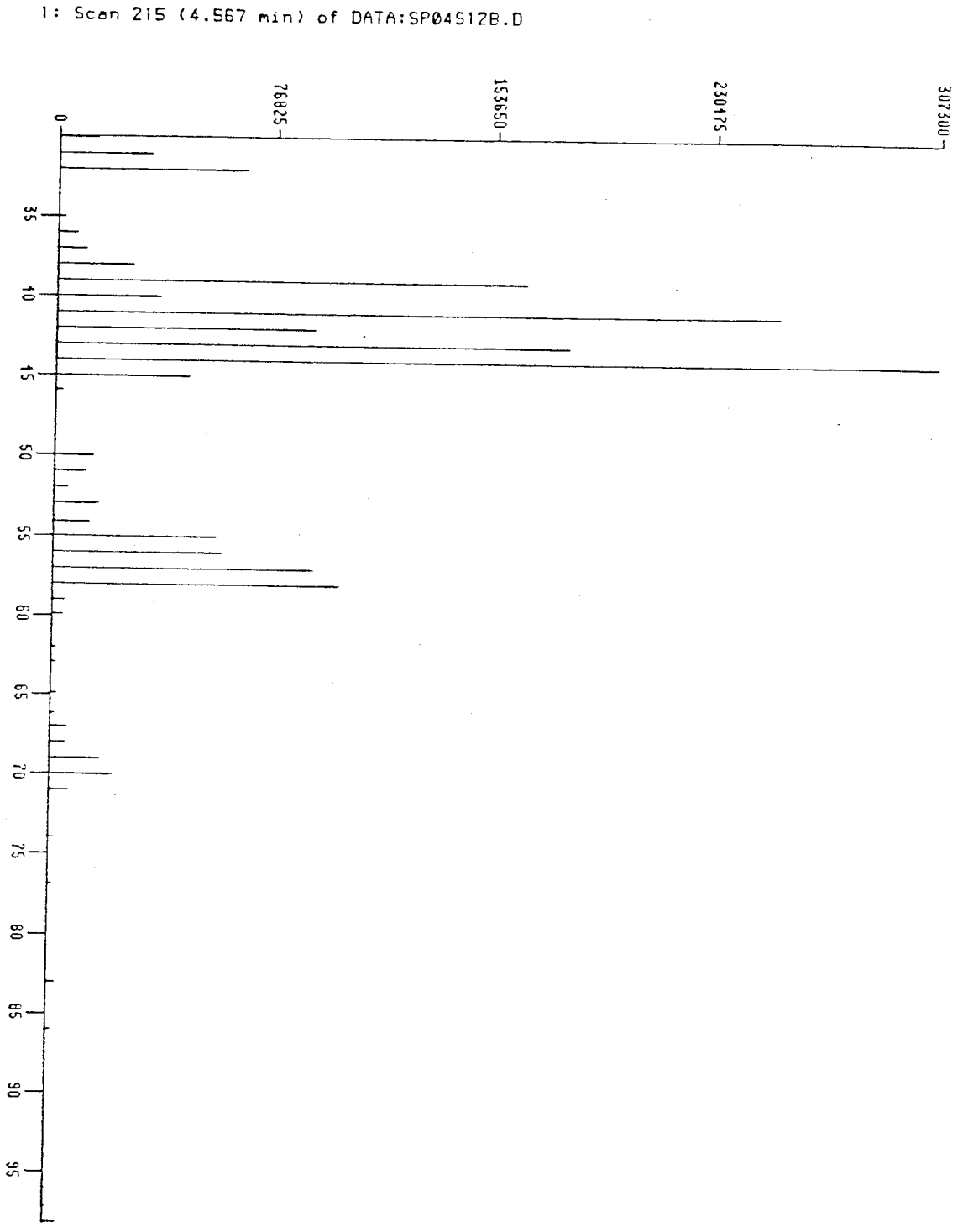


Figure A3.33. Ion current (ordinate) vs mass/charge (amu) (abscissa). File and retention time as indicated. Unidentified.

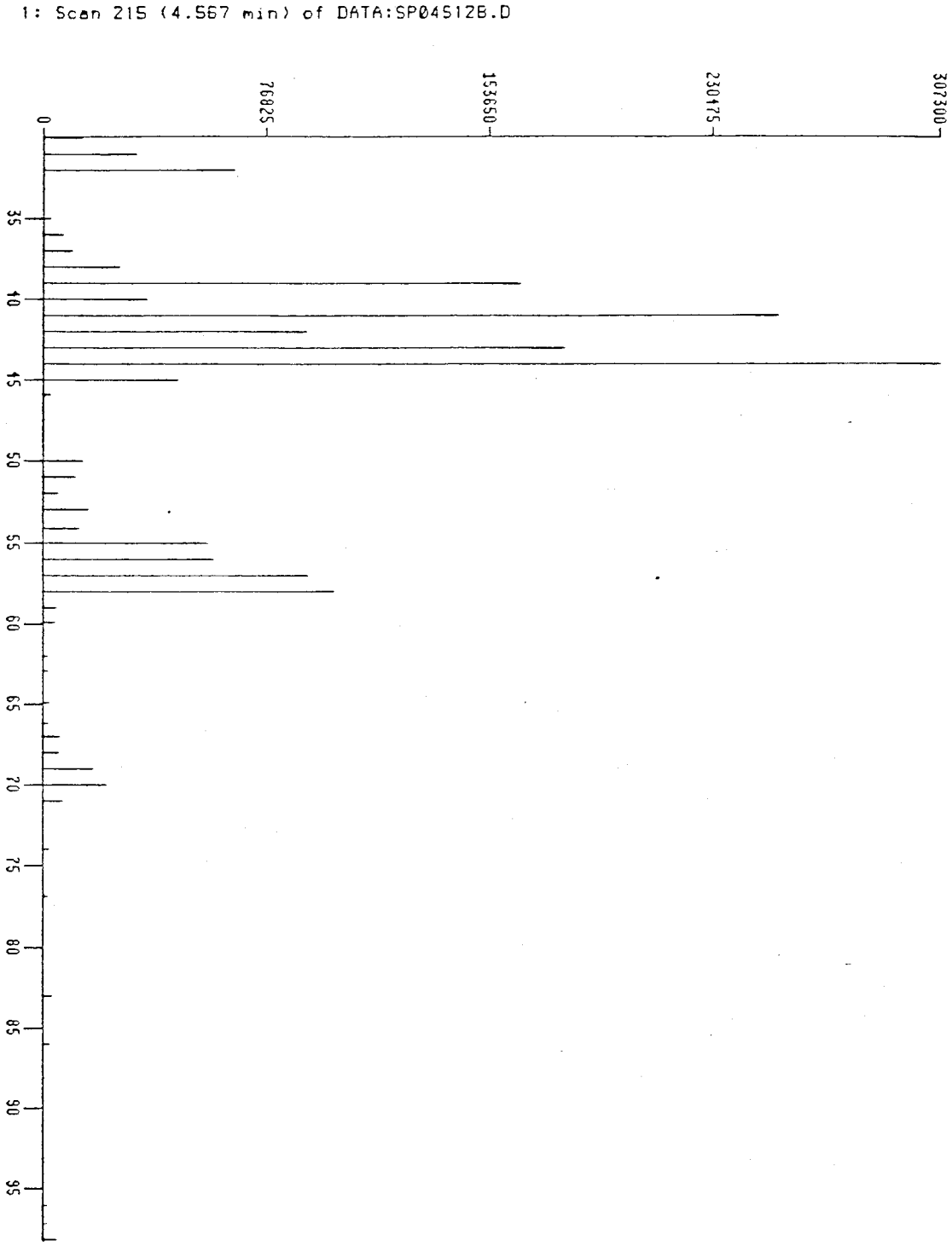


Figure A3.34. Ion current (ordinate) vs mass/charge (amu) (abscissa). File and retention time as indicated. Unidentified.

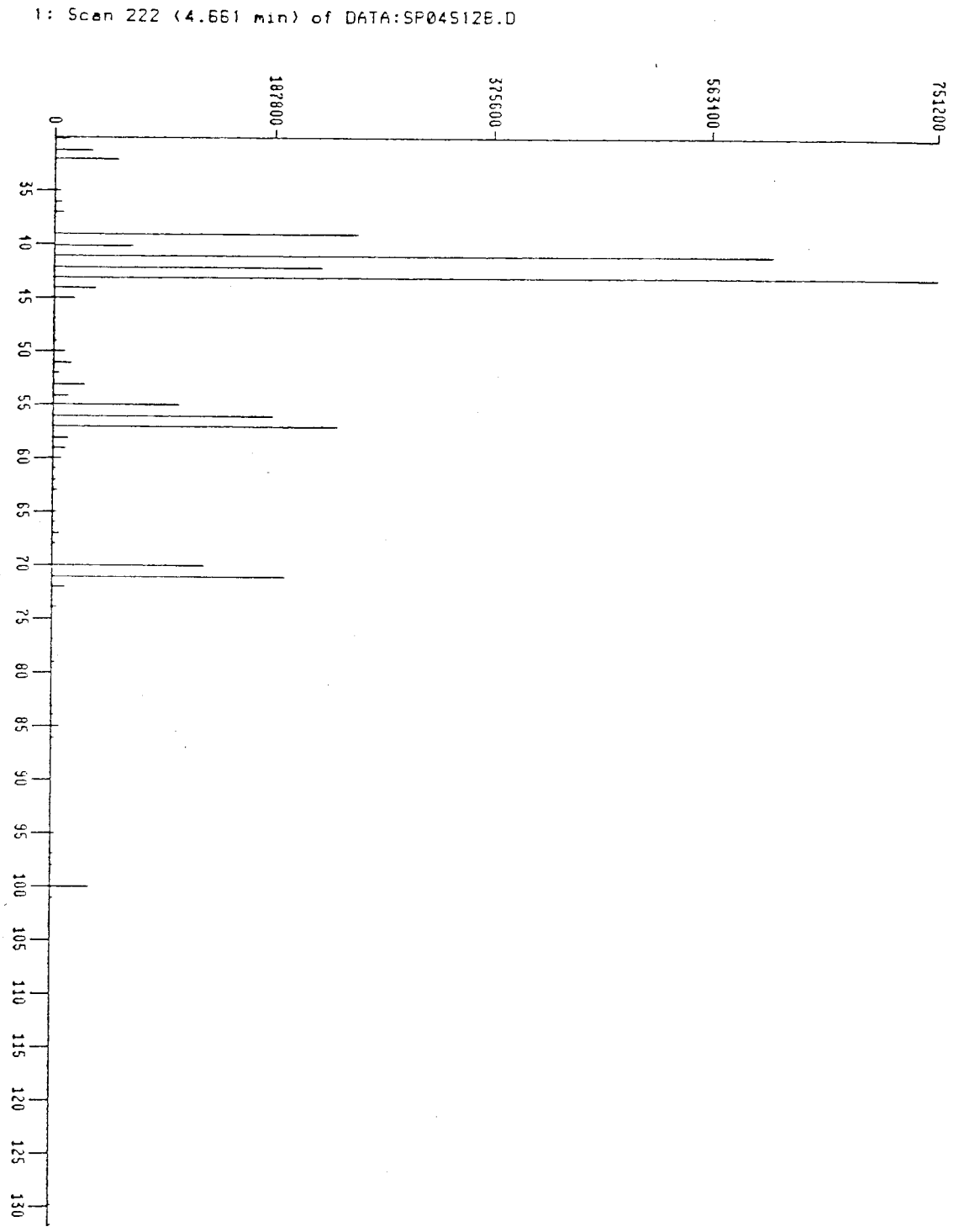


Figure A3.35. Ion current (ordinate) vs mass/charge (amu) (abscissa). File and retention time as indicated. Unidentified.

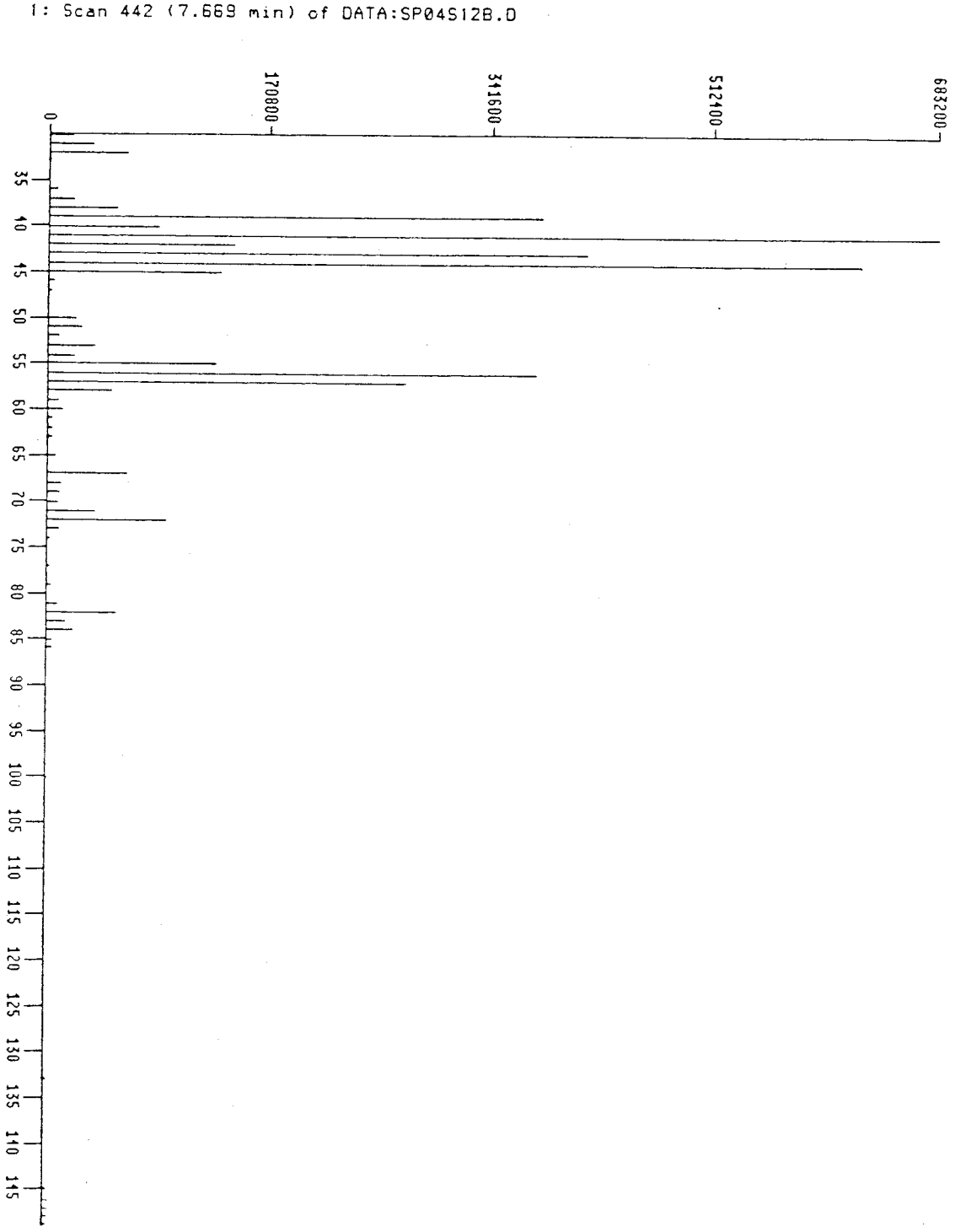


Figure A3.36. Ion current (ordinate) vs mass/charge (amu) (abscissa). File and retention time as indicated. Unidentified.

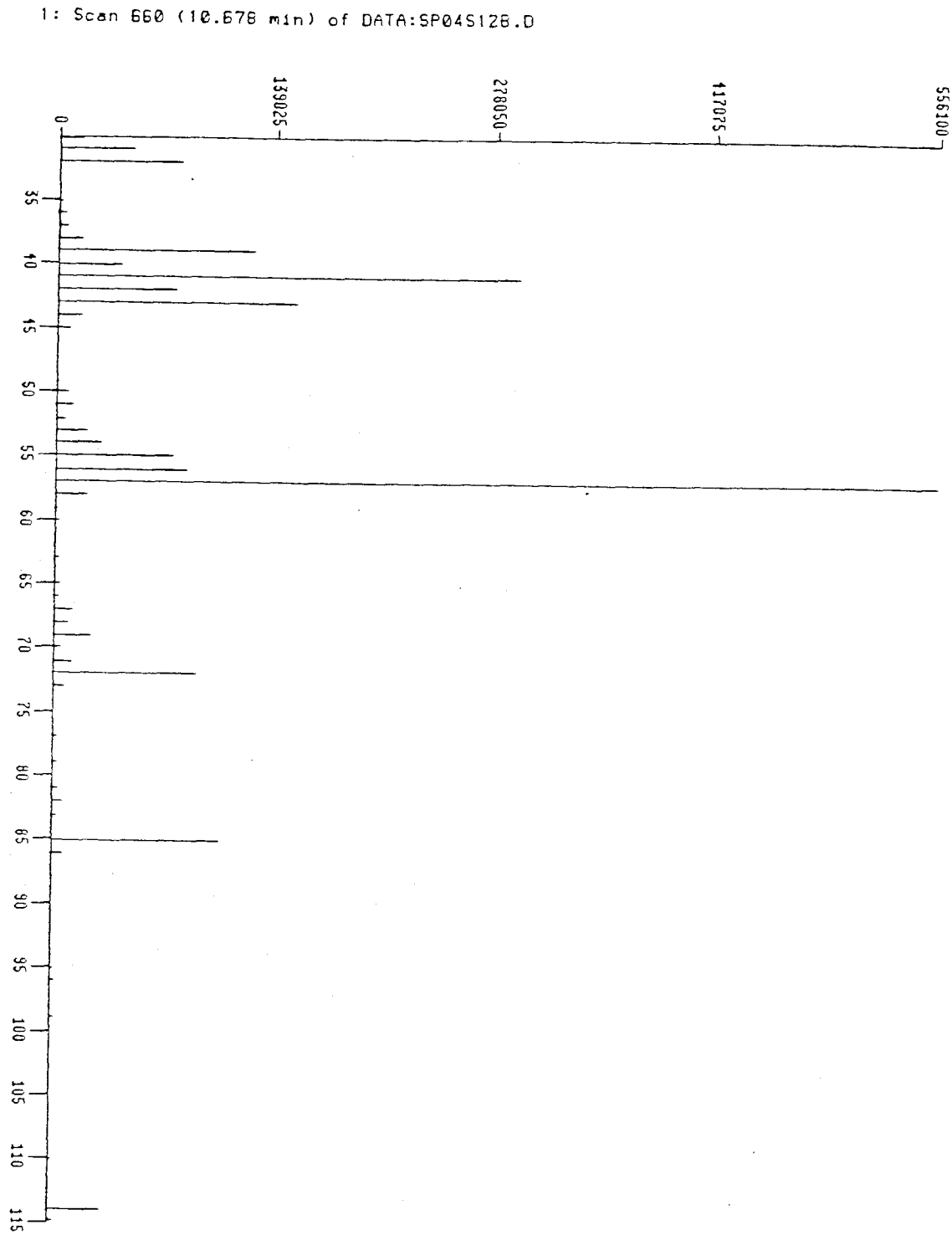


Figure A3.37. Ion current (ordinate) vs mass/charge (amu) (abscissa). File and retention time as indicated. Identified as 3-heptanone.

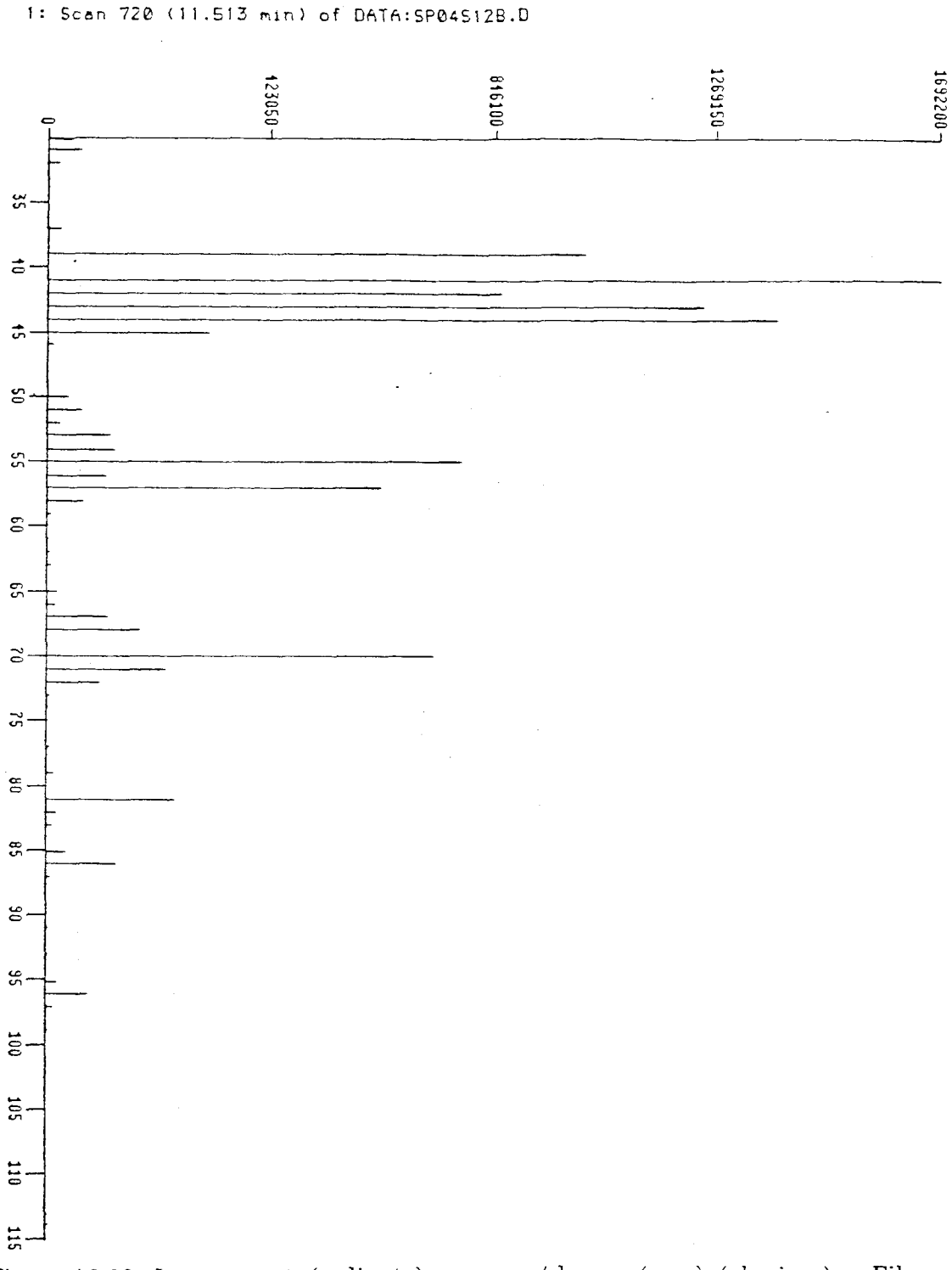


Figure A3.38. Ion current (ordinate) vs mass/charge (amu) (abscissa). File and retention time as indicated. Identified as heptanal.

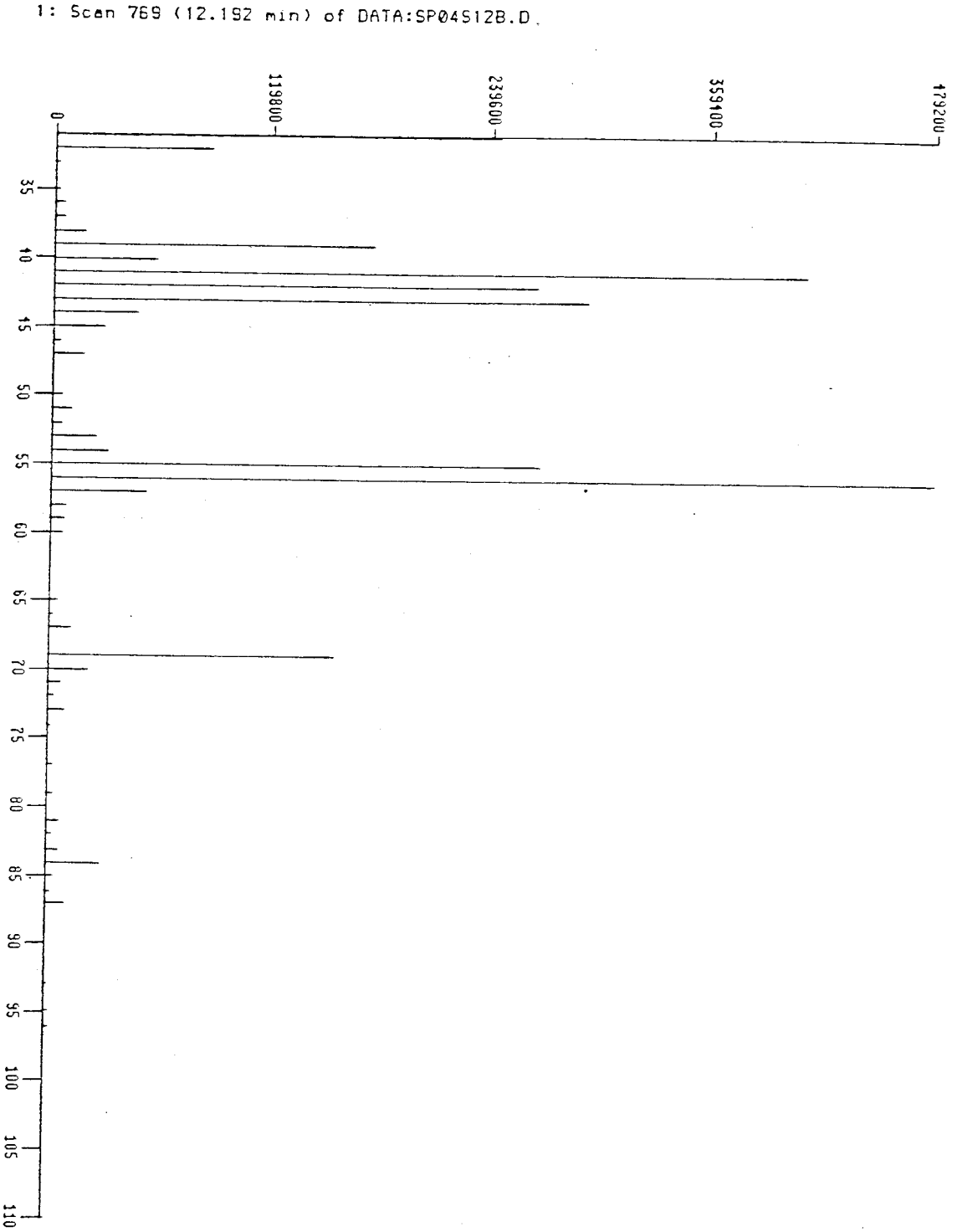


Figure A3.39. Ion current (ordinate) vs mass/charge (amu) (abscissa). File and retention time as indicated. Unidentified.

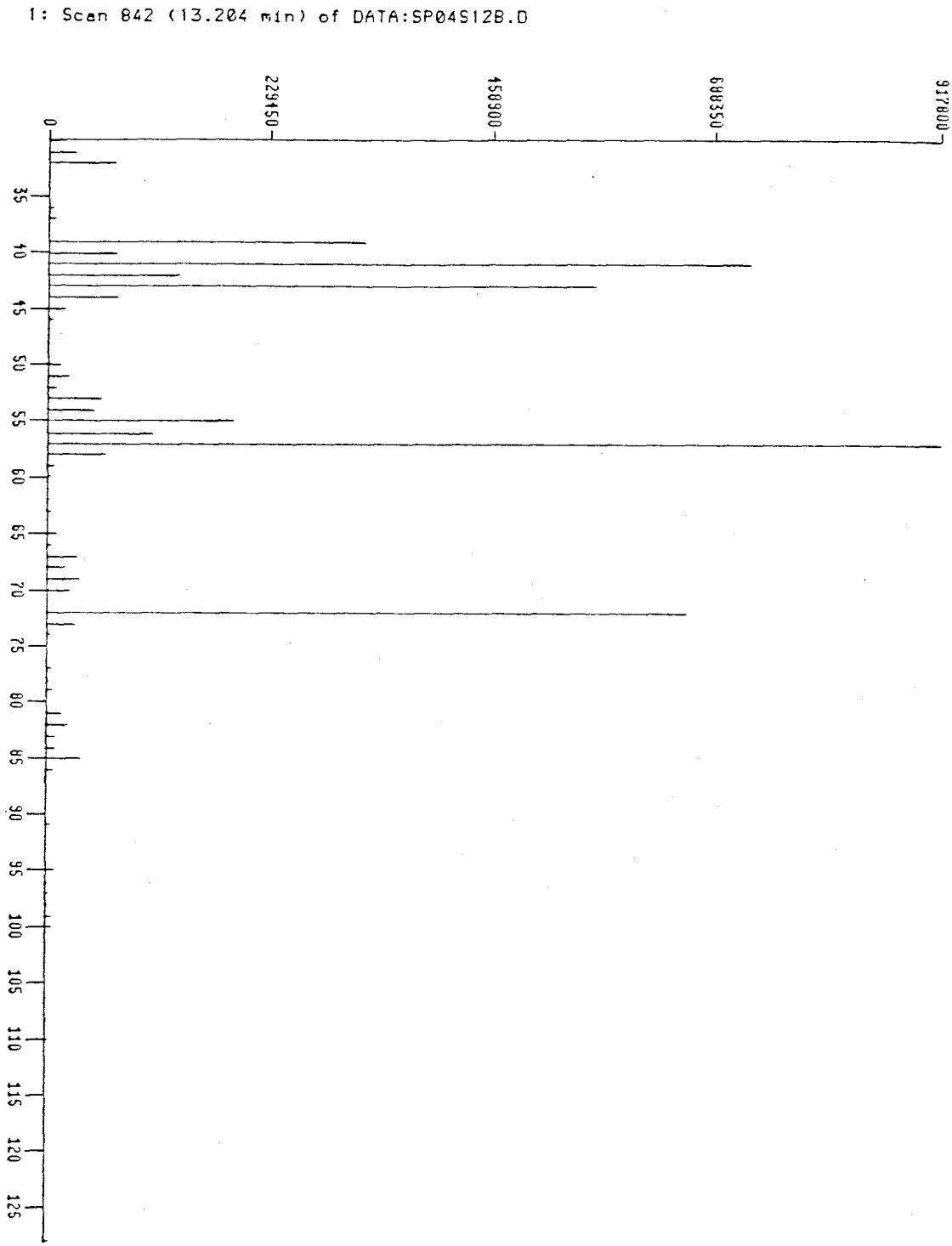


Figure A3.40. Ion current (ordinate) vs mass/charge (amu) (abscissa). File and retention time as indicated. Identified as 2-ethyl hexanal.

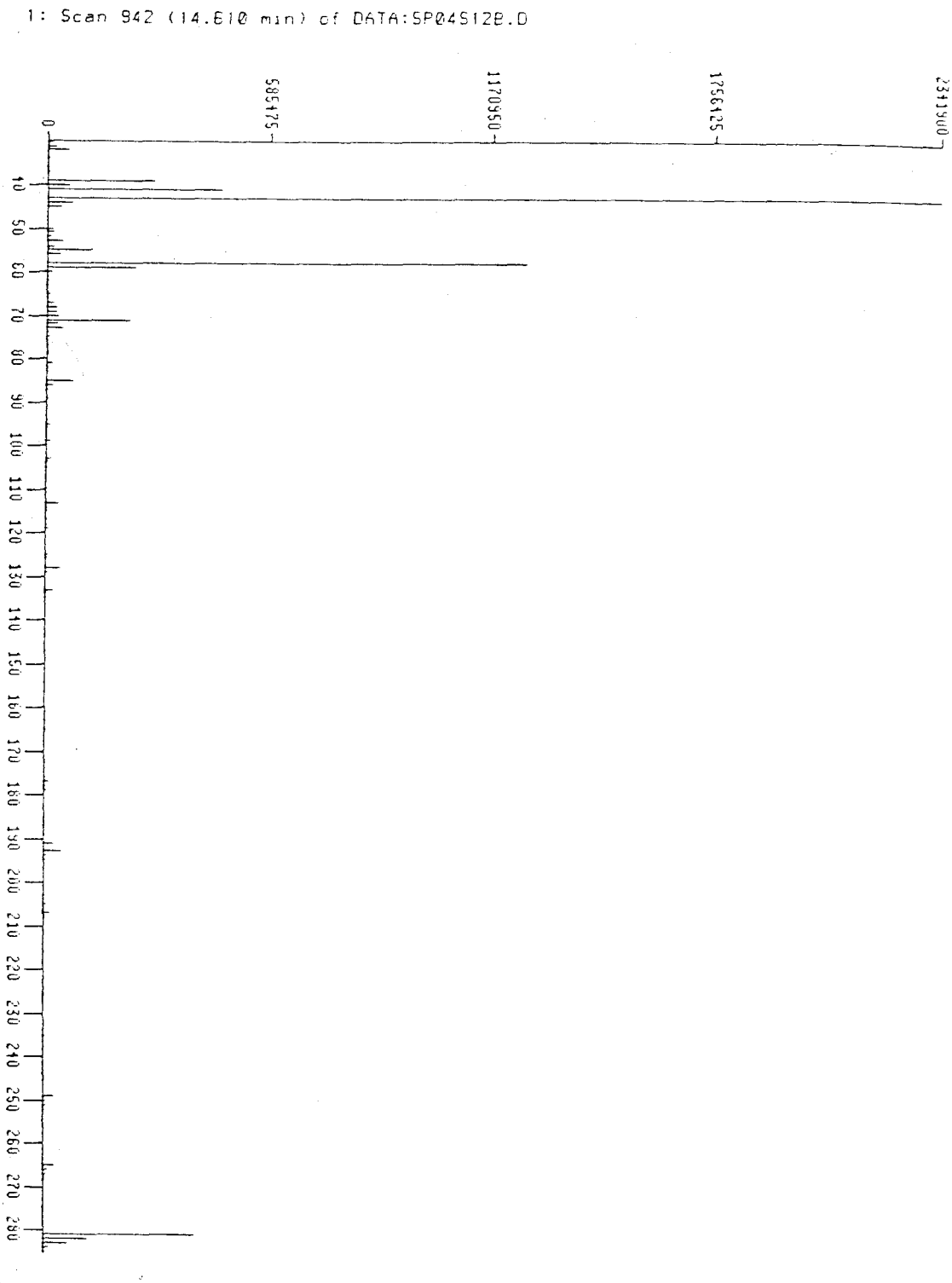


Figure A3.41. Ion current (ordinate) vs mass/charge (amu) (abscissa). File and retention time as indicated. Identified as 2-octananal; current at 280+ is from background noise in GC/MS (a result of the polymer chemists).

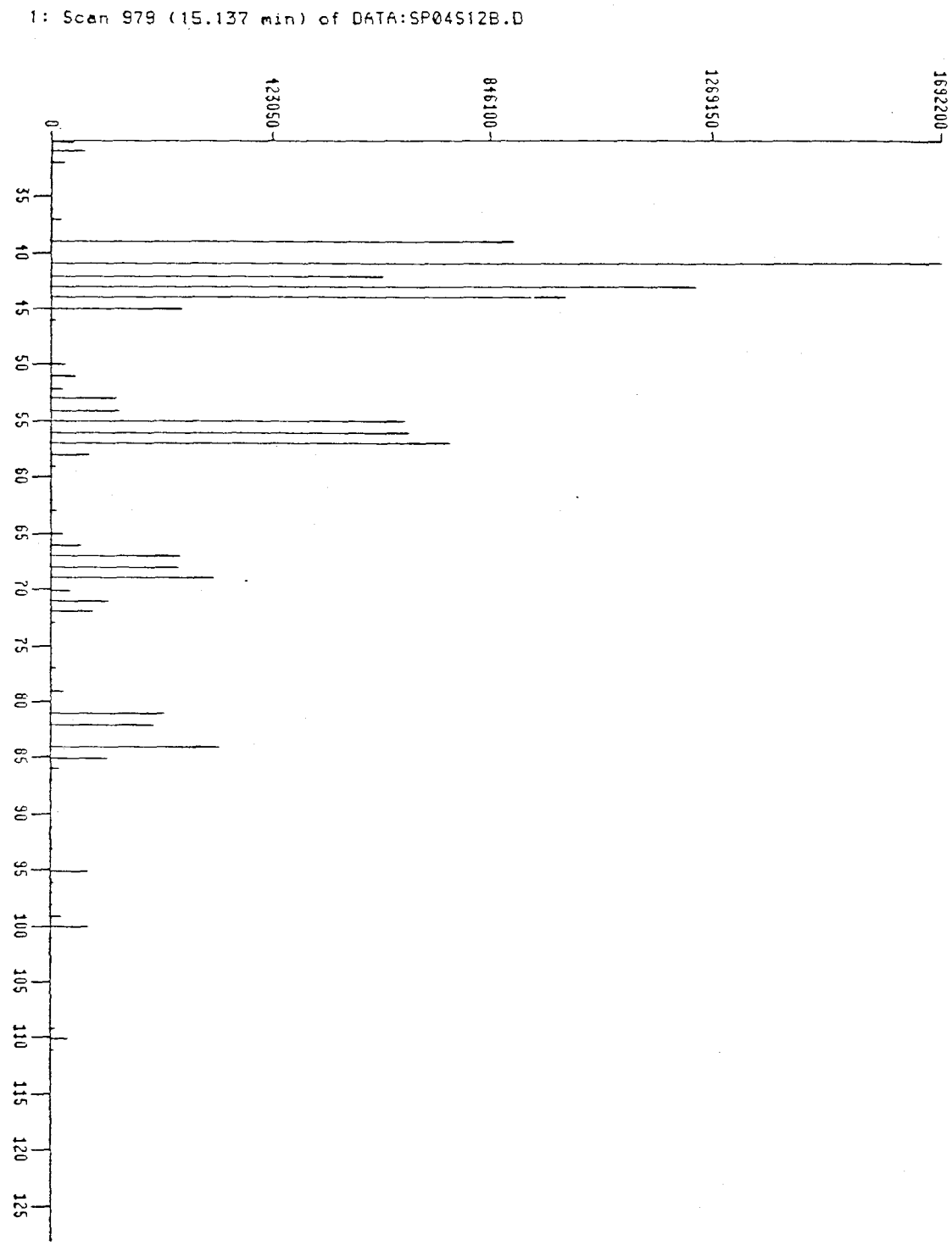


Figure A3.42. Ion current (ordinate) vs mass/charge (amu) (abscissa). File and retention time as indicated. Identified as octanal.

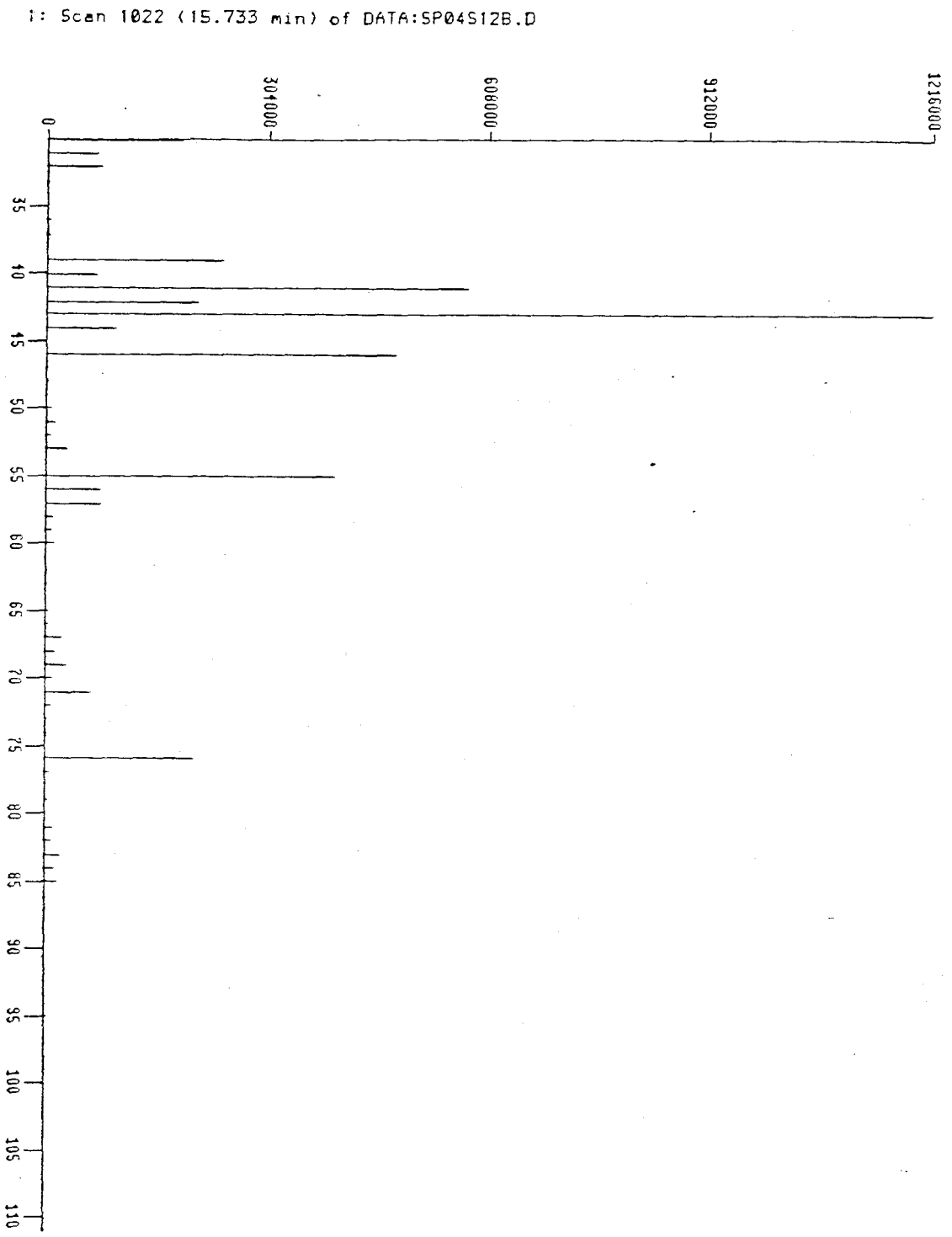


Figure A3.43. Ion current (ordinate) vs mass/charge (amu) (abscissa). File and retention time as indicated. Unidentified; probable nitrate peak.

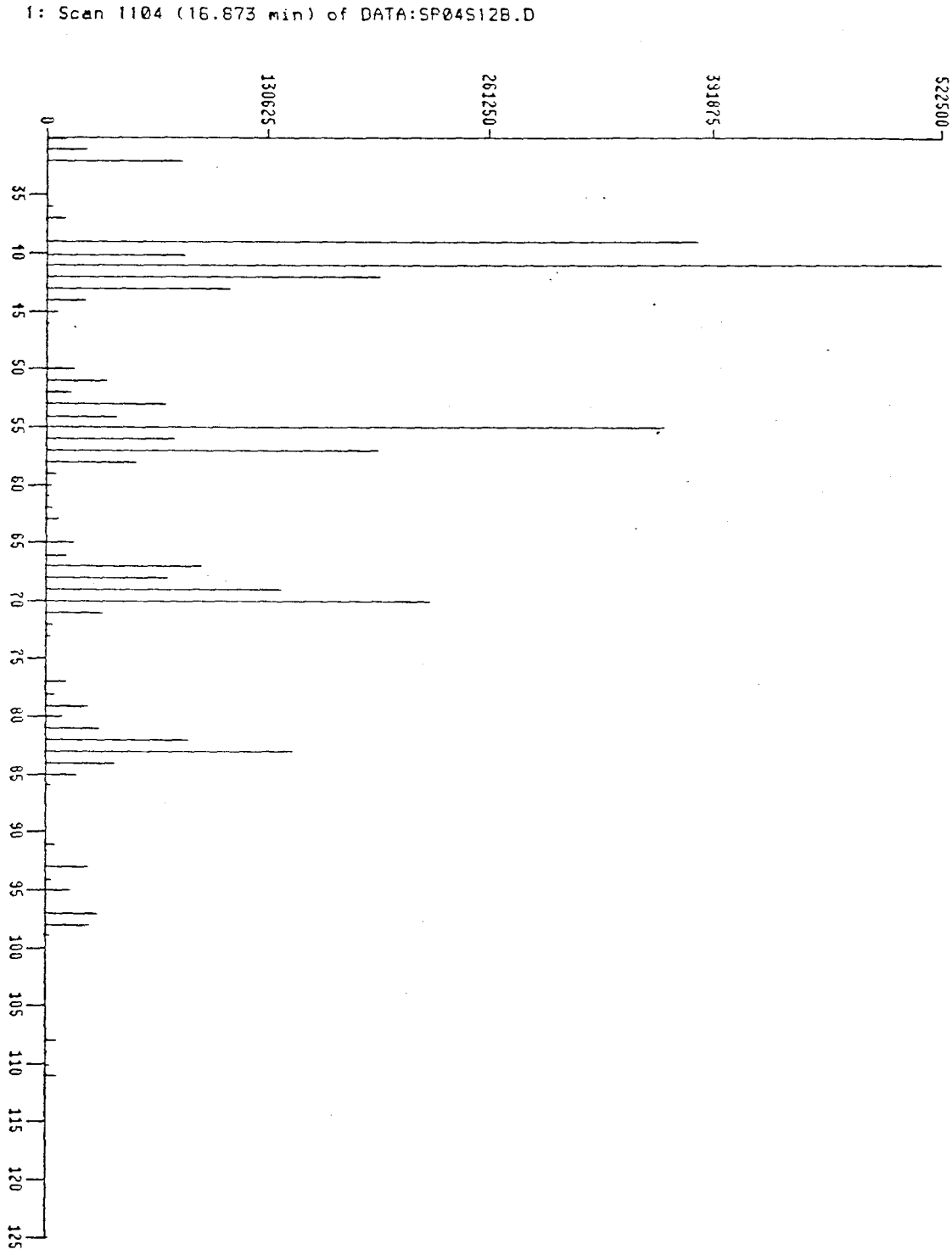


Figure A3.44. Ion current (ordinate) vs mass/charge (amu) (abscissa). File and retention time as indicated. Unidentified.

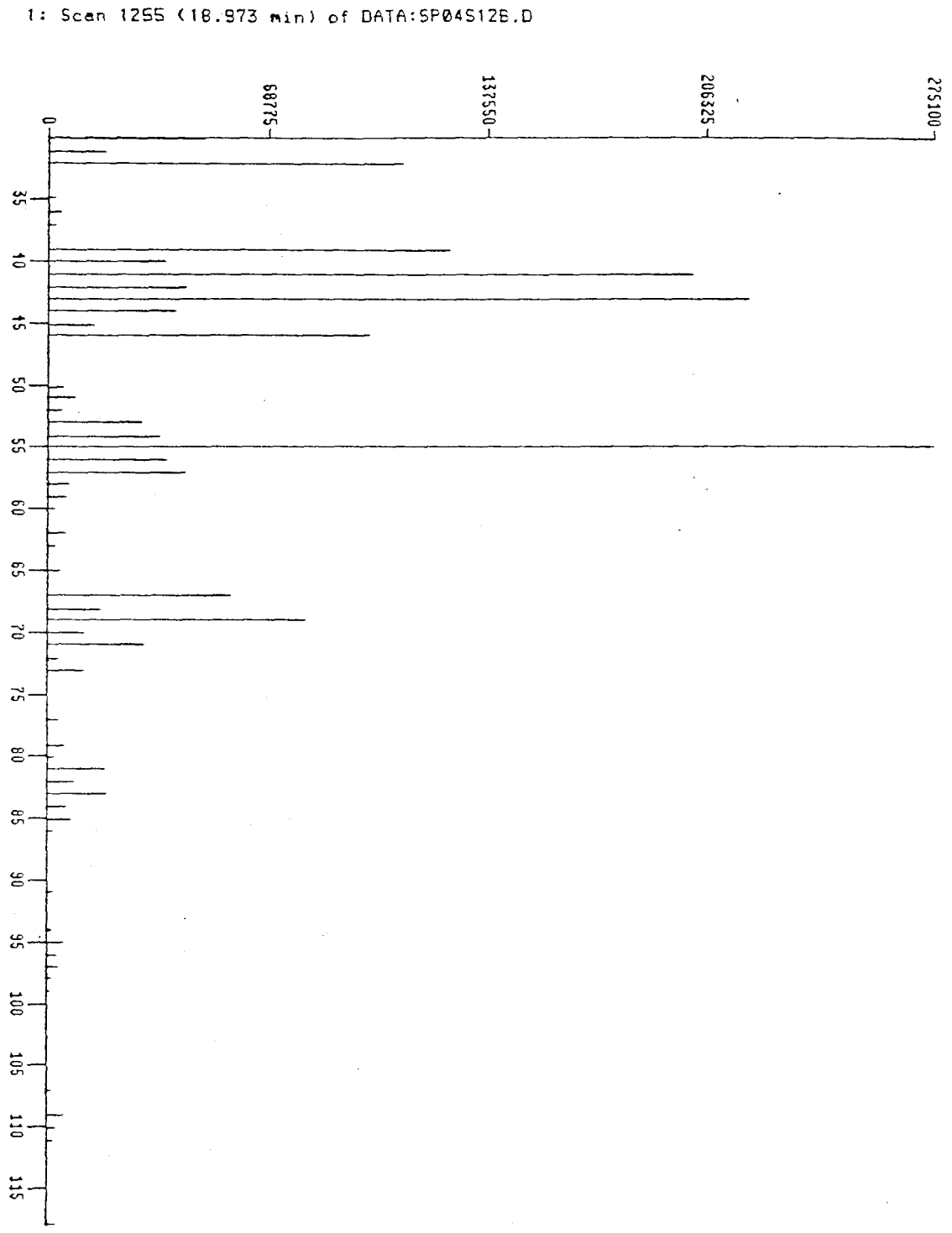


Figure A3.45. Ion current (ordinate) vs mass/charge (amu) (abscissa). File and retention time as indicated. Unidentified; probable nitrate.

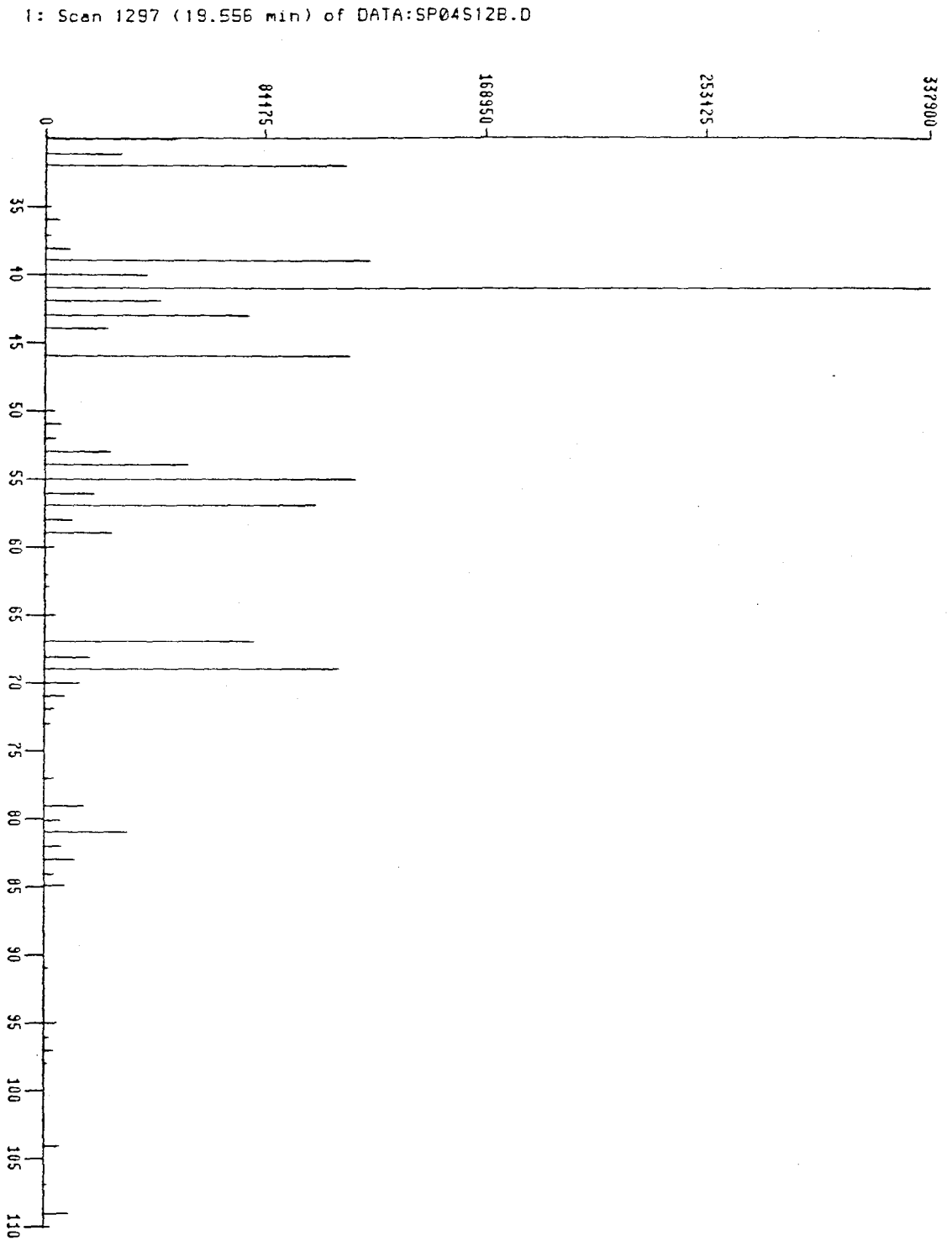


Figure A3.46. Ion current (ordinate) vs mass/charge (amu) (abscissa). File and retention time as indicated. Unidentified; probable nitrate.

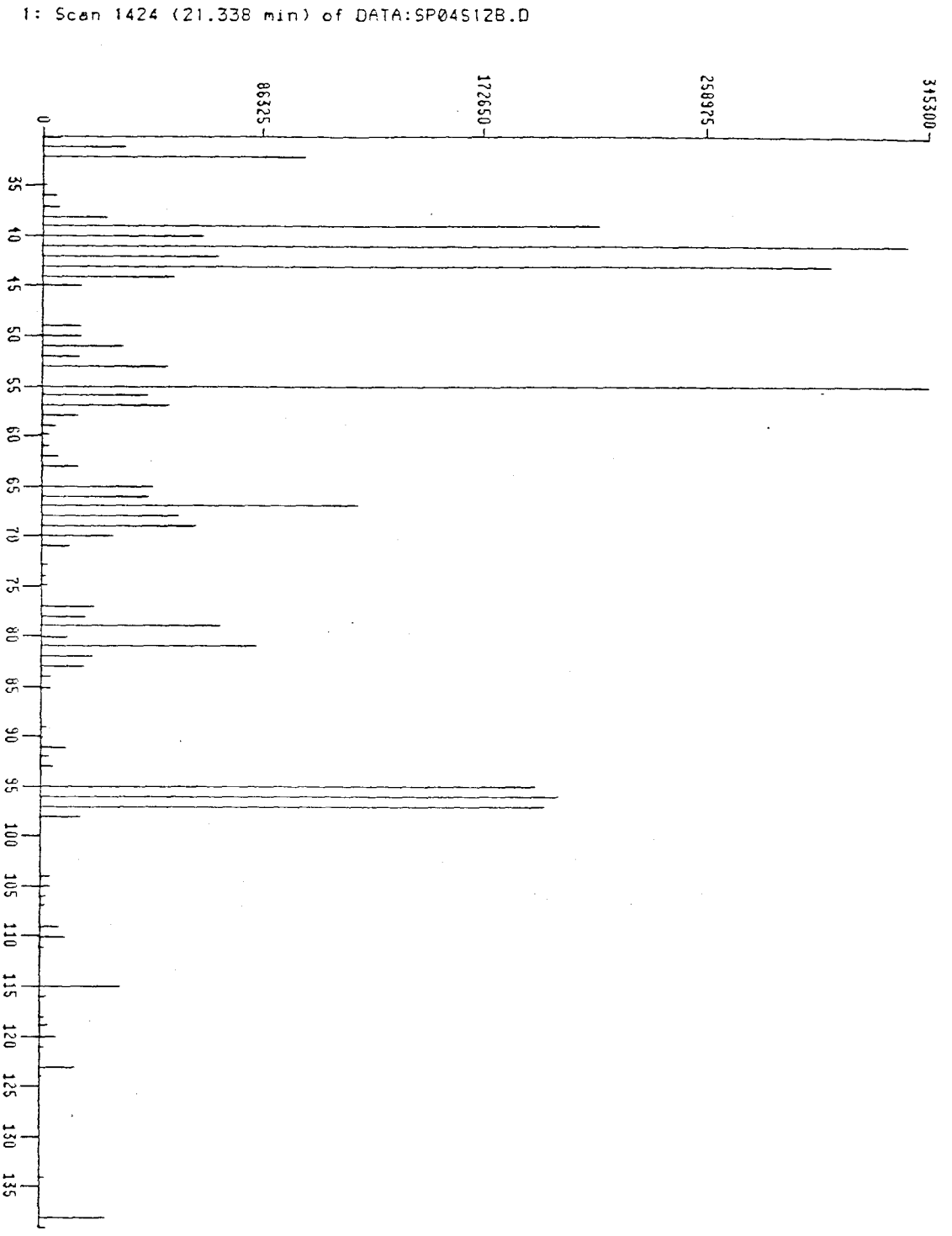


Figure A3.47. Ion current (ordinate) vs mass/charge (amu) (abscissa). File and retention time as indicated. Unidentified.

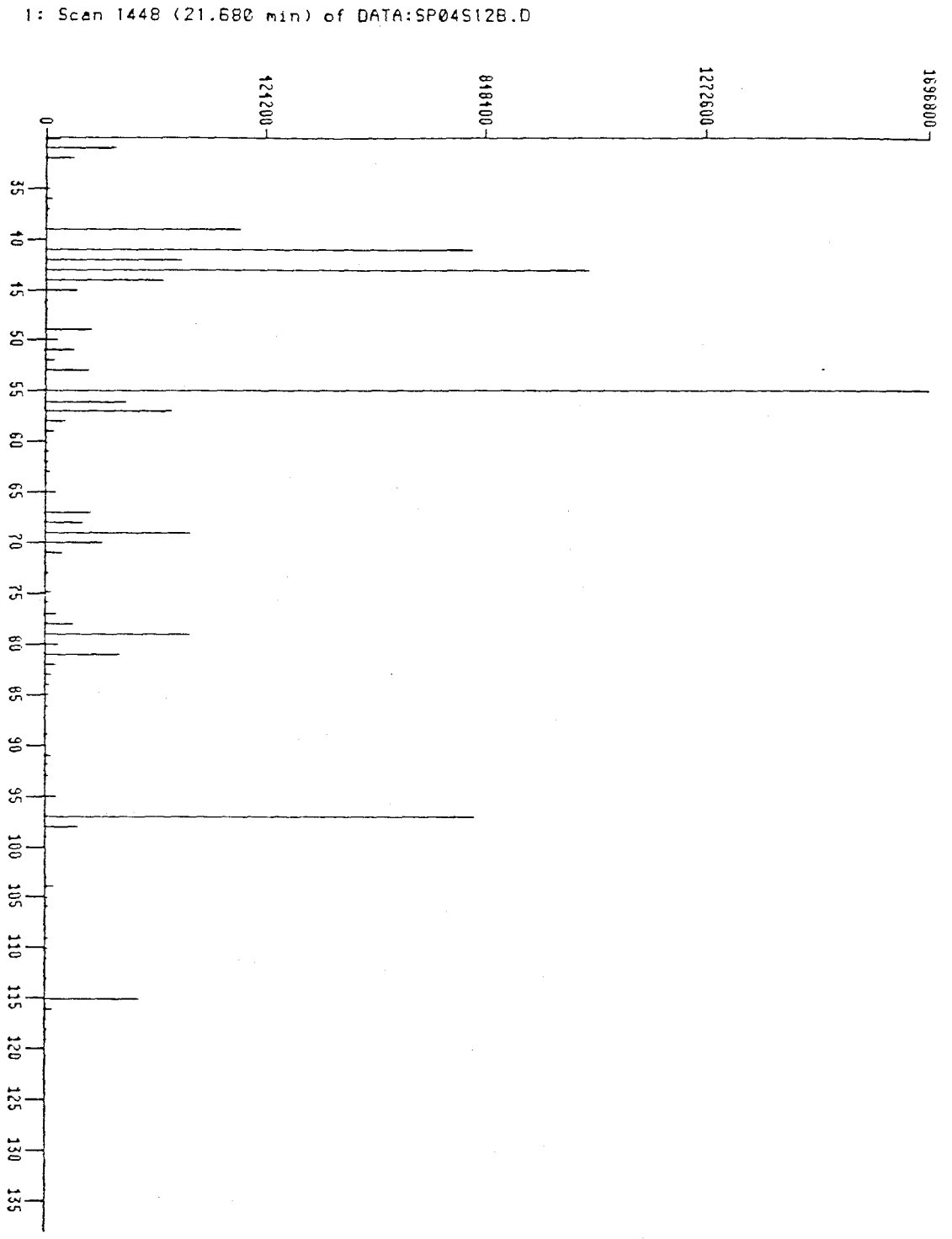


Figure A3.48. Ion current (ordinate) vs mass/charge (amu) (abscissa). File and retention time as indicated. Unidentified.

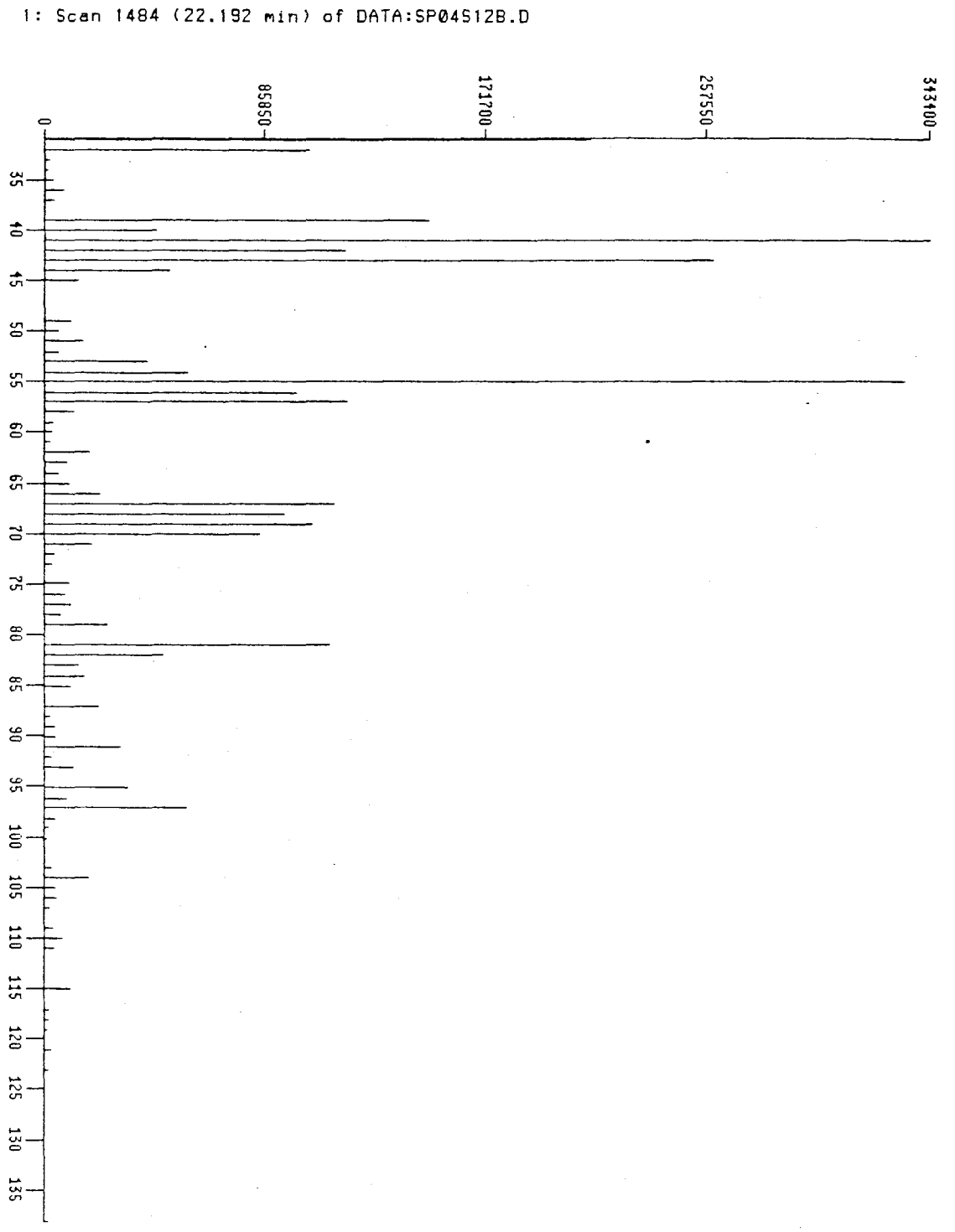


Figure A3.49. Ion current (ordinate) vs mass/charge (amu) (abscissa). File and retention time as indicated. Unidentified.

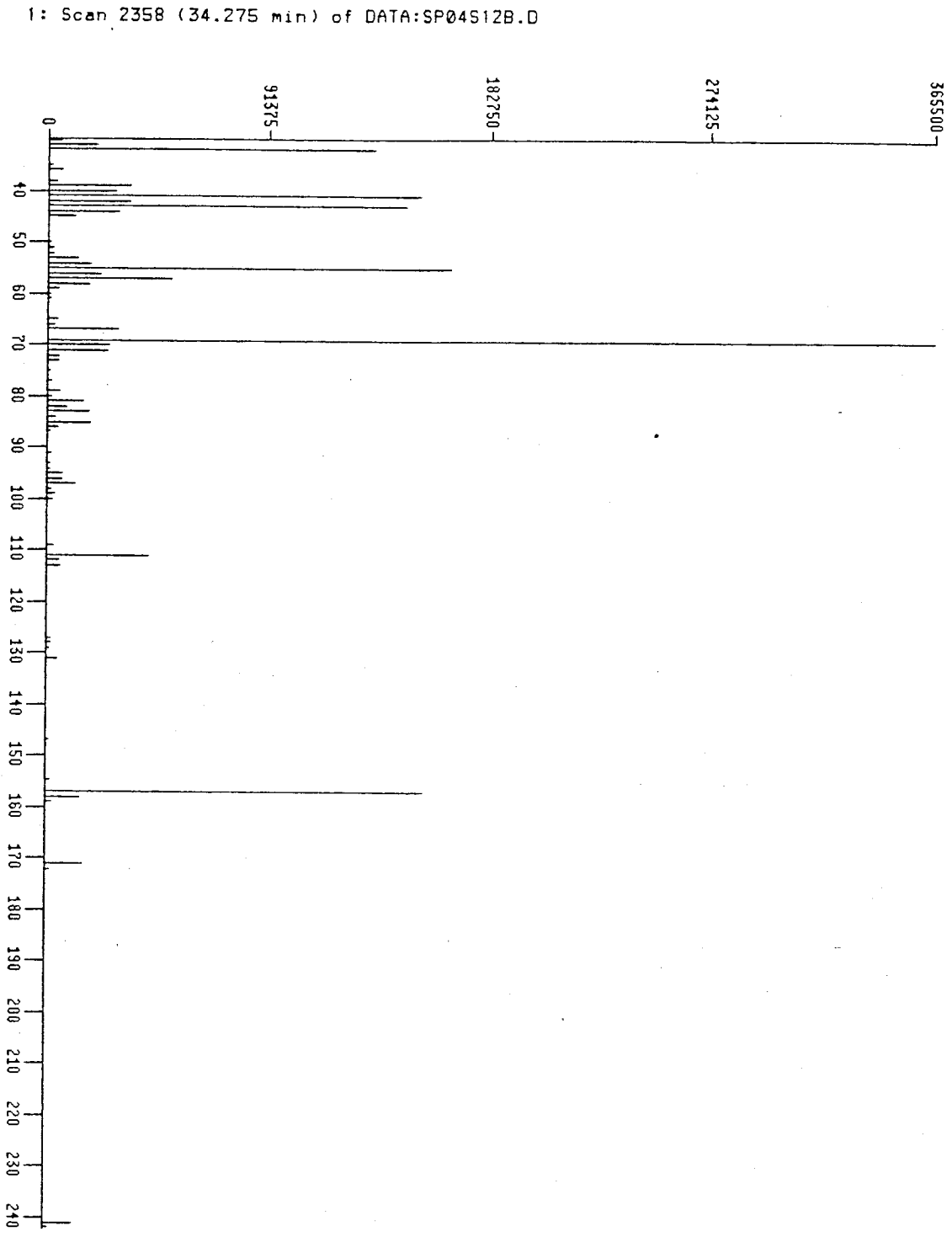


Figure A3.50. Ion current (ordinate) vs mass/charge (amu) (abscissa). File and retention time as indicated. Unidentified.

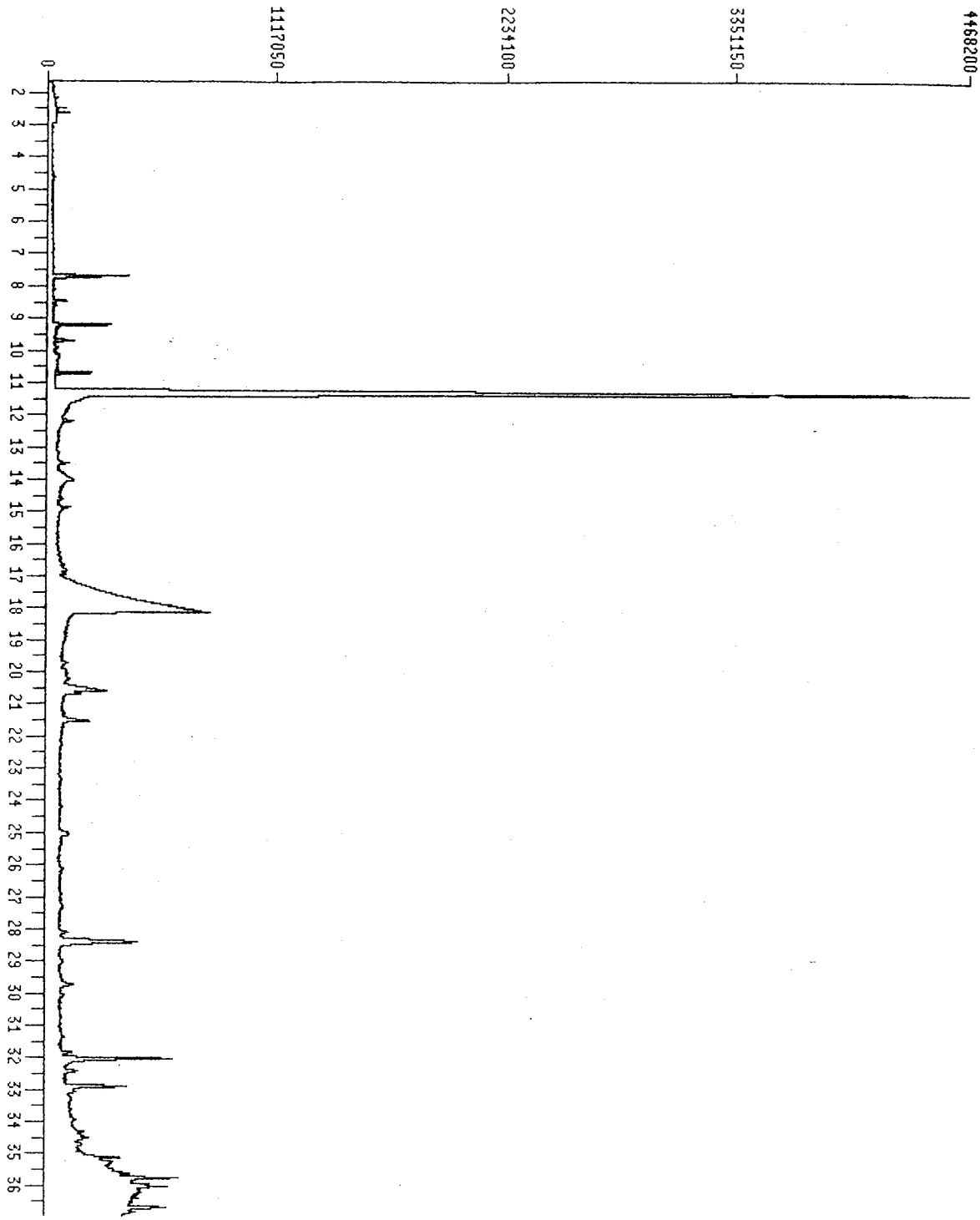


Figure A3.51. Total ion chromatogram from experiment 1O31. Ordinate: relative units. Abscissa: retention time. Data file V3:SP11J15E.D. Mass spectra similarly identified correspond to this chromatogram. Peak at 11.4 mins. is heptanal.

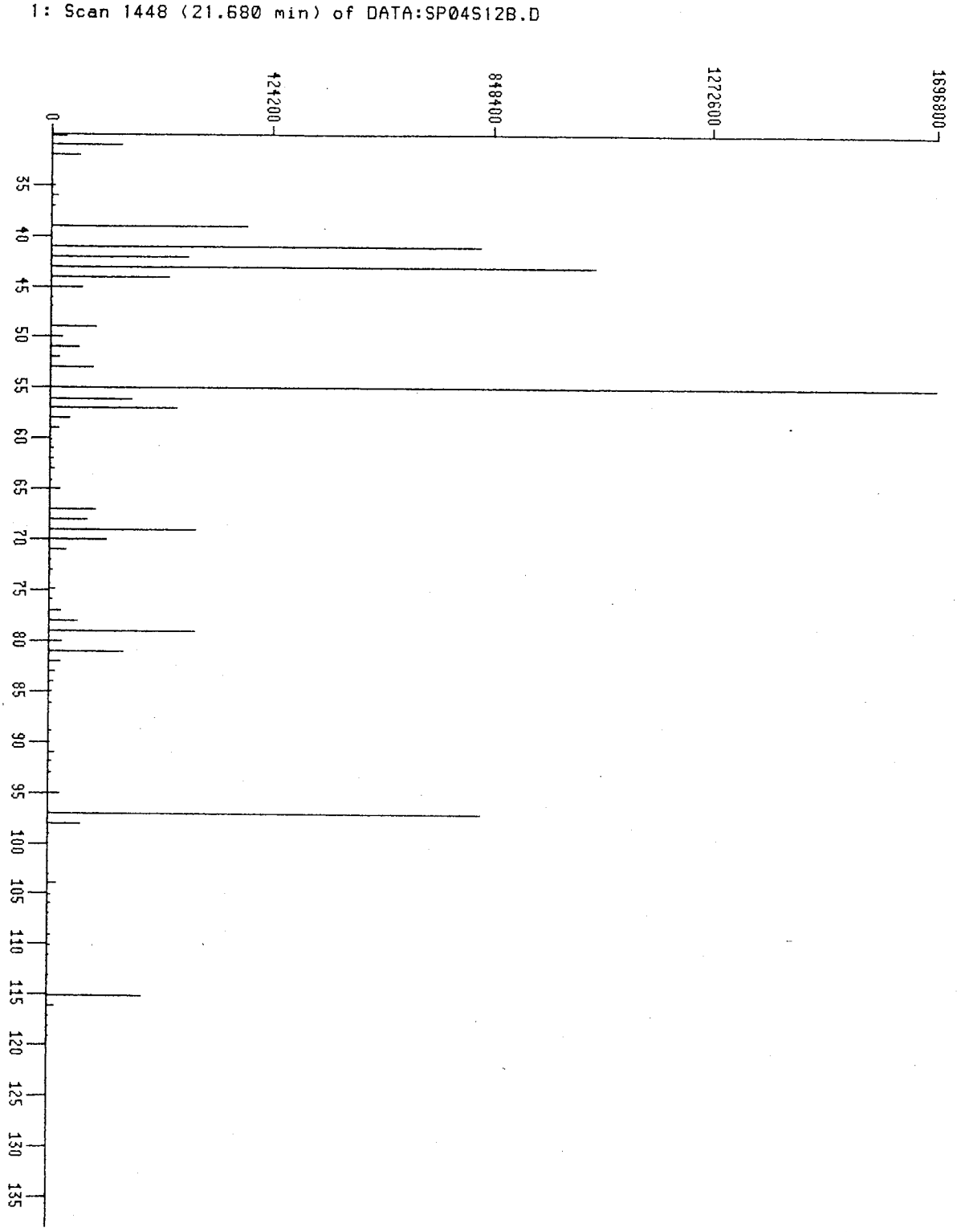


Figure A3.52a. Ion current (ordinate) vs mass/charge (amu) (abscissa). File and retention time as indicated. Unidentified.

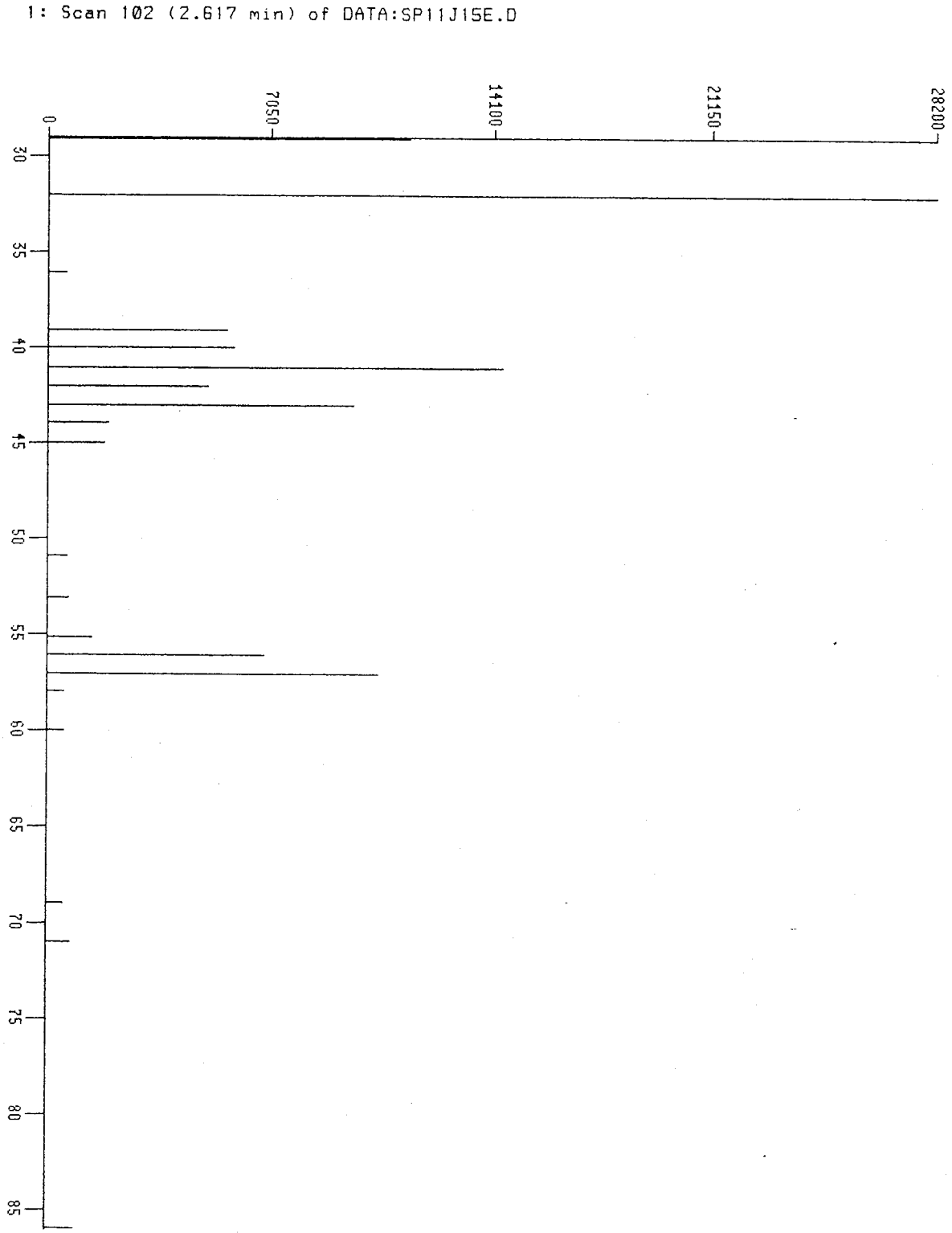


Figure A3.52b. Ion current (ordinate) vs mass/charge (amu) (abscissa). File and retention time as indicated. Identified as hexane.

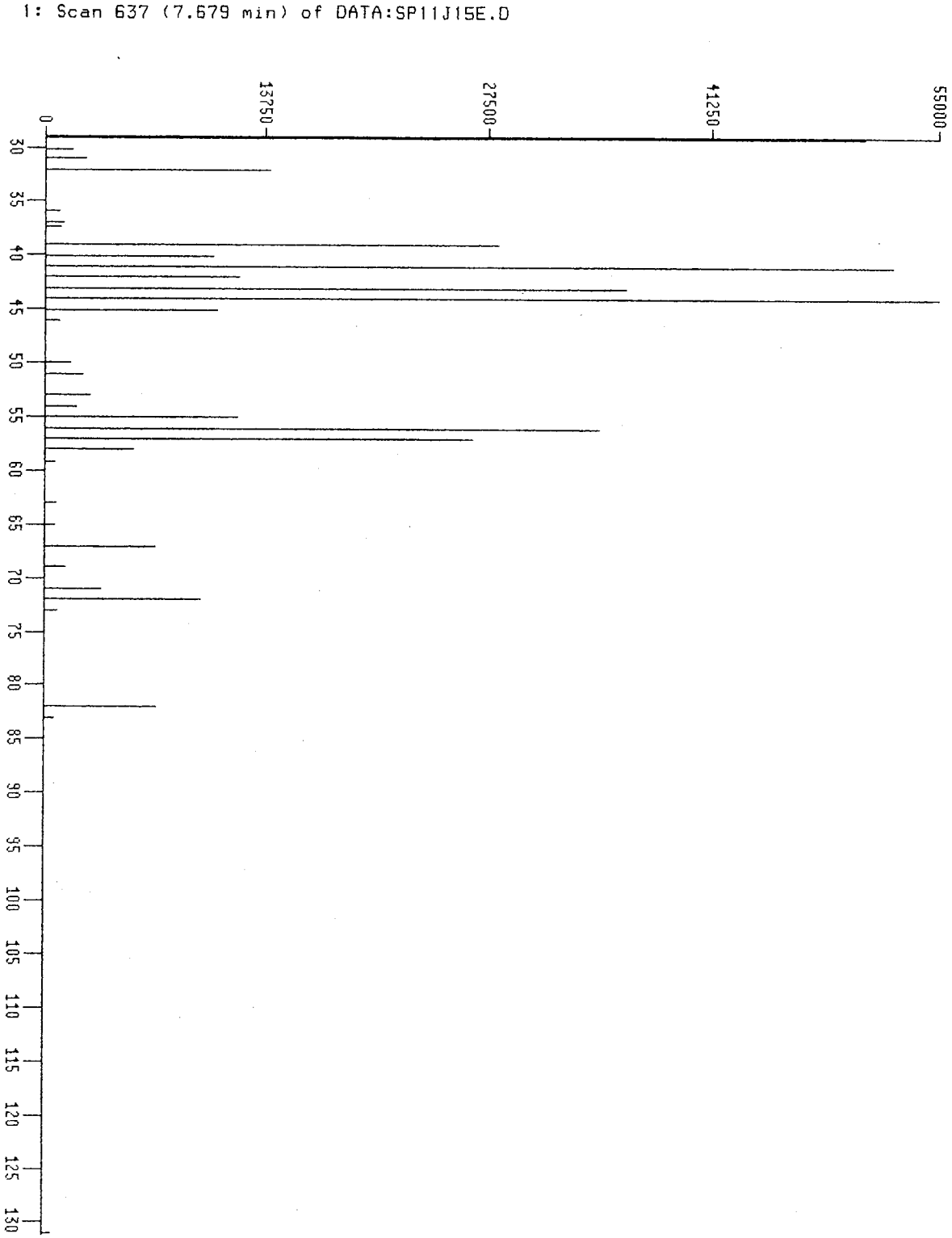


Figure A3.53. Ion current (ordinate) vs mass/charge (amu) (abscissa). File and retention time as indicated. Unidentified.

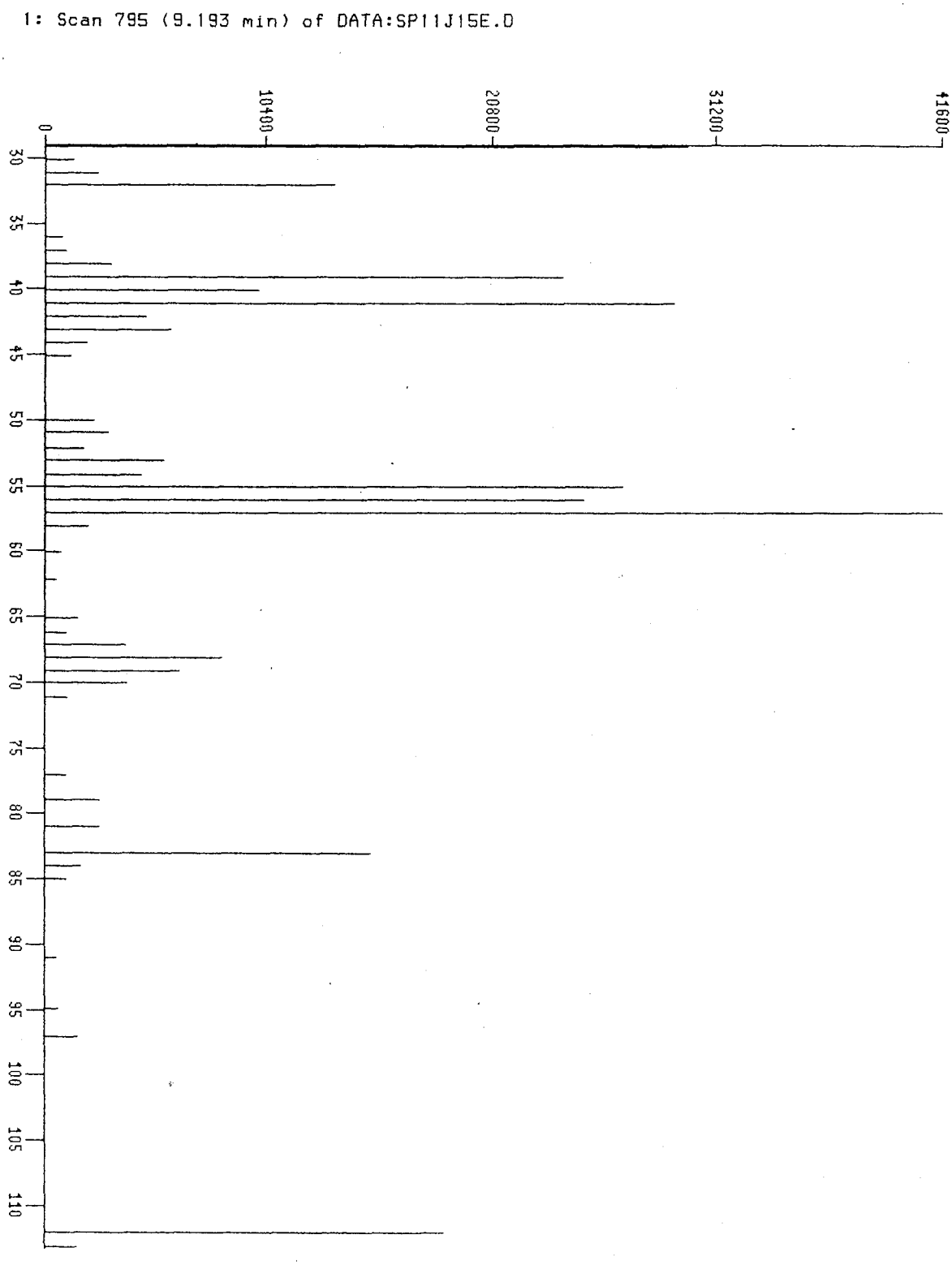


Figure A3.54. Ion current (ordinate) vs mass/charge (amu) (abscissa). File and retention time as indicated. Unidentified.

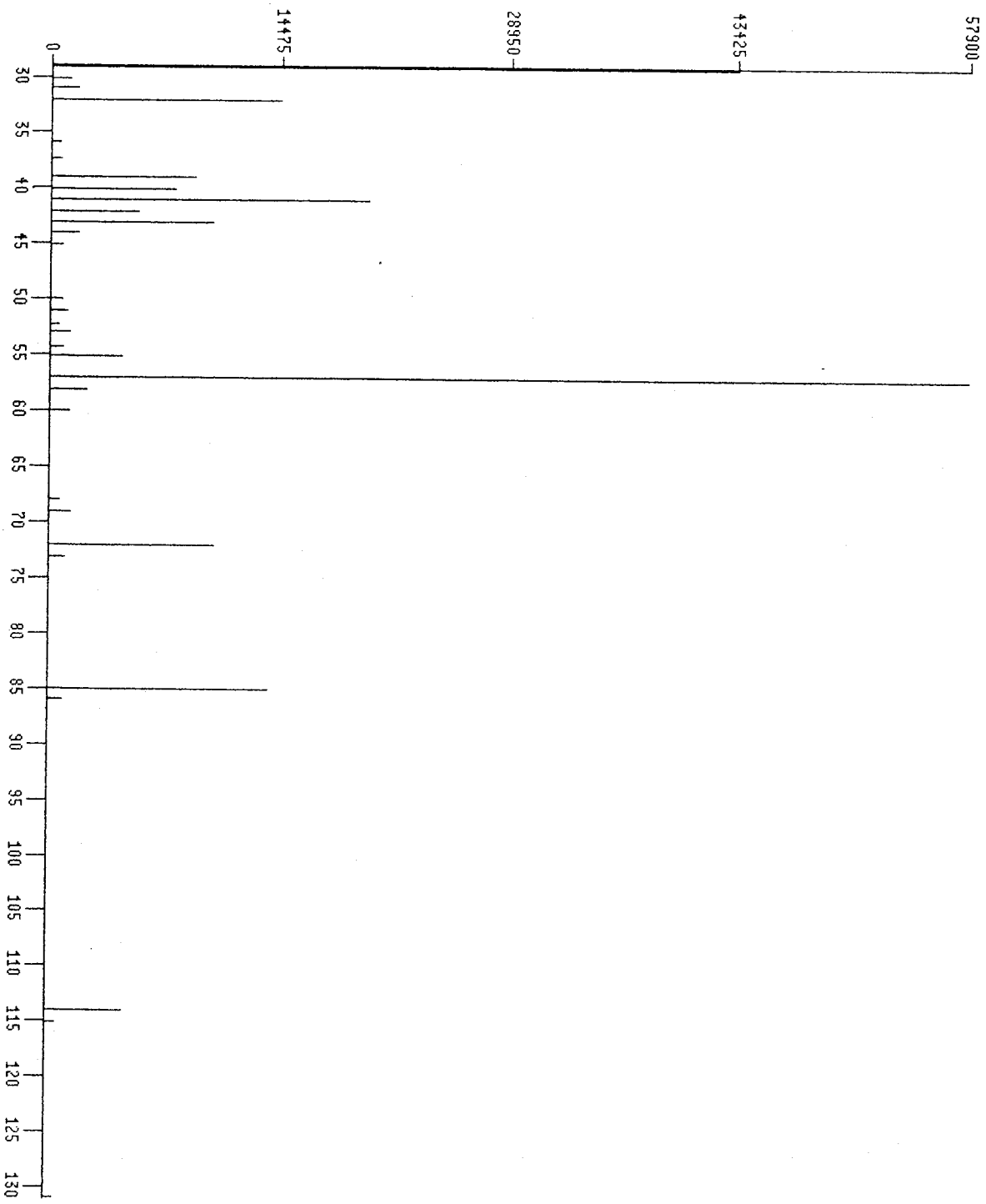


Figure A3.55. Ion current (ordinate) vs mass/charge (amu) (abscissa). File and retention time as indicated. Unidentified.

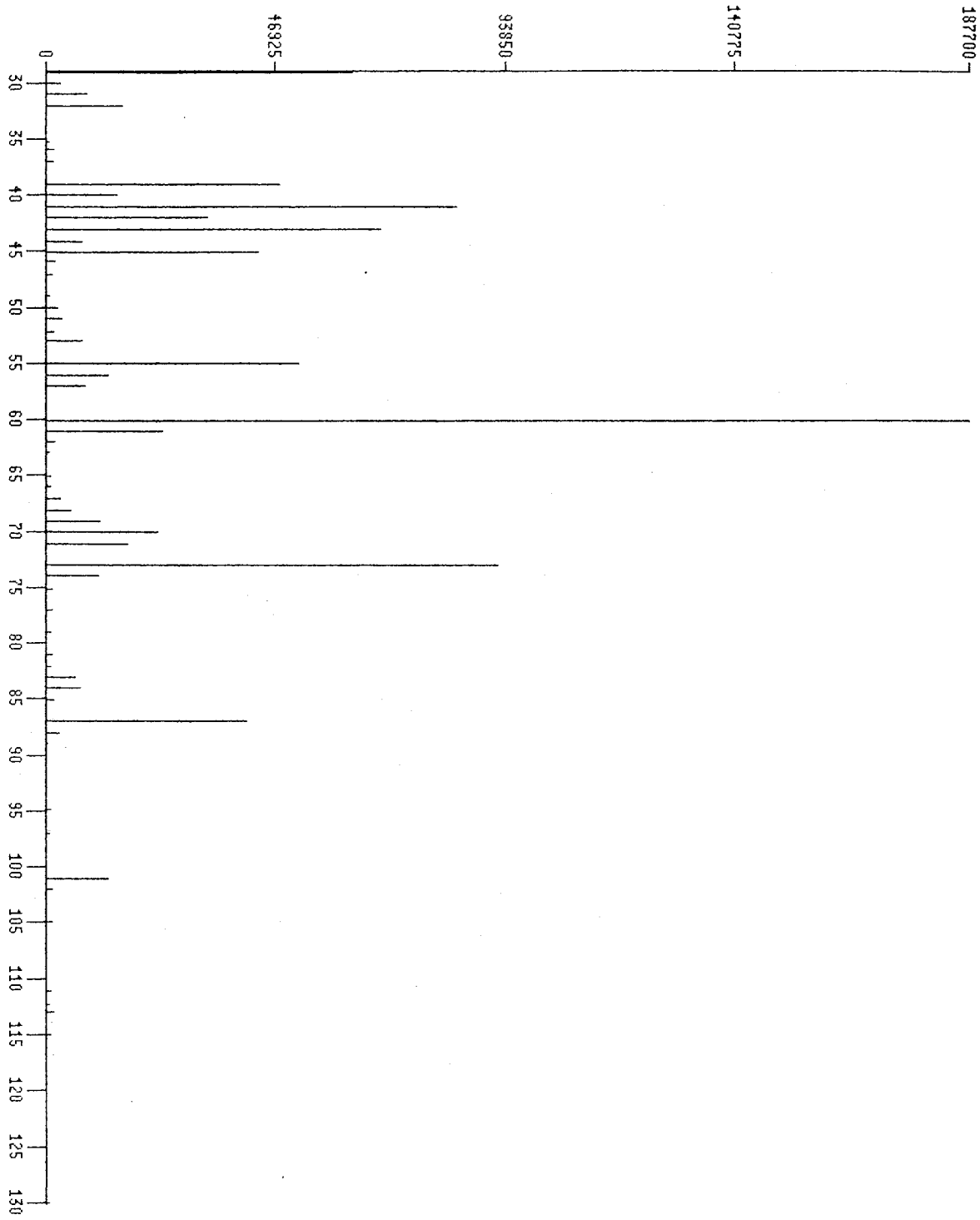


Figure A3.56. Ion current (ordinate) vs mass/charge (amu) (abscissa). File and retention time as indicated. Identified as heptanoic acid.

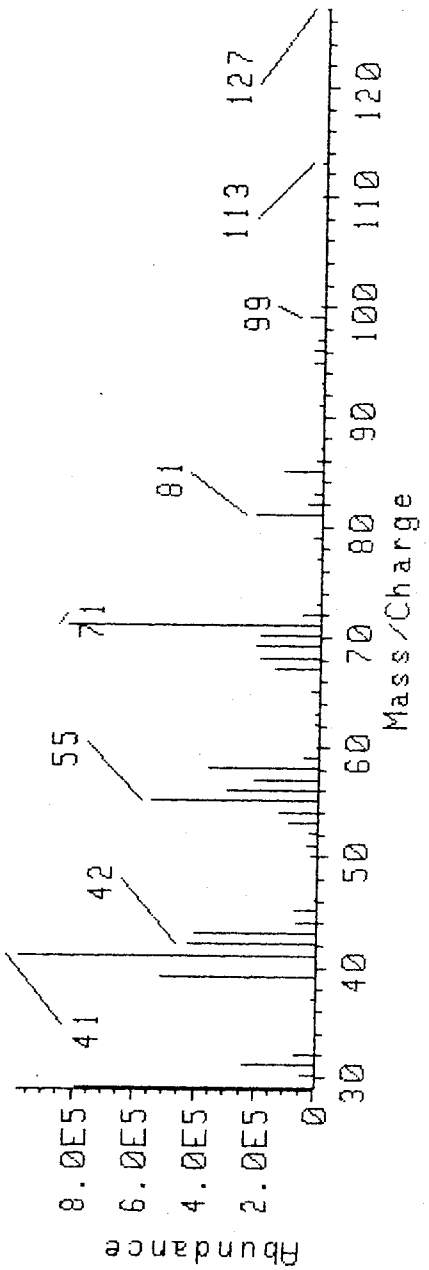


Figure A3.57. Ion current (ordinate) vs mass/charge (amu) (abscissa). 1-Octene library: 1, 2 octyl epoxide (standard obtained from Aldrich).

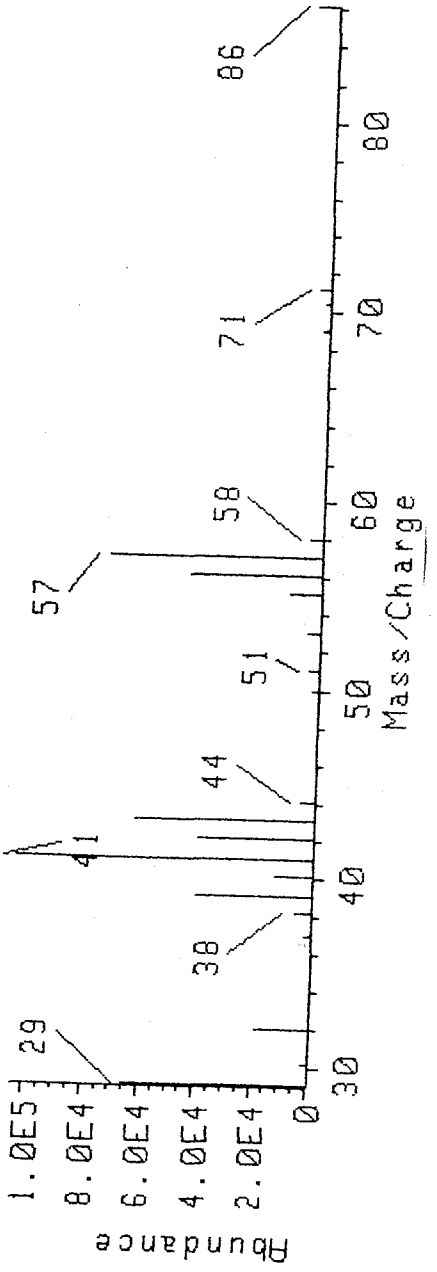


Figure A3.58. Ion current (ordinate) vs mass/charge (amu) (abscissa). 1-Octene library: hexane (standard obtained from Aldrich).

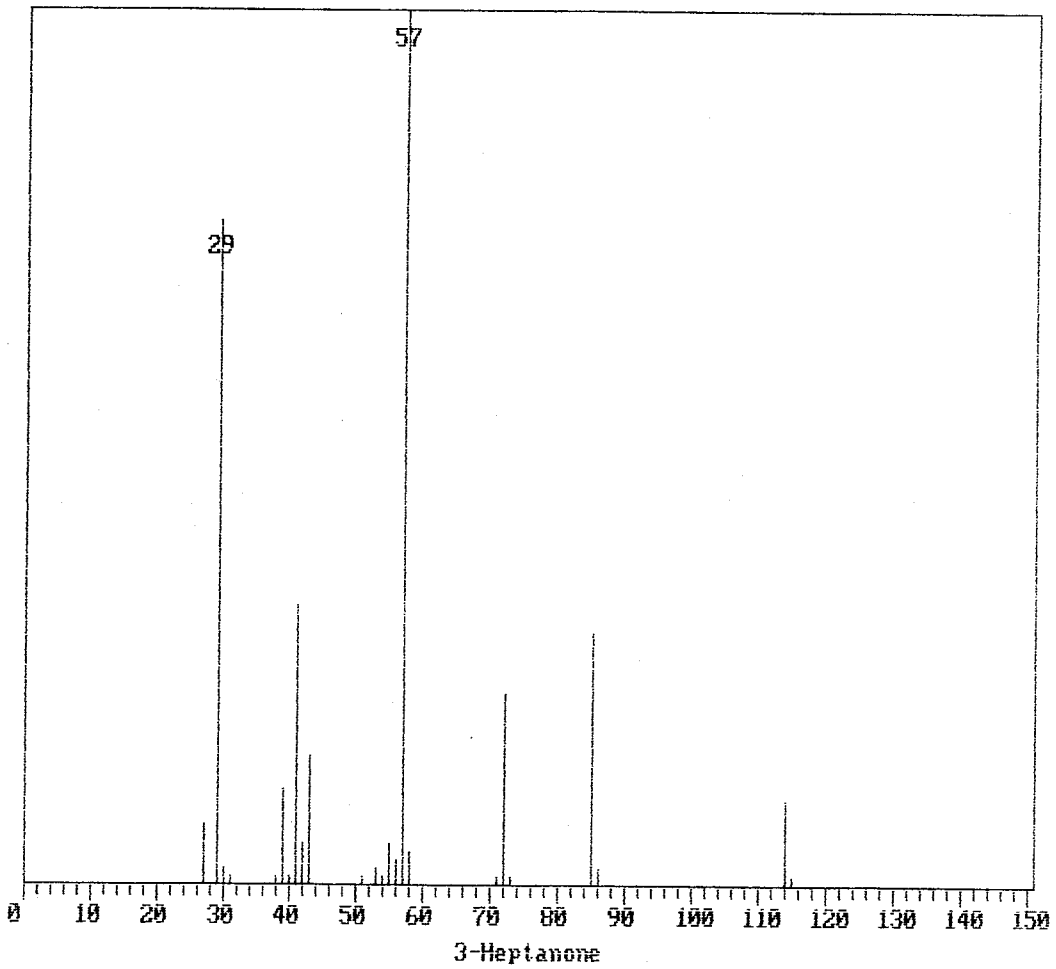


Figure A3.59. Ion current (ordinate) vs mass/charge (amu) (abscissa). 1-Octene library: 3-heptanone (from National Institute of Standards and Technology Mass Spectral Library (1990)).

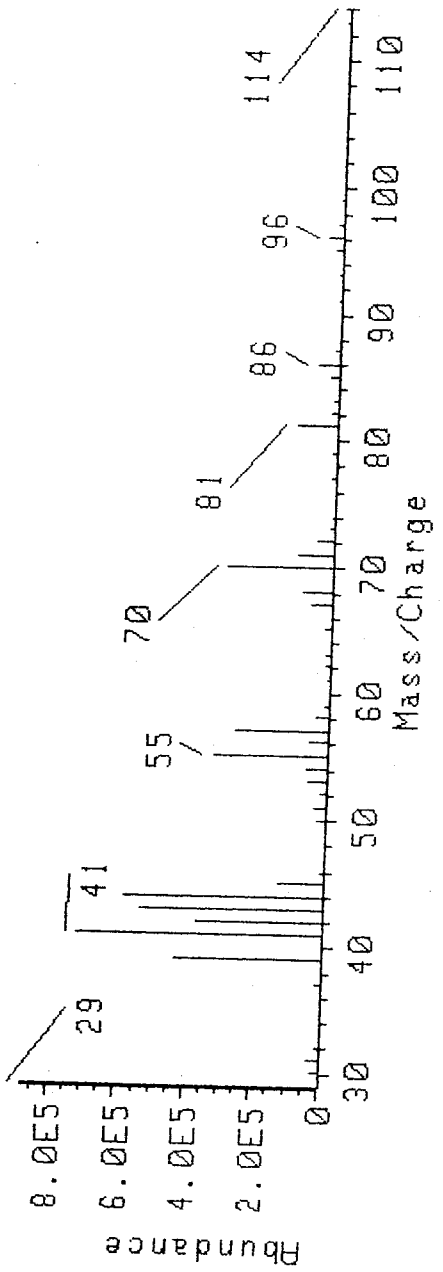


Figure A3.60. Ion current (ordinate) vs mass/charge (amu) (abscissa). 1-Octene library: heptanal (standard obtained from Aldrich).

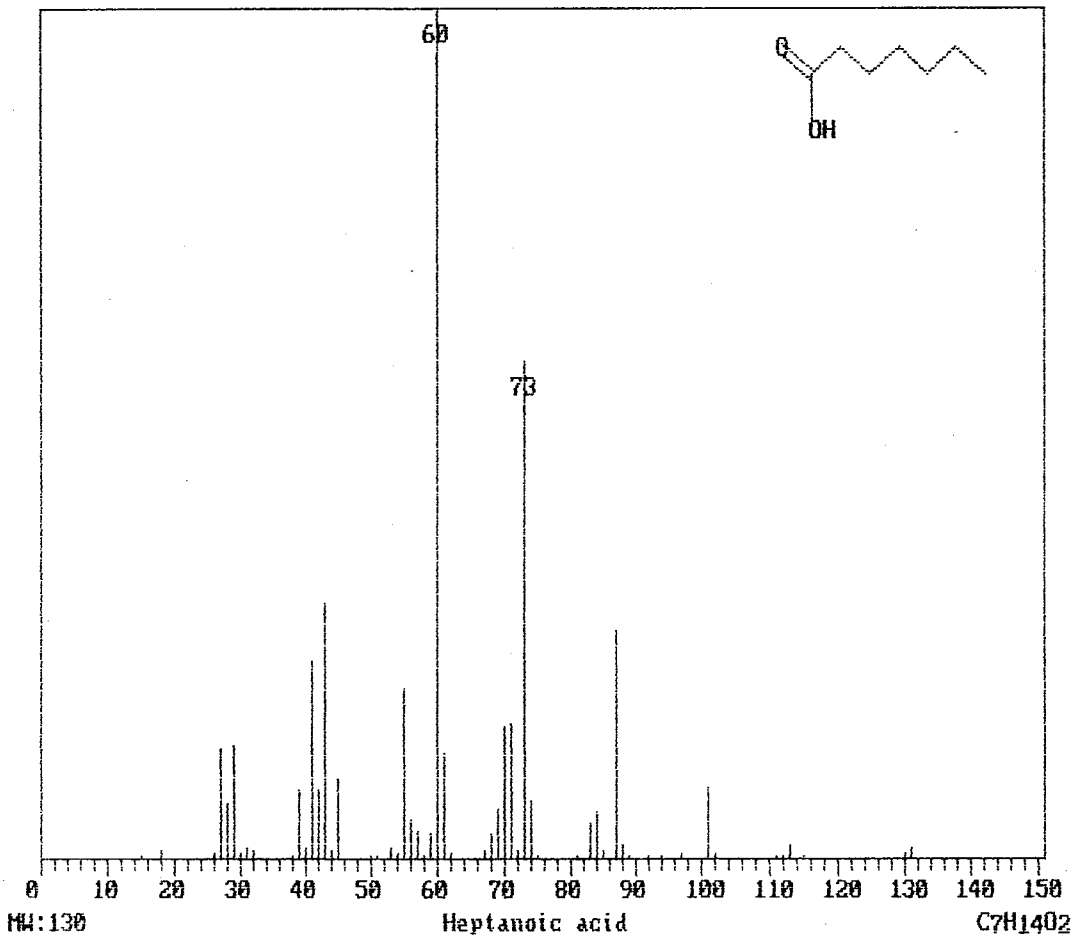


Figure A3.61. Ion current (ordinate) vs mass/charge (amu) (abscissa). 1-Octene library: heptanoic acid (from National Institute of Standards and Technology Mass Spectral Library (1990)).

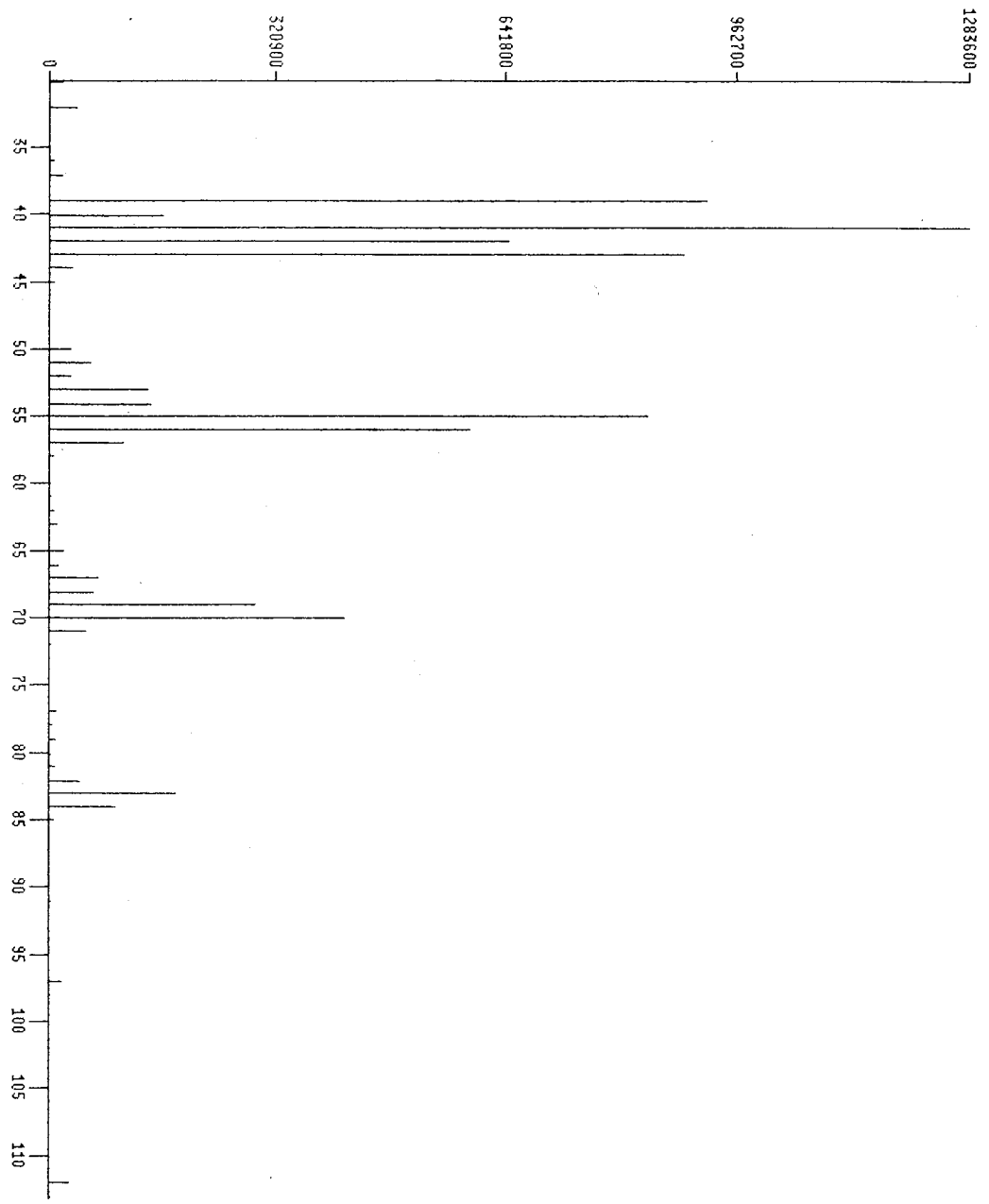


Figure A3.62. Ion current (ordinate) vs mass/charge (amu) (abscissa). 1-Octene library: 1-octene (standard obtained from Aldrich).

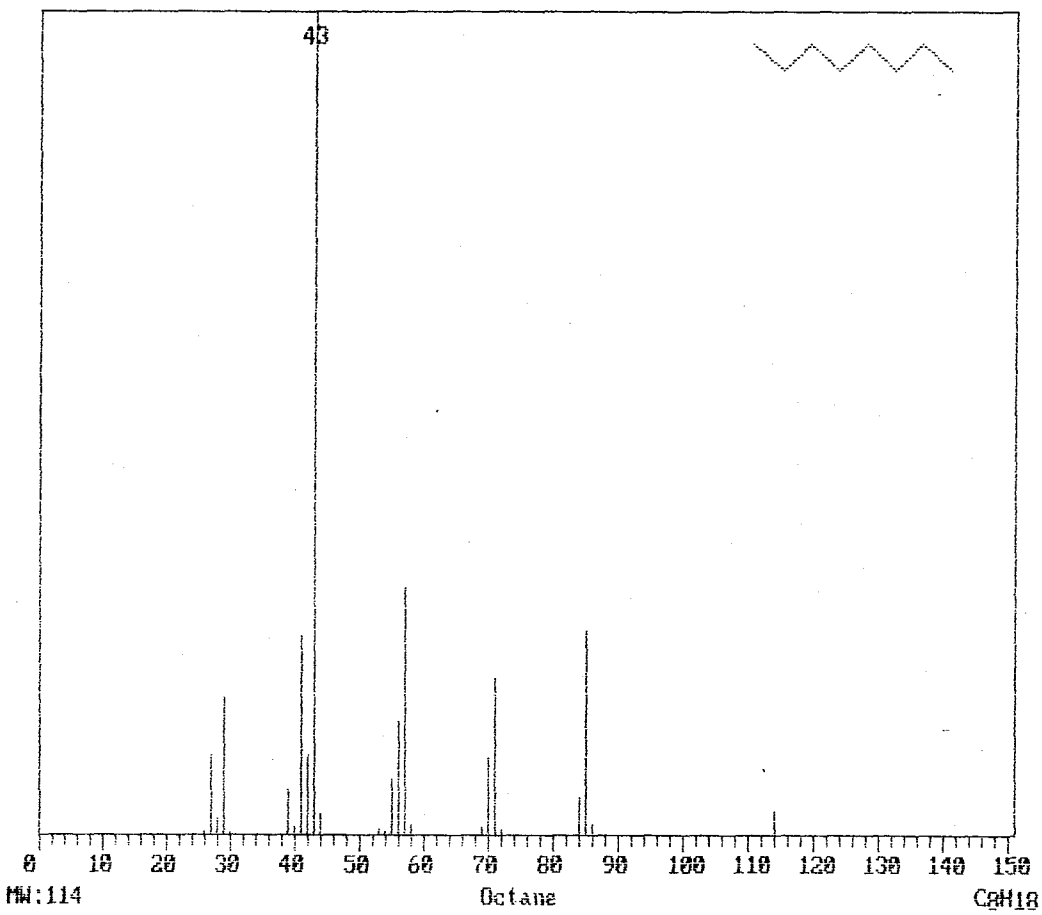


Figure A3.63. Ion current (ordinate) vs mass/charge (amu) (abscissa). 1-Octene library: n-octane (from National Institute of Standards and Technology Mass Spectral Library (1990)).

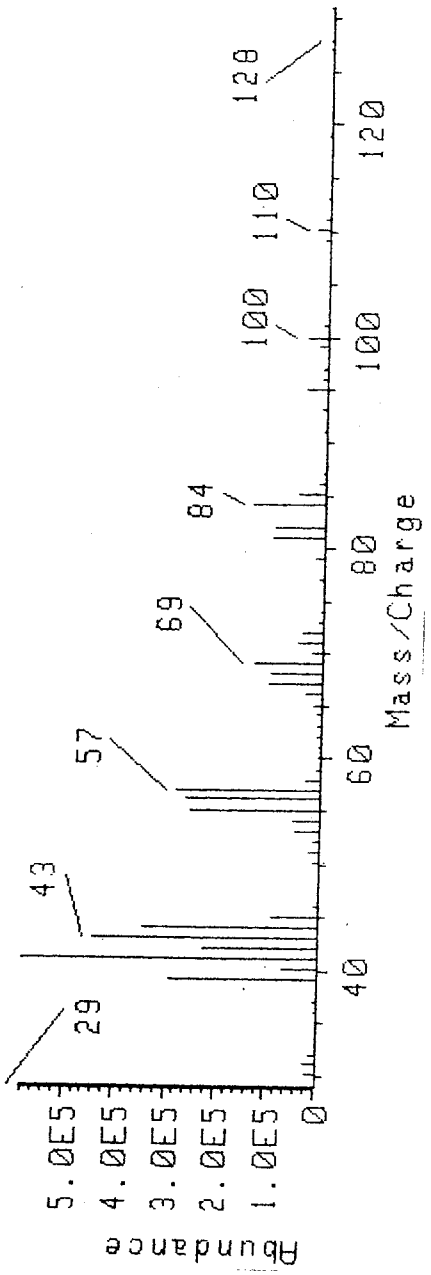


Figure A3.64. Ion current (ordinate) vs mass/charge (amu) (abscissa). 1-Octene library: octanal (standard obtained from Aldrich).

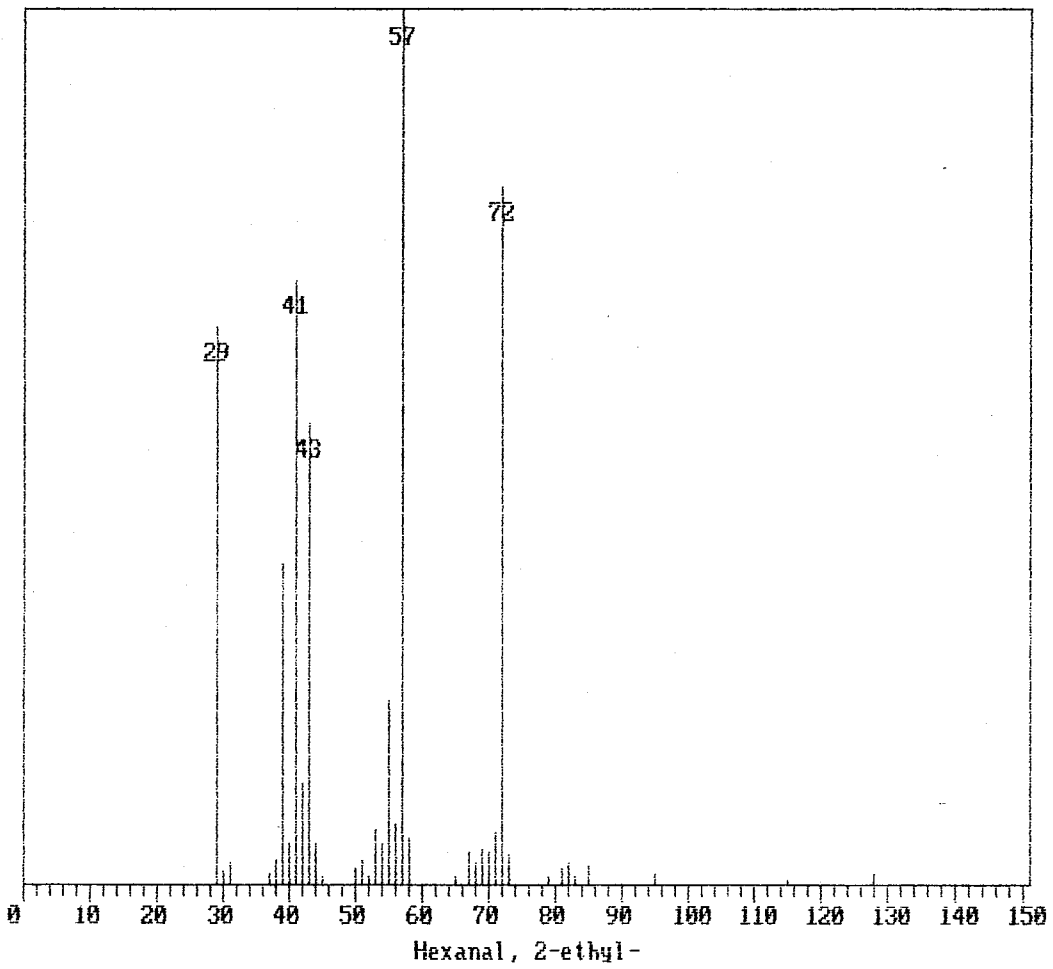


Figure A3.65. Ion current (ordinate) vs mass/charge (amu) (abscissa). 1-Octene library: 2-ethyl hexanal (from National Institute of Standards and Technology Mass Spectral Library (1990)).

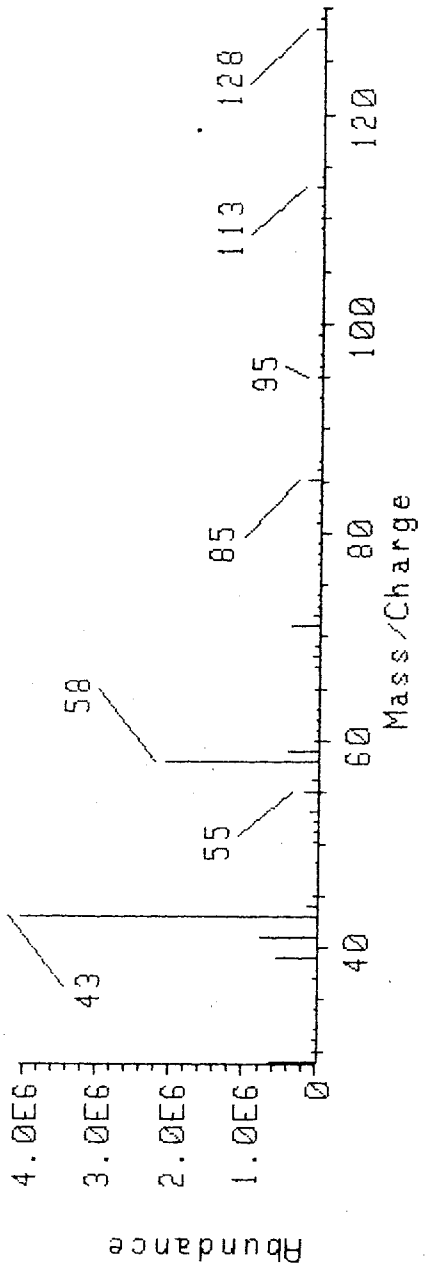


Figure A3.66. Ion current (ordinate) vs mass/charge (amu) (abscissa). 1-Octene library: 2-octanone (standard obtained from Aldrich).

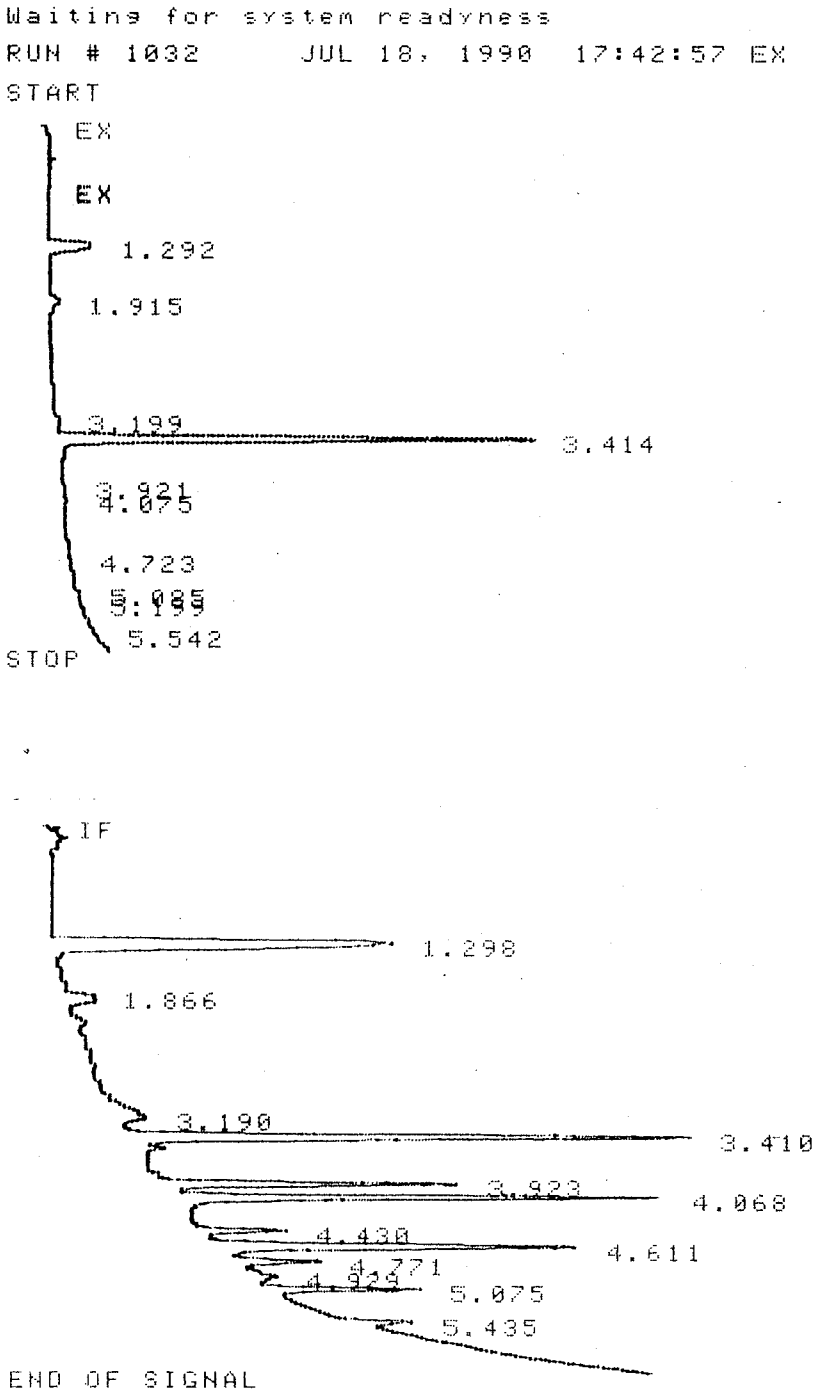


Figure A3.67. FID traces, no pre-concentration, experiment IOH8, (a) before uncovering, and (b) at end of experiment. Peak at 1.3, methane, 3.4, isoprene, 3.9, methacrolein, 4.1, methyl vinyl ketone, 4.4, 3-methyl furan, 4.6., 2-methyl 3-butene oxide, 5.1, 3,3-methyl butene oxide.

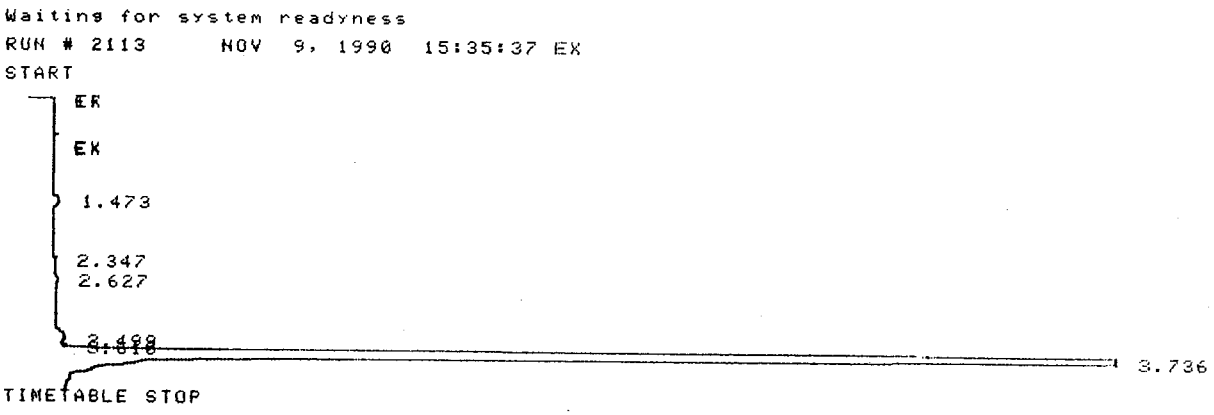


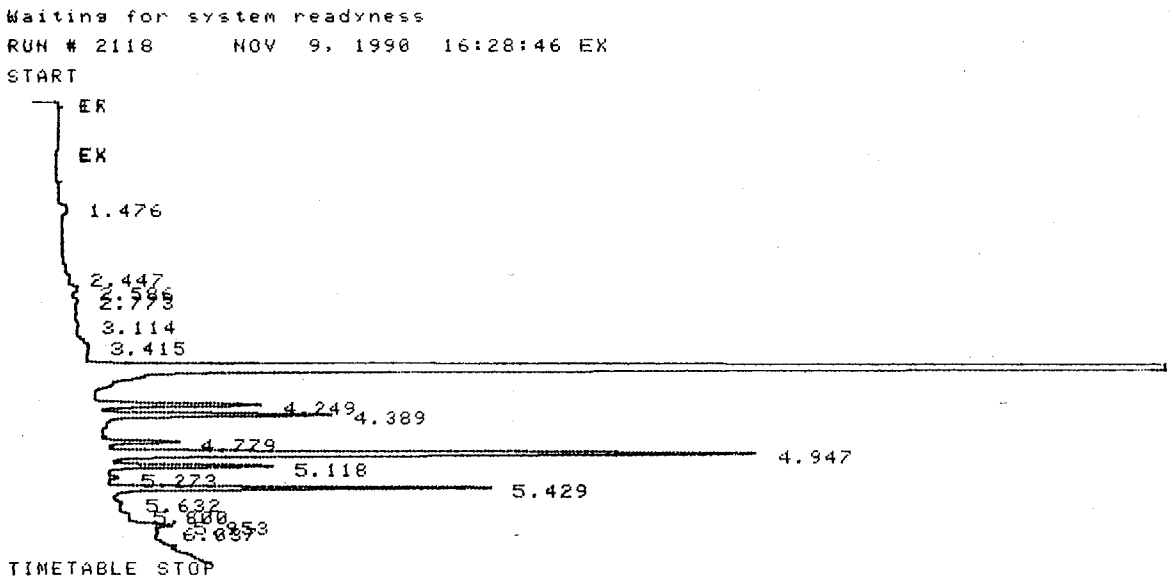


Figure A3.68. FID traces, no pre-concentration, experiment IO3P2, (a) before uncovering, and (b) at end of experiment. Peak at 1.3, methane, 3.7, isoprene, 4.25, methacrolein, 4.4, methyl vinyl ketone, 5., 2-methyl 3-butene oxide, 5.4, 3,3-methyl butene oxide.

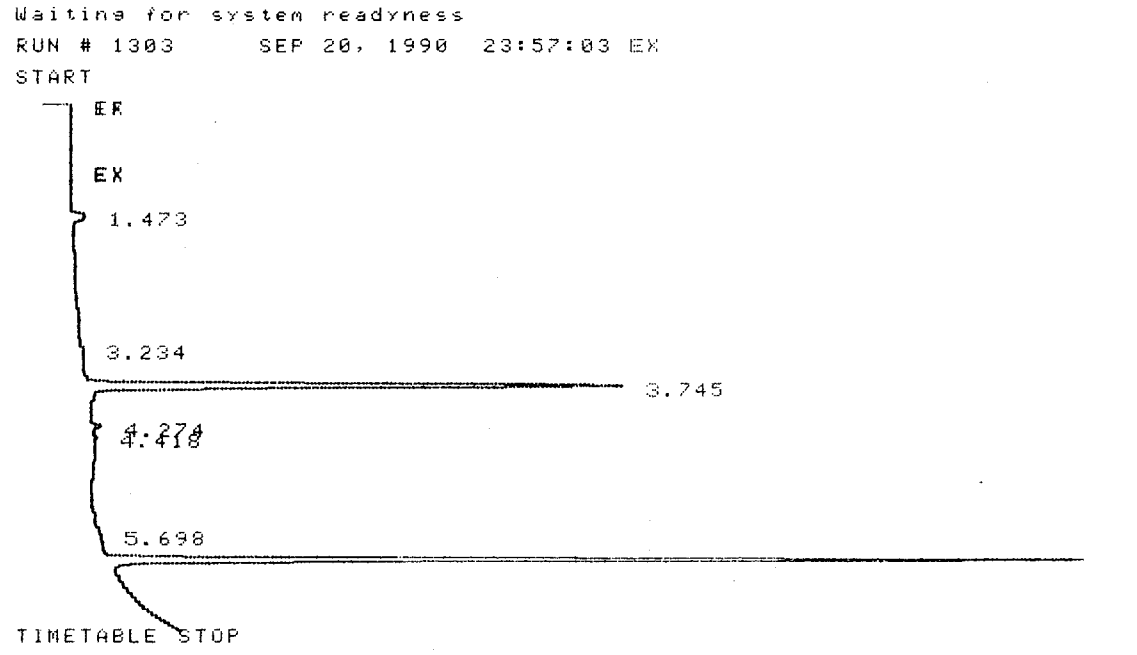


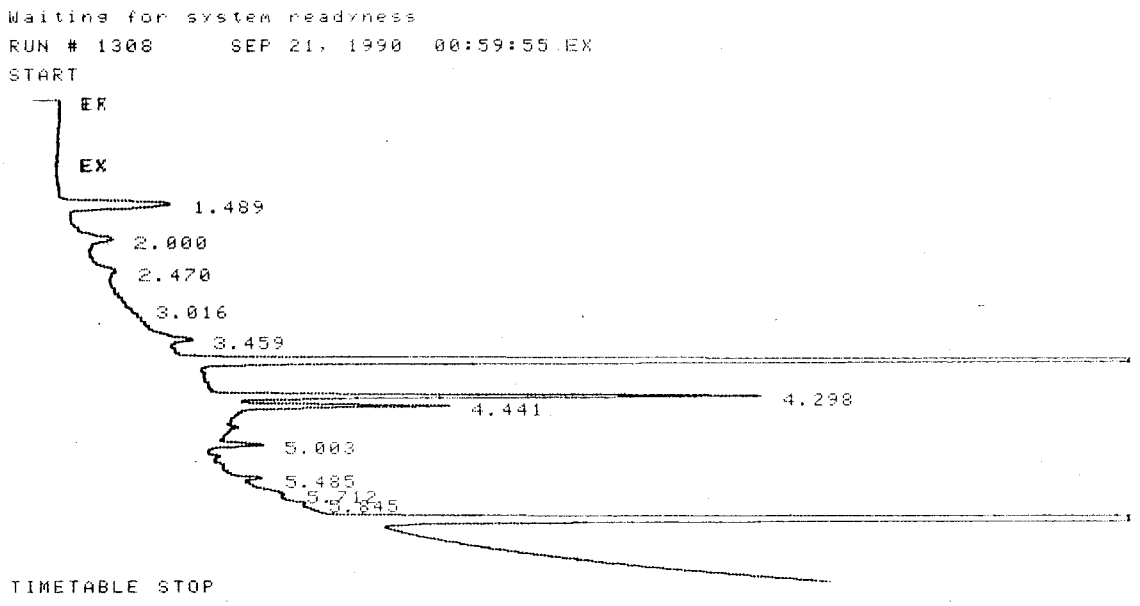


Figure A3.69. FID traces, no pre-concentration, experiment MIO31, (a) before uncovering, and (b) at end of experiment. Peak at 1.3, methane, 3.7, isoprene, 4.3, methacrolein, 4.44, methyl vinyl ketone, 5.003, 2-methyl 3-butene oxide, 6., methyl cyclohexane.

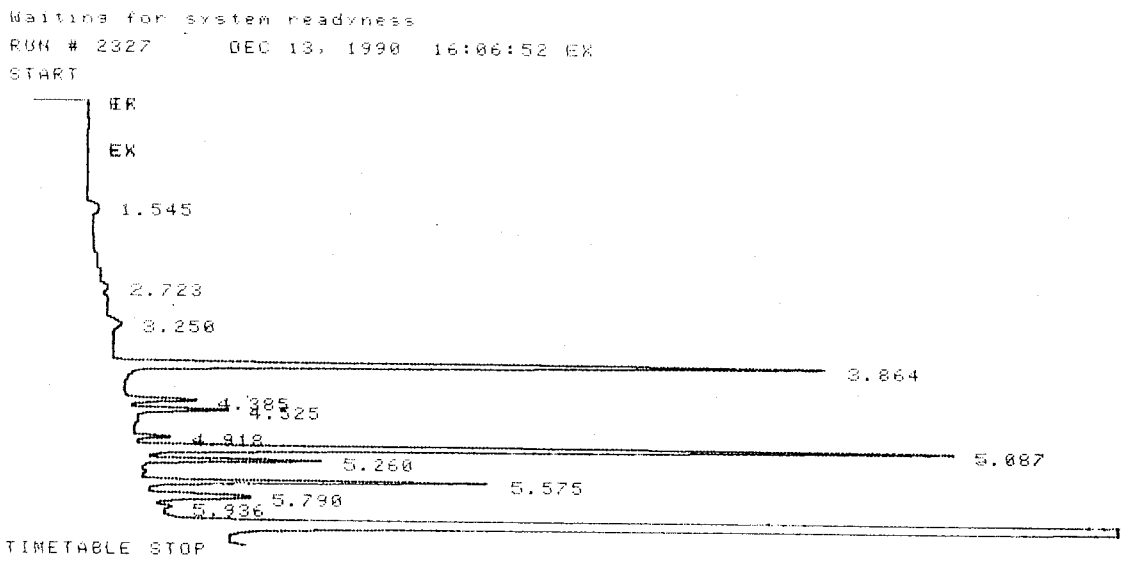


Figure A3.70. FID traces, no pre-concentration, experiment MIO3P1, at end of experiment. Peak at 1.3, methane, 3.9, isoprene, 4.4, methacrolein, 4.5, methyl vinyl ketone, 5.1, 2-methyl 3-butene oxide, 5.3, unknown 1, 5.6, 3,3-methyl butene oxide, 6., methyl cyclohexane.

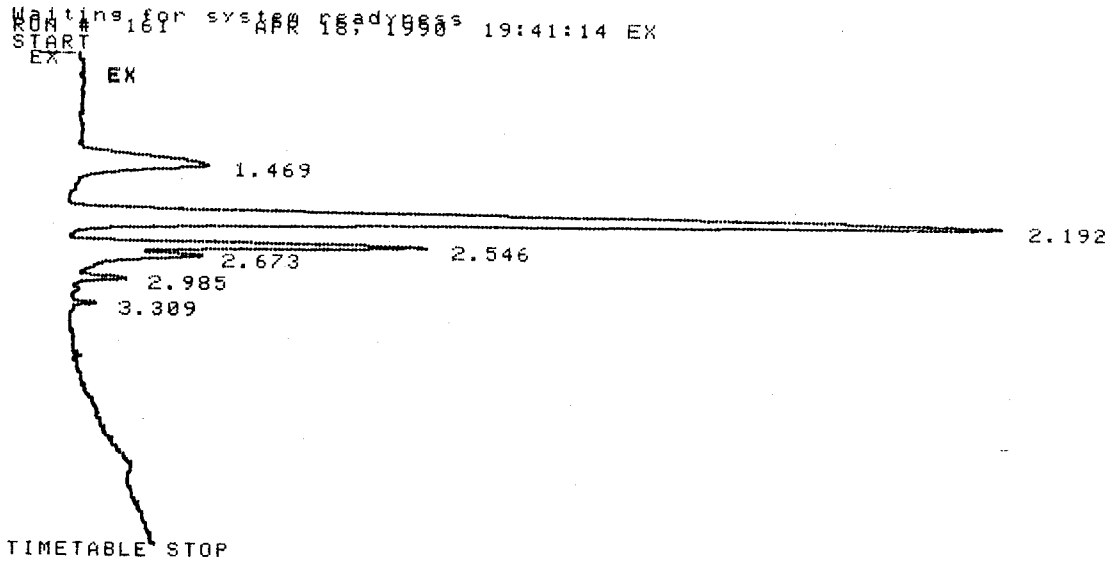


Figure A3.71. FID traces, no pre-concentration, experiment IO32, at end of experiment. Peak at 1.3, methane, 2.2, isoprene, 2.55, methacrolein, 2.68, methyl vinyl ketone, 2.99, 2-methyl 3-butene oxide, 3.3, 3,3-methyl butene oxide.

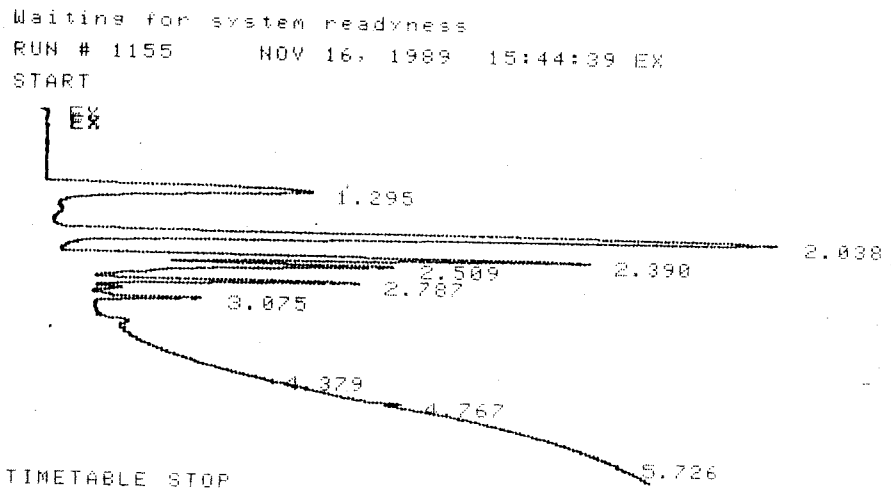


Figure A3.72. FID traces, no pre-concentration, experiment IO32, at end of experiment. Peak at 1.3, methane, 2.1, isoprene, 2.4, methacrolein, 2.5, methyl vinyl ketone, 2.8, 2-methyl 3-butene oxide, 3.1, 3,3-methyl butene oxide.

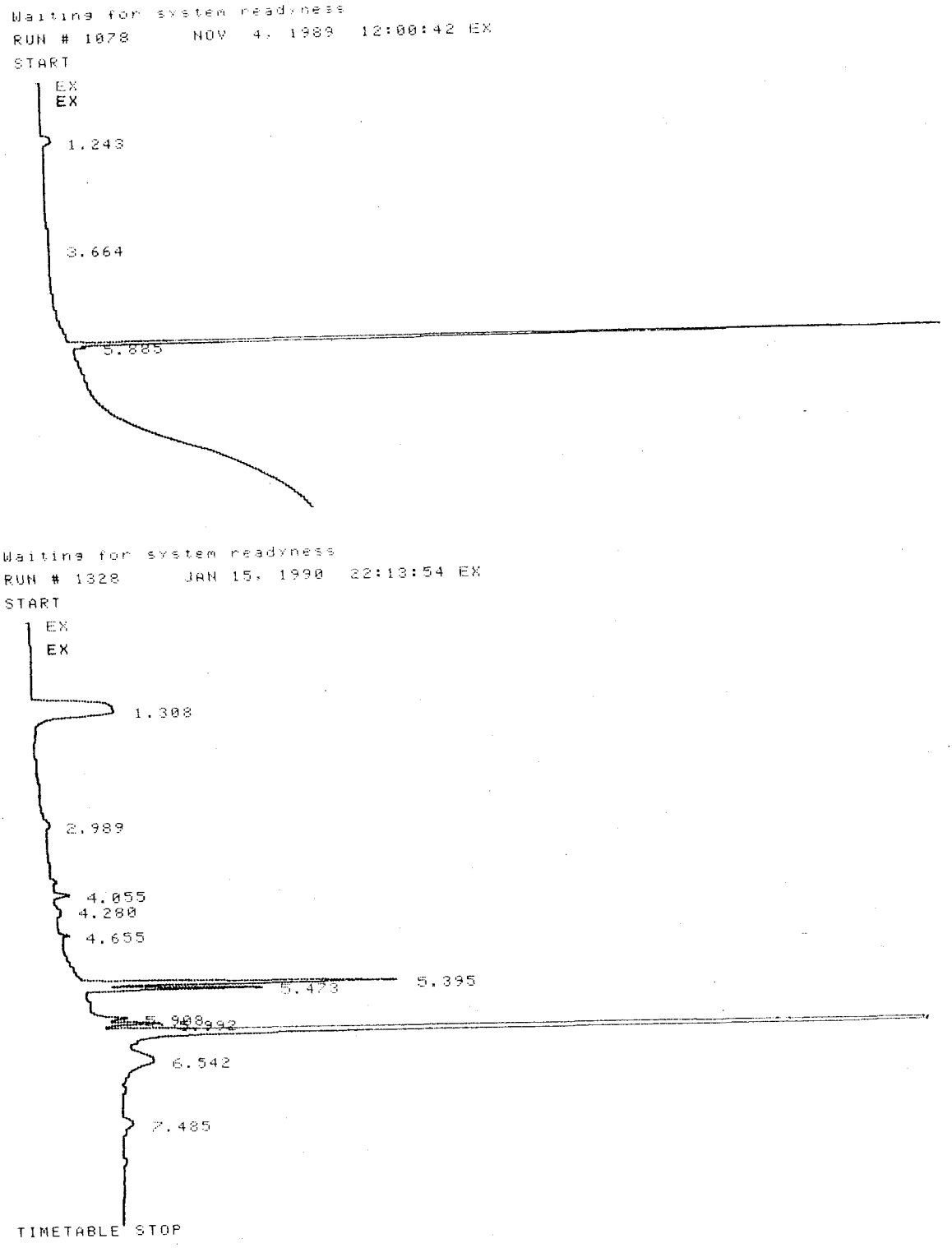


Figure A3.73. FID traces, no pre-concentration, experiment 1O31, (a) before introduction of ozone, and (b) at end of experiment; (b) scale is 4x (a). Peak at 1.3, methane, 5.8 (a) and 5.4 (b), 1-octene, (b) 5.5, n-octane, 6.2 heptanal, 7.5, heptanoic acid.

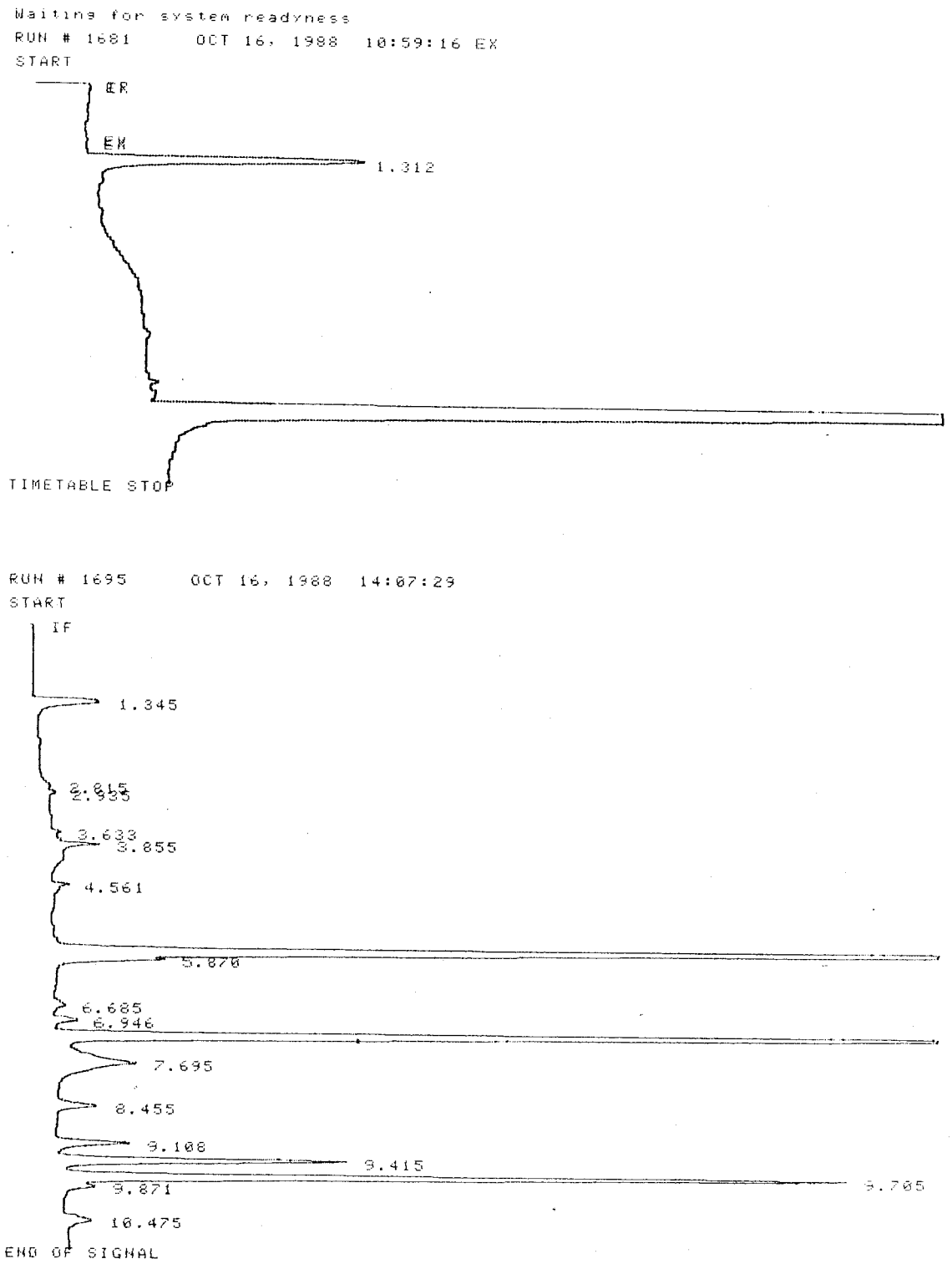


Figure A3.74. FID traces, no pre-concentration, experiment 1NOX5, (a) before introduction of ozone, and (b) at end of experiment; (a) scale is 4x (b). Peak at 1.3, methane, 5.7, 1-octene, 5.8, n-octane, 6.9, 3-heptanone, 7.2 heptanal, 9.4, 2-octanone, 9.7, octanal + 1, 2 octyl epoxide.

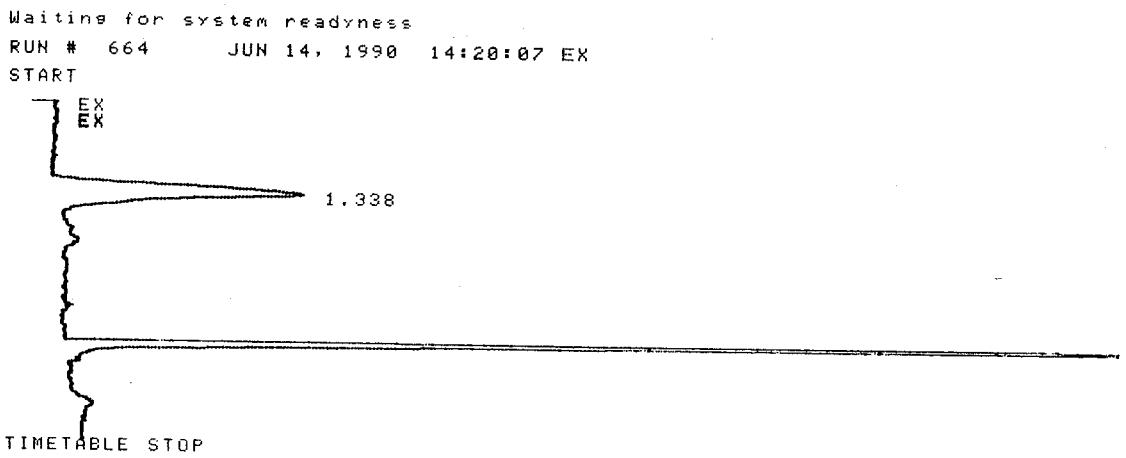


Figure A3.75. FID traces, no pre-concentration, experiment 1OH2, at end of experiment. Peak at 1.3, methane, 3.5, 1-octene.

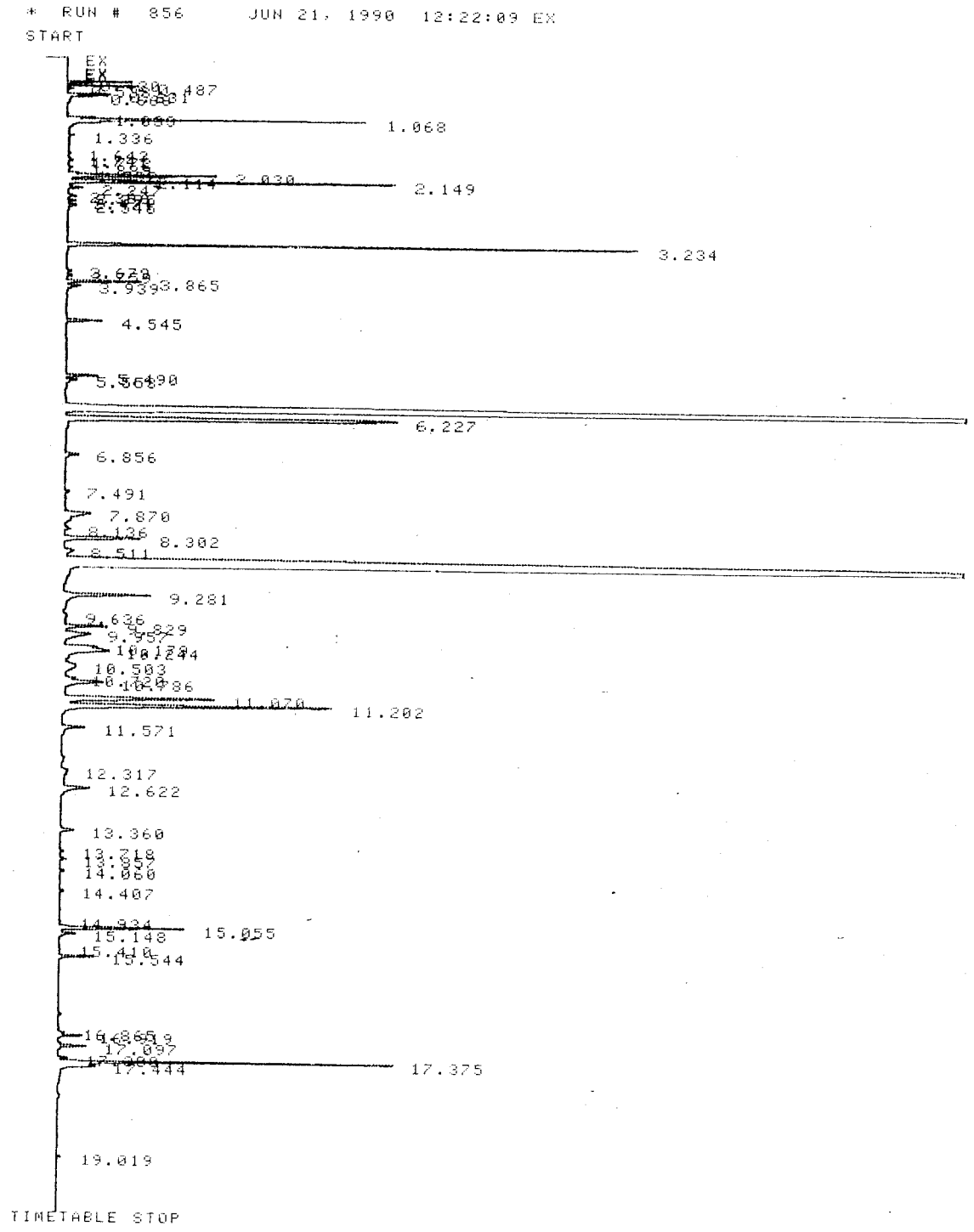


Figure A3.76. FID traces, with pre-concentration, experiment 1NOXJ21. Peak at 6., 1-octene, 8.8, heptanal.

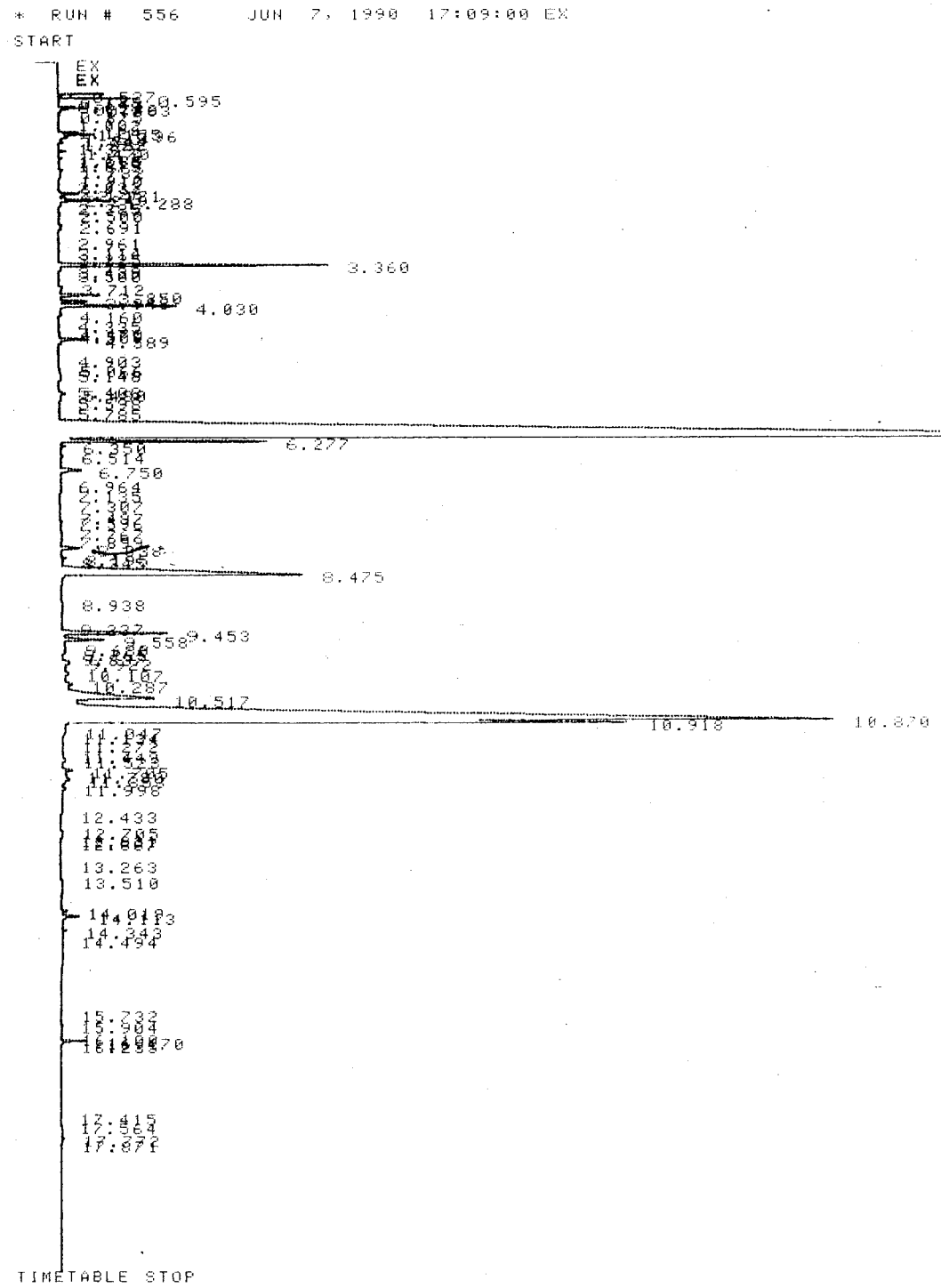


Figure A3.76. FID traces, with pre-concentration, experiment 1NOXJ21. Peak at 6., 1-octene, 8.8, heptanal.

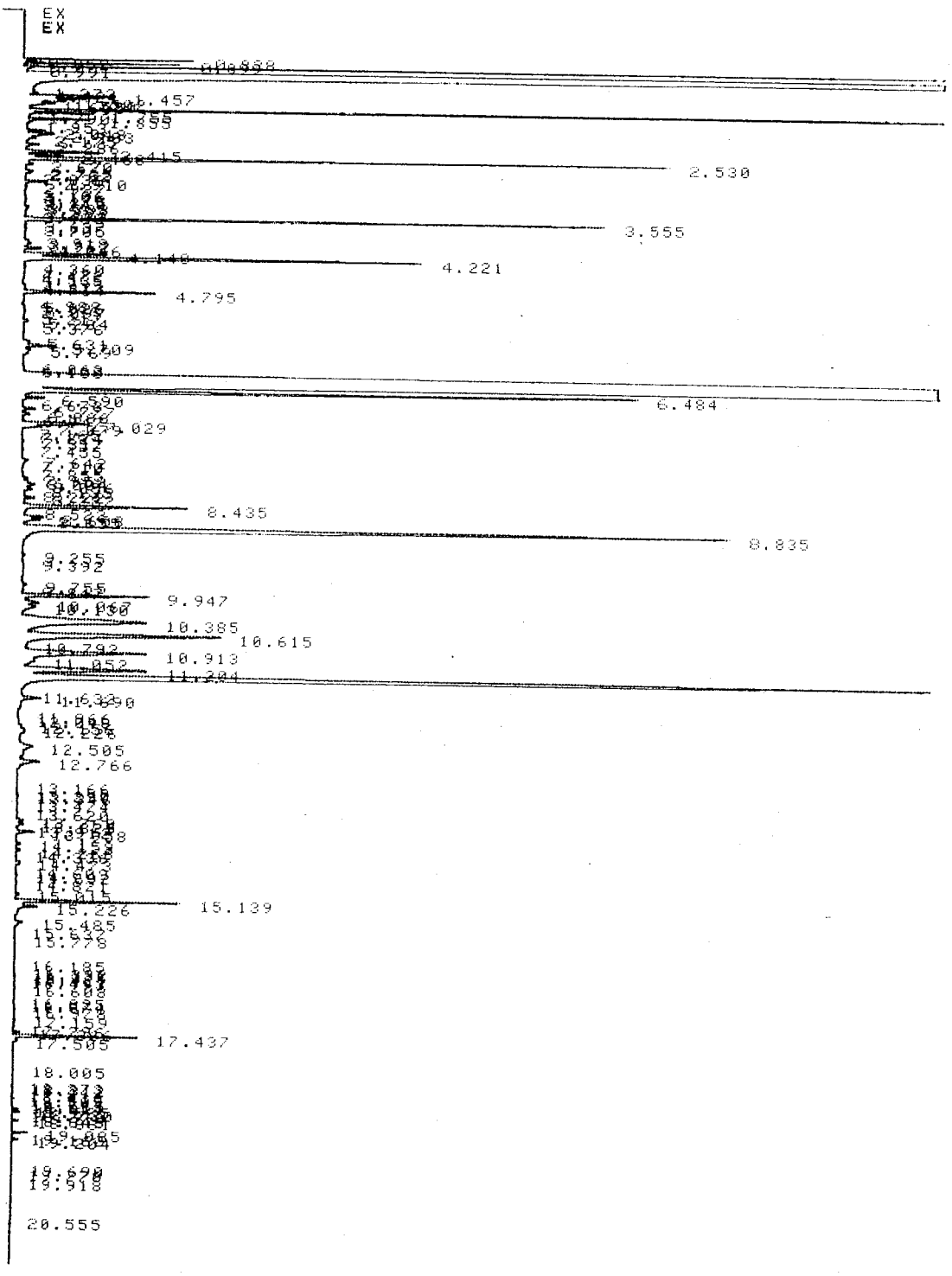


Figure A3.78. FID traces, with pre-concentration on Tenax, experiment 1OH1. Peak at 6.4, 1-octene, 8.8, heptanal, 11.4, octanal and 1, 2 octyl epoxide.